UNIVERSITY OF COPENHAGEN
FACULTY OR DEPARTMENT

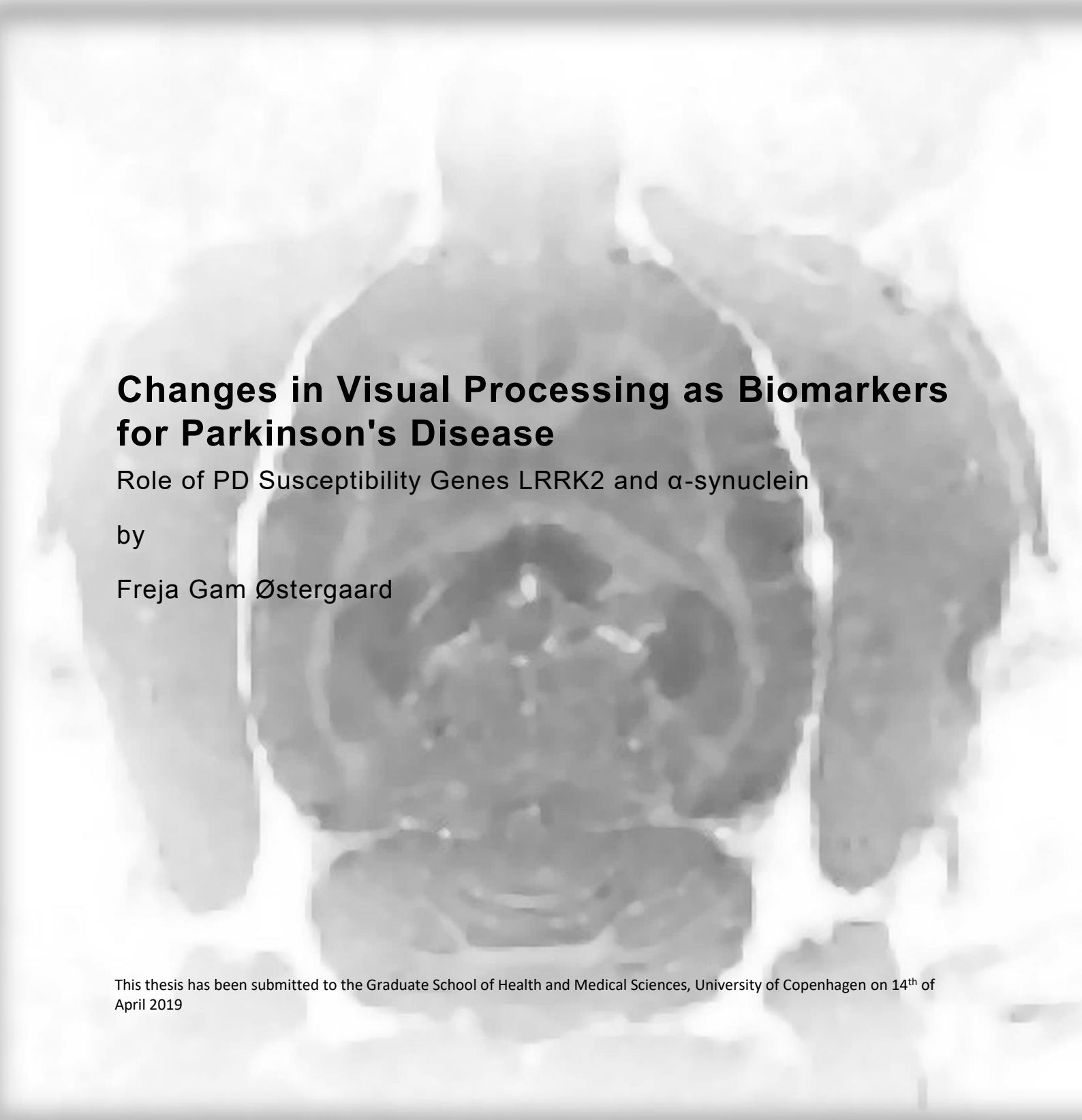

Changes in Visual Processing as Biomarkers for Parkinson's Disease

Role of PD Susceptibility Genes LRRK2 and α-synuclein

by

Freja Gam Østergaard

This thesis has been submitted to the Graduate School of Health and Medical Sciences, University of Copenhagen on 14th of April 2019

Changes in Visual Processing as Biomarkers for Parkinson's Disease: Role of PD Susceptibility Genes LRRK2 and α-synuclein

PhD thesis
by
Freja Gam Østergaard, MSc.

Supervisors:
Hartwig Roman Siebner, Professor,
Danish Research Centre for Magnetic Resonance, Copenhagen University Hospital Hvidovre, Denmark

Kenneth Vielsted Christensen, PhD, Project Director,
Neuropsychiatry Center for Therapeutic Innovation, Institut de Recherches Servier, France

Alex R. Wade, Professor,
Department of Psychology, University of York, United Kingdom

Bettina Laursen, PhD, Research Scientist,
Translational Biology, H. Lundbeck A/S, Denmark

Tim Bjørn Dyrby, Associated Professor,
Danish Research Centre for Magnetic Resonance, Copenhagen University Hospital Hvidovre, Denmark

This project has received funding from the European Union's Horizon 2020 research and innovation programme under the Marie Sklodowska-Curie grant agreement No 641805

UNIVERSITY of York

DANISH RESEARCH CENTRE FOR MAGNETIC RESONANCE

Preface

This thesis is the result of three years of PhD fellowship. The work was a collaboration between Lundbeck, the Danish Research Centre for Magnetic Resonance (DRCMR) and the University of York. The primary funding source was the European Union's Horizon 2020 research and innovation programme under the Marie Skłodowska-Curie grant agreement No 641805. This was a grant given to the training the next generation of European visual neuroscientist (NextGenVis). Supplementary funding was provided by Lundbeck.
The focus of the project was to investigate the potential of using changes in visual processing as biomarkers for the progression of Parkinson's disease.
The project was carried out in the period from March 2016 to April 2019.

This thesis is a synopsis based on three manuscripts and a study report:

I- Progressive effects of sildenafil on visual processing in rats

Freja Gam Østergaard, Alex R. Wade, Hartwig Roman Siebner, Kenneth Vielsted Christensen & Bettina Laursen

II- A visual assay for detection of α-synuclein-related pathology in a rat model of Parkinson's Disease

Freja Gam Østergaard, Bettina Laursen, Marc M. Himmelberg, Hartwig R. Siebner, Alex R. Wade, & Kenneth Vielsted Christensen

III- Mapping visual processing with functional MRI in a rodent model of α-synuclein overexpression

Freja Gam Østergaard, Christian Skoven, Alex R. Wade, Hartwig R. Siebner, Bettina Laursen, Kenneth Vielsted Christensen & Tim B. Dyrby

Study report- Electrophysiological investigation of the role of LRRK2 in visual processing of rats

Acknowledgements

Most of the work was carried out on the Valby site of H. Lundbeck A/S under the supervision of Bettina Laursen and Kenneth Vielsted Christensen. The MR scans were carried out at Hvidovre Hospital at the Danish Research Center for Magnetic Resonance (DRCMR) under the supervision of Tim Dyrby. I would like to thank Sascha Gude for her invaluable help with venflons and preparing animals for scanning, and Yi He for sparring about stimulus paradigm and live visualization of fMRI. A great thanks to my fellow sufferer at the DRCMR, Christian Skoven for designing the anaesthetic paradigm and helping out at scans.
The analysis of the fMRI data was carried out using the pipeline from the University of York under the supervision of Alex Wade, and kindly guided by Milena Kaestner.
Analysis and especially statistical analysis can be a tough job therefore I would like to thank Lars Arvastson for statistical guidance.
Pia and Kirsten provided indispensable help with histology for which I am grateful.

I would like to thank the NextGenVis network for being an international support group to air and discuss frustrations.
Last, but not least, I would like to thank my former office-mates Christian and Sara for their support and advice throughout the project, and off course for the cake and coffee breaks.

Contents

1 Summaries

1.1 Dansk

Parkinsons sygdom (PD) er en almindelig neurodegenerativ sygdom der rammer den ældre del af befolkningen. Der er en generel mangel på behandlinger, der kan ændre eller stoppe sygdomsforløbet. For at udvikle nye behandlinger er det nødvendigt at karakterisere biomarkører, der er brugbare til at stille diagnosen tidligere. For indeværende er der ingen godkendte biomarkøre til sygdomsmodificerende behandlinger i PD. Forskning peger på at der er visuelle ændringer i PD. Disse blev først opdaget ved måling af 'visuelle fremkaldte potentialer' (VEP). Siden da har det vist sig, at PD-patienter har et signifikant forsinket VEP, og desuden er kontrastfølsomhed reduceret.

I dette projekt var der fokus på at validere ændringer i synsbanerne i gnavermodeller af PD svarende til dem, der observeres i hvirvelløse modeller, dette kan resultere i en biomarkør for PD, der er pålidelig på tværs af arter.

Først etableredes et VEP-system der kunne måle på gnavere. Dette indebar en undersøgelse af, hvordan synsbanerne kunne påvirkes farmakologisk. Dernæst blev gnavermodeller af PD karakteriseret i VEP-systemet. Fokus var på, hvordan α-synuclein i de basale ganglier påvirker synsbanerne, og om modulering af sygdomsbiologier som LRRK2 og α-synuclein kunne forbedre disse ændringer.

Det var muligt at etablere et VEP-system til måling af synsbanerne i vågne gnavere. Undersøgelsen af AAV-α-synuclein-modellen viste, at vi kunne detektere ændringer i VEP induceret ved overudtrykket af α-synuclein. Den viste yderligere, at en 'support vector machine' var følsom nok til at detektere disse ændringer tidligt i forløbet og derved kunne klassificere individer i den korrekte sygdomsgruppe. En fMRI-undersøgelse viste, at synsbanerne kunne afbildes, men det var ikke muligt at måle ændringer fremkaldt ved overudtrykket af α-synuclein.

Undersøgelse af LRRK2-KO-modellen viste, at LRRK2 spiller en rolle i farvesyn svarende til det, der er blevet rapporteret både hos mennesker og bananfluer. Yderligere blev det bekræftet, at LRRK2 har forskellige roller i hjernebarken og subkortikale strukturer.

Samlet set peger resultaterne på, at synsbanerne er påvirket i prækliniske modeller af PD, hvilket gør synsbanerne til en funktionel biomarkør, der kan drages nytte af i udviklingen af nye behandlinger af PD.

1.2 English

Parkinson's disease (PD) is the second most common neurodegenerative disorder with a prevalence of 0.5% of the entire population. There is a huge unmet need for treatments that alter the progression or even modifies the disease. Biomarkers suitable for early diagnosis and useful to monitor disease progression are the cornerstone of the development of such disease-modifying treatments for PD, and at this stage no regulatory approved biomarker for disease-modifying treatments in PD is available. Evidence for visual deficits in PD was first obtained using measurements of visual evoked potentials (VEP). Since then it has been shown that PD patients have significant delayed VEP and reduced contrast sensitivity.

In this project the focus was to validate changes in visual processing in rodent models of PD similar to those observed in invertebrate models leading to a reliable, cross-species biomarker for the presence of PD.

Firstly, a VEP assay in rodents was established. Included was an assessment of how a visual processing can be modulated pharmacologically. Secondly, rodent models of PD were characterized in the established visual assay. Here, focus was how α-synuclein pathology in the basal ganglia affects the visual system and whether modulation of disease biologies such as the LRRK2 and the α-synuclein could alleviate visual system deficits.

It was possible to establish a VEP assay for measuring visual processing in awake and freely-moving rodents. Studying the AAV-model in this assay showed that VEP could detect changes in the VEP induced by overexpressing α-synuclein it further showed that a support vector machine was sensitive enough to detect these changes early and could accurately classify rats into the correct disease group. Using fMRI to detect changes of the visual system showed that the visual system could be imaged, but it was not possible to detect changes induced by overexpressing α-synuclein.

Investigating the LRRK2-KO model suggested that LRRK2 plays a role in colour vision similar to what has been shown in both humans and fruit flies. Further LRRK2 was confirmed to have differential roles in cortex and subcortical structures.

Collectively, these results point to the visual system being affected in preclinical models of PD making it a functional biomarker useful in the development of new therapeutics for PD.

2 Abbreviations

AAV- adeno-associated virus
BG – Basal ganglia
BOLD – blood oxygen level dependent
bp - basepair
COPE – contrast of parameter estimate
COR – C-terminal of ROC
dLGN - dorsolateral geniculate nucleus
EEG - electroencephalography
EPI – echo planar image
ERG - electroretinogram
ERP – event-related potential
Feat – FSL expert analysis tool
fMRI – functional magnetic resonance imaging
FSL- FMRIB software library
GABA - γ-aminobutyric acid
GLM – general linear model
GP - Globus pallidus
HE - hematoxylin-eosin
KO – knock-out
LB – Lewy bodies
LE – Long-evans
LRRK2 – Leucine rich repeat kinase 2
MAPKKK - mitogen-activated protein kinase kinase kinase
MRI – magnetic resonnance imaging
MSN – medium spiny neurons
NAC – non-amyloidogenic core
PD – Parkinson's disease
PDE6 – Phosphodiesterase 6
RF – radio frequency
RGC – Retinal ganglion cell
ROC - Ras of complex
ROI – Region of interest
ROS – reactive oxygen species
rsMRI – resting-state MRI
SC – superior colliculus
SD – Sprague-dawley
SN – substantia nigra
SNc – substantia nigra pars compacta
SNr – substantia nigra pars reticulata
SNR – signal-to-noise ratio
SSVEP – steady-state VEP
STN - subthalamic nucleus
SVM – Support vector machine
SWB – Short-wave blue
TE – Echo time
TH – tyrosine hydroxylase
TR – repetition time
VC – visual cortex
VEP – visual evoked potential
Voxel – volume pixel
WT – wildtype

3 Introduction

Parkinson's disease is diagnosed late in the progression of the disease. Biomarkers suitable for early diagnosis and monitoring the disease are crucial for the development of disease preventing therapies.

In this chapter Parkinson's disease will be introduced, along with a detailed description of the susceptibility genes relevant for the project. Further, the visual system of rodents and humans will be presented in parallel. The last two sections are dedicated to introducing the methods of electrophysiology and magnetic resonance imaging.

3.1 Parkinson's Disease

Parkinson's disease (PD) is the second most common neurodegenerative disorder affecting 0.5% of people worldwide [1]. One of the first thorough descriptions of the disease was published in 1817 by James Parkinson in 'an essay on the shaking palsy'. In this early scientific essay the disease is described to be 'extremely slow in its progress' [2]. Parkinson further noticed that this slowness obscured the commencement of the disease. Since then the relative contributions of genetics and environment have been speculated. In 1996, a hereditary cause of PD was reported for the first time [3] since then, several other genes have been discovered [4]. These underlying genetic factors have been shown to cause the 'beginning' of the disease to be decades before the occurrence of the motor symptoms [5], that typically bring patients to the clinic. The cardinal symptoms of PD are progressive development of bradykinesia, akinesia, rigidity, tremor, and postural instability. These symptoms are caused by the loss of dopaminergic neurons in the substantia nigra pars compacta (SNc). Hence, standard therapy for PD builds on replacing the neurotransmitter dopamine, by administration of levodopa or dopamine agonists [6]. At later stages of the disease, deep brain stimulation can be applied to electrically compensate for the dopamine dysfunction [7]. Both treatment strategies aim at alleviating symptoms, but neither halt nor slow the progression of the disease.

PD is also associated with a wide range of non-motor symptoms, which adversely impact on the patients' quality of life and may precede the emergence of motor symptoms for years [8]. Non-motor symptoms comprise sleep-disturbances [9], constipation [2], [10], depression [11], anosmia and visual processing disorders [12], [13]. It should be noted that not all of these symptoms involve dopamine [14]. The prodromal phase of PD is gaining interest as it may provide an opportunity for early diagnosis [11]. So far research in early diagnosis and neuroprotective therapies have been unsuccessful [15], one challenge comes from the early symptoms not being specific to PD nor

sensitive enough to provide accurate measures of the disease progression [11]. Hence improving knowledge of the prodromal phase of PD may facilitate the development of new neuroprotective therapeutics that will slow or halt the progression of the disease [16].

3.2 Basal Ganglia

The basal ganglia (BG) is a system of deep grey matter nuclei, that receive input from the entire cortex and play a pivotal role in diverse functions such as: voluntary movement, learning of habits, evaluation of time, and action evaluation [17]. As BG has a prominent role in action control, disintegration of neural processing in these nuclei leads to movement disorders such as tremor, ballism, chorea, and dystonia [18].

The BG is located in the midbrain, central to the fornix in both hemispheres. This system is well conserved among vertebrae [19]. It consists of the globus pallidus, striatum, subthalamic nucleus, and the substantia nigra. These nuclei are anatomically and functionally linked in separate circuits [20], [21]. The rate model of the BG is a simplified but useful model describing the functional circuitry of the basal ganglia (shown in Figure 1A). In this model, the striatum is the primary input of the BG [19], [21], [22] it receives input from all over the cortex. The subthalamic nucleus (STN), which is gaining interest as an input structure, receives cortical input from the frontal areas of the cortex via the so-called hyper-direct pathway [22].

The striatum consists of three parts: the caudate nucleus, nucleus accumbens and the putamen. The primary projection neurons from the striatum are GABAergic medium spiny neurons (MSN) which are targeted by nigrostriatal dopaminergic neurons. They are divided into two types based on the neuroproteins and type of dopamine receptor they express. One type of MSNs is enkephalin-positive and expresses D_2-receptors, they are inhibited by dopamine. The other type is substance P-positive, express D_1-receptors, and are excited by dopamine [20], [21]. Both types of MSNs project to each their part of the globus pallidus (GP). This division has given rise to the direct and the indirect pathways of the BG, referring to the path from the striatum to the output structures: internal segment of globus pallidus (GPi), and the substantia nigra pars reticulata (SNr).

The two pathways have opposing effects on the output structures. In the direct path the striatum inhibits the output structures. In the indirect path the striatal MSN inhibits the external segment of the GP, disinhibiting the STN, causing excitation of the output structures.

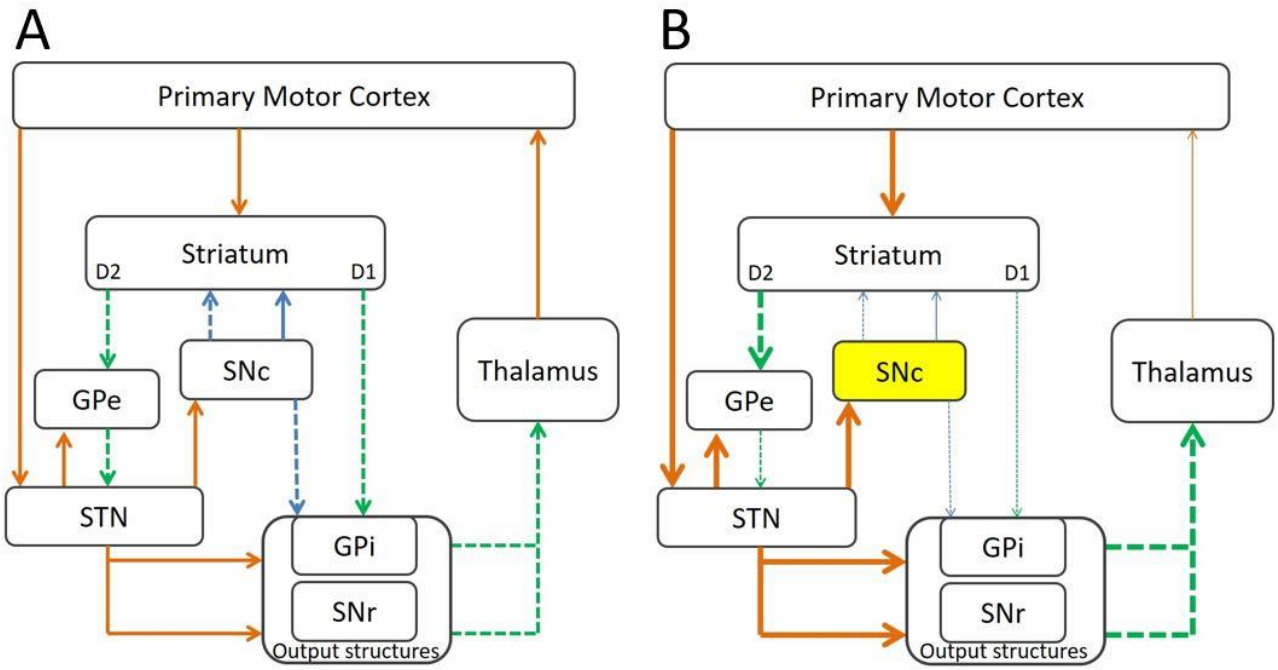

Figure 1 Schematic drawing of the canonical circuits of the basal ganglia. A) normal function B) Parkinson's disease. The direct pathway is the inhibitory connection from the striatum to the output structures. The indirect pathway is the inhibitory connection from striatum to the GPe, which inhibits the STN. The STN excites the output structures. orange=glutamatergic, green=GABAergic, blue= dopaminergic. Dashed arrows are inhibitory, unbroken are excitatory. The weight of the arrows indicates the activation in those projections. GPe, Globus pallidus external segment; GPi, Globus pallidus internal segment; SNc, substantia nigra pars compacta; SNr, substantia nigra pars reticulata; STN, subthalamic nucleus.

The SNr consists primarily of GABAergic neurons [23], along with the GPi it projects primarily to the thalamus, but also to the superior colliculus (section 3.5.3). The SNc consist of dopaminergic neurons, exhibiting natural pacemaker activity [24] and is responsible for motor initiation. The SNc can be inhibited by the thalamus and the superior colliculus [25]. The cardinal symptoms of Parkinson's disease emerge because of a progressive nigrostriatal denervation of the BG [20]. It has been hypothesized that the projections from the SNc to the putamen degenerate before the nigral projections to the other parts of the striatum [22].

The D_2-receptors are under normal circumstances inhibited by the dopaminergic signalling from the SNc, depletion of this signal will lead to overinhibition of the GPe and disinhibition of the STN causing hyperactivity in the parkinsonian state (Figure 1B). In turn, leading to overinhibition of the thalamus, making the circuit for motor initiation work like a car with a stuck brake.

3.3 Braak's Staging Hypothesis

The pathogenesis of PD is incompletely understood. A prevailing theory was proposed two decades ago by Braak, on the basis of histological staining of protein aggregates in post-mortem brains of PD patients. Aggregates seemed to spread in a stereotypic pattern; showing if there were aggregates in the cortex there would also be aggregates in the brainstem, while the reverse was not true (Figure 2). This sparked the hypothesis that these aggregates spread from the brainstem, moving out through the midbrain and into the cortex [26]. Later studies showed aggregates in the enteric nervous system connecting the gut with the central nervous system. This finding expanded the hypothesis of pathogenesis to start by an unknown pathogen entering via the gut, initiating the aggregation process, that would eventually reach the brain [27], [28]. It was further hypothesized, that these aggregates may be detectable or cause detectable symptoms early in the progression of the disease.

These aggregates are proteinaceous inclusions termed lewy bodies (LB) or lewy neurites. They consist of misfolded proteins such as parkin, neurofilament, and especially α-synuclein [29]. LBs are not specific for PD, but are also found in other neurodegenerative diseases such as Alzheimer's disease, multiple systems atrophy and dementia with lewy body pathology [30].

According to the staging hypothesis proposed by Braak, there are six stages of PD which can be defined as follows: at the first stage the LBs are largely confined in the medulla oblongata, and dorsal motor nucleus. In the second stage, the LBs are present in the coeruleus complex. In the third stage the midbrain is affected. In the fourth stage, the first pathology is detectable in the mesocortex. In stage five, the pathology has spread to the neocortex. In the sixth stage, LBs are present in the premotor areas, the primary sensory and motor areas [26].

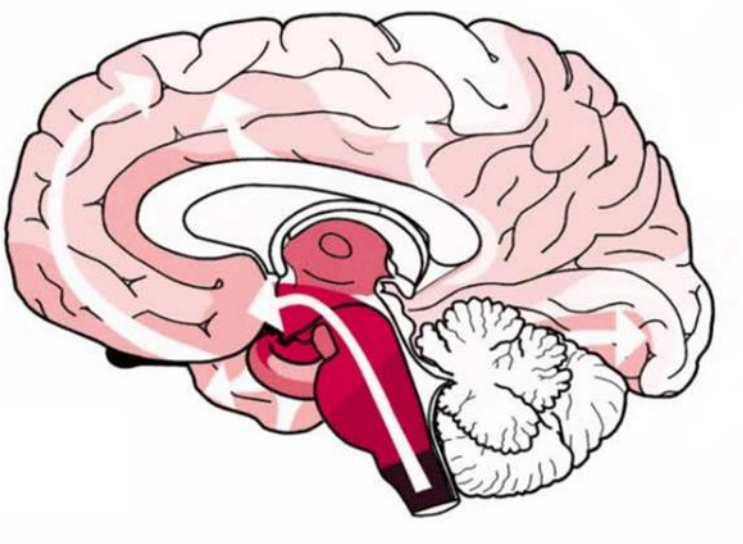

Figure 2 Illustration of Braak staging. The gradual change in shading intensity represents the spreading of protein aggregates in the direction of the white arrows. Reprinted from [26] with permission.

The mechanisms for the propagation of LB pathology are still under investigation, but it has been hypothesized that these aggregates can spread from cell-to-cell and induce conditions favourable for the formation of more aggregates similar to what is seen in prion disease [31], [32]. Braak's staging hypothesis has gained interest, but it is still controversial: Surmeier et al. argues that, in spite of LBs being considered a defining feature of PD, they are not predictive of disease severity or even present in all cases of PD [33]. George et al. presented the counter argument that LBs are considered the defining feature while the phenotype may be caused by smaller protein aggregates that are not taken into consideration [32]. Surmeier et al. further noticed that the LBs are not equally present in all types of neurons and pointed out that they have yet to be reported in GABAergic neurons. Collectively, this suggests that Braak's hypothesis is not exhaustive, but a contributing factor in the pathogenesis of PD [30].

3.4 Susceptibility Genes

Parkinson's disease is primarily sporadic (~90%), but there are familial cases linked to genes first referred to as PARK 1-23 [4], [34] (see S 1). As more research emerged on the subject, the genes and their gene products were identified, and assigned more descriptive names, such as *SNCA* (α-synuclein) or *LRRK2* (leucine rich repeat kinase 2). Seven of the PARK genes are linked to monogenic PD [4], [35]. The autosomal dominantly inherited forms of PD have been robustly associated with *SNCA*, *LRRK2, EIFAG1* and *VPS35*. While *parkin, PINK1* and *DJ-1* have an autosomal recessive inheritance pattern [35]. These genes have also been linked to increased risks

of sporadic PD, but mutations are rare. Many of the genes related to PD are associated with lysosomal degradation and autophagy leading some to speculate that PD is caused by a failure in damage response [34].

3.4.1 α-synuclein

α-synuclein is a small protein, abundantly expressed in the brain, but also expressed in other tissues [36], [37]. In the brain, it is primarily located around the presynaptic terminals of neurons [38]. The gene coding for this protein was formerly known as *PARK1* and *PARK4* [4], but is now named *SNCA* and is highly conserved among vertebrae. The gene consists of six exons and span about 117kb [39]. The protein product contains an amino-terminal lipid binding α-helix, a non-amyloidogenic core (NAC) domain and an unstructured carboxy-terminus [40].

α-synuclein is natively unfolded as a soluble monomer in the cytosol, but changes to α-helical conformation when bound to a lipid membrane [41], [42]. The cellular function is largely unclear, but has been related to vesicle-membrane association and it is thought to play a role in endocytosis, vesicle recycling [43] and neurotransmitter release [44].

Aggregation of this protein have been associated with prodromal PD, therefore it is considered to have potential as a biomarker [45]. The presence of the protein in peripheral tissues and body fluid makes it convenient as a biomarker [45][46].

3.4.1.1 Pathological α-synuclein

α-synuclein is a major constituent of LBs. Several missense mutations in the *SNCA* gene as well as duplication and triplication of the gene have been associated with familial PD [47]–[49]. Collectively this leads to misfolding and overexpression, causing the protein to aggregate into LBs [29]. When misfolded the NAC domain has changed conformation from α-coil to β-sheets [44]. This domain is considered to be necessary for the aggregation of α-synuclein [42] in to oligomers and fibrils. The fibrillar type is both a 'precursor' of LBs and they seem more prone to spread compared to other types of aggregates. Rey et al. have found that α-synuclein fibrils introduced in the olfactory bulb can spread throughout the brain [50].

A wide range of physiological factors have been shown to affect the aggregation of α-synuclein. These include posttranslational modifications, physiological stress and neuroinflammation. Most of the 140 residues of α-synuclein can undergo post-translational modifications [44] influencing aggregation and toxicity [40]. LBs have been reported to contain large quantities of nitrated α-synuclein [51]. This has been proposed to be a result of a reaction with reactive nitrogen species, rather than a cause of aggregation, as nitration of α-synuclein have been shown to inhibit fibril

formation [52]. Further phosphorylation of serine 129 seems to increase toxicity while enhancing phosphatase level seemed to be protective against α-synuclein induced toxicity [53]. The influence of the these post-translational modification is ambiguous and it is not yet known which arise as a function of pathology, and which are physiologically relevant [44].

Oxidative stress may induce the aggregation of α-synuclein, which in turn increases oxidative stress, thereby amplifying its own aggregation. It has been shown in primary cortical neurons that an overexpression of α-synuclein increases mitochondrial production of reactive oxygen species (ROS) [54]. Along with oxidative stress, iron metabolism and especially the presence of ferric iron (Fe^{+3}) can contribute to the oligomerization of α-synuclein [55]. Overaccumulation of α-synuclein in cultured cells have shown to spark a cell death cascade, dependent on ROS and endogenous dopamine production [56], [57]. This correlation of neurotoxic effect of α-synuclein aggregates and endogenous dopamine [58], may be the reason for the selective loss of dopaminergic cells in PD. The aggregation of α-synuclein has also been reported to interact with microglia, initiating neuroinflammation which may also induce the cell death cascade. Taken together there are a plethora of ways in which α-synuclein aggregation can cause neurodegeneration, whether some of these factors are more important than others remain to be elucidated. Further, the excitability of α-synuclein overexpressing neurons is diminished [54]. This causes dysfunction of the neuronal network independent of neurodegeneration, and primarily in aging neurons.

Along with changes in synaptic functioning, α-synuclein has been shown to play a role in regulating excitotoxicity, by selectively regulating the fusion pore [59]. The aggregation of α-synuclein is more often resulting in cell deaths compared to overexpression of other proteins such as the green fluorescent protein (GFP) [54], [60].

3.4.1.2 Animal Models of Pathological α-synuclein and PD

Several transgenic mouse lines modelling α-synuclein overexpression have been developed, these have proven useful in studying the α-synuclein biology, though the endogenous expression pattern has not been similar to that of PD patients [61]. However, transgenic models usually fail to show a progressive phenotype, and the phenotype may be caused by differential function of the protein in the developmental stages (neurogenesis). An alternative is to use viral overexpression of α-synuclein, in which a virus expressing a variant of α-synuclein is injected directly into the nigrostriatal system of rodents. This overexpression develops over several weeks, and may be a better model of the progressive nature of PD. Adeno-associated virus (AAV) have been widely used to express PD-relevant forms of α-synuclein [62]–[64]. Overexpression of human α-synuclein in the nigrostriatal system of rats, causes a progressive loss of dopaminergic fibres in the striatum

and of cells in the SNc. This loss causes significant changes in motor activity [64]. Further, there are functional changes related to firing pattern of the affected neurons [65]. The spreading pattern in these models vary with the serotype of the AAV and possibly the version of α-synuclein as mutated types have been shown to be more prone to formation of exogenous α-synuclein [60] than wildtype. Similar observations of spreading are present in models where fibrils are injected either in the SNc or the olfactory bulb [50].

Lesion models are commonly used to model PD. In the 6-OHDA model, 6-OHDA selectively targets the dopaminergic system. This model have had great value for investigating the consequences of loss of dopamine [66]. However, the mechanism of cell death may not be similar to that of clinical PD [61].

A caveat with preclinical models is that they often model one very specific mechanistic feature of the disease and often use young animals. The perfect model would display age-related degeneration of the SNc and motor symptoms such as tremor [67]. The genetic models here have construct validity because they are based on underlying genetic mechanisms of Parkinson's disease, but they have little face validity. Where lesion models may display more face validity, but rarely display the progressive nature of the disease [22]. Neuroprotective strategies effective in lesion models may not translate into the human condition, where strategies based on the underlying genetic profile may be more relevant [61]. In this thesis the AAV-mediated overexpression of α-synuclein is used to model the early phase of PD.

3.4.2 Leucine-Rich Repeat Kinase

Mutations in the *LRRK2* gene accounts for up to 6% of inherited PD cases and 1-2% of sporadic PD patients [68], [69]. LRRK2 is a large protein with diverse functions, it is highly expressed in the kidneys, lungs and other peripheral tissues [70]. Though, it is not specific to neurons, it plays an important role in neuronal development [71]. In adult subjects it has been localized to the presynapses of neurons in the cortex and the striatum of rodents [72] and in cortical neurons of humans [73].

The gene *LRRK2* consists of 51 exons spanning 144 kb [74]. This multi-domain protein consists of: leucine-rich repeat (LRR), Ras-of complex (Roc), C-terminal of Roc (COR), a mitogen-activated protein kinase kinase kinase (MAPKKK) and a C-terminal WD40 repeat domain.

It possesses mixed-linage kinase activity, the cellular function is still poorly understood, but it has been shown to support intracellular trafficking [75] by phosphorylating Rab GTPases [76], rearrange the cytoskeleton [71], [77], involved in lysosomes [77], [78], autophagosomes [79], and

overexpression of LRRK2 have been shown to cause changes the structure of the Golgi apparatus [56], [80].

LRRK2 can undergo post-translational modifications such as phosphorylation including autophosphorylation of serine and threonine. Phosphorylation of the serine cluster located just upstream of the LRR domain [81] is associated with target-engagement. Phosphorylation of ser935 precedes dimerization and translocation [82]. Decline in the phosphorylation status of LRRK2 in the SNc have been associated to PD [73].

3.4.2.1 Pathological LRRK2

Missense mutations in LRRK2 are among the common causes for autosomal-dominantly inherited PD. These mutations are primarily located in the Roc-COR and kinase domains [75], [83]. Often these mutations are gain-of-function mutations and have been shown to increase the phosphorylation of specific Rab proteins or disrupt binding of 14-3-3, which LRRK2 binds when inactive, causing increased LRRK2 activity [84]–[87]. Apart from increased kinase activity, LRRK2's effect on the Golgi apparatus seems to increase oxidative stress. Interactions between oxidative stress and mutated LRRK2 have been shown to increase cell death in primary cultures [83].

LRRK2 has been suggested to play a role in the spreading pathology of α-synuclein [56], [78] and LRRK2 overexpression seems to promote the accumulation of α-synuclein [56] possibly because of impaired lysosomal function, leading to a decrease in clearance of insoluble protein aggregates [78]. The general idea is that LRRK2 regulates the mechanism α-synuclein uses to spread between neurons, as increased LRRK2 kinase activity enhances α-synuclein-induced neurodegeneration, and inhibition has shown to be neuroprotective in viral models of α-synuclein pathology [88], [89]. A polymorphism in *SNCA* have shown to decrease the age of onset *G2019S*-LRRK2 PD [90] this interplay may be a two-way. Collectively this suggests that inhibition of LRRK2 could be a potential therapeutic for α-synuclein pathology.

3.4.2.2 LRRK2 Kinase Inhibition and a Knock-out Model

There has been quite a development in tool compounds inhibiting the kinase activity of LRRK2 [91][92]. These have been tested in various rodent models, and chronic treatment have shown to rescue α-synuclein induced changes [65].

To test the safety of LRRK2 kinase inhibition [70] a model of LRRK2 knock out, has been produced by a 10 bp deletion in exon 30, located upstream of Roc, COR and kinase domain. These rats develop normally, but a consistent adverse effects of both pharmacological inhibition, as well

as knock-out models are the cellular changes of especially the kidneys [93], [94] and lungs [70], [94]. Visual processing in this model is investigated in the **study report**.

3.5 Visual System

The canonical path of vision starts with a photon being received by rhodopsin in the outer segment of photoreceptors in the back of the eye. This initiates the cascade of phototransduction, where this one photon is translated to an electrochemical signal in the brain. A process which is well-conserved in vertebrae. In humans 90 % of the fibres from the retina pass through the chiasm and synapse in the dorsolateral geniculate nucleus of the thalamus (dLGN), before reaching the visual cortex. A second pathway projects to the superior colliculus. A third pathway extends to the pretectal area of the midbrain [95]. In the rodent the pathways are the same, but the distribution of retinal fibres differs, as more than 90 % of retinal fibres project directly to the superior colliculus, but a subset of these fibres branch and project to the dLGN, which projects to the visual cortex.

Parkinson's disease is not known for causing visual system defects. Visual symptoms due to PD may be obscured by other age-related conditions as the typical patient belong to an older segment of the population and normal aging, causes a wide range of visual defects [96]. Yet some changes in the visual system seem more common in PD, in particular contrast insensitivity, colour discrimination and visuospatial deficits [97]–[103]. Differences of electrophysiology of the visual system will be presented in section 3.6.

3.5.1 Retina

The mammalian retina is very well conserved. It consists of six layers (Figure 3A): photoreceptor layer (contains the outer segments of the photoreceptors), outer nuclear layer (cell bodies of the photoreceptors), outer plexiform layer, inner nuclear layer (bipolar cells, amacrine cells, and horizontal cells), inner plexiform layer, and nerve fibre layer (retinal ganglion cells).
Phototransduction starts with rhodopsin being excited by a photon in the photoreceptors. This starts a PDE6-dependent mechanism hyperpolarizing the cell and initiating a graded potential [104]. The photoreceptors are divided into two types: cones and rods. Cones are responsible for colour vision. Rod are primarily considered to provide information about luminance levels. The photoreceptors release glutamate to the connecting bipolar cells when light is decreased. The bipolar exists in two types ON and OFF types named after their response to light, these project to the retinal ganglion cells. The axons of the retinal ganglion cells make up the optic nerve. This three neuron chain seems simple, but the mammalian retina have been proposed to contain more

than 60 different types of neurons [105], [106], giving rise to several parallel channels for detecting low-level visual features such as luminance, wavelength, contrast and direction. In addition to these three cells types there are also horizontal cells and amacrine cells.

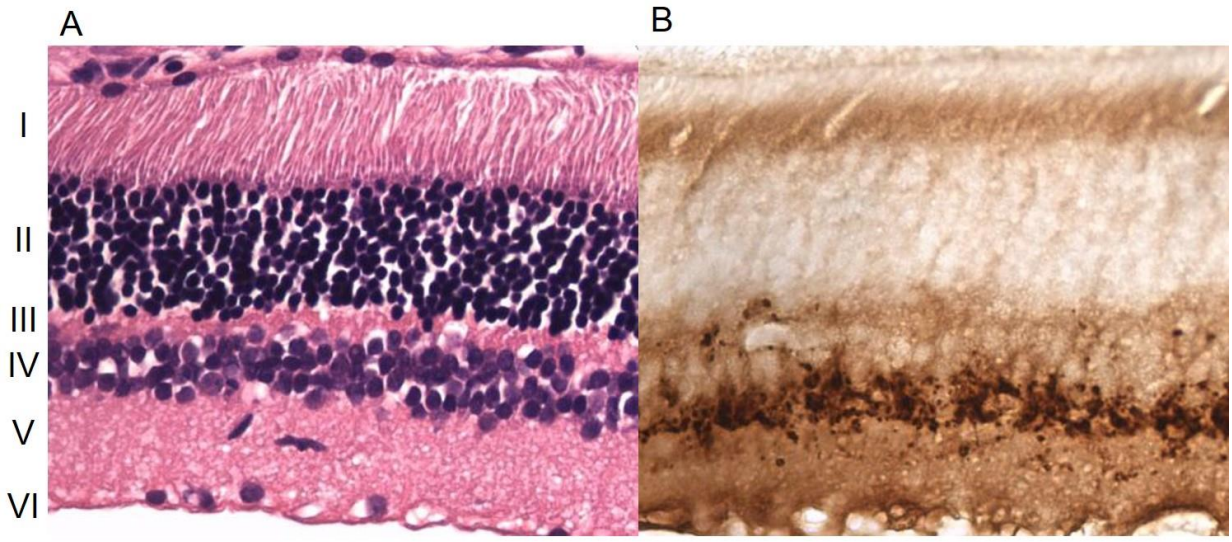

Figure 3 Transversal section of retina from an SD rat. The top of the image is towards the back of the eye: Layer I contains the outer segments of the photoreceptors, layer II is the outer nuclear layer, layer III is the outer plexiform layer, layer IV is the inner nuclear layer, layer V is the inner plexiform layer and the layer VI is the nerve fibre layer. The bottom is towards the vitreous. A) hematoxylin-eosin (HE) staining of a piece of retina. The HE stain, stains nuclei purple making the three nuclear layers distinguishable from the interplexiform layers. B) Tyrosine hydroxylase (TH) stain of a piece of retina. TH is the delimiting enzyme in dopamine production. The stain shows the amacrine cells and their processes reaching out into the other layers. Magnification is 40x.

The amacrine cells of mammalian retina are related to a plethora of functions in visual processing [107] most of them contain GABA or glycine, but a subset are dopaminergic (Figure 3B). They have been implicated in vision at high luminance levels as well as contrast sensitivity [108]. Dopamine affects the amacrine cells and uncouples the rod pathway from the cone pathway in bright light conditions leading to perception of sharper contrast. The release of dopamine is determined by rods [108], [109].

Early-stage PD patients are likely to report unspecific visual disturbances, probably due to dopamine deficiency in the retina. Post-mortem analysis of retinas from PD patients have found a reduction in dopaminergic cells [110]. The involvement of the dopaminergic system in these visual processing impairments of the retina is supported by studies showing that the contrast sensitivity improves when patients are treated with levodopa [98], [111]. Patients with idiopathic PD have shown thinning of the photoreceptor layer of the retina [112] . This could be related to susceptibility genes. PD-related mutations in LRRK2 in a *drosophila* model show considerable

changes in the visual response to flickering light, compared to wildtype flies [113]. Colour discrimination has also been linked to LRRK2 in human carriers of PD [114].

Colour discrimination is changed in PD, this may arise from deficits of the retina [115]. α-synuclein is naturally present in the retina, but aggregates have been shown to be present in PD patients [116]. Whether this is the underlying cause of dopaminergic deficiency in the retina remains elusive [117]. Further, a *Drosophila* model of PD showed that genes related to PD in combination with light stimuli causes retinal degeneration [118], this is consistent with the finding in five lesion models of PD using rats [119].

3.5.2 Visual Cortex

In the human visual chiasm 50% of retinal fibres cross over to the contralateral hemisphere and 50% continues to the ipsilateral the visual cortex is located in the cortex of the occipital lobe. Each side of this symmetric structure receives equal numbers of fibres from the ipsi- and contralateral eye. The primate visual cortex is divided into four primary parts (V1-4) with a hierarchical relation. The V1 receives input from the retina and relays for the V2 and V3, which in turn passes the signal further to the V4 and middle temporal cortex for higher level vision [95]. The V1 balances information from both eyes, giving rise to depth perception and contour integration.

Unlike humans, rodents have more than 97% (depending on the stock) of the retinal fibres cross over in the chiasm and synapse in the contralateral hemisphere [120]. Most of the visual nuclei receive direct input from the retina. Retino-recipient nuclei include: dLGN, superior colliculus (SC), pregeniculate nucleus, intergeniculate leaflet, pretectum, and pretectal nuclei [120]. The rodent visual cortex subdivided into multiple parts: V1, striate cortex, area 17, area V1. Hierarchy might not be as canonical in rats (rodents) as it is in primates [120]. The area 17 is considered to correspond to the human V1.

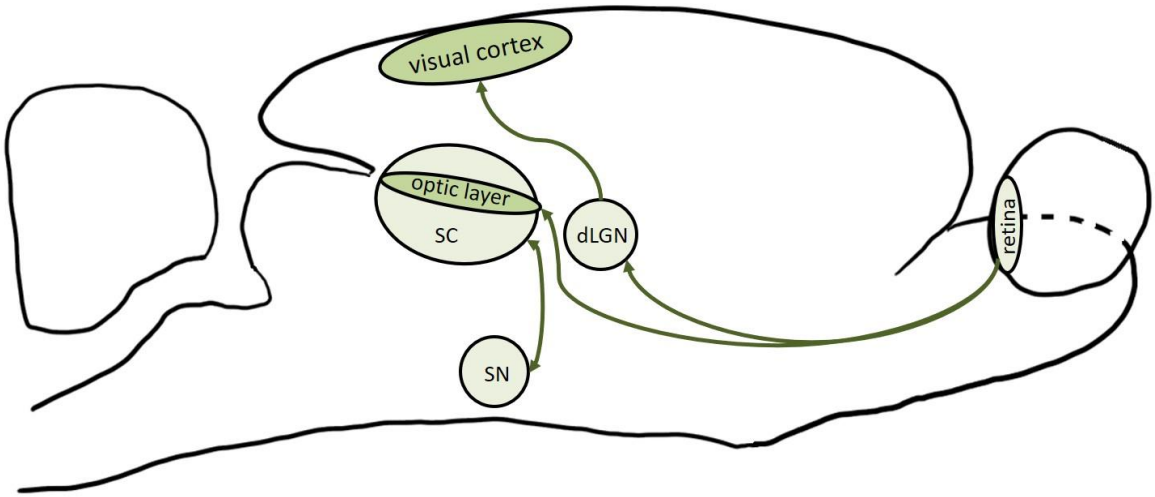

Figure 4 Simplified schematic drawing of the rodent visual system. From the retina >90 % of fibres go to the optic layer of the SC, a fraction of the fibres also supplies the dLGN with a retinal input. The visual cortex receives retinal input via the dLGN, and other less canonical structures. The SC and the SN are connected via GABAergic projections. dLGN: dorsolateral geniculate nucleus, SC: superior colliculus, SN: substantia nigra pars compacta and pars reticulate. From descriptions by [120]**.**

3.5.3 Superior Colliculus

In all mammals, the superior colliculus (SC) is a layered structure, commonly divided into the two parts a visuosensory part, and a motor part. Input to the superior colliculus is considered important for subconscious movements such as saccadic eye movements, and reorienting the organism to visual cues [121], [122]. In rodents, the SC is responsible for visual inputs to the basal ganglia (Figure 4) and receives a majority of the fibres from the retina [120]. The primary projections from the intermediate and deep tectal layers in the SC, to the BG extend via the STN [120], [123], [124]. However, there are GABAergic projections between the SNr and SC. The SC have been suggested to provide the SNc with a short-latency visual input, via dopaminergic neurons in order to make reward predictions [125]–[127]. In humans, the superior colliculus receives ~10 % of the projections from the retinal ganglion cells. This is relayed to the V2. The connection between the SC and BG is not well described, but there are suggestions of the projections between the striatum and visual cortex. In dementia with LBs and Parkinson's disease, LBs have been found in the SC. This finding has been associated to hallucinations in PD [128].

3.6 Electrophysiology

Electrophysiology describes the electrical activity of living organisms. Cells of the nervous system are traditionally considered to communicate via electrochemical discharges of neurotransmitter in

the synapse. This neurotransmitter causes a change in the potential of the post-synaptic neuron, lasting for tens of milliseconds [129], allowing for a summation of these post-synaptic potentials which will cause changes in the local field relative to a reference. When this change is measured on the scalp it is usually referred to as electroencephalography (EEG), and as local field potentials (LFPs) when measured in the brain [130]. In this thesis, we will focus on the event-related changes in LFPs, called event-related potentials (ERPs). This measures the change in electrical potentials to a specific event and is suggested to arise from a summation of postsynaptic potentials across local fields [131]. The exact mechanism which generates ERPs is not well known, but a popular theory describes the ERP being a result of oscillations changing phase [132], [133]. Cortical ERPs have been shown to arise from afferent activity of the pyramidal cells as local field potentials tends to have a strict phase relationship to cortical discharge [134].

The temporal resolution of the technique is in the order of milliseconds [131], but a disadvantage of the technique is that volume conductance blurs the source of the electrical activity even more so if the ERP is recorded on the surface of the skull (usual in humans). The spatial resolution of EEG is limited by the number and placement of electrodes.

3.6.1 Visual Evoked Potential

The visual evoked potential (VEP) is a variant of ERP, where the sensory event is visual, either a flash of light or a pattern presented on a screen. The VEPs are extracted from EEG traces by averaging over many, single trials [135]. The stimuli should be repeated at irregular intervals or at a frequency of ≤ 3 Hz, to make the response to the stimulus independent of any previous trials. The VEPs are used to quantify the functional integrity of the visual pathways, and gives an integrated view of neural activity and sensory processing [136], [137] both in the clinic and in animal research. Clinically, most often a pattern stimulus is used to detect abnormalities of the central visual pathways, but the flash VEP is useful to examine whether there is cortical response to the illumination of the retina, especially in difficult subjects or subjects with motor impairments [97]. The VEP is primarily sensitive to ‘robust’ changes of the integrity of the visual system. However, changes in VEPs are traditionally considered symptomatic, and not diagnostic [135].

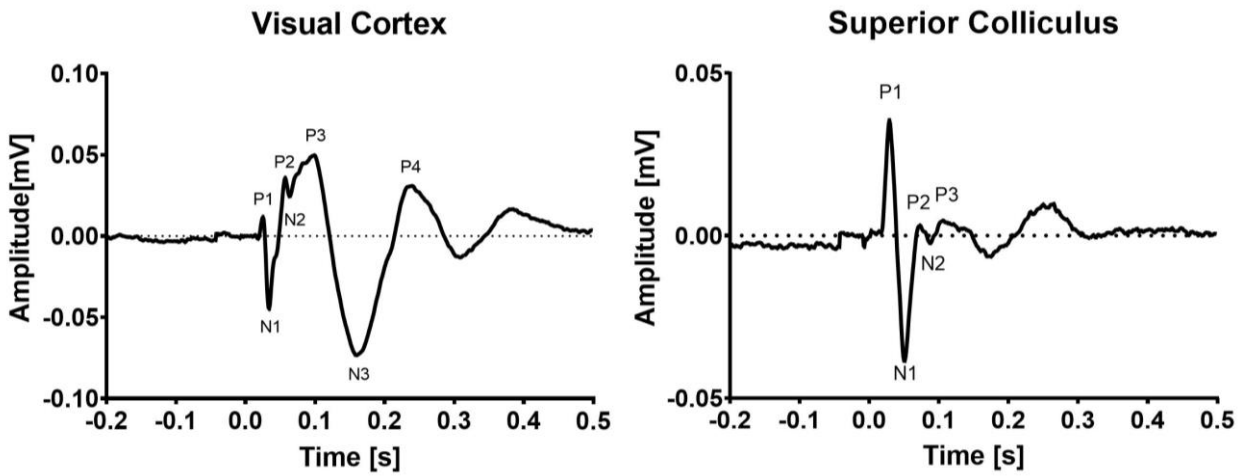

Figure 5 A VEP recorded from the visual cortex and superior colliculus of a rat. The stimulus was a 10 ms flash of white light, turning off at time 0. There is nothing special about the peaks, instead the waveform is considered an expression of the electrophysiological integrity of the visual system.

The VEP waveform (Figure 5) is quantified by measuring the amplitude and latency of each peak separately. The peaks are named so the first positive deflection of the waveform is referred to as P1, and the first negative deflection as N1. Naming of the peaks in the visual cortex of rodents is guided by [138], [139]. The peak designation may appear arbitrary, as the naming is unrelated to the underlying generator. Peaks with similar time domains, such as the P2-N2-P3 complex in visual cortex can on occasion obscure each other [131].

In rodents, the first peaks appear within 50ms after stimulus onset. These first peaks have been suggested to be principally affected by the transduction of the illumination information via the retino-geniculate fibres [135], [137] and might be of extrastriate origin [140]. Later peaks are more likely to have been influenced by higher visual areas and potentially consciousness.

In humans, VEPs are usually measured with extracranial electrodes placed on the scalp, causing a loss of information compared to intracranial measurements [130] therefore both the timing and the appearance of the peaks are different, but they are still measures of the postsynaptic potentials. However, the deeper structures such as the superior colliculus are rather hard to measure in humans.

VEPs have been investigated in relation to Parkinson's disease for more than four decades [97], [141]–[145]. One of the primary reasons for wanting to use this technique have been the non-invasiveness and independence of motor function [97]. Evidence for a functional abnormality of visual processing in PD was first obtained by measurements of the VEP showing delayed cortical latencies, an abnormality that was improved by dopamine replacement [97], [141], [146]. Several studies have shown delays in the peaks of the VEP waveform from the occipital lobe [12], [97],

[142], [144], [145], [147]–[149], but so far the efforts to correlate these changes with disease severity have been unsuccessful [150]. However, Miri et al. have suggested that combining VEP with measurements of contrast sensitivity and foveal thickness can give a more accurate diagnosis [142].

3.6.2 Steady-state Visual Evoked Potential

The steady-state VEP (SSVEP) is any case where the stimulation frequency is more than 3Hz [135], [151], and presented in regular intervals [131], [131], this causes the electrical activity to sum because the VEP to a single trial does not 'finish' before the next stimulation is presented. This shapes the EEG as smaller more uniform peaks, called a steady-state response or photic driving [152], [153]. This waveform should be constant in amplitude and phase over an infinitely long exposure to the flickering stimuli [154]. The generation of oscillations is not fully understood [155], but SSVEPs are considered to be very stable within subjects, because of more robustness against artefacts [135].

These oscillations are considered useful in discerning networks of the brain [151], [156], and have gained some attention in connection to brain computer interfaces as a mean to encode information [153]. SSVEPs have a solid mathematical basis [154], and waveforms should be analysed in the frequency domain instead of the time domain [157], yielding the amplitudes of the frequencies as the absolute number and the phase as a complex number. Analysis of the SSVEP yields three harmonics of the stimulation frequency. The first harmonic will have the same frequency as the stimulus, and have been hypothesised to come from photoreceptor activity where the second harmonic may reflect the activity of the ganglion cells [156]. The third harmonic is a result of nonlinearities in the visual system [113]. Another theory concerning the interpretation of the SSVEP is referred to as the superimposition theory, because it states that the amplitude and phase can be completely predicted by superimposing the VEP with the frequency of the stimulus presented [158]. A disadvantage of the SSVEP, it does not contain as precise temporal information as the ERP [131].

3.7 Magnetic Resonance Imaging

Magnetic resonance imaging (MRI) is a non-invasive imaging technique for visualizing anatomy and metabolism of tissues. It utilizes the natural nuclear spin of hydrogen atoms, to produce a spatial map of the proton density and physical properties of the tissue. An advantage of the technique is the excellent soft-tissue contrast even for incarcerated tissues such as the brain [159]. The signal strength depends on the density of protons, the strength of the magnet, and the induced

voltage. The signal comes from applying a radio frequency (RF) pulse, pushing the proton nuclei out of their equilibrium state. The frequency of the precessing back to equilibrium is measured with the receiver coils. The 3D image is a reconstruction based on frequency information from each volume pixel (voxel) [159].

This technique is used to image anatomy. In PD it has been used to look for structural biomarkers [160]. So far the thinning of the visual cortex [102], [161], and changes in the structure of the SNc [23], [162] have been reported in PD patients.

3.7.1 fMRI

To image the function of the brain a technique called blood-oxygenation level dependent functional MRI (BOLD-fMRI) can be applied. This technique utilizes the fact the magnetic moment for haemoglobin depends on the binding of oxygen. It images the ratio of oxygenated and deoxygenated blood within each voxel, by multiple, consecutive repetitions of the RF pulse changes in the neurons metabolic demand (neurovascular coupling) can be measured.

How the neurovascular coupling relates to spiking activity is not well understood [163], but have been hypothesised to correlate with changes in the frequency power of electrophysiological activity [164]. Unlike the EEG techniques the temporal resolution of fMRI is quite low, but the possibility of whole-brain imaging is an advantage of the technique [165].

3.7.1.1 fMRI of Rodent Models

The neurovascular coupling and the functional dynamics of the brain are expected to be similar between all animals (including humans) therefore fMRI is considered to translate well [165]. The biggest challenge of preclinical fMRI is that rodents have to be restrained mechanically or sedated by the use of anaesthetics and muscle relaxants [166]. Restraining in restrainment tubes requires the animal to be trained and causes considerable stress in the animal, though it has been argued to be more translationally relevant than anaesthetics [167]. Anaesthetics change the neuronal dynamics, thereby changing the basis for neurovascular coupling [167], [168].

Rodent models have the advantages of the ability to genetically engineer and pharmacological inventions compared to humans [165]. Further, they have been used in basic research of especially subcortical structures, as these can be difficult to measure in human subjects [169].

In Parkinson's models fMRI have been used to look for biomarkers because of the translational ease and it has been found that fMRI is sensitive enough to detect changes in the dopaminergic release of a rodent model overexpressing α-synuclein [170].

4 Objectives

The objective of the entire project is to gain translational knowledge on visual biomarker discoveries initially obtained in genetic models of PD. Initial data demonstrates profound visual contrast gain control abnormalities in invertebrate models of genetic forms of PD [113], [171]. Quantification of similar changes in neuronal function in rodent models of PD will be pursued using VEP and SSVEP. Ultimately, this could form the basis of a reliable, cross-species biomarker for the presence of PD.

4.1 Aims

4.1.1 Establishing a VEP assay

The first aim is to build a setup for measuring VEPs, and SSVEPs in awake and moving rats, further it is necessary to validate that the established assay measures visual activity. The assay will be tested with sildenafil and ketamine, to test the possibility of modulating the response measured using the assay, and how sensitive the assay is to different types of modulation.

4.1.2 Testing if visual processing is compromised in rodent models of PD

A link between PD susceptibility genes and functional changes of the visual system are investigated in two different models: a model of α-synuclein overexpression and a knock-out model of LRRK2. In the rat model of overexpression of human wild-type α-synuclein in the substantia nigra leads to progressive changes in motor function, dopamine homeostasis and basal ganglia function. The aim is to investigate if the progression can be monitored by using the established assay. Furthermore, the possibility to detect the overexpression of α-synuclein using fMRI will be studied.

As the results from *drosophila* suggests a direct link between the modulation of LRRK2 and changes in visual processing, a LRRK2-KO model is studied in the established assay.

4.1.3 Exploring if modulations of disease relevant biologies can alleviate the visual phenotype

The third aim is to test if the modulations of visual processing, possibly detected in the two PD models can be rescued by pharmacologically modulating LRRK2 kinase activity.

5 Materials and methods

This section aims at providing an overview of all the methods used in this project, including the methods described in the appended manuscripts and supplementary materials.
During this project, six cohorts of animals were used in a wide range of studies Figure 6.

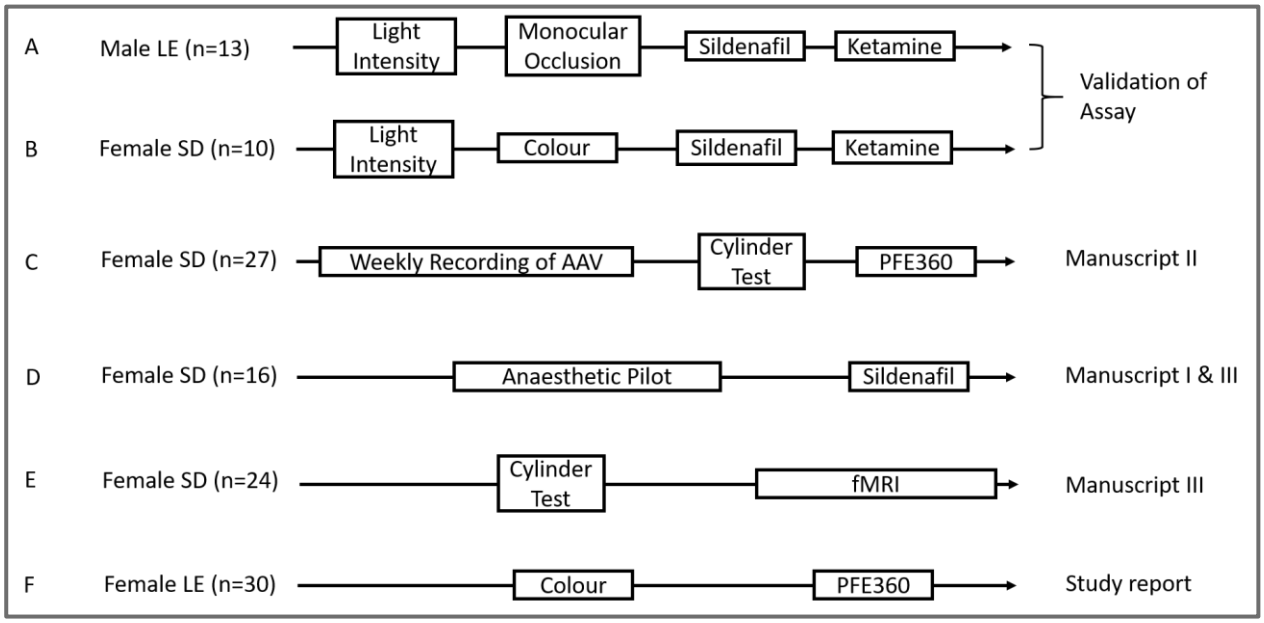

Figure 6 Schematic diagram of all studies carried out in the project. The letters on the left is cohort designation. Cohorts A and B were used for the setting up the assay. Cohorts C, E and F were used for modelling PD. Cohort D was used for the sildenafil study presented in manuscript I, and for piloting an anaesthetic regime for the fMRI study presented in the supplementary material of manuscript III. LE= Long-Evans, SD= Sprague-Dawley.

5.1 Animals

All animal experiments were carried out in compliance with EU community council directive (86/609/EEC) and Danish legislation on the care and handling of experimental animals. The cohort A Figure 6, were male Long-Evans (LE) (Charles River, Denmark), as these are pigmented, there would be a smaller risk of unexpected visual damage during surgery, and in case of suboptimal housing light compared to an albino stock [172]. Cohorts B-E were female Sprague-Dawley (SD) (Taconic, Denmark) as females display slower growth curve than males, thereby diminishing physiological stress regarding body weight in the course of the ten weeks the AAV-α-synuclein model develops. Cohort F consisted of female LE LRRK2-KO (SAGE Laboratories, US). This KO model has a homozygous deletion of 10 bp in exon 30, it was developed by SAGE laboratories in collaboration with the Michael J. Fox foundation.

5.1.1 Husbandry

All rats were single-housed post-surgery in controlled temperature (22±1.5 °C), humidity (55-65%) and kept on reverse day in a 12/12 hour dark/light cycle (lights off at 06:00 h). Food and water were available *ad libitum*. The cages were enriched with a red house, nesting material and food enrichment once a week.

5.2 Stereotaxic surgery

Rats weighing 225 g at arrival (ten weeks of age) were anesthetized using subcutaneous (SC) injections of Hypnorm® (Lundbeck, Denmark), midazolam 5 mg/ml (B.Braun, Germany) and saline in a 2:1:1 relation (2.0 ml/kg), yielding 157 µg/kg fentanyl and 5 mg/kg fluanisone. The head was shaved and disinfected with 0.2% chlorhexidine, and the animal was placed in a stereotactic frame. The eyes were covered with tinfoil to prevent retinal damage from the light of the surgical lamp. The rat was covered with a surgical cover, with a hole exposing the top of the head. Local anaesthesia, Marcain (2.5 mg/ml bupivacaine, AstraZeneca, Denmark), was injected prior to incision.

Six holes were drilled in bilaterally in os paritalis and os frontale coordinates were guided by Paxinos and Watson [173] for visual cortex (AP: -6, ML: ±4), superior colliculus (AP: -6, ML: ±1, DV: -3.5), reference electrode (AP: +8, ML: -2) and ground electrode (AP: -2, ML: +4). The electrodes for recording in the superior colliculus were stranded electrodes E363/3/Spc (PlasticsOne, US). The other four electrodes were E363/20/2.4/S screw electrodes (PlasticsOne, US). The electrode leads were collected in a plastic pedestal MS363 (PlasticsOne, US) and fixed to the skull with RelyX^{TM} Unicem dental cement (3M, Denmark) and GC Fuji (GC, US) as a chronic implant. Sutures were placed to close the wound around the pedestal.

In total the animals were fully anaesthetized for 90-120 minutes, and then placed under a heating lamp while recovering from the anaesthesia. Norodyl (carprofen 5 mg/kg) (ScanVet, Denmark) and Noromox prolongatum (amoxicillintrihydrat 150 mg/kg) (ScanVet, Denmark) were administered during surgery and for five days post-surgery. The animals were allowed recovering for 14 days before the first exposure to stimuli. This procedure was carried out for cohort A, B, D and F.

5.3 Viral injection

The viral injections were carried out both in combination with the electrode implantation (cohort C), and alone (cohort E). The AAV-model, models the mechanistic consequences of

overexpressing α-synuclein [63]. The animals were anaesthetized with hypnorm/midazolam as described above. A hole was drilled over the SNc (AP: -5.5 ML: +2 DV: -7.2) of the left hemisphere. 3 µl rAAV2/5 viral vector ($3x10^{10}$ GC/ml) (Vector biolabs, US) expressing human wildtype *SNCA* with a chimeric promoter containing part cytomegalovirus and a part of the synthetic chicken β-actin promoter, was injected into the SNc using a 32 G cannula (Hamilton, US), at an injection rate of 0.2 µl/min. Prior to injection, the tissue got two minutes to adjust. After the injection, the cannula would stay for five minutes, before being removed, to allow diffusion of the vector. This was a unilateral injection therefore the un-injected side could function as a control. Furthermore, one half of the animals worked as controls by having the empty viral vector injected. If it was only the injection the animals would be pain treated for 24 hours with Temgesic® (buprenorphine 0.05 mg/kg every eight hours) (Cohort E). If it was in combination with the electrodes the analgesia period would be extended to five days (Cohort C). The animals were single-housed after the surgery with enrichment in the form a red plastic house and nesting material. Antibiotics were not administered to avoid compromising the effect of the AAV.

5.4 Cylinder test

The animals receiving the unilateral injection of AAV (cohort C and E) were subjected to a test of motor asymmetry to validate the development of the overexpression of α-synuclein.

The lesion is fully developed after ten weeks [65]. As the lesion is unilateral in an area related to motor initiation it is expected that animals with an overexpression of α-synuclein will display asymmetry of movement by a relative reduction of movement of the paw contralateral of the injection [63].

To test for motor asymmetry induced by the injection of α-synuclein in the SNc. The animal was placed in a transparent, plastic cylinder and recorded for five minutes using a video camera. The number of touches on the plastic was scored offline, and the ratio of contralateral touches to total number of touches was computed.

5.5 VEP recording

VEP was recorded for cohorts A, B, C, D and F. The animals were awake and freely-moving in a homecage, with wood bedding, placed in a dark and sound proof chamber. The pedestal is threaded to keep it tethered when the rat is exploring the homecage. Though [174], [175] have shown a changes in the VEP from the SC with movement then the VEP stimulus was repeated 400 times as this yielded a robust signal.

The animals were exposed to both flash VEPs (1 Hz), and SSVEPs (14 Hz) in five different colours. Short-wave blue (SWB) (405 nm), blue (455-460 nm), green (525-530 nm), red (620-625 nm) and white 5050 SMD LEDs. Though this type of EEG has been accused of temporal changes we have not seen marked variation from week to week. There have been trends but nothing significant. Also the LEDs have been shown to cause variability in other setups [137], but this is not detectable in the current setup.

The flashes were 10 ms as this gives a robust waveform (based on pilot experiments). The light intensity was 20 lx (based on pilot experiments, Figure 9) as measured on the floor of the homecage with a LED luxmeter (Extech instruments, US).

The stimulus was programmed using Spike2 7.20 (Cambridge electronic design (CED), UK), which also recorded the electrical activity via a micro1401 (CED, UK), and a Brownlee amplifier (Model 410, Brownlee precision, US). High (1 Hz) and low pass (200 Hz) filtering was done by the amplifier, which recorded with a bandwidth of 1000 Hz.

5.5.1 Data Analysis

The VEP was extracted by averaging across the 400 trials using Spike2. The VEP waveform was visualized in the temporal range of 190 ms before the stimulus and 500 ms after the stimulation. The peaks were named according to their position e.g. first negative deflection is called N1 [138], [139]. Crude quality assessment is done visually on the VEP, this was only to remove dead channels. The time and amplitude of each peak was extracted manually, and exported for statistics in R. The peaks were analysed separately, because they may vary independently. Measuring the amplitude from peak-peak assumes that the underlying components overlap to an extent were the early component will distort the late [131]. That assumption was not met, and the method was deemed suboptimal.

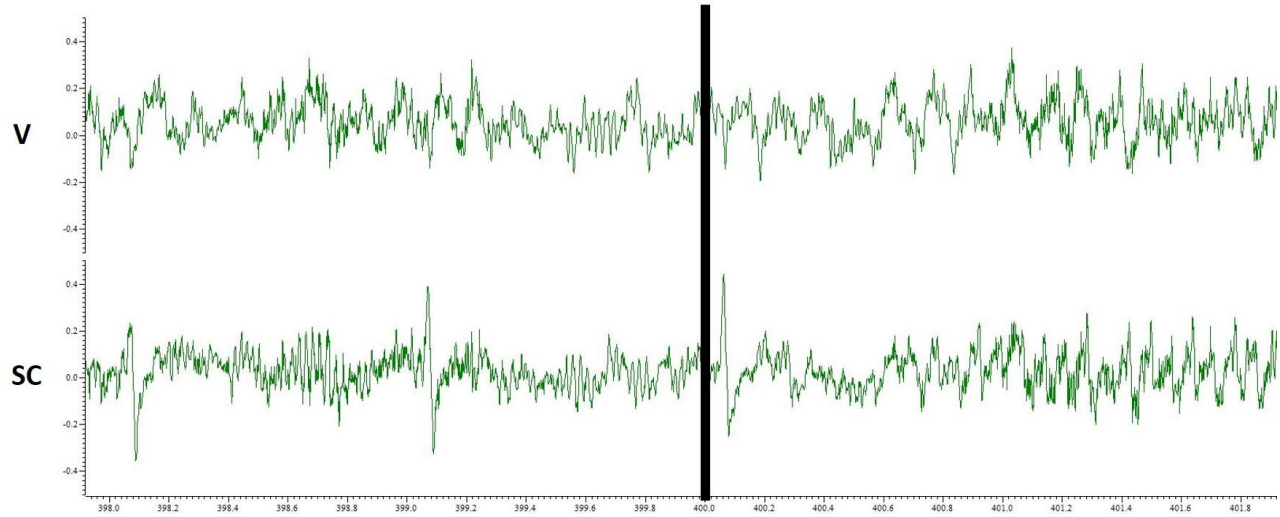

Figure 7 Raw EEG trace of transition from VEP to SSVEP. The black line marks the change of stimulation frequency, on the left side are two seconds of 1 Hz flashes, and on the right side the first two seconds with 14 Hz. There is a noticeable transition effect during the first second. V: visual cortex, SC: superior colliculus.

5.6 The steady-state VEPs

The SSVEPs were recorded for cohorts C, D and F. The 14 Hz stimulus was presented for 100 s after the flash VEP stimulation. The SSVEPs were exported to Matlab (2016a, Mathworks, US), where it was analysed. The first five seconds of the recording were discarded due to noise from the transition effects (shown in Figure 7). When the steady-state is reached the electrical activity is presented as a regular continuous sine wave.

5.6.1 Data Analysis

A fast Fourier transform was performed to get amplitude of the first and second harmonic. The four bins adjacent to the frequency of interest were averaged to yield the mean noise level. The signal-to-noise ratio (SNR) was computed, as the amplitude divided by the mean noise, and this was used as the measure of the electrophysiological activity because the SNR is less vulnerable to variation in noise, than amplitude.

The amplitude data was analysed using a support vector machine (SVM) for cohort C. The basic principle of an SVM is trying to find a hyperplane separating two groups and compute the accuracy with which an unlabelled value would be assigned to the correct group. The SVM can only show if a value can be classified, and not the difference between two groups.

The phase data is briefly represented, as the SSVEP is a summation of activity the temporal information is not accurate.

5.7 Drugs

5.7.1 Ketamine

Ketamine is a non-competitive NMDA-antagonist, working as a dissociative anaesthetic and hallucinogenic. Subanaesthetic doses have gained interest in the field of depression, as a potential treatment for treatment-resistant major depression disorder [176]. To discern the effect of ketamine on neural processing, EEG has been employed showing changes in both auditory and visual ERPs in humans [177].

For this project it was used in cohort A and B, to validate the VEP assay. Further, ketamine was used to explore the translational value of rodent VEP, by comparing them to findings in human VEP. Ketamine was dissolved in saline and 10 mg/kg was administered SC in the flank in randomized cross-over design, with a week in between dosing to avoid lingering effects. Recordings were started ten minutes after administration.

5.7.2 Sildenafil

Sildenafil is a hypotensive agent targeting phosphodiesterase type 5 (PDE5) but it has been reported to have adverse effects on PDE6 with a 10-fold lower efficacy [178]. PDE6 is of interest to this project because it is specific to the retina. Furthermore, sildenafil causes a temporary increase in intra ocular blood pressure [179]. As the adverse effects of sildenafil are expected to be local in the eye, administering a high dose was expected to cause decreases in the measured VEP. Sildenafil-citrate was extracted from Viagra® (Pfizer, US). The sildenafil was administered in three different studies. In cohort A and B it was administered in a randomized cross-over design to validate the visual input for the assay. Cohort D was used in a longitudinal study aiming at profiling the electrophysiological changes induced by sildenafil (manuscript I). In all three the dose was 50 mg/kg, which was dissolved in 1 M HCl and titrated with 1 M NaOH to a pH>2. This dose was around the saturation point of the solution, because the administered volume was to comply with the guidelines from the veterinarians on PO dosing.

5.7.3 PFE360

PFE360 is a LRRK2-kinase inhibitor developed by Pfizer it was first described by Baptista et al. [180]. It has previously been shown to rescue changes in electrophysiological activity induced by overexpressing α-synuclein [65]. This small-molecule inhibitor was synthesized at H. Lundbeck A/S. The compound was dissolved in 10% captisol, pH adjusted to >2 with methanesulphonic acid and administered at a dose of 7.5 mg/kg, which have been shown to cause full inhibition [65]. It was administered in a randomized cross-over design for the animal cohorts D and F.

5.7.4 Anaesthesia

This section describes the anaesthetic regime used for fMRI acquisition. The commonly used anaesthetic isoflurane is a gas anaesthetic with vasodilating properties, thereby changing the neurovascular coupling in a dose-dependent manner [181] and abolishing the BOLD signal at high doses. Comparing anaesthetic regimes used to record visual stimulation in literature (Table 1). It was decided to base the anaesthetic regime on a combination of isoflurane and dexmedetomidine. Dexmedetomidine is an α_2-adrenoceptor agonist, sedative and a muscle relaxant with strong vasoconstrictive properties. This effect of vasoconstriction causes a large drop in heart rate after administration. It exerts its effect on the locus coeruleus [182] and is considered to induce an anaesthesia similar to natural sleep [183].

The following regime was tested in the VEP assay (**supplementary of Manuscript III**) prior to the initiation of the fMRI study (**manuscript III**). This was to test the effect of the anaesthetic on synaptic transmission. The anaesthesia was induced with isoflurane 5%, while placing a tail-vein catheter. As soon as possible thereafter the dexmedetomidine (dexdormitor, Orion Pharma, Finland) was infused at 0.05 mg/kg/hr, and isoflurane decreased to 0.5% (in 1L of oxygen:medical air, 8:2). The animals were breathing spontaneously during scans, the breathing rate was monitored throughout the study, using a breathing pad (SA instruments, US). Temperature of the animals was monitored with a rectal probe and adjusted to 37.5±1 °C using heated air. After one hour the infusion of dexmedetomidine was increased to 0.1 mg/kg/hr (based on pilot studies, and literature).

Initiation		Maintenance		Paper	Stimuli	Response
Isoflurane	4%	Urethane	1.3g/kg bolus (IP), 0.13g/kg supplements (IV)	[184]	RGB LEDs, optical cables	SC VC dLGN
Isoflurane	2.5%	Medetomidine, pancuronium bromide	0.1mg/kg/h 2mg/kg/h	[163]	5ms, 465nm (blue) LED	SC VC dLGN
Ketamine, Xylazine	75 mg/kg 5 mg/kg	Medetomidine	Bolus 0.08mg/kg → 0.15mg/kg/h (IM)	[185]	Strobe unit (bi-, monocular)	SC VC
Isoflurane	4%	Isoflurane	1%	[169], [186]	Green LED 10Hz, Fiber optics	SC dLGN (VC)
Isoflurane	2%	Medetomidine	Bolus 0.04mg/kg → 0.08mg/kg (SC)	[187]	cold white LED	SC VC dLGN
Isoflurane	5→2.5 %	Isoflurane Dexmedetomidine	0.5% 0.05→0.1 mg/kg/h (IV)	**Manuscript III**	White LED, fiber optics	SC VC (dLGN)

Table 1 Comparison of anaesthetic regimes used in the literature of visual stimulation in a MR scanner. (IV) intravenous; (IM) intramuscular; (SC) subcutaneous. (RGB) red, green, blue referring to the wavelength of the LEDs.

5.8 MRI

Cohort E underwent viral injection and the cylinder test at the site H. Lundbeck A/S. they were transported to the DRCMR using an approved transport company. The animals acclimatized to the new facility for two weeks before participating in any experimentation, the cages and enrichment were similar at the two sites. After five months the rats were anesthetized and scanned in a 7T preclinical Bruker system controlled through Paravision 6.0.1. The animals were scanned on separate days at approximately the same time of the day, to minimize variation caused by the circadian rhythm.

The imaging data was obtained using an 80 mm RF transmit quandrature coil and a 20 mm surface receiver coil, which was fixed on the top of the head. The signal covered the whole brain, with maximal SNR above the regions of interest (ROIs): superior colliculus, and visual cortex. Sticky tack was placed in the ears of the rats to prevent damage to the auditory system, by reducing scanner noise.

Before the functional scans were commenced a high-resolution structural T1 scan was carried out using the Bruker-standard T1_Flash_3D_iso protocol (Paravision 6.0.1). This protocol imaged the entire brain with 80 transversal slices, and a voxel size of 0.2 mm isotropic.

5.8.1 fMRI

During the scans, it was possible to run online analysis of the BOLD through Analysis of Functional NeuroImages (AFNI) [188] (the pipeline for online analysis was provided by Yi He). This allowed a rough estimate of the changes in the BOLD signal to the stimulus, during the scans. The BOLD was stabile three hours after reduction of the isoflurane concentration. The echo-planar image (EPI) had a voxel size of .313 mm x 0.313 mm x 0.500 mm and was obtained using a slice package of 42 slices covering from the caudal part of the olfactory bulb to the caudal part of the cerebellum. The repetition time (TR) was 1500 ms, and the echo time (TE) was 8.348 ms. The flip angle of 64° was based on T1 measurement of the grey matter obtained from a separate session. The stimulus paradigm was a block design consisting of six task blocks per trial. Each task block contained 14 TRs of stimulation of either 1Hz or 14Hz, and then 14 TRs of no stimulation (Figure 8). The flickering light was controlled from Spike2 and synchronized with the scanning by transistor-transistor logic (TTL) triggers (red arrows) before each stimulation cycle. There was no light in the scanner between stimulation presentations.

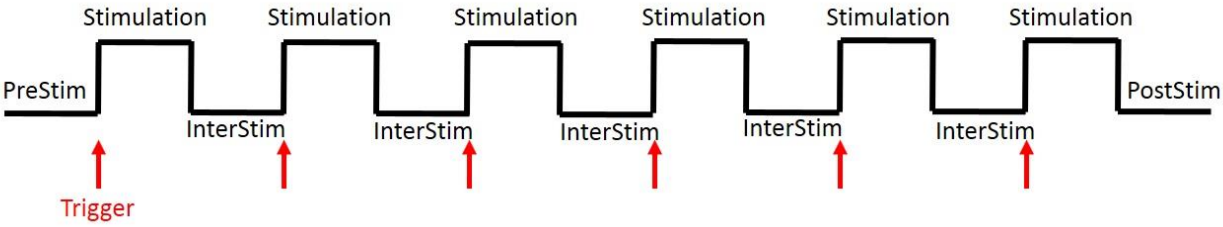

Figure 8 Block design of stimulus. The PreStim, Stimulation, Interstim and postStim all have the duration of 14 TRs (21 s). The stimulation was white light flickering at either 1 Hz or 14 Hz.

Each rat was scanned five times for each temporal frequency. This stimulation paradigm was an adaptation of the stimulation used in the electrophysiological experiment. The stimulus was emitted by warm white LEDs, at 20 lx (based on EEG pilot) measured at the approximate position of the animals' eyes with a LED luxmeter (Extech, US) and conducted through ten (five on either side of the head) 1.5mm, 2m long fibre optics.

5.8.2 Data analysis

Data was analysed using FMRIB software library (FSL) [189]. A standard brain was constructed by aligning and averaging the EPIs from all animals, using FSLmaths.

All scans were registered to the standard brain using FMRIB's linear image registration tool (FLIRT). After checking the quality of the scans four rats were discarded, only 16 rats were analysed: nine control rats and seven AAV-α-synuclein rats.

Functional MRI data were analysed using a three-level statistical analysis pipeline implemented in the FSL expert analysis tool (FEAT). In the first level, the time course of each voxel was fitted with a general linear model (GLM) to produce a statistical map of the z-scores of the correlation for each voxel within each of the scans. Each voxel was corrected for family-wise error with a p-threshold of $p<0.05$. Spatial smoothing was then applied using a Gaussian kernel with full width half maximum of 0.5 mm. In the second level, the z-score maps were averaged for each stimulation frequency within each subject, yielding two averaged statistical maps per animal. Each voxel within the averaged statistical map was corrected for family-wise error with a p-threshold of $p<0.05$. At the third and last level, the averaged statistical maps were averaged within the two groups for each of the two stimulation frequencies. The group statistical maps were compared using an unpaired comparison of the z-score maps between the two groups within each frequency. For the visualization, the statistical maps were superimposed on the high resolution T1.

Were the third level analysis gives the overall differences between the groups, we are interested in the difference within the groups, and if the stimulation frequency influences the intensity of the time course. We extracted the intensity of the signal using masks of the regions of interest (ROIs) specifically the superior colliculus and the visual cortex. The masks of structural ROIs were made using the brain atlas the NITRC and the scalable brain [190]–[192]. The percent changes between on and off state of the time series were extracted from each animal using FEATquery. The data was extracted for final analysis in R, through R studio.

5.9 Perfusion fixation

At the end of the scan session, the animal was first given an SC bolus of hypnorm midazolam. The animal was then perfused intracardially with saline and heparin for three minutes, and then with 4% paraformaldehyde (PFA) (premade with methanol). After 10-15 minutes the rat was decapitated, and the brain extracted. The brain was immersed in 4% PFA for 24 hours, then placed in phosphate buffer with <1% PFA, and then placed in KPBS [152.3 mM NaCl, 2.7 mM KCl, 1.9 mM $NaH_2PO_4 \cdot H_2O$, 8.5 mM Na_2HPO_4 in H_2O]. They were stained as described in section 5.11.2.

5.10 Post-mortem assessments of drug exposure

Drug exposure measurements were carried out on cohorts C and F for PFE360, and cohort D for sildenafil. After decapitation the cerebellum was weighed and transferred to a Covaris glass tube. This was snap-frozen and stored at -80 °C until analysis. The cerebellum was thawed and homogenized using the Covaris 220X. The concentration of PFE360 was quantified in a LC-MS/MS platform (Xevo TQS triple quadrupole (TQ) mass spectrometer operated in electrospray MS/MS mode (multiple reaction mode, MRM) and coupled to a Waters Acquity UPLC controlled by Mass Lynx software version 4.1). Mass spectrometry methods gave the concentration of drug in the tissue sample.

5.11 Histology

5.11.1 Validation of Electrode Placement

After EEG recording the animals were decapitated. The brains extracted and frozen on dry ice after decapitation. Brains were sectioned in the coronal plane at a thickness of 20µm, on a freeze microtome (Leica Microsystems Inc., Germany) and picked up on glass slides. The placement of the stranded electrodes was assessed visually by using a light microscope, the electrode leaves a straight-line separation of the tissue. The location of the electrodes was assessed for all animals in cohorts A, B, C, D, and F.

Electrodes placed below the optic layer of the superior colliculus caused a reversed potential. This was accounted for in the data analysis.

5.11.2 Immunohistochemistry

72H before slicing the brains, they were fixed in 30% sucrose. 40 µm coronal sections were cut on a freezing microtome and placed in KPBS immediately after cutting. The slices were stained within five days after sectioning. Briefly, the sections were washed in phosphate buffered saline (PBS, Thermo Fisher Scientific, USA), and any endogenous peroxidase was quenched with a 3 % hydrogen peroxide solution. The tissue was the washed and incubated over night with primary antibody (see Table 2). The tissue was then washed and incubated with 1:500 biotine conjungated secondary antibody either E0464 anti mouse or E0353 anti rabbit (DAKO, Denmark), and then incubated with Elite avidin-biotin complex (ABC kit, Vector labs, USA). After washing with PBS the immunostaining was then visualized with 3,3-diaminobenzidine (DAB-reaction) (Vector labs, USA).

Target	Host	Concentration	Name	Producer
Human wildtype α-synuclein	Mouse	1:1000	4B12	Thermo scientific
pSer129-α-synuclein	Rabbit	1:500	AB51253	Abcam
Tyrosine hydroxylase	Rabbit	1:1000	AB152	Millipore

Table 2 Antibodies used for histology

The stained sections were placed on gelatine covered glass slides and examined with a light microscope (Axio scope.A1, Carl Zeiss Microimaging, Germany).

5.12 Biochemistry

5.12.1 Western blotting

Western blotting was used as a supplement to the histological analysis to test the presence of α-synuclein in the superior colliculus and the striatum. Tissue punches were taken from the striatum and the superior colliculus and homogenized using the Precellys lysing kit 0.5ml with a cellLysis M buffer (Sigma, USA) containing Complete Protease Inhibitor 40x (Roche, Switzerland), and PhosSTOP (Roche, Switzerland). The Precellys homogenizer was set to 30 s 2x 5000rpm. Then the samples were spun at 300g for 30 min at 4 °C. The supernatant was collected, and the protein concentration determined with the BCA Protein Assay (Thermo Scientific, USA). For the loading sample, the concentration was adjusted to 0.5µg/µl using MilliQ, and 5µl loading buffer NuPAGE LDS sample buffer (Invitrogen, USA) with 100mM DTT (Sigma, USA), was added. For α-synuclein siliconized pipette tips and test tubes were used as the protein is 'sticky'.

Samples were loaded on a 4-12% Bis-Tris Gels (Life Technologies, UK) or 3-8% tris-acetate gel (Life Technologies, UK) for LRRK2. Gels were run at 200V for approx. 45 minutes. The proteins were blotted to immobilon-FL PVDF membranes (Millipore, USA). Membranes for α-synuclein detection were boiled in PBS prior to incubation with overnight primary antibody (Table 3).

Target	Host	Concentration	Name	Producer
GABA Transporter 1	Rabbit	1:500	ab1570w	Merck
Human wildtype α-synuclein	Mouse	1:10 000	4B12	Thermo scientific
pSer129-α-synuclein	Rabbit	1:1000	ab51253	Abcam
Tyrosine hydroxylase	Rabbit	1:2000	ab152	Millipore
LRRK2	Mouse	1:2000	N241A/34	Neuromab
pSer935-LRRK2	Rabbit	1:1000	ab133450	Abcam

Table 3 Primary antibodies for western blotting

The membranes were then washed and incubated with infrared dye conjungated secondary antibody. This was visualized using the Odessey CLx infrared scanner (LI-COR, USA) and quantified using Image Studio v3.1 (LI-COR, USA).

5.13 Statistical analysis

Data was tested for normality using QQ plots. Most statistical analysis was carried out in R (3.4.2) via Rstudio, the exceptions are the SSVEPs which were analysed in Matlab.

The randomized cross-overs with ketamine, were all tested using paired t-tests. Otherwise a model of linear mixed effects was made with the appropriate number of variables (this was tested by autocorrelating the residuals). The models included a random effect of individual rats, to account for bilateral electrodes. Subsequently, ANOVAs were applied to the models, then they were combined with the backward elimination strategy removing insignificant higher-order interaction, to secure the robustness of the test performed [193].

In the data from VEPs there would be at least 24 repeated ANOVA causing a multiple testing problem this was handled by adjusting the p-values using false discovery rate [194] to scrutinize potential false positives. This test is not as conservative as the Bonferroni.

6 Summary of Results

The primary results of the thesis are presented in the appended manuscripts, but here the results will be presented in the context of the entire project, which includes results from pilots, which were used to characterize the potential of the established assay.

6.1 Model Validation

In developing the stimulus paradigm, the length of the stimulus was determined to 10 ms. The shape of the stimulus pulse was determined to be a square wave (on-off). The light intensity was tested in the range 1:200 lx and subsequently adjusted to 20 lx as this light intensity provides the possibility of detecting both potentiation and depression of the signal in pigmented as well as in albino rats (**Figure 9**).

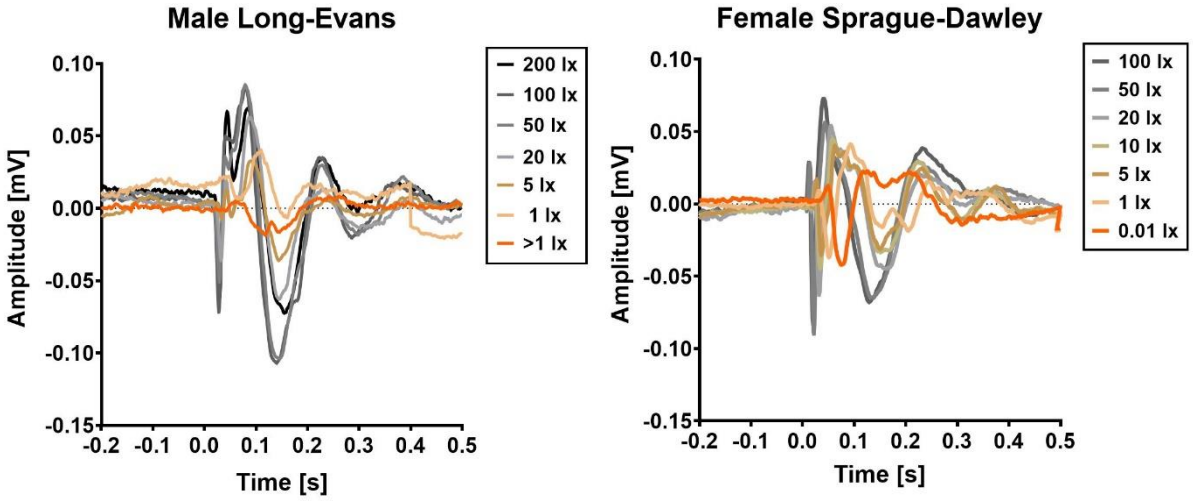

Figure 9 Changes in the VEP from the visual cortex as a response to change in light intensity. The left panel shows the grand average of VEPs from male LE rats. This is a pigmented stock. The right panel shows the VEPs from female SD rats. As these are albinos, they were not exposed to the 200lx flash as it might damage their retinas. Overall, a decrease in intensity of light causes reduction in the amplitude and increases in the latency of the waveform.

The waveforms from the SC and VC were comparable in shape to what has been described previously [125], [195]. The amplitudes of the responses were not as similar, but this measure varies with the type of electrodes, amplifier and EEG setup.

The setup was validated by patching one eye of the rat (cohort A) (**Appendix #2**). The purpose was to validate the origin of the VEP response as well as testing if the assay would be sensitive to unilateral differences. The eye patch is effective because rodents have a >97% cross-over of retinal

fibres, and therefore a patch is expected to deplete the signal of the contralateral hemisphere. As the recordings had to be made with the chamber open the VEP contains more noise, but the trend of the signal is a marked reduction in the signal recorded contralateral to the patch. This confirms both that we are in fact measuring a visual response as well as the assay's ability to measure unilateral stimuli.

The literature on VEPs in rats use different wavelengths of stimuli, usually green or white. Rats are dichromats, but a majority of their cones have a peak response at approximately 510 nm [120] which is in the green part of the spectrum, but a subset of these also respond to light in the ultra-violet part of the spectrum. Five wavelengths were tested to gain an impression of the significance of this variable. The grand averages from the visual cortex and the superior colliculus are shown in **Figure 10**. The quantifications of amplitude and latency data can be found in **Appendix #3**. One-way ANOVA using the white as control, shows that all five wavelengths cause significant changes of the waveforms from both the VC and the SC.

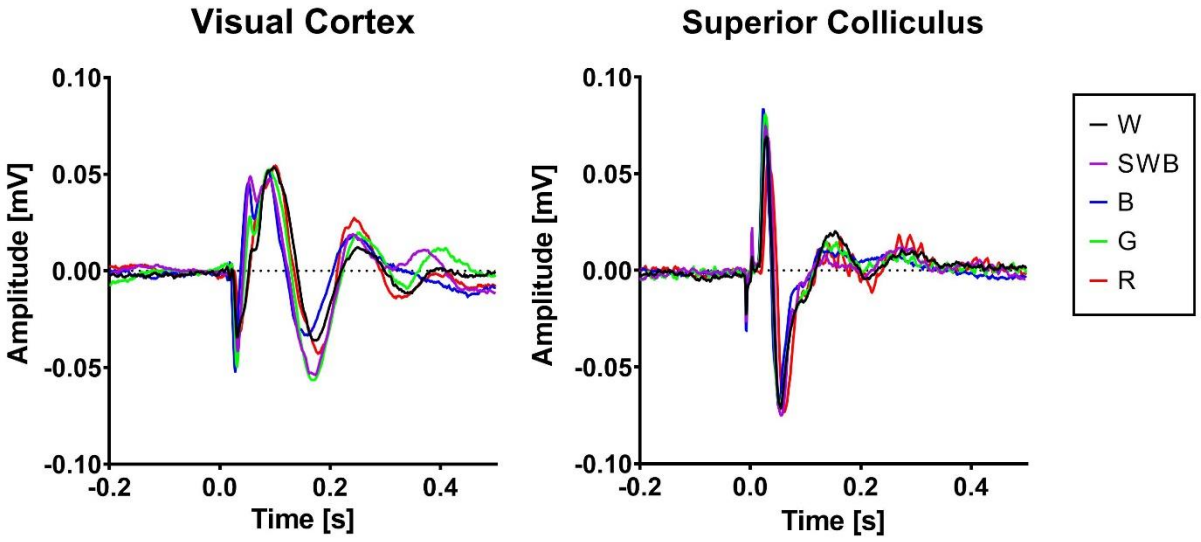

Figure 10 Superimposition of VEPs recorded under five wavelength conditions. These are recordings from cohort B. Left panel: the grand averages from the visual cortex. Right panel: the grand averages from the superior colliculus. W: white, SWB: short-wave blue, B: blue, G: green, R: red.

6.1.1 Ketamine

As subanaesthetic doses of ketamine have been reported to cause changes in the electrophysiological activity measured in humans [177]. A randomized cross-over of 10 mg/kg

ketamine was carried out in two cohorts, male LE (cohort A), and female SD rats (cohort B) (for figures see **Appendix #4**). The VEP from the superior colliculus and the visual cortex were measured ten minutes after administration of ketamine. The VEP waveforms show that ketamine does not affect the SC but induce changes in the VC. Ketamine modulates the thalamo-cortical network. The primary relay nucleus of the visual cortex, the dLGN is located in the thalamus, suggesting that the change is caused by ketamine modulating this relay of the visual system. Further, this suggests the SC are not directly connected to the dLGN. In humans, ketamine has been shown to cause a robust reduction of the P300 in the VEP [177], here we see changes in several peaks. This can be considered a proof-of-concept that the rodent visual system is comparable to the human, and that the VEPs measured are translational, though the direct translation of specific peaks may not be feasible.

6.1.2 Sildenafil

(Results from **manuscript I**) To test if the assay could measure longitudinal effects of neuromodulation, high-doses of sildenafil were administered to four animals (cohort D) with bilateral electrodes in the superior colliculus and visual cortex. The EEG was recorded nine times during the 28 hours after the administration, using three different wavelength conditions: white, blue and SWB. Overall, the administration of sildenafil caused statistically significant reductions of the amplitude of the VEP from both the visual cortex and the superior colliculus after 30 minutes. Further, there were significant increases of the latencies of the peaks. **Figure 11** displays the grand averages from the VC and SC, this is only the data for stimulation with white light for a more comprehensive description of the changes see **manuscript I.**

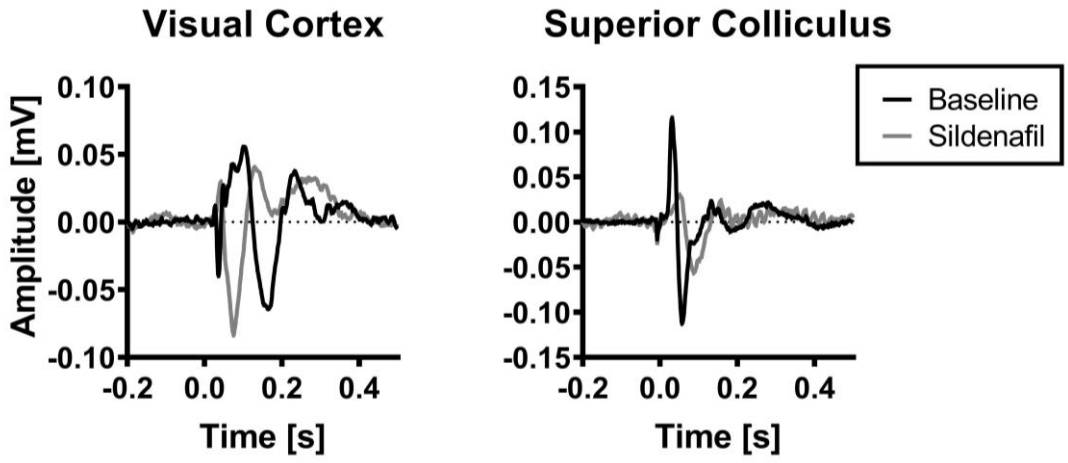

Figure 11 Waveform of grand averages recorded in the visual cortex (left) and the superior colliculus (right). The baseline measurements are shown in black, and the VEP from 30 minutes after the administration of sildenafil is shown in grey. The waveform is recorded with white light.

The results show statistical significance for the interaction between colour and sildenafil. The magnitude of change of the VEP is affected less if the wavelength is blue compared to white and SWB. In the first harmonic of the SSVEP recorded from the VC, the SNR is decreased of the in the blue and the SWB conditions, the second harmonic is unaffected in all three wavelength conditions. In the first harmonic from the superior colliculus, the SNR is reduced in the white wavelength condition, but not in the other two. The SNR of the second harmonic is affected in all three wavelength conditions.

For both techniques the magnitude of change depends on the wavelength of the stimuli. As inhibiting PDE6 inhibits the response to photons, where dimming the light lowers the number of photons received. It can be speculated that the effect of inhibiting PDE6 should be comparable to dimming the light. Assuming the effect of using light at a lower intensity causes a reduction of the amplitude and an increase of the latency, the VEP recorded in the SC display this change in waveform. However, the VC displays a change unlike a simple reduction of light intensity, this could give the impression that it receives light information from cells that utilises PDE6-independent phototransduction. In conclusion the established assay can monitor the progression of neuromodulation of the visual system. Further research is needed to investigate why the changes in the visual cortex does not mimic a reduction in phototransduction.

6.2 Visual Processing in the AAV-model

(Results from **manuscript II**) To test if the development of α-synuclein overexpression could be detected using electrophysiological measurements. AAV-α-synuclein was unilaterally injected in 13 rats, another 13 rats received an injection with the empty viral vector (cohort C). EEG was recorded bilaterally from the visual cortex and the superior colliculus from week three post-injection to week 11 (counted from the first day of surgery).

We hypothesised that the functional effect of the overexpression of α-synuclein would be detectable after 11 weeks of the injection. This was validated in the cylinder test. When comparing the VEPs recorded in the SC, ipsi- vs. contralateral to the injection of the α-synuclein we found a significant delay in the P1 of the superior colliculus (two-way ANOVA, $F(1,24)=12.3$, p-adjusted=0.0022) (**Figure 12**). This difference was not present in the control animals. There were no significant changes in the VEP recorded from the visual cortex. A comprehensive description of the results can be found in **manuscript II.**

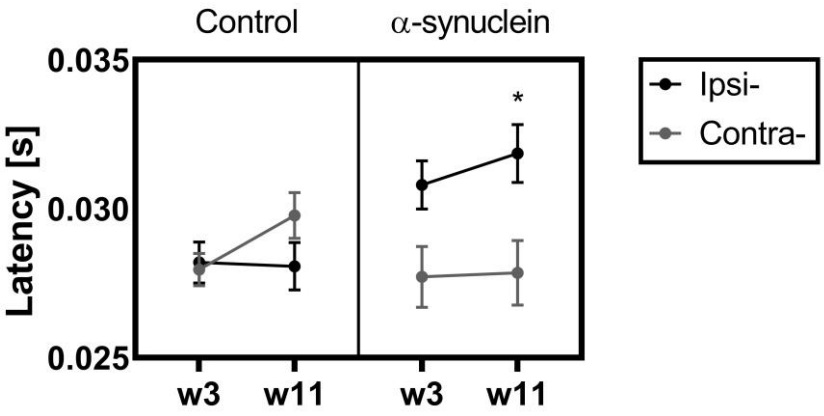

Figure 12 Change in the latency of P1 of the superior colliculus. The latency is shown as mean±SEM for the control and the α-synuclein animals at the first week of recording (w3) and at week 11 (w11). The mean latency of P1 recorded from the electrode contralateral to the injection (grey). The mean latency from the electrode ipsilateral to the injection (black).

Similarly, the support vector machine was able to classify the SSVEPs from the superior colliculus ipsi- and contralateral to the injection in the α-synuclein expressing animals in all weeks but week 10. In week 11 the classification accuracy was 73%, showing that the SVM would classify an electrode from an animal correctly into injected and un-injected side 73% of the time when only including the electrodes of the α-synuclein rats. The SVM was also used for classifying the animals into PD and control when including all electrode (both SC and VC). This showed that the SVM could classify an 'undiagnosed' animal correctly 83.7% of the time as soon as week three. The spread of α-synuclein was confirmed with histological staining of the cerebrum after ended recordings. Immunohistochemistry of the AAV-α-synuclein model showed that α-synuclein is highly expressed in the processes originating in the substantia nigra, both dopaminergic and GABAergic. Therefore, α-synuclein was detectable in the striatum and the superior colliculus.

As LRRK2 inhibition has been shown to rescue functional consequences of overexpressing α-synuclein [65], the animals were dosed with the LRRK2-kinase inhibitor PFE360. The acute administration of PFE360 did not rescue increase of latency induced by overexpressing α-synuclein. The PFE360 further showed that inhibition of the LRRK2-kinase caused a general increase in the latency of the peaks from the VC and the SC. The inhibition of LRRK2 was validated with western blotting showing a decrease in the expression of p-ser935 LRRK2, which is necessary for the target engagement of LRRK2. Taken together, the VEP assay did detect functional changes induced by overexpression of α-synuclein. PFE360 did not rescue these changes.

6.3 fMRI of the AAV-model

(Results from **manuscript III**) As intracranial EEG is an invasive technique it could be interesting to test for the effect induced by overexpressing α-synuclein, using a non-invasive technique such as fMRI. Seven animals had the AAV-expressing α-synuclein injected unilaterally in the SNc, while nine animals had the empty AAV-vector injected (cohort E). After five months the animals were scanned in a preclinical MR scanner. The stimulus was comparable to the paradigm described in **manuscript II** but adapted to a block design to accommodate the use of the hemodynamic response function.

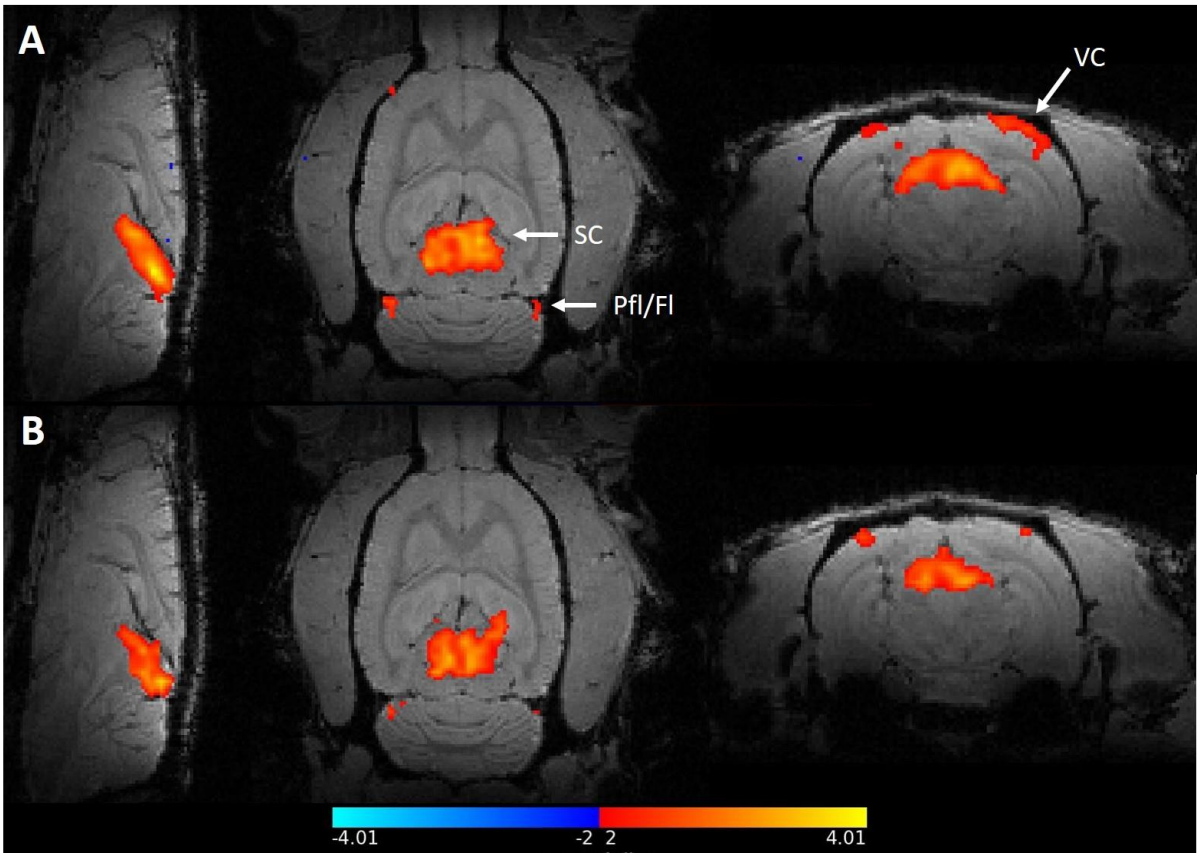

Figure 13 Z-score maps from the A) control and B) α-synuclein animals. The colour bar shows the z-score thresholds for the colour maps. SC: superior colliculus, VC: visual cortex, Pfl/Fl: paraflocculus and flocculus complex. The left side of the image corresponds to the left side of the animal.

The z-score maps show BOLD activation in the visual system (**Figure 13**). However, when extracting the difference of the ON and OFF state of the BOLD-response from the SC and the VC, there was no significant asymmetry of the response in the SC, as there was in the VEP assay. Further, there is no overall difference between the two groups. The presence of α-synuclein in the SN, SC and striatum was validated using immunohistochemistry. Collectively this shows that the overexpression of α-synuclein cannot be detected using the BOLD-fMRI with a visual stimulus.

Suggesting that the overexpression of α-synuclein does not cause detectable changes in blood flow nor in oxygen demands.

6.4 Visual Processing in the LRRK2-KO

(**Study report**) Studies in flies and humans have suggested a link between LRRK2 and visual processing. As administering PFE360 caused significant changes in the VEP of the AAV model, we wanted to explore the role of LRRK2 in visual processing. The LRRK2-KO rats were subjected to the VEP assay (cohort E). A pilot study with five wavelengths showed a significant interaction between genotype and wavelength. As the magnitude of difference between the two genotypes was largest in the blue wavelength condition, and this wavelength was used for subsequent experimentation. When comparing the VEPs from LRRK2-KO (KO) rats to wildtype (WT) rats, the amplitudes of the waveform showed significant differences in both the VC and the SC (**Figure 14**). Further there were significant differences in the latencies. The KO displayed significantly shorter latencies in the VEP from the SC compared to the WT, while the latencies were longer in the VEP from the VC. Suggesting differential roles of LRRK2 in these two regions. A more comprehensive description of the results can be found in the **study report**.

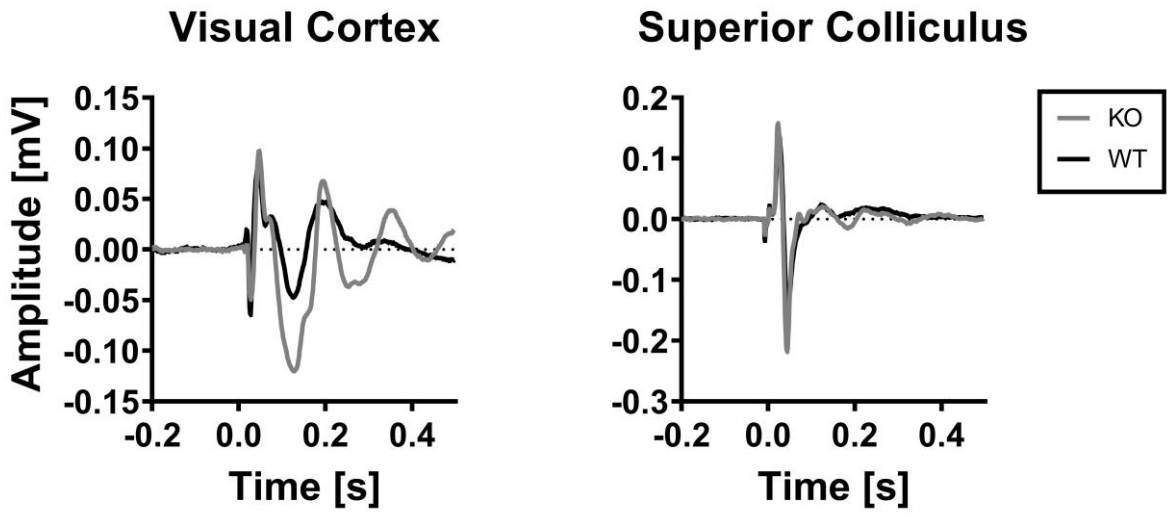

Figure 14 Grand average waveforms from the VC and the SC. The grey trace is the grand average from the LRRK2-KO rats and the black trace is from the wildtype rats.

Subsequent, to the characterization of differences in the VEP between KO and WT, PFE360 was administered to the two groups. Here we found that PFE360 induced changes in the LRRK2-KO suggesting off-target effects. Another interesting finding was that the KO exhibited shorter

latencies on peaks from the SC were the addition of PFE360 caused increased latencies, similar to what was shown in the EEG-study of the AAV-model. Taken together these results suggest a role for LRRK2 in visual processing.

7 Discussion

This section will discuss the overall points made in the appended manuscripts along with a general discussion combining the results from **manuscript I, II, III** and the **study report**.

7.1 Visual System as a Biomarker

Parkinson's disease is among the most common neurodegenerative disorders worldwide [1]. It is typically diagnosed very late in the disease progression. In order to improve the potential for intervention biomarkers are needed to develop new therapeutics [16]. The main purpose of this project was to determine whether modulations of PD relevant biologies would be detectable by measuring on visual processing, and if these modulations could be used to monitor disease severity and progression. Biomarkers in the visual system have so far failed to give unambiguous predictions of disease severity [196]. Though, there are several visual dysfunctions in PD, related to the oculomotor function as well as visual processing [14], a meta-study have reported robust changes of the P1 of the VEP in PD patients [149].

7.1.1 Establishing the VEP Assay

The first aim of the thesis was to establish an assay for measuring visual processing of awake and freely-moving rats. The visual cortex was chosen because the area 17 is considered to be comparable to the V1 in humans. SC was chosen as it is the primary visual nucleus of the rodent visual system, and because of the 'intimate' relation with the substantia nigra. The AAV-model uses a unilateral injection, bilateral recordings allowed comparisons within subject, increasing the statistical power of the assay.

The results from **manuscript I** showed that changes locally in the eye changed the VEPs validating the necessity of input from the eye in the generation of the VEP and the SSVEP. Confirming that the ERP measured is indeed a VEP. These results further showed that the progression of a pharmacological modulation can be monitored using the assay. The assay does not measure the electrophysiological activity of the retina, but the direct connection from the retina to the SC gives a 'pure' visual response comparable to the ERG. **Manuscript I** demonstrates that the VEP from the SC is influenced similarly to the ERG recorded in humans [197], [198].

Pharmacologically modulating a relay of the visual processing with subanaesthetic doses of ketamine, induced changes of the VEP measured at the level of the cortex. Similar to what has been reported in humans [177]. Supporting the translational value of the rodent visual system.

7.2 Spreading of α-synuclein in the AAV-model

In the AAV-model used in both **manuscript II** and **III** the overexpression of α-synuclein appears to stay within the cells originally transduced: α-synuclein is present in the entire SN, striatum and optic layer of the SC. Most of the projections between the superior colliculus and the substantia nigra are GABAergic processes from the pars reticulata and not the pars compacta [126], but there are proposed to be dopaminergic processes from the SNc to the SC [125]. Surmeier et al. mentions that α-synuclein is not detected in GABAergic processes in post-mortem samples from PD patients [33]. The presence of α-synuclein in GABAergic cells may be a feature of the AAV not preferring certain cell types. Though, α-synuclein is primarily found in dopaminergic cells it has been found in the SC of PD patients [128], and it is not exclusively expressed in dopaminergic cells.

The induced phenotype of the AAV-model appears to depend on the serotype of the AAV, the promoter and possibly the version of α-synuclein, as mutated types have been suggested to be more prone to formation of exogenous α-synuclein [60] than wildtype α-synuclein. Furthermore, Albert et al. use an AAV serotype comparable to the one used in this thesis, but with a different promoter and do not detect α-synuclein in the SC [199].

7.3 Functional Changes Caused by Overexpressing α-synuclein

Manuscript II aims at addressing the potential for monitoring the development of the overexpression of α-synuclein using electrophysiology. The overexpression of α-synuclein caused a statistically significant delay of 4 ms in the VEP of the superior colliculus 11 weeks after the injection of the AAV-α-synuclein, when the overexpression was fully developed. This shows that the established assay can monitor the changes induced by the α-synuclein overexpression at the late stages of progression.

Previous electrophysiological studies of the AAV-model have identified changes in the firing pattern of the subthalamic nucleus (STN) ten weeks after injection [65]. The STN is directly connected to the SNc vis dopaminergic processes. The electrophysiological techniques differ, as Andersen et al. used single-unit recording and VEPs are used in **manuscript II** it can only be speculated if the mechanism causing the change is the same. The increase in burst firing could potentially lead to a desynchronization of the local field, thereby causing an increase in the latency. A lesion model of PD shows enhanced visual response in SC [123]. Rolland et al. argue that this could be caused by 6-OHDA affecting the SNr and disinhibiting the SC. Similarly, Vila et al., shows that the activity of SNr is increased in the parkinsonian state [200], suggesting a cause for the changes in saccadic movements and visuospatial functions seen in PD [201], furthermore they showed that these effects could be partially reversed with levodopa treatment. ‘Express’ saccades

are controversial, but have been reported in PD as dyskinesias arising from increased inhibition of the SC [202] and neuronal loss in the SC [203]. Tölo et al. have described a mild inhibition of functional connectivity in neurons overexpressing α-synuclein [54], possibly by impairing vesicle recycling [204] and the release of neurotransmitters, which should cause a disinhibition of the SC. Taken together these results suggest an enhanced response from the SC, which is contrary to the increased latency seen in **manuscript II**. This discrepancy can be caused by variation in the expression of α-synuclein within the cells, causing a delayed synchronization of the post-synaptic potentials. It is not possible to measure VEPs in the SC of human, but the changes in saccadic movements may provide the necessary surrogate marker. Further, it can be speculated that the delays seen in VEPs measured from the visual cortex of humans [149] is similarly caused by aggregated α-synuclein. If this is the case, then according the Braak staging theory the delayed VEP will not be detectable until the aggregates reach the cortex i.e. in the late stages of the disease.

However, if the delay in latency seen in **manuscript II** is caused by the post-synaptic potentials of the local field being desynchronized it would be fair to assume a decrease in amplitude as well. There is no effect on the amplitude of the VEP response. This may be due to the VEP analysis providing some drawbacks as a multiple comparisons problem arises, when every peak must be analysed separately. There is a difference in the amount of variation on the amplitude and the latency data, as the amplitude data seems to be more sensitive to the accuracy of the electrode placement, i.e. whether the SC electrode was exactly in the middle of the optic layer or closer to the layer above or below. This induces a larger variation in amplitude between subjects compared to latency. The rats are freely moving during the EEG recordings, which produces noise, but the stimulus length has been adjusted so the many repeats cause a robust signal, with very little intertrial variation, and little batch variation on the grand averages.

The SNR of the SSVEP showed a trend for a difference when comparing the α-synuclein group to the control group. The SSVEP is considered to be less vulnerable to noise than the VEP. A downside to the technique is the lack of a temporal information, as the signal results from a summation of peaks the phase of the signal cannot be directly interpreted as latency.
The SVM (**manuscript II**) was able to classify the amplitude data from the SSVEPs. Suggesting that the overexpression of α-synuclein causes a change in the amplitude, but it requires a very sensitive technique to detect it. The SVM found that it was possible to classify the difference already at week three after the injection of the AAV, suggesting very subtle differences. An individual animal could be classified to the correct group (control or α-synuclein) with an accuracy

of 83.7%, using all electrodes. This is promising for the development of a biomarker. The VEP did not detect any difference at this early timepoint, but as the SVM is very sensitive, it is likely that there are subtle changes in the electrophysiological activity at this early time point. Kirik et al. shows that α-synuclein is present in the nigrostriatal system at three weeks after injection of AAV. However, functional pathology have been shown to develop slower than the immunoreactivity [205].

It would be relevant to study if the phenotypes detected can be rescued by using other treatments for PD on the models presented. Though, the α-synuclein model was only a small difference, reversal of α-synuclein aggregation would probably rescue the latency changes.

7.3.1 fMRI

The results from **manuscript III** show that the BOLD response is the same in the two groups. There are responses in the visual areas the SC and VC, however, it was not possible to detect the unilateral overexpression of α-synuclein. Suggesting that the overexpression of α-synuclein does not induce detectable changes in oxygen requirements of the neurons of the visual system. Though, a previous study have shown that it changes in the energy metabolism specifically in the glucose-lactate switch of the striatum, when the AAV was injected bilaterally in this structure [206]. This was assed using MRI-spectrometry, were the chemical composition of a ROI is assessed rather than the functional activity of the entire brain.

The fMRI study has limitations both in the use of an anaesthetic regime and the time variance of two months between the first and the last scan, inducing an age variation. We estimated that the variation induced by circadian rhythm would cause more noise in the data than the age variation.

The anaesthesia was tested in the EEG setup to study how it influenced the electrophysiological activity in the areas of interest (**section 17.1**). Though the VEP is almost normalized after three hours, there were still some individual variation in anaesthetic depth.

fMRI might not be the ideal technique for α-synuclein, as temporal resolution of fMRI makes it insensitive to small changes of latency. Kuebler et al. have shown that α-synuclein is detectable if the stimulus is combined with an amphetamine challenge because of the effect on dopaminergic cells [170].

The usefulness of α-synuclein as a biomarker in patients is still debated as aggregated α-synuclein is also present in healthy people [207]. Further the aggregation is not unique to PD it is also present in Alzheimer's disease and Lewy body dementia.

The sensitivity and potential of machine learning techniques may provide the models with sensitivity that has been missing in the detection of prodromal PD.

7.4 LRRK2 and α-synuclein

Studies have shown a great potential for LRRK2 inhibition as a treatment for PD [89], [208]. The increase of latency in the VEP from the SC (**manuscript II**) was not rescued by a single acute dose of the LRRK2 kinase inhibitor PFE360. LRRK2-inhibtion however caused general increases in the latency of all peaks from both the VC and the SC. The LRRK2-inhibition did not rescue the α-synuclein induced changes possibly because it was administered as a single acute dose, where other studies have used long-term treatments. Furthermore, the overexpression of α-synuclein was already developed at the time of the intervention. There is no literature suggesting that inhibiting LRRK2 can clear the aggregation of α-synuclein once developed. LRRK2 seems to primarily play a role in the spreading of the aggregated protein and not necessarily in reversing already existing aggregation. Though, Andersen et al. showed a reversal of the electrophysiological phenotype in the single-unit recordings in the STN of the AAV model [65] the results from **manuscript II** do not support the efficacy of acute administration of LRRK2 kinase inhibitors as a therapeutic for α-synuclein induced changes.

This thesis further showed off-target effects of PFE360 (**study report**), as an acute dosis of PFE360 caused increased latencies in the VEPs from the LRRK2-KO group. Off-target effects of PFE360 were also seen in human blood cells [76]. Off-target effects have been primarily demonstrated in kinases related to damage response, which are unlikely to affect post-synaptic potentials [180].

7.5 LRRK2

The **study report** showed significant interactions between the expression of LRRK2 and the wavelength of the light. The function of LRRK2 in vision is supported by the literature associated with gain-control in flies [113], [209], [210] and colour discrimination in humans [114], [115], [211]. Interestingly the human study found differences between the carriers and PD carriers of LRRK2-G2019S in a test of colour discrimination [114]. Furthermore, a fly study reported a relation between mutated LRRK2 and degeneration of the photoreceptor cells [171], a similar study is yet to be conducted in rodents and humans. Taken together this suggests a role for LRRK2 in the retina, possibly in the cones. This could contribute to the change of contrast sensitivity seen in PD patients. However, localization studies of LRRK2 in the retina have yet to be conducted.

Localisation studies of LRRK2 in the adult rodent brain have shown that LRRK2 is present in the striatum and the cortex [72]. When comparing the VEP of the KO to wildtype it became evident that the latency of the VEP from VC is increased, while it is decreased in the VEP from the SC. Suggesting differential roles of LRRK2 in the cortex and grey matter nuclei. The LRRK2-KO showed considerable changes of the VEP supposedly resulting from the developmental lack of LRRK2, as similar effects were not induced in the wildtype, when treated with PFE360. It is worth speculating whether a time limited inhibition of the kinase domain of LRRK2 is comparable to knocking out the gene, as LRRK2 has multiple effects unrelated to neuronal signal transduction. Knocking out LRRK2 have been reported to change the development in progenitor cells [212]. Supporting that the effect in the SC is developmental, as Zechel et al. notices that in the murine brain LRRK2 is more widely expressed during development [212]. The increase in latency may be a result of developmental deficiency of LRRK2, where the decrease in latency in the cortex, may come from a combination of developmental lack and the function of LRRK2 missing.
This data correlates with data from *drosophila* showing that modulations of LRRK2 affects the electrophysiological activity in the visual system [209]. This suggests that changes in LRRK2 causes subtle changes in the visual system across species. A future step would be to look at a model of the *G2019S* mutation.

8 Conclusion

The aim of this thesis was to establish an assay for detecting changes in visual processing as a result of modulating Parkinson's disease related genes.

In the course of this study we managed to establish an EEG assay for measuring both VEPs and SSVEPs in awake and freely moving rats. We show that the two PD-related models: the AAV-model and the LRRK2-KO model display differences in the visual processing compared to controls. Finding changes in the SC of the AAV-model suggests that α-synuclein may be involved in the abnormal saccadic movements seen in PD patients, adding to the translational value of the AAV-model.

These models the disease in animals of ages corresponding to young adults and did not take an interaction of disease biology and age into account. However, these subtle effects may be what that specific disease biology contributes to the overall disease picture and forms the basis for the changes seen in human subjects, as the real disease is a multifactorial disorder.

Further, we showed that acute dosing of the LRRK2-kinase inhibitor PFE360 did not rescue the increases in the latency induced by α-synuclein, and it may not be as specific to LRRK2 as anticipated.

9 Perspectives

There is still some way to go before the ideal biomarker for PD is well-established in flies, rodents and human patients.

LRRK homologs exist in all three species and as it has a considerable effect on visual processing, more research would be needed to understand mechanisms underlying this relation. Further there is a need to map the location of this protein, as several studies indicate a role in the retina. In this thesis LRRK2 is either knocked out or inhibited. PD is primarily associated with increased activity of LRRK2, therefore it would be relevant to investigate if these modulations cause similar changes in visual processing. This would be promising for the development of a trans-species biomarker spanning from *Drosophila*, via rodents to humans.

The AAV-model shows a potential as a future way of modelling early PD, which could be an additional tool in the toolbox for developing neuroprotective strategies to modify the course of PD in the human condition.

There is still a problem with the biomarkers not being unique to PD, therefore functional profiling of the effects of multiple potential biomarkers may pave the way for early diagnosis of PD. As LRRK2 has the specificity of PD, and SSVEP seems to have the sensitivity that has been missing, so the combination of these two may be ideal to diagnose LRRK2-related PD early. Further, the combination may prove useful in the development of neuroprotective strategies to be used in PD. Though the LRRK2-kinase inhibition is considered to have a great potential, more specificity is warranted, both in terms of tissue specificity and efficacy. A potential to overcome this may arise from the field RNA interference rather than small molecule inhibitors.

References

10 References

[1] T. Pringsheim, N. Jette, A. Frolkis, and T. D. L. Steeves, "Prevalence of Parkinson's disease: A systematic review and meta-analysis," *Mov. Disord.*, vol. 29, no. 13, pp. 1583–1590, 2014.

[2] J. Parkinson, "An Essay on the Shaking Palsy (Originally published in 1817)," *J. Neuropsychiatr.*, vol. 14, no. 2, pp. 223–236, 2002.

[3] M. H. Polymeropoulos *et al.*, "Mapping of a Gene for Parkinson ' s Disease to Chromosome 4q21-q23," *Science (80-.).*, vol. 274, no. 5290, pp. 1197–1199, 1996.

[4] C. Klein and A. Westenberger, "Genetics of Parkinson's Disease," *Cold Spring Habor Perspect. Med.*, vol. 2, pp. 1–15, 2012.

[5] A. J. Noyce, A. J. Lees, and A.-E. Schrag, "The prediagnostic phase of Parkinson's disease," *J. Neurol. Neurosurg. Psychiatry*, vol. 87, no. 8, pp. 871–878, 2016.

[6] J. A. Obeso *et al.*, "Past, Present, and Future of Parkinson's Disease: A Special Essay on the 200th Anniversary of the Shaking Palsy," *Mov. Disord.*, vol. 32, no. 9, pp. 1264–1310, 2017.

[7] Y. Liu *et al.*, "Improvement of Deep Brain Stimulation in Dyskinesia in Parkinson's Disease: A Meta-Analysis," *Front. Neurol.*, vol. 10, no. February, pp. 1–8, 2019.

[8] P. Mahlknecht, K. Seppi, and W. Poewe, "The concept of prodromal Parkinson's disease," *J. Parkinsons. Dis.*, vol. 5, no. 4, pp. 681–697, 2015.

[9] M. Ansari, F. Rahmani, M. Dolatshahi, A. Pooyan, and M. H. Aarabi, "Brain pathway differences between Parkinson's disease patients with and without REM sleep behavior disorder," *Sleep Breath.*, vol. 21, no. 1, pp. 155–161, 2017.

[10] J. Kaye, H. Gage, A. Kimber, L. Storey, and P. Trend, "Excess burden of constipation in Parkinson's disease: A pilot study," *Mov. Disord.*, vol. 21, no. 8, pp. 1270–1273, 2006.

[11] N. Visanji and C. Marras, "The relevance of pre-motor symptoms in Parkinson's disease," *Expert Rev. Neurother.*, vol. 15, no. 10, pp. 1205–1217, 2015.

[12] C. Fearon, J. S. Butler, L. Newman, T. Lynch, and R. B. Reilly, "Audiovisual processing is abnormal in Parkinson's disease and correlates with Freezing of Gait and Disease Duration," *J. Parkinsons. Dis.*, vol. 5, no. 4, pp. 925–936, 2015.

[13] R. B. Postuma, J.-F. Gagnon, M. Vendette, C. Desjardins, and J. Y. Montplaisir, "Olfaction and color vision identify impending neurodegeneration in rapid eye movement sleep behavior disorder," *Ann. Neurol.*, vol. 69, no. 5, pp. 811–818, 2011.

[14] R. A. Armstrong, "Oculo-visual dysfunction in Parkinson's disease," *J. Parkinsons. Dis.*, vol. 5, no. 4, pp. 715–726, 2015.

[15] A. E. Lang and A. J. Espay, "Disease Modification in Parkinson's Disease: Current Approaches, Challenges, and Future Considerations," *Mov. Disord.*, vol. 33, no. 5, pp. 660–677, 2018.

[16] L. S. Shihabuddin, P. Brundin, J. T. Greenamyre, D. Stephenson, and S. P. Sardi, "New Frontiers in Parkinson's Disease: From Genetics to the Clinic," *J. Neurosci.*, vol. 38, no. 44, pp. 9375–9382, 2018.

[17] M. Stephenson-Jones *et al.*, "A basal ganglia circuit for evaluating action outcomes," *Nature*, vol. 539, no. 7628, pp. 289–293, 2016.

[18] N. Yanagisawa, "Review Functions and dysfunctions of the basal ganglia in humans," *Proc. Jpn. Acad., Ser. B*, vol. 94, no. 7, pp. 275–304, 2018.

[19] A. B. Nelson and A. C. Kreitzer, "Reassessing Models of Basal Ganglia Function and Dysfunction," *Annu. Rev. Neurosci.*, vol. 37, pp. 117–135, 2014.

[20] A. Galvan and T. Wichmann, "Pathophysiology of Parkinsonism," *Clin. Neurophysiol.*, vol. 119, no. 7, pp. 1459–1474, 2008.

[21] J. Obeso *et al.*, "Pathophysiology of the basal ganglia in Parkinson ' s disease," *Trends Neurosci.*, vol. 23, no. 10, pp. S8–S19, 2000.

[22] D. J. Ellens and D. K. Leventhal, "Electrophysiology of basal ganglia and cortex in models of parkinson disease," *J. Parkinsons. Dis.*, vol. 3, no. 3, pp. 241–254, 2013.

[23] S. Lehéricy, E. Bardinet, C. Poupon, M. Vidailhet, and C. François, "7 tesla magnetic resonance imaging: A closer look at substantia nigra anatomy in Parkinson's disease," *Mov. Disord.*, vol. 29, no. 13, pp. 1574–1581, 2014.

[24] G. Di Giovanni, V. Di Matteo, and E. Esposito, Eds., *Birth, Life and Death of Dopaminergic Neurons in the Substantia Nigra*, Supplement. Journal of Neural Transmission, 2009.

[25] J. Tepper, L. Martin, and D. Anderson, "GABAA receptor-mediated inhibition of rat substantia nigra

dopaminergic neurons by pars reticulata projection neurons," *J. Neurosci.*, vol. 15, no. 4, pp. 3092–3103, 1995.
[26] H. Braak, K. Del Tredici, U. Rüb, R. A. I. De Vos, E. N. H. Jansen Steur, and E. Braak, "Staging of brain pathology related to sporadic Parkinson's disease," *Neurobiol. Aging*, vol. 24, no. 2, pp. 197–211, 2003.
[27] A. Mulak and B. Bonaz, "Brain-gut-microbiota axis in Parkinson's disease," *World J. Gastroenterol.*, vol. 21, no. 37, pp. 10609–10620, 2015.
[28] H. Braak, R. A. I. De Vos, J. Bohl, and K. Del Tredici, "Gastric α-synuclein immunoreactive inclusions in Meissner's and Auerbach's plexuses in cases staged for Parkinson's disease-related brain pathology," *Neurosci. Lett.*, vol. 396, no. 1, pp. 67–72, 2006.
[29] M. G. Spillantini, M. L. Schmidt, V. M.-Y. L. Lee, J. Q. Trojanowski, R. Jakes, and M. Goedert, "Alpha-Synuclein in Lewy bodies Lewy," *Nature*, vol. 388, no. 28 August, pp. 839–840, 1997.
[30] P. Brundin and R. Melki, "Prying into the Prion Hypothesis for Parkinson's Disease," *J. Neurosci.*, vol. 37, no. 41, pp. 9808–9818, 2017.
[31] M. Polymenidou and D. W. Cleveland, "Prion-like spread of protein aggregates in neurodegeneration: Figure 1.," *J. Exp. Med.*, vol. 209, no. 5, pp. 889–893, 2012.
[32] S. George, N. L. Rey, N. Reichenbach, J. A. Steiner, and P. Brundin, "α-Synuclein: The long distance runner," *Brain Pathol.*, vol. 23, no. 3, pp. 350–357, 2013.
[33] D. J. Surmeier, J. A. Obeso, and G. M. Halliday, "Parkinson's Disease Is Not Simply a Prion Disorder," *J. Neurosci.*, vol. 37, no. 41, pp. 9799–9807, 2017.
[34] J. Brás, R. Guerreiro, and J. Hardy, "SnapShot: Genetics of Parkinson's disease," *Cell*, vol. 160, no. 3, p. 570–570.e1, 2015.
[35] A. Puschmann, "Monogenic Parkinson's disease and parkinsonism: Clinical phenotypes and frequencies of known mutations," *Park. Relat. Disord.*, vol. 19, no. 4, pp. 407–415, 2013.
[36] S. Baltic *et al.*, "A-Synuclein Is Expressed in Different Tissues During Human Fetal Development," *J. Mol. Neurosci.*, vol. 22, no. 3, pp. 199–203, 2004.
[37] I. Rodriguez-Leyva *et al.*, "The Presence of Alpha-Synuclein in Skin from Melanoma and Patients with Parkinson's Disease," *Mov. Disord. Clin. Pract.*, vol. 4, no. 5, pp. 724–732, 2017.
[38] L. Maroteaux, J. T. Campanelli, and R. H. Scheller, "Synuclein: A Neuron-Specific Protein Localized to the Nucleus and Presynaptic Nerve Terminal," *J. Neurosci.*, vol. 8, no. 8, pp. 2804–2815, 1988.
[39] M. Decressac *et al.*, "Alpha-Synuclein Produces Early Behavioral Alterations via Striatal Cholinergic Synaptic Dysfunction by Interacting With GluN2D N -Methyl-D-Aspartate Receptor Subunit," *Biol. Psychiatry*, vol. 79, no. 5, pp. 402–414, 2015.
[40] M. Emanuele and E. Chieregatti, "Mechanisms of alpha-synuclein action on neurotransmission: Cell-autonomous and non-cell autonomous role," *Biomolecules*, vol. 5, no. 2, pp. 865–892, 2015.
[41] T. S. Ulmer, A. Bax, N. B. Cole, and R. L. Nussbaum, "Structure and dynamics of micelle-bound human α-synuclein," *J. Biol. Chem.*, vol. 280, no. 10, pp. 9595–9603, 2005.
[42] L. Stefanis, "Alpha synuclein in parkinson's disease," *Cold Spring Habor Perspect. Med.*, vol. 4, p. a009399, 2012.
[43] D. J. Busch *et al.*, "Acute increase of -synuclein inhibits synaptic vesicle recycling evoked during intense stimulation," *Mol. Biol. Cell*, vol. 25, no. 24, pp. 3926–3941, 2014.
[44] J. Burré, M. Sharma, and T. C. Südhof, "Cell Biology and Pathophysiology of α-Synuclein Jacqueline," *Cold Spring Habor Perspect. Med.*, vol. 8, p. a024091, 2018.
[45] A. Atik, T. Stewart, and J. Zhang, "Alpha-Synuclein as a Biomarker for Parkinson's Disease," *Brain Pathol.*, vol. 26, no. 3, pp. 410–418, 2016.
[46] U. J. Kang *et al.*, "Comparative study of cerebrospinal fluid α-synuclein seeding aggregation assays for diagnosis of Parkinson's disease," *Mov. Disord.*, pp. 1–9, 2019.
[47] R. Krüger *et al.*, "AlaSOPro mutation in the gene encoding α-synuclein in Parkinson's disease," *Nat. Genet.*, vol. 18, no. 2, pp. 106–108, 1998.
[48] M. H. Polymeropoulos *et al.*, "Mutation in the alpha-Synuclein Gene Identified in Families with Parkinson ' s Disease," *Science (80-.).*, vol. 276, no. June, pp. 2045–2048, 1997.
[49] A. B. Singleton *et al.*, "α-Synuclein Locus Triplication Causes Parkinson's Disease," *Science (80-.).*, vol. 302, no. 5646, p. 841 LP-841, Oct. 2003.
[50] N. L. Rey *et al.*, "Widespread transneuronal propagation of α-synucleinopathy triggered in olfactory bulb mimics prodromal Parkinson's disease," *J. Exp. Med.*, vol. 213, no. 9, pp. 1759–1778, 2016.
[51] B. I. Giasson *et al.*, "Oxidative Damage Linked to Neurodegeneration by Selective alpha -Synuclein Nitration in Synucleinopathy Lesions," *Science*, vol. 290, no. 5493, pp. 985–989, 2000.
[52] R. Hodara *et al.*, "Functional Consequences of α-Synuclein Tyrosine Nitration," *J. Biol. Chem.*, vol. 279, no.

46, pp. 47746–47753, 2004.
[53] K.-W. Lee *et al.*, "Enhanced Phosphatase Activity Attenuates -Synucleinopathy in a Mouse Model," *J. Neurosci.*, vol. 31, no. 19, pp. 6963–6971, 2011.
[54] J. Tolö *et al.*, "Pathophysiological Consequences of Neuronal α-Synuclein Overexpression: Impacts on Ion Homeostasis, Stress Signaling, Mitochondrial Integrity, and Electrical Activity," *Front. Mol. Neurosci.*, vol. 11, no. March, pp. 1–21, 2018.
[55] J. Levin *et al.*, "Generation of ferric iron links oxidative stress to α-synuclein oligomer formation," *J. Parkinsons. Dis.*, vol. 1, no. 2, pp. 205–216, 2011.
[56] X. Lin *et al.*, "Leucine-Rich Repeat Kinase 2 Regulates the Progression of Neuropathology Induced by Parkinson's-Disease-Related Mutant α-synuclein," *Neuron*, vol. 64, no. 6, pp. 807–827, 2009.
[57] J. Xu, S.-Y. Kao, F. J. S. Lee, W. Song, L.-W. Jin, and B. A. Yankner, "Dopamine-dependent neurotoxicity of α-synuclein: A mechanism for selective neurodegeneration in Parkinson disease," *Nat. Med.*, vol. 8, no. 6, pp. 600–606, 2002.
[58] Jin Xu, Shyan-Yuan Kao, Frank J.S. Lee, Weihong Song, Lee-Way Jin &, and Bruce A. Yankner, "Dopamine-dependent neurotoxicity of α-synuclein: A mechanism for selective neurodegeneration in Parkinson disease," *Nat. Med.*, vol. 8, no. 6, pp. 600–606, 2002.
[59] T. Logan, J. Bendor, C. Toupin, K. Thorn, and R. H. Edwards, "α-Synuclein promotes dilation of the exocytotic fusion pore," *Nat. Neurosci.*, vol. 20, no. 5, pp. 681–689, 2017.
[60] H. Niu *et al.*, "Alpha-synuclein overexpression in the olfactory bulb initiates prodromal symptoms and pathology of Parkinson's disease," *Transl. Neurodegener.*, vol. 7, no. 1, pp. 1–17, 2018.
[61] M. F. Chesselet, "In vivo alpha-synuclein overexpression in rodents: A useful model of Parkinson's disease?," *Exp. Neurol.*, vol. 209, no. 1, pp. 22–27, 2008.
[62] O. S. Gorbatyuk *et al.*, "α-synuclein expression in rat substantia nigra suppresses phospholipase D2 toxicity and nigral neurodegeneration," *Mol. Ther.*, vol. 18, no. 10, pp. 1758–1768, 2010.
[63] M. Decressac, B. Mattsson, M. Lundblad, P. Weikop, and A. Björklund, "Progressive neurodegenerative and behavioural changes induced by AAV-mediated overexpression of α-synuclein in midbrain dopamine neurons," *Neurobiol. Dis.*, vol. 45, no. 3, pp. 939–953, 2012.
[64] L. A. Volpicelli-Daley, D. Kirik, L. E. Stoyka, D. G. Standaert, and A. S. Harms, "How can rAAV-α-synuclein and the fibril α-synuclein models advance our understanding of Parkinson's disease?," *J. Neurochem.*, vol. 139, pp. 131–155, 2016.
[65] M. A. Andersen *et al.*, "Parkinson's disease-like burst firing activity in subthalamic nucleus induced by AAV-α-synuclein is normalized by LRRK2 modulation," *Neurobiol. Dis.*, vol. 116, no. April, pp. 13–27, 2018.
[66] W. Dauer and S. Przedborski, "Parkinson's disease: Mechanisms and models," *Neuron*, vol. 39, no. 6, pp. 889–909, 2003.
[67] A. Van der Perren, C. Van den Haute, and V. Baekelandt, "Viral Vector-Based Models of Parkinson's Disease," in *Behavioral Neurobiology of Huntington's Disease and Parkinson's Disease*, H. H. P. Nguyen and M. A. Cenci, Eds. Berlin, Heidelberg: Springer Berlin Heidelberg, 2015, pp. 271–301.
[68] C. Wang *et al.*, "Penetrance of LRRK2 G2385R and R1628P is modified by common PD-associated genetic variants," *Park. Relat. Disord.*, vol. 18, no. 8, pp. 958–963, 2012.
[69] D. G. Healy *et al.*, "Phenotype, genotype, and worldwide genetic penetrance of LRRK2-associated Parkinson's disease: a case-control study," *Lancet Neurol.*, vol. 7, no. 7, pp. 583–590, 2008.
[70] M. A. S. Baptista *et al.*, "Loss of leucine-rich repeat kinase 2 (LRRK2) in rats leads to progressive abnormal phenotypes in peripheral organs," *PLoS One*, vol. 8, no. 11, pp. 1–16, 2013.
[71] C. Schulz *et al.*, "Leucine-rich repeat kinase 2 modulates retinoic acid-induced neuronal differentiation of murine embryonic stem cells," *PLoS One*, vol. 6, no. 6, 2011.
[72] P. Davies *et al.*, "Comprehensive characterization and optimization of anti-LRRK2 (leucine-rich repeat kinase 2) monoclonal antibodies," *Biochem. J.*, vol. 453, no. 1, pp. 101–113, 2013.
[73] N. Dzamko *et al.*, "LRRK2 levels and phosphorylation in Parkinson's disease brain and cases with restricted Lewy bodies," *Mov. Disord.*, vol. 32, no. 3, pp. 423–432, 2017.
[74] A. Zimprich *et al.*, "Mutations in LRRK2 Cause Autosomal-Dominant Parkinsonism with Pleomorphic Pathology families, we have found six disease-segregating muta- tions (five missense and one putative splice site muta- tion) in a gene encoding a large, multifunctional pro- kinase," *Neuron*, vol. 44, pp. 601–607, 2004.
[75] M. Steger *et al.*, "Phosphoproteomics reveals that Parkinson's disease kinase LRRK2 regulates a subset of Rab GTPases," *Elife*, vol. 5, pp. 1–28, 2016.
[76] K. Thirstrup *et al.*, "Selective LRRK2 kinase inhibition reduces phosphorylation of endogenous Rab10 and Rab12 in human peripheral mononuclear blood cells," *Sci. Rep.*, vol. 7, no. 1, pp. 1–18, 2017.

[77] P. N. Gandhi, X. Wang, X. Zhu, S. G. Chen, and A. L. Wilson-Delfosse, “The Roc domain of leucine-rich repeat kinase 2 is sufficient for interaction with microtubules,” *J. Neurosci. Res.*, vol. 86, no. 8, pp. 1711–1720, 2008.
[78] J. Schapansky, J. D. Nardozzi, and M. J. Lavoie, “The complex relationships between microglia, alpha-synuclein, and LRRK2 in Parkinson’s disease,” *Neuroscience*, vol. 302, pp. 74–88, 2015.
[79] D. A. Roosen and M. R. Cookson, “LRRK2 at the interface of autophagosomes, endosomes and lysosomes,” *Mol. Neurodegener.*, vol. 11, no. 1, pp. 1–10, 2016.
[80] P. Rivero-Ríos *et al.*, “Alterations in late endocytic trafficking related to the pathobiology of LRRK2-linked Parkinson’s disease,” *Biochem. Soc. Trans.*, vol. 43, no. 3, pp. 390–395, 2015.
[81] C. J. Gloeckner *et al.*, “Phosphopeptide analysis reveals two discrete clusters of phosphorylation in the N-terminus and the Roc domain of the Parkinson-disease associated protein kinase LRRK2,” *J. Proteome Res.*, vol. 9, no. 4, pp. 1738–1745, 2010.
[82] J. Schapansky, J. D. Nardozzi, F. Felizia, and M. J. LaVoie, “Membrane recruitment of endogenous LRRK2 precedes its potent regulation of autophagy,” *Hum. Mol. Genet.*, vol. 23, no. 16, pp. 4201–4214, 2014.
[83] H. Y. Heo, J. M. Park, C. H. Kim, B. S. Han, K. S. Kim, and W. Seol, “LRRK2 enhances oxidative stress-induced neurotoxicity via its kinase activity,” *Exp. Cell Res.*, vol. 316, no. 4, pp. 649–656, 2010.
[84] N. Dzamko *et al.*, “Inhibition of LRRK2 kinase activity leads to dephosphorylation of Ser 910 /Ser 935 , disruption of 14-3-3 binding and altered cytoplasmic localization,” *Biochem. J.*, vol. 430, no. 3, pp. 405–413, 2010.
[85] R. J. Nichols *et al.*, “14-3-3 binding to LRRK2 is disrupted by multiple Parkinson’s disease-associated mutations and regulates cytoplasmic localization,” *Biochem. J.*, vol. 430, no. 3, pp. 393–404, 2010.
[86] X. Li *et al.*, “Phosphorylation-dependent 14-3-3 binding to LRRK2 is impaired by common mutations of familial parkinson’s disease,” *PLoS One*, vol. 6, no. 3, pp. 1–13, 2011.
[87] K. B. Fraser *et al.*, “LRRK2 secretion in exosomes is regulated by 14-3-3,” *Hum. Mol. Genet.*, vol. 22, no. 24, pp. 4988–5000, 2013.
[88] J. P. L. Daher, L. A. Volpicelli-Daley, J. P. Blackburn, M. S. Moehle, and A. B. West, “Abrogation of -synuclein-mediated dopaminergic neurodegeneration in LRRK2-deficient rats,” *Proc. Natl. Acad. Sci.*, vol. 111, no. 25, pp. 9289–9294, 2014.
[89] J. P. L. Daher *et al.*, “Leucine-rich repeat kinase 2 (LRRK2) pharmacological inhibition abates α-synuclein gene-induced neurodegeneration,” *J. Biol. Chem.*, vol. 290, no. 32, pp. 19433–19444, 2015.
[90] T. Botta-Orfila *et al.*, “Age at onset in LRRK2-associated PD is modified by SNCA variants,” *J. Mol. Neurosci.*, vol. 48, no. 1, pp. 245–247, 2012.
[91] P. Cohen and D. R. Alessi, “Kinase Drug Discovery – What ’ s Next in the Field ?,” *ACS Chem. Biol.*, vol. 8, no. 1, pp. 96–104, 2013.
[92] J.-M. Taymans and E. Greggio, “LRRK2 Kinase Inhibition as a Therapeutic Strategy for Parkinson’s Disease, Where Do We Stand?,” *Curr. Neuropharmacol.*, vol. 14, no. 3, pp. 214–25, 2016.
[93] M. A. Andersen *et al.*, “PFE-360-induced LRRK2 inhibition induces reversible, non-adverse renal changes in rats,” *Toxicology*, vol. 395, no. December 2017, pp. 15–22, 2018.
[94] M. C. Herzig *et al.*, “LRRK2 protein levels are determined by kinase function and are crucial for kidney and lung homeostasis in mice,” *Hum. Mol. Genet.*, vol. 20, no. 21, pp. 4209–4223, 2011.
[95] C. D. Gilbert, “Intermediate-Level Visual Processing and Visual Primitives,” in *The Principles of Neural Science*, 5th ed., E. R. Kandel, J. H. Schwartz, T. H. Jessell, S. A. Siegelbaum, and A. J. Hudspeth, Eds. McGraw-Hill Companies, 2013, pp. 602–620.
[96] C. Owsley, D. Ghate, and S. Kedar, “Vision and aging,” *Annu. Rev. Vis. Sci.*, vol. 2, pp. 255–271, 2016.
[97] I. Bodis-Wollner and M. D. Yahr, “Measurements of visual evoked potentials in Parkinson’s disease.,” *Brain*, vol. 101, no. 4, pp. 661–71, 1978.
[98] C. Bulens, J. D. Meerwaldt, G. J. Van der Wildt, and J. B. P. Van Deursen, “Effect of levodopa treatment on contrast sensitivity in Parkinson’s disease,” *Ann. Neurol.*, vol. 22, no. 3, pp. 365–369, 1987.
[99] J. Birch, R. U. Kolle, M. Kunkel, W. Paulus, and P. Upadhyay, “Acquired colour deficiency in patients with Parkinson’s disease,” *Vision Res.*, vol. 38, no. 21, pp. 3421–3426, 1998.
[100] V. Pieri, N. J. Diederich, R. Raman, and C. G. Goetz, “Decreased color discrimination and contrast sensitivity in Parkinson’s disease,” *J. Neurol. Sci.*, vol. 172, no. 1, pp. 7–11, 2000.
[101] I. Bodis-Wollner, “Foveal vision is impaired in Parkinson’s disease,” *Park. Relat. Disord.*, vol. 19, no. 1, pp. 1–14, 2013.
[102] A. I. Garcia-Diaz *et al.*, “Structural Brain Correlations of Visuospatial and Visuoperceptual Tests in Parkinson’s Disease,” *J. Int. Neuropsychol. Soc.*, vol. 24, no. 1, pp. 33–44, 2018.
[103] M. Price, R. G. Feldman, D. Adelberg, and H. Kayne, “Abnormalities in Color Vision and Contrast Sensitivity

in Parkinson's Disease," *Neurology*, vol. 42, no. April, pp. 887–890, 1992.
[104] J. R. Heckenlively and G. B. Arden, Eds., *Principles and Practice of Clinical Electrophysiology of Vision*, 2nd ed. The MIT press, 2006.
[105] T. Baden, P. Berens, K. Franke, M. Román Rosón, M. Bethge, and T. Euler, "The functional diversity of retinal ganglion cells in the mouse," *Nature*, vol. 529, no. 7586, pp. 345–350, 2016.
[106] R. H. Masland, "The Neuronal Organization of the Retina," *Neuron*, vol. 76, no. 2, pp. 266–280, 2012.
[107] R. H. Masland, "The tasks of amacrine cells," *Vis. Neurosci.*, vol. 29, no. 01, pp. 3–9, 2012.
[108] V. Pérez-Fernández *et al.*, "Rod Photoreceptor Activation Alone Defines the Release of Dopamine in the Retina," *Curr. Biol.*, vol. 29, no. March 4, pp. 763–774, 2019.
[109] T. Munteanu, K. J. Noronha, A. C. Leung, S. Pan, J. A. Lucas, and T. M. Schmidt, "Light-dependent pathways for dopaminergic amacrine cell development and function," *Elife*, vol. 7, pp. 1–10, 2018.
[110] B. Nowacka, W. Lubiński, K. Honczarenko, A. Potemkowski, and K. Safranow, "Bioelectrical function and structural assessment of the retina in patients with early stages of Parkinson's disease (PD)," *Doc. Ophthalmol.*, vol. 131, no. 2, pp. 95–104, 2015.
[111] J. T. Hutton, J. L. Morris, and J. W. Elias, "Levodopa Improves Spatial Contrast Sensitivity in Parkinson ' s Disease," *Arch Neurol*, vol. 50, pp. 721–724, 1993.
[112] N. M. Roth *et al.*, "Photoreceptor layer thinning in idiopathic Parkinson's disease," *Mov. Disord.*, vol. 29, no. 9, pp. 1163–1170, 2014.
[113] F. Afsari *et al.*, "Abnormal visual gain control in a Parkinson's disease model," *Hum. Mol. Genet.*, vol. 23, no. 17, pp. 4465–4478, 2014.
[114] C. Marras *et al.*, "Phenotype in parkinsonian and nonparkinsonian LRRK2 G2019S mutation carriers," *Neurology*, vol. 77, no. 4, pp. 325–333, 2011.
[115] A. U. Brandt, H. G. Zimmermann, T. Oberwahrenbrock, J. Isensee, T. Müller, and F. Paul, "Self - perception and determinants of color vision in Parkinson ' s disease," *J. Neural Transm.*, vol. 125, no. 2, pp. 145–152, 2018.
[116] I. Bodis-Wollner, P. B. Kozlowski, S. Glazman, and S. Miri, "a-Synuclein in the Inner Retina in Parkinson Disease," *Ann. Neurol.*, vol. 75, no. 6, pp. 964–966, 2014.
[117] L. Veys *et al.*, "Retinal α-synuclein deposits in Parkinson's disease patients and animal models," *Acta Neuropathol.*, vol. 137, no. 3, pp. 379–395, 2019.
[118] S. J. Hindle and C. J. H. Elliott, "Spread of neuronal degeneration in a dopaminergic, Lrrk-G2019S model of Parkinson disease," *Autophagy*, vol. 9, no. 6, pp. 936–938, 2013.
[119] G. L. Willis, C. Moore, and S. M. Armstrong, "Parkinson's disease, lights and melanocytes: Looking beyond the retina," *Sci. Rep.*, vol. 4, no. 3921, pp. 1–10, 2014.
[120] A. J. Sefton, B. Dreher, A. R. Harvey, and P. R. Martin, *Visual System*. 2014.
[121] M. A. Basso and P. J. May, "Circuits for Action and Cognition: A View from the Superior Colliculus," *Annu. Rev. Vis. Sci.*, vol. 15, no. 3, pp. 197–226, 2017.
[122] N. Sahibzada, P. Dean, and P. Redgrave, "Movements resembling orientation or avoidance elicited by electrical stimulation of the superior colliculus in rats.," *J. Neurosci.*, vol. 6, no. 3, pp. 723–33, 1986.
[123] M. Rolland, C. Carcenac, P. G. Overton, M. Savasta, and V. Coizet, "Enhanced visual responses in the superior colliculus and subthalamic nucleus in an animal model of Parkinson's disease," *Neuroscience*, vol. 252, pp. 277–288, 2013.
[124] G. D. R. Watson, J. B. Smith, and K. D. Alloway, "The Zona Incerta Regulates Communication between the Superior Colliculus and the Posteromedial Thalamus : Implications for Thalamic Interactions with the Dorsolateral Striatum," *J. Neurosci.*, vol. 35, no. 25, pp. 9463–9476, 2015.
[125] E. Comoli *et al.*, "A direct projection from superior colliculus to substantia nigra for detecting salient visual events," *Nat. Neurosci.*, vol. 6, no. 9, pp. 974–980, 2003.
[126] M. Takada, Z. K. Li, and T. Hattori, "Dopaminergic nigrotectal projection in the rat," *Brain Res.*, vol. 457, no. 1, pp. 165–168, 1988.
[127] O. Hikosaka, K. Nakamura, and H. Nakahara, "Basal Ganglia Orient Eyes to Reward," *J. Neurophysiol.*, vol. 95, no. 2, pp. 567–584, 2006.
[128] D. Erskine *et al.*, "Neuronal Loss and A-Synuclein Pathology in the Superior Colliculus and Its Relationship to Visual Hallucinations in Dementia with Lewy Bodies," *Am. J. Geriatr. Psychiatry*, vol. 25, no. 6, pp. 595–604, 2017.
[129] G. Buzsáki, *Rhythms of the Brain*, 1st ed. New York: Oxford University Press Inc., 2006.
[130] G. Buzsáki, C. A. Anastassiou, and C. Koch, "The origin of extracellular fields and currents — EEG, ECoG, LFP and spikes," *Nat. Rev. Neurosci.*, vol. 13, no. 6, pp. 407–420, 2012.
[131] S. J. Luck, *An Introduction to the Event-Related Potential Technique*, 1st ed. MIT press, 2005.

[132] P. Sauseng, W. Klimesch, W. R. Gruber, S. Hanslmayr, R. Freunberger, and M. Doppelmayr, "Are event-related potential components generated by phase resetting of brain oscillations? A critical discussion," *Neuroscience*, vol. 146, no. 4, pp. 1435–1444, 2007.
[133] S. Makeig *et al.*, "Dynamic brain sources of visual evoked responses," *Science (80-.).*, vol. 295, no. January, pp. 690–694, 2002.
[134] J. A. Goldberg, U. Rokni, T. Boraud, E. Vaadia, and H. Bergman, "Spike Synchronization in the Cortex-Basal Ganglia Networks of Parkinsonian Primates Reflects Global Dynamics of the Local Field Potentials," *J. Neurosci.*, vol. 24, no. 25, pp. 6003–6010, 2004.
[135] D. J. Creel, "Visually Evoked Potentials," in *The Organization of the Retina and Visual System*, 2012, pp. 1–28.
[136] Y. Iwamura, Y. Fujii, and C. Kamei, "The effects of certain H1-antagonists on visual evoked potential in rats," *Brain Res. Bull.*, vol. 61, no. 4, pp. 393–398, 2003.
[137] Y. You, A. Klistorner, J. Thie, and S. L. Graham, "Improving reproducibility of VEP recording in rats: Electrodes, stimulus source and peak analysis," *Doc. Ophthalmol.*, vol. 123, no. 2, pp. 109–119, 2011.
[138] D. Creel, R. E. Dustman, and E. C. Beck, "Intensity of flash illumination and the visually evoked potential of rats, guinea pigs and cats," *Vision Res.*, vol. 14, no. 8, pp. 725–729, 1974.
[139] H. K. M. Meeren, E. L. J. M. Van Luijtelaar, and A. M. L. Coenen, "Cortical and thalamic visual evoked potentials during sleep-wake states and spike-wave discharges in the rat," *Electroencephalogr. Clin. Neurophysiol. - Evoked Potentials*, vol. 108, no. 3, pp. 306–319, 1998.
[140] M. Onofrj, C. Harnois, and I. Bodis-Wollner, "The hemispheric distribution of the transient rat VEP: a comparison of flash and pattern stimulation," *Exp. Brain Res.*, vol. 59, no. 3, pp. 427–433, 1985.
[141] M. Onofrj, M. F. Ghilardi, M. Basciani, and D. Gambi, "Visual evoked potentials in parkinsonism and dopamine blockade reveal a stimulus-dependent dopamine function in humans.," *J. Neurol. Neurosurg. Psychiatry*, vol. 49, no. 10, pp. 1150–1159, 1986.
[142] S. Miri, S. Glazman, L. Mylin, and I. Bodis-Wollner, "A combination of retinal morphology and visual electrophysiology testing increases diagnostic yield in Parkinson's disease," *Park. Relat. Disord.*, vol. 22, pp. S134–S137, 2016.
[143] L. B. Quagliato, C. Domingues, E. M. A. B. Quagliato, E. B. de Abreu, and N. Kara-Junior, "Applications of visual evoked potentials and fourier-domain optical coherence tomography in Parkinson's disease: A controlled study," *Arq. Bras. Oftalmol.*, vol. 77, no. 4, pp. 238–242, 2014.
[144] S. Calzetti, a Franchi, G. Taratufolo, and E. Groppi, "Simultaneous VEP and PERG investigations in early Parkinson's disease.," *J. Neurol. Neurosurg. Psychiatry*, vol. 53, no. 2, pp. 114–117, 1990.
[145] A. Tartaglione, N. Pizio, G. Bino, L. Spadavecchia, and E. Favale, "VEP changes in Parkinson's disease are stimulus dependent.," *J. Neurol. Neurosurg. Psychiatry*, vol. 47, no. 3, pp. 305–307, 1984.
[146] I. Bodis-Wollner, M. D. Yahr, L. Mylin, and J. Thornton, "Dopaminergic deficiency causes delayed visual evoked potentials in rats," *Ann. Neurol.*, vol. 11, no. 5, pp. 478–483, 1982.
[147] C. Liu, Y. Zhang, W. Tang, B. Wang, B. Wang, and S. He, "Evoked potential changes in patients with Parkinson's disease," *Brain Behav.*, vol. 7, no. 5, p. e00703, 2017.
[148] G. Özmüş *et al.*, "Demonstration of early cognitive impairment in Parkinson's disease with visual p300 responses," *Noropsikiyatri Ars.*, vol. 54, no. 1, pp. 21–27, 2017.
[149] S. He *et al.*, "Meta-Analysis of Visual Evoked Potential and Parkinson's Disease," *Parkinsons. Dis.*, vol. 2018, pp. 1–8, 2018.
[150] E. Cubo *et al.*, "Lack of association of morphologic and functional retinal changes with motor and non-motor symptoms severity in Parkinson's disease," *J. Neural Transm.*, vol. 121, no. 2, pp. 139–145, 2014.
[151] P. Xu *et al.*, "Cortical network properties revealed by SSVEP in anesthetized rats," *Sci. Rep.*, vol. 3, pp. 1–11, 2013.
[152] C. S. Herrmann, "Human EEG responses to 1-100 Hz flicker: Resonance phenomena in visual cortex and their potential correlation to cognitive phenomena," *Exp. Brain Res.*, vol. 137, no. 3–4, pp. 346–353, 2001.
[153] F. B. Vialatte, M. Maurice, J. Dauwels, and A. Cichocki, "Steady-state visually evoked potentials: Focus on essential paradigms and future perspectives," *Prog. Neurobiol.*, vol. 90, no. 4, pp. 418–438, 2010.
[154] D. Regan, *Human Brain Electrophysiology: Evoked Potentials and Evoked Magnetic Fields in Science and Medicine*. New York: Elsevier Science Publishing Co., Inc., 1989.
[155] M. Labecki, R. Kus, A. Brzozowska, T. Stacewicz, B. S. Bhattacharya, and P. Suffczynski, "Nonlinear Origin of SSVEP Spectra—A Combined Experimental and Modeling Study," *Front. Comput. Neurosci.*, vol. 10, no. December, pp. 1–10, 2016.
[156] P. Lennie and V. H. Perry, "Spatial contrast sensitivity of cells in the lateral geniculate nucleus of the rat.," *J. Physiol.*, vol. 315, no. 1, pp. 69–79, 1981.

[157] A. M. Norcia, L. G. Appelbaum, J. M. Ales, B. R. Cottereau, and B. Rossion, “The steady-state visual evoked potential in vision research: A review,” *J. Vis.*, vol. 15, no. 6, p. (4); 1-46, 2015.
[158] A. Capilla, P. Pazo-Alvarez, A. Darriba, P. Campo, and J. Gross, “Steady-state visual evoked potentials can be explained by temporal superposition of transient event-related responses,” *PLoS One*, vol. 6, no. 1, 2011.
[159] C. Westbrook, C. K. Roth, and J. Talbot, *MRI in Practice*, 4th ed. Wiley-Blackwell, 2011.
[160] U. Saeed *et al.*, “Imaging biomarkers in Parkinson’s disease and Parkinsonian syndromes: current and emerging concepts,” *Transl. Neurodegener.*, vol. 6, no. 1, p. 8, 2017.
[161] Y. Zhao, X. Zheng, Q. Wang, J. Xu, X. Xu, and M. Zhang, “Altered activation in visual cortex: unusual functional magnetic resonance imaging finding in early Parkinson’s disease.,” *J. Int. Med. Res.*, vol. 42, no. 2, pp. 503–15, 2014.
[162] D. H. Kwon *et al.*, “Seven-tesla magnetic resonance images of the substantia nigra in Parkinson disease,” *Ann. Neurol.*, vol. 71, no. 2, pp. 267–277, 2012.
[163] C. P. Pawela *et al.*, “Modeling of region-specific fMRI BOLD neurovascular response functions in rat brain reveals residual differences that correlate with the differences in regional evoked potentials,” *Neuroimage*, vol. 41, no. 2, pp. 525–534, 2008.
[164] A. D. Engell, S. Huettel, and G. McCarthy, “The fMRI BOLD signal tracks electrophysiological spectral perturbations, not event-related potentials,” *Neuroimage*, vol. 59, no. 3, pp. 2600–2606, 2012.
[165] E. Jonckers, D. Shah, J. Hamaide, M. Verhoye, and A. Van der Linden, “The power of using functional fMRI on small rodents to study brain pharmacology and disease,” *Front. Pharmacol.*, vol. 6, no. OCT, pp. 1–19, 2015.
[166] M. Desai *et al.*, “Mapping brain networks in awake mice using combined optical neural control and fMRI,” *J. Neurophysiol.*, vol. 105, no. 3, pp. 1393–1405, 2011.
[167] Y. R. Gao *et al.*, “Time to wake up: Studying neurovascular coupling and brain-wide circuit function in the un-anesthetized animal,” *Neuroimage*, vol. 153, no. April 2016, pp. 382–398, 2017.
[168] C. Martin, J. Martindale, J. Berwick, and J. Mayhew, “Investigating neural-hemodynamic coupling and the hemodynamic response function in the awake rat,” *Neuroimage*, vol. 32, no. 1, pp. 33–48, 2006.
[169] C. Lau, I. Y. Zhou, M. M. Cheung, K. C. Chan, and E. X. Wu, “BOLD temporal dynamics of rat superior colliculus and lateral geniculate nucleus following short duration visual stimulation,” *PLoS One*, vol. 6, no. 4, 2011.
[170] L. Kuebler *et al.*, “Quantification of molecular and functional changes in a rat model of Parkinson’s disease using a simultaneaous PET/fMRI protocol.” SfN, p. session 455.07, 2017.
[171] S. Hindle *et al.*, “Dopaminergic expression of the Parkinsonian gene LRRK2-G2019S leads to non-autonomous visual neurodegeneration, accelerated by increased neural demands for energy,” *Hum. Mol. Genet.*, vol. 22, no. 11, pp. 2129–2140, 2013.
[172] M. A. Contín, M. M. Arietti, M. M. Benedetto, C. Bussi, and M. E. Guido, “Photoreceptor damage induced by low-intensity light: model of retinal degeneration in mammals.,” *Mol. Vis.*, vol. 19, no. May 2012, pp. 1614–25, 2013.
[173] G. Paxinos and C. Watson, *The Rat Brain: in stereotaxic Coordinates*, 4th ed. San Diego, London: Academic Press, An imprint of Elsevier, 1998.
[174] A. Bringmann and F. Klingberg, “Behavior-Dependent and Drug-Induced Changes of Rat VEP,” *Neuropsychobiology*, vol. 31, pp. 89–97, 1995.
[175] J. Brankack and F. Klingberg, “Behaviour-dependent Changes of Visually Evoked Potential Components in the Superior Colliculus of Freely Moving Rats,” *Biomed. Biochim Acta*, vol. 44, no. 5, pp. 743–748, 1985.
[176] T. H. Pham and A. M. Gardier, “Fast-acting antidepressant activity of ketamine: highlights on brain serotonin, glutamate, and GABA neurotransmission in preclinical studies,” *Pharmacol. Ther.*, 2019.
[177] A. Schwertner, M. Zortea, F. V. Torres, and W. Caumo, “Effects of Subanesthetic Ketamine Administration on Visual and Auditory Event-Related Potentials (ERP) in Humans: A Systematic Review,” *Front. Behav. Neurosci.*, vol. 12, no. April, 2018.
[178] R. M. Wallis, “The pharmacology of sildenafil, a novel and selective inhibitor of phosphodiesterase (PDE) type 5.,” *Nihon Yakurigaku Zasshi.*, vol. 114 Suppl, no. Table 1, p. 22P–26P, 1999.
[179] M. M. Moschos and E. Nitoda, “Pathophysiology of visual disorders induced by phosphodiesterase inhibitors in the treatment of erectile dysfunction,” *Drug Des. Devel. Ther.*, vol. 10, pp. 3407–3413, 2016.
[180] M. A. S. Baptista *et al.*, “LRRK2 Kinase Inhibitors of Different Structural Classes Induce Abnormal Accumulation of Lamellar Bodies in Type II Pneumocytes in Non-Human Primates but are Reversible and Without Pulmonary Functional Consequences Workflow and Study Design,” p. 94080, 2015.
[181] K. Masamoto, M. Fukuda, A. Vazquez, and S. G. Kim, “Dose-dependent effect of isoflurane on neurovascular coupling in rat cerebral cortex,” *Eur. J. Neurosci.*, vol. 30, no. 2, pp. 242–250, 2009.

[182] M. A. S. Weerink, M. M. R. F. Struys, L. N. Hannivoort, C. R. M. Barends, A. R. Absalom, and P. Colin, "Clinical Pharmacokinetics and Pharmacodynamics of Dexmedetomidine," *Clin. Pharmacokinet.*, vol. 56, no. 8, pp. 893–913, 2017.
[183] H. Benveniste *et al.*, "Anesthesia with dexmedetomidine and low-dose isoflurane increases solute transport via the glymphatic pathway in rat brain when compared with high-dose isoflurane," *Anesthesiology*, vol. 127, no. 6, pp. 976–988, 2017.
[184] C. J. Bailey, B. G. Sanganahalli, P. Herman, H. Blumenfeld, A. Gjedde, and F. Hyder, "Analysis of time and space invariance of BOLD responses in the rat visual system," *Cereb. Cortex*, vol. 23, no. 1, pp. 210–222, 2013.
[185] N. Van Camp, M. Verhoye, C. I. De Zeeuw, and A. Van der Linden, "Light Stimulus Frequency Dependence of Activity in the Rat Visual System as Studied With High-Resolution BOLD fMRI," *J. Neurophysiol.*, vol. 95, no. 5, pp. 3164–3170, 2006.
[186] C. Lau *et al.*, "BOLD responses in the superior colliculus and lateral geniculate nucleus of the rat viewing an apparent motion stimulus," *Neuroimage*, vol. 58, no. 3, pp. 878–884, Oct. 2011.
[187] A. Niranjan, I. N. Christie, S. G. Solomon, J. A. Wells, and M. F. Lythgoe, "fMRI mapping of the visual system in the mouse brain with interleaved snapshot GE-EPI," *Neuroimage*, vol. 139, pp. 337–345, 2016.
[188] R. W. Cox, "AFNI : Software for Analysis and Visualization of Functional Magnetic Resonance Neuroimages," *Comput. Biomed. Res.*, vol. 29, pp. 162–173, 1996.
[189] M. W. Woolrich *et al.*, "Bayesian analysis of neuroimaging data in FSL.," *Neuroimage*, vol. 45, no. 1 Suppl, pp. S173–S186, 2009.
[190] E. A. Papp, T. B. Leergaard, E. Calabrese, G. A. Johnson, and J. G. Bjaalie, "Waxholm Space atlas of the Sprague Dawley rat brain," *Neuroimage*, vol. 97, pp. 374–386, 2014.
[191] M. Sergejevaa *et al.*, "Anatomical landmarks for registration of experimental image data to volumetric rodent brain atlasing templates," *J. Neurosci. Methods*, vol. 240, pp. 161–169, 2015.
[192] L. J. Kjonigsen, S. Lillehaug, J. G. Bjaalie, M. P. Witter, and T. B. Leergaard, "Waxholm Space atlas of the rat brain hippocampal region: Three-dimensional delineations based on magnetic resonance and diffusion tensor imaging," *Neuroimage*, vol. 108, pp. 441–449, 2015.
[193] R. R. Hocking, "The Analysis and Selection of Variables in Linear Regression," *Biometrics*, vol. 32, no. 1, pp. 1–49, 1976.
[194] Y. Benjamini and D. Yekutieli, "The Control of the False Discovery Rate in Multiple Testing under Depency," *Ann. Stat.*, vol. 29, no. 4, pp. 1165–1188, 2001.
[195] O. Szabo-Salfay, J. Palhalmi, E. Szatmari, P. Barabas, N. Szilagyi, and G. Juhasz, "The electroretinogram and visual evoked potential of freely moving rats," *Brain Res.Bull.*, vol. 56, no. 1, pp. 7–14, 2001.
[196] A. Ridder, M. L. T. M. Müller, V. Kotagal, K. A. Frey, R. L. Albin, and N. I. Bohnen, "Impaired contrast sensitivity is associated with more severe cognitive impairment in Parkinson disease," *Park. Relat. Disord.*, vol. 34, pp. 15–19, 2017.
[197] L. Nivison-Smith *et al.*, "Sildenafil alters retinal function in mouse carriers of Retinitis Pigmentosa," *Exp. Eye Res.*, vol. 128, pp. 43–56, 2014.
[198] M. A. Vobig, T. Klotz, M. Staak, K. U. Bartz-Schmidt, U. Engelmann, and P. Walter, "Retinal side effects of sildenafil," *Lancet*, vol. 353, p. 375., 1999.
[199] K. Albert *et al.*, "Downregulation of tyrosine hydroxylase phenotype after AAV injection above substantia nigra: Caution in experimental models of Parkinson's disease," *J. Neurosci. Res.*, vol. 97, no. 3, pp. 346–361, 2019.
[200] M. Vila *et al.*, "Consequences of nigrostriatal denervation on the gamma-aminobutyric acidic neurons of substantia nigra pars reticulata and superior colliculus in parkinsonian syndromes," *Neurology*, vol. 46, no. 3, pp. 802–809, 1996.
[201] M. S. Ekker *et al.*, "Ocular and visual disorders in Parkinson's disease: Common but frequently overlooked," *Park. Relat. Disord.*, vol. 40, pp. 1–10, 2017.
[202] Y. Terao, H. Fukuda, Y. Ugawa, and O. Hikosaka, "New perspectives on the pathophysiology of Parkinson's disease as assessed by saccade performance: A clinical review," *Clin. Neurophysiol.*, vol. 124, no. 8, pp. 1491–1506, 2013.
[203] D. Erskine *et al.*, "Specific patterns of neuronal loss in the pulvinar nucleus in dementia with lewy bodies," *Mov. Disord.*, vol. 32, no. 3, pp. 414–422, 2017.
[204] R. B. Walsh *et al.*, "Acute increase of -synuclein inhibits synaptic vesicle recycling evoked during intense stimulation," *Mol. Biol. Cell*, vol. 25, no. 24, pp. 3926–3941, 2014.
[205] D. Kirik *et al.*, "Parkinson-like neurodegeneration induced by targeted overexpression of alpha-synuclein in the nigrostriatal system.," *J. Neurosci.*, vol. 22, no. 7, pp. 2780–91, 2002.

[206] S. Cuellar-Baena *et al.*, “Assessment of brain metabolite correlates of adeno-associated virus-mediated over-expression of human alpha-synuclein in cortical neurons by in vivo 1H-MR spectroscopy at 9.4 T,” *J. Neurochem.*, vol. 137, no. 5, pp. 806–819, 2016.
[207] S. Daniele *et al.*, “α-Synuclein Aggregated with Tau and β-Amyloid in Human Platelets from Healthy Subjects: Correlation with Physical Exercise,” *Front. Aging Neurosci.*, vol. 10, no. January, pp. 1–14, 2018.
[208] E. J. Bae *et al.*, “LRRK2 kinase regulates α-synuclein propagation via RAB35 phosphorylation,” *Nat. Commun.*, vol. 9, no. 1, 2018.
[209] R. J. H. West, C. J. H. Elliott, and A. R. Wade, “Classification of Parkinson’s Disease Genotypes in Drosophila Using Spatiotemporal Profiling of Vision,” *Sci. Rep.*, vol. 5, no. October, p. 16933, 2015.
[210] M. M. Himmelberg, R. J. H. West, C. J. H. Elliott, and A. R. Wade, “ Abnormal visual gain control and excitotoxicity in early-onset Parkinson’s disease Drosophila models ,” *J. Neurophysiol.*, vol. 119, no. 3, pp. 957–970, 2017.
[211] L. Sun and P. Chan, “LRRK2-associated Parkinson’s disease patients have better stereopsis than idiopathic Parkinson disease,” *Clin. Neurol. Neurosurg.*, vol. 169, no. November 2016, pp. 174–177, 2018.
[212] S. Zechel, A. Meinhardt, K. Unsicker, and O. von Bohlen und Halbach, “Expression of leucine-rich-repeat-kinase 2 (LRRK2) during embryonic development,” *Int. J. Dev. Neurosci.*, vol. 28, no. 5, pp. 391–399, 2010.

Appendices

11 Appendix #1

park designation	symbol	name	location	possible pathway	type
park1/4	SNCA	alpha-synuclein	4q21	Synaptic function; mitochondrial function; autophagy/lysosomal degradation	mendelian
park2	PRKN	Parkin RBR E3 ubiquitin protein ligase	6q25.2-q27	Mitochondrial function/mitophagy; ubiquitination; synaptic function	mendelian
park3			2p13		
park5	(UCHL1)?		4p13		
park6	PINK1	PTEN -induced putative kinase 1	1p36	Mitochondrial function/mitophagy	mendelian
park7	DJ-1	Parkinson protein 7	1p36.23	Inflammation/immune system; mitochondrial function	mendelian
park8	LRRK2	Leucine-rich repeat kinase 2	12q12	Synaptic function; inflammation/immune system; autophagy/lysosomal degradation	mendelian
park9	ATP13A2	ATPase type 13A2	1p36	Mitochondrial function; autophagy/lysosomal degradation	mendelian
park10			1q32		
park11	GIGYF2	GRB10-interacting GYF protein 2	2q37.1	IGF signaling	
park12			Xq21-25		
park13	HTRA2	HTRA Serine peptidase 2	2p13.1	Cellular stress response; apoptosis	
park14	PLA2G6	Phospholipase A2, group VI	22q13.1	Mitochondrial function	mendelian
park15	FBXO7	F-box protein 7	22q12.3	Ubiquitination; mitochondrial function/mitophagy	mendelian
park16		SNP upstream of RAB7L1	1q32		
park17	VPS35	Vacuolar protein sorting 35 homolog (S. cerevisiae)	16q12	Autophagy/lysosomal degradation; endocytosis;	mendelian
park18	EIF4G1	Eukaryotic translation initiation factor 4-γ , 1	3q27.1	Protein synthesis	
park19	DNAJC6	DnaJ (Hsp40) homolog, subfamily C, member 6	1p31.3	Synaptic function; endocytosis	mendelian
park20	SYNJ1	Synaptojanin 1	21q22.2	Synaptic function; endocytosis	mendelian
park21			3q22		
park22	CHCHD2	Coiled-coil-helix-coiled-coil-helix domain-containing protein 2	7p11.2	Cellular stress response	
park23	VPS13C	Vacuolar protein sorting 13 homolog C (S. cerevisiae)	15q22.2	Endocytosis	risk loci
	GBA	Glucosidase, beta, acid	1q21	Inflammation/ immune system; autophagy/lysosomal degradation; metabolic pathways	risk gene
	MAPT	Microtubule-associated protein tau	17q21.1	Microtubule stabilization and axonal transport	risk loci
	RAB7L1	RAB7, member RAS oncogene family-like 1	1q32	Autophagy/lysosomal degradation	risk loci

	BST1	Bone marrow stromal cell antigen 1	4p15	Immune system	risk loci
	HLA-DRB5	Major histocompatibility complex, class II, DR beta 5	6p21.3	Inflammation/immune system	risk loci
	GAK	Cyclin-G-associated kinase	4p16	Autophagy/lysosomal degradation; synaptic function; endocytosis	risk loci
	ACMSD	Aminocarboxymuconate semialdehyde decarboxylase	2q21.3	Tryptophan metabolism; metal ion binding; metabolic pathways	risk loci
	STK39	Serine threonine kinase 39	2q24.3	Inflammation/immune system; protein kinase binding; cellular stress response	risk loci
	SYT11	Synaptotagmin XI	1q21.2	Synaptic function; transporter activity; metal ion binding; substrate for PARK2	risk loci
	FGF20	Fibroblast growth factor 20	8p22	Growth factor activity; FGF receptor binding	risk loci
	STX1B	Syntaxin 1B	16p11.2	Synaptic function; SNAP receptor activity; protein domain-specifi c binding	risk loci
	GPNMB	Glycoprotein (transmembrane) nmb	7p15	Integrin binding; heparin binding; cancer pathways	risk loci
	SIPA1L2	Signal-induced proliferation-associated 1 like 2	1q42.2	GTPase activator activity	risk loci
	INPP5F	Inositol polyphosphate-5-phosphatase F	10q26.11	Phosphoric ester hydrolase activity	risk loci
	MIR4697HG	MIR4697 host gene (non-protein coding)	11q25		risk loci
	GCH1	GTP cyclohydrolase 1	14q22.1-q22.2	GTP binding; calcium ion binding; BH4 metab; metabolic pathways	risk loci
	DDRGK1	DDRGK domain containing 1	20p13	Protein binding	risk loci
	MCCC1	Methylcrotonoyl-CoA carboxylase 1 (alpha)	3q27	Biotin carboxylase activity; methylcrotonoyl-CoA carboxylase activity; metabolic pathways	risk loci
	SCARB2	Scavenger receptor class B, member 2	4q21.1	Autophagy/lysosomal degradation; receptor activity (lysosomal receptor for GBA targeting); enzyme binding	risk loci
	CCDC62	Coiled-coil domain containing 62	12q24.31	Nuclear receptor coactivator; cancer pathways	risk loci
	RIT2	Ras-like without CAAX 2	18q12.3	Synaptic function; calmodulin binding; GTP binding	risk loci
	SREBF1	Sterol regulatory element binding transcription factor 1 cholesterol and steroid metabolic processes	17p11.2	Chromatin binding; cholesterol and steroid metabolic processes	risk loci

S 1 Table of genes associated with Parkinson's disease. The type says mendelian for the genes that are confirmed to have a mendelian pattern. Not all of the PARK genes are well described and may only have been found in one family. Modified from [34] **with the use of omim.org.**

12 Appendix #2

Monocular Occlusion

To confirm the origin of the responses measured in the assay. The VEPs were recorded while one eye was patched, and the responses from the two hemispheres were compared. Showing that the VEP is indeed modulated when one eye is patched.

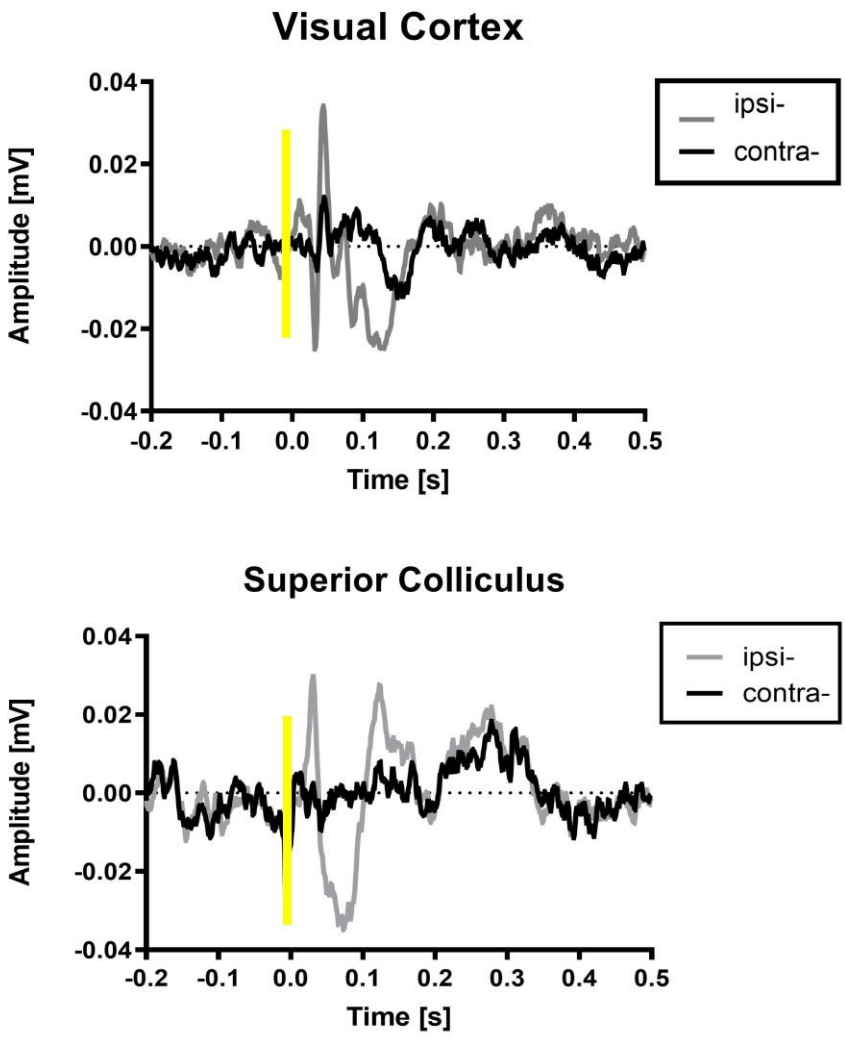

S 2 Recording of Long-Evans rats with one eye patched from the visual cortex (top) and superior colliculus (bottom). The recording from bilateral electrodes are superimposed, the recording from the electrode ipsilateral to the injection (grey), the electrode contralateral to the injection (black). The yellow bar is the 10 ms stimulus.

13 Appendix #3

Quantification of amplitudes and latencies of waveforms shown in Figure 10

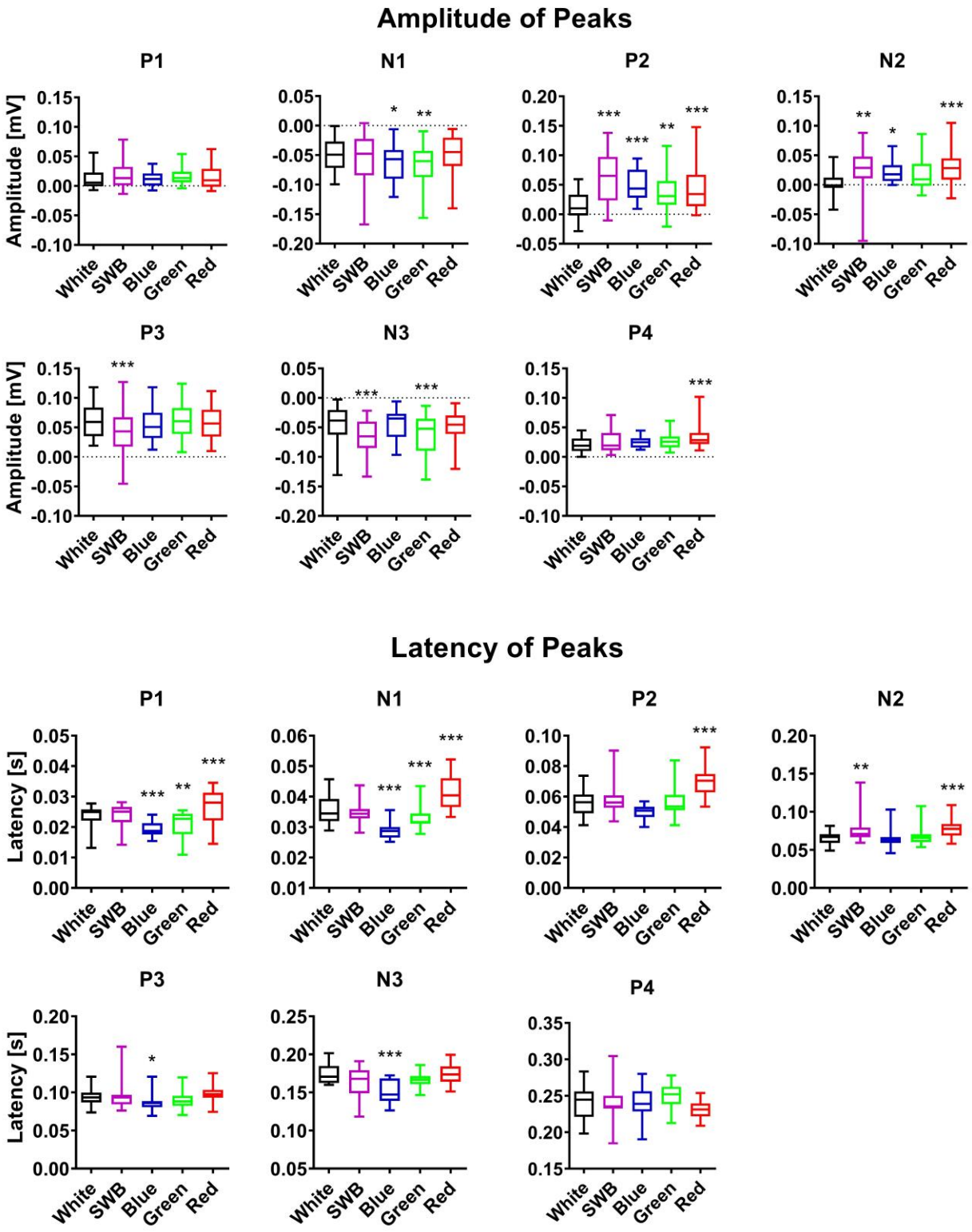

S 3 Amplitude and latency data from the peaks of the visual cortex Figure (10). are the result of a one-way ANOVA asterisks refer to the post-hoc test comparing to the white wavelength condition. * p<0.05, ** p<0.01 *** p<0.001

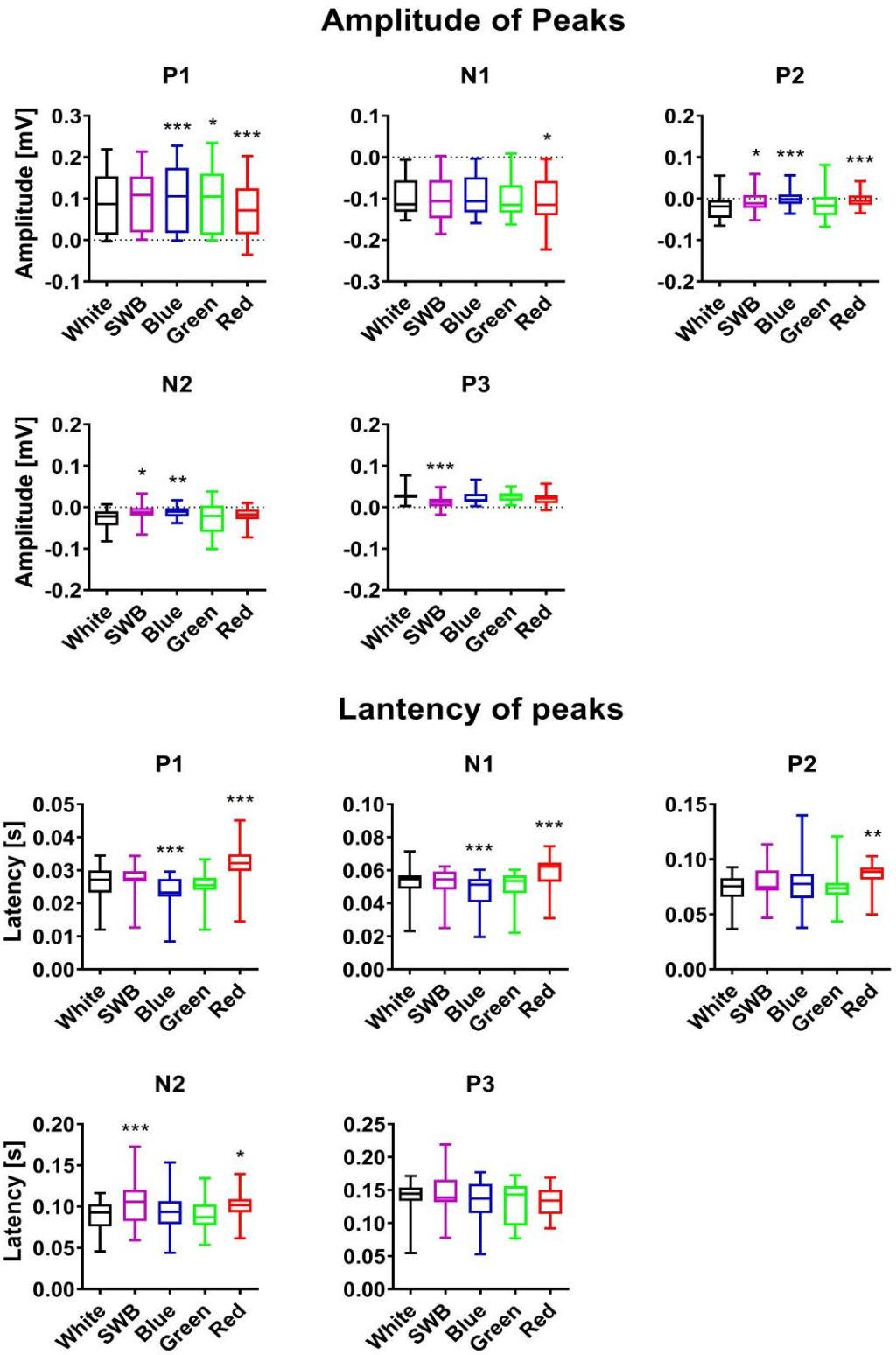

S 4 Quantification of amplitude and latency data from the superior colliculus Figure (10). are the result of a one-way ANOVA asterisks refer to the post-hoc test comparing to the white wavelength condition. * p<0.05, ** p<0.01 *** p<0.001

14 Appendix #4

Randomized cross-over with ketamine

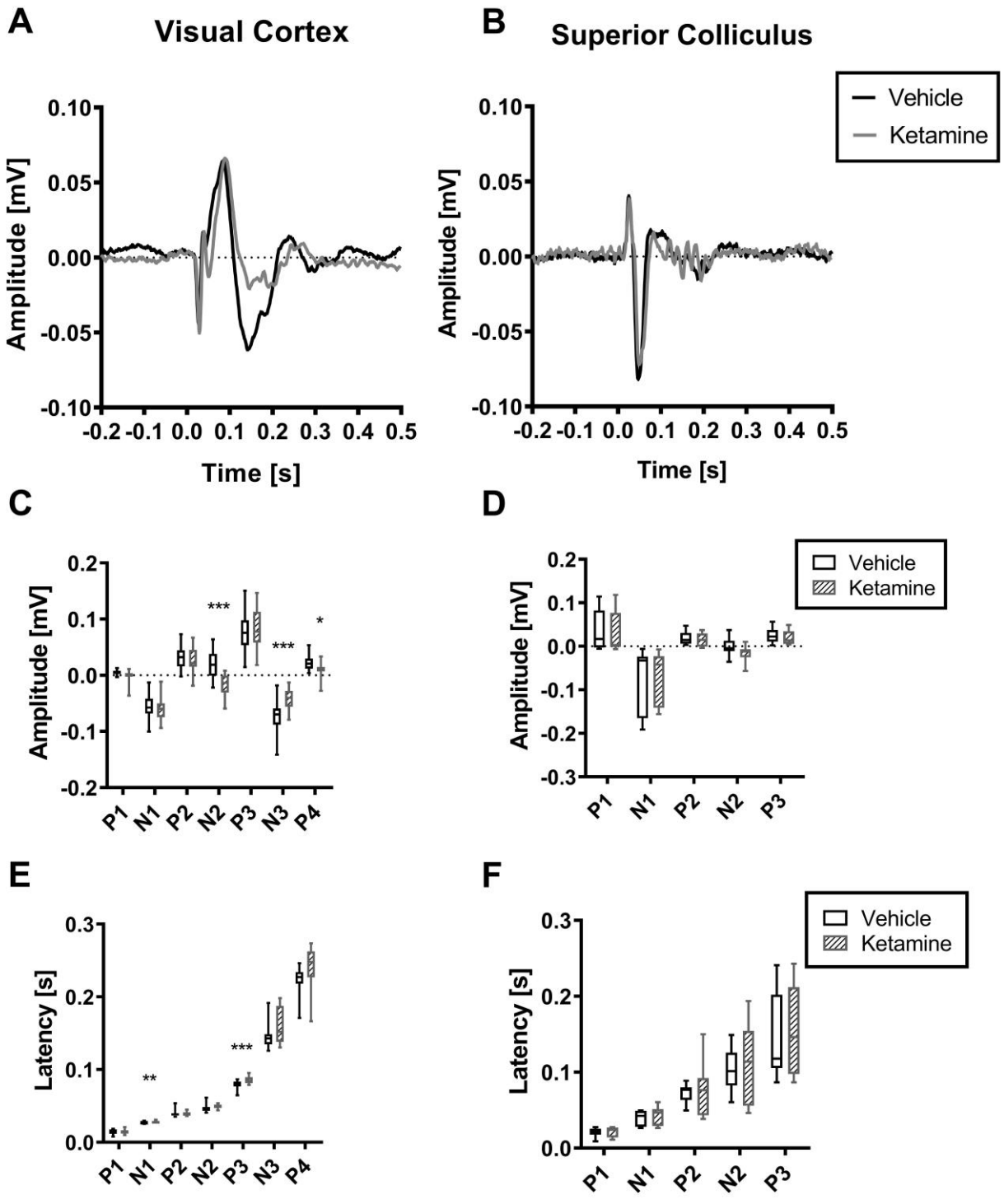

S 5 Response to 10mg/kg ketamine in male LE (Cohort A). A)-B) show the grand average waveforms from the visual cortex and superior colliculus. C)-D) show the quantification of amplitudes. E)-F) the quantification of latencies. The asterisks refer to paired t-test, * p<0.05, ** p<0.01 *** p<0.001.

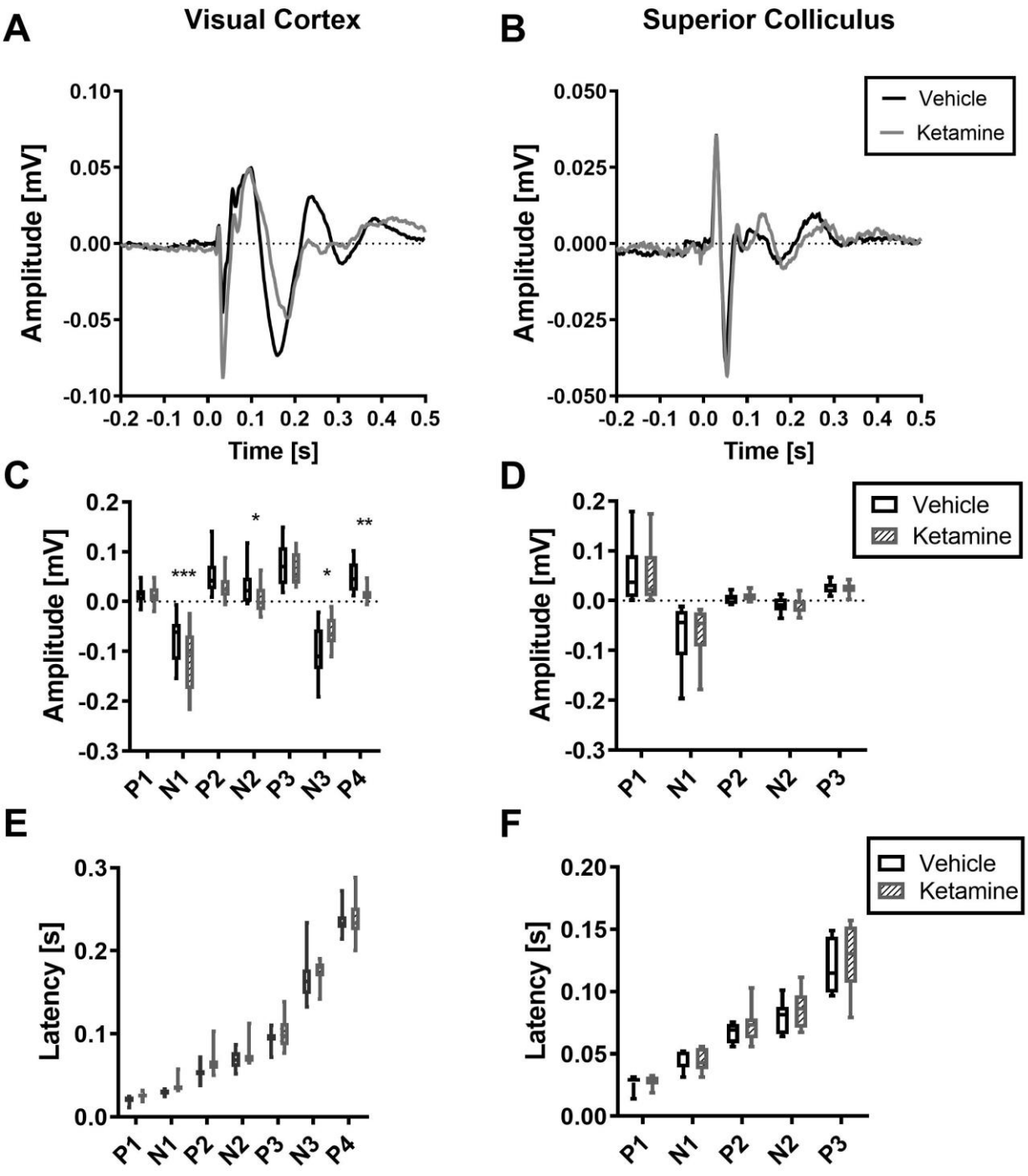

S 6 Response to 10mg/kg ketamine in female SD (Cohort B). A)-B) show the grand average waveforms from the visual cortex and superior colliculus. C)-D) show the quantification of amplitudes. E)-F) the quantification of latencies. The asterisks refer to paired t-test, * p<0.05, ** p<0.01 *** p<0.001.

Manuscripts

15 Manuscript I

Progressive effects of sildenafil on visual processing in rats

Authors: Freja Gam Østergaard[1], Alex R. Wade[2], Hartwig Roman Siebner[3], Kenneth Vielsted Christensen[4] and Bettina Laursen[1].

[1]Translational Biology, H. Lundbeck A/S, Ottiliavej 9. DK-2500 Valby, Denmark. [2] Department of Psychology, The University of York, Heslington, York, YO10 5DD, United Kingdom. [3] Danish Research Centre for Magnetic Resonance, Copenhagen University Hospital Hvidovre, Denmark [4] Institut de Recherches Servier – IDRS, 125 Chemin de Ronde, 78290 Croissy sur Seine, France

Corresponding author: Freja Gam Østergaard

Target journal: Journal of Neuropharmacology

Abstract

Retinitis pigmentosa is a heterogenous group of diseases, causing retinal degeneration. In some cases, this degeneration commences with death of the rod photoreceptors, causing night blindness. Photoreceptors are not be the only cells in the retina responding to light stimulation. Sildenafil is a phosphodiesterase type 5 and 6 (PDE5 and 6) inhibitor effective as treatment for e.g. erectile dysfunction. One of the frequently reported side effects is altered vision, even causing transient blindness at high doses. An effect that may be attributed to modulation of PDE inhibition. In this study, we characterized the effects of sildenafil on the electrophysiological activity of the rodent visual system.

The effect of sildenafil on phototransduction was investigated in female Sprague dawley™ rats by measuring progressive changes of neuronal electrophysiology using flash visual evoked potentials (VEP), and the steady-state version of the same technique (SSVEP), at 0.5, 5 and 28 hours after per oral administration of sildenafil (50 mg/kg). Recording electrodes were implanted in the superior colliculus and visual cortex allowing characterization different aspects of functional connectivity in the visual system. To study the effect of wavelengths flickering light with three wavelengths conditions, corresponding to short-wave blue, blue and white light were applied.

Sildenafil caused a significant reduction in the amplitude of both VEPs and SSVEPs in the superior colliculus and visual cortex along with a delay in the latency of VEP peaks. The effects of sildenafil depended on the wavelength condition suggesting that phototransduction might not only be driven by the PDE´s in the photoreceptors.

Keywords: sildenafil, PDE6, visual evoked potential, retinal ganglion cells

Introduction

Worldwide, diseases impacting retinal function such as age-related macular degeneration and retinitis pigmentosa represent some of the most common forms of neurodegenerative disorders (Hartong et al., 2006). Retinitis pigmentosa causes progressive photoreceptor death and is among the most common causes of retinal degeneration (He et al., 2014).

The photoreceptors at the outermost surface of the retina are critical for light detection. The transduction from light into a chemical signal happens in the outer segment of the photoreceptors, where a photon excites rhodopsin which in turn, activates a retina-specific phosphodiesterase (PDE), PDE type 6 (PDE6)(Wert et al., 2014). PDE6 hydrolyzes cyclic guanosine monophosphate (cGMP) which acts as the primary second messenger and triggers a cascade of cellular processes which transform the light signal into electrical signals. Retinitis pigmentosa is often associated with mutations in phototransduction and especially genes directly related to cGMP (Zhang et al., 2005) pathway such as *PDE6A,* and *PDE6B* coding for subunits of the PDE6 holoenzyme, *CNGA1* coding for a cGMP-gated ion channel and others (Heckenlively and Arden, 2006).

Besides the rods and cones, the retinal ganglion cells (RGCs) and especially the intrinsic photosensitive (ipRGCs) also transduce light information. The ipRGCs have been implicated in triggering light-induced reflexes such as pupillary constriction and in regulating circadian rhythms (Jiang et al., 2018; Reifler et al., 2015). The exact mechanism of photoreception in ipRGCs is not fully elucidated, but studies report an involvement of melanopsin which may not involve cGMP (Warren et al., 2006) suggesting that light in the RGCs is transduced by a PDE6-independent mechanism (Jiang et al., 2018). While the contribution of RGCs in image formation is still controversial, these cells project to relays of the visual cortex i.e. the dorsolateral geniculate nucleus (Reifler et al., 2015).

Sildenafil citrate (henceforth, `sildenafil´) is a phosphodiesterase (PDE) inhibitor which mainly acts on PDE type 5. Sildenafil also inhibits PDE type 6, but with a 10-fold lower efficacy (Wallis, 1999). Sildenafil (marketed as Viagra®) is generally well tolerated, but some patients experience temporary visual impairments such as changes in color discrimination (Laties and Zrenner, 2002; Martins et al., 2015), transient blindness and reductions in the amplitude of electroretinograms (ERGs) (Vobig et al., 1999). Due to the localization of PDE6 in the internal membranes of retinal photoreceptors (Cote, 2004) and bipolar cells (Moschos and Nitoda, 2016), these visual disturbances have been ascribed to an inhibition of PDE6. Inhibition of PDEs increases cytoplasmic levels of cGMP (Loughney and Ferguson, 1996) affecting the hyperpolarization of the outer segment of the photoreceptors (Wert et al., 2014). Apart from the photoreceptors, PDE6 is also expressed in the bipolar cells of the retina (Shiells and Falk, 2002). Furthermore, sildenafil

is a hypotensive agent causing decreases in systemic blood pressure (Moschos and Nitoda, 2016) temporarily increasing the intraocular blood pressure which have been related to the drug-induced reductions in retinal electrical potentials as measured by ERG (Moschos and Nitoda, 2016).

The transient or flash visual evoked potential (VEP) is an event-related potential (ERP) representing net changes in post-synaptic electrical potentials as a response to sensory stimulations. The VEP is considered to be a measure of neurological integrity of the visual pathway (Iwamura et al., 2003; You et al., 2011). For consistency, this type of VEP will be referred to as flash VEP throughout this paper. Steady-state visual evoked potentials (SSVEP) are VEPs evoked at a frequency high enough for the VEPs to overlap, presumably causing a summation of the VEPs (Vialatte et al., 2010). The SSVEP most appropriately analyzed in the frequency domain by Fourier transformed yielding one amplitude measure, and one phase measure for each condition (Luck, 2005; Norcia et al., 2015; Regan, 1989). As opposed to VEPs, it has been proposed that SSVEPs may be used to measure neuronal response amplitudes (Afsari et al., 2014) enabling differentiation between different cell types in the retina of *Drosophilae.* Photoreceptors are believed to respond to the frequency of the stimulus while RGCs seem to respond at double rate corresponding to the second harmonic. Whether this interpretation is also applicable for rodents remains to be elucidated.

In rodents, the superior colliculus is the major retino-recipient nucleus (Sefton et al., 2014) and the visual evoked potential here is similar to that of the ERG. The rodent visual cortex receives visual information relayed from different parts of the brain, but no direct signal from the retina (Sefton et al., 2014), yet it is still considered translationally relevant. Here, we aim to characterize rodent electrophysiological responses during visual processing measured with flash VEPs and SSVEP in the superior colliculus, and the visual cortex. We study how net electrophysiological activity changes over time from the administration of sildenafil which at high dose inhibits PDE6, thereby modelling the progressive change in PDE6 function.

Material and Methods

All animal experimentation was carried out according to European Communities Council Directive (86/609/EEC) and Danish legislation on care for laboratory animal.

Animals

Eight Sprague dawley™ (SD) female rats (Taconic, Denmark), weighing 225g on arrival. The animals were kept on a reversed 12h circadian circle (lights on at 18:00h) and recordings were made during the dark phase. They were single housed in home cages with food and water ad libitum. The cages were enriched with feed enrichment (one a week), a red house, nesting material and wood for gnawing. The room was controlled at temperature of 22±1.5 °C and humidity of 55-65%.

Surgery

The animals were anesthetized using subcutaneous (SC) injections of Hypnorm® (Lundbeck, Valby, Denmark), midazolam 5 mg/ml (B.Braun, Melsungen, Germany) and saline in a 2:1:1 relation (2.0 ml/kg), yielding 157 µg/kg fentanyl. Norodyl (carprofen 5 mg/kg) (ScanVet, Fredensborg, Denmark) and Noromox prolongatum (amoxicillintrihydrat 150 mg/kg) (ScanVet, Fredensborg, Denmark) were administered during surgery and for five days post-surgery. The animals were mounted in a stereotactic frame and Marcain (2.5 mg/ml bupivacaine, AstraZeneca, Albertslund, Denmark), was administered locally (SC) prior to incision. Coordinates were guided by (Paxinos and Watson, 1998). Holes were made bilaterally for visual cortex (AP: -6, ML: ±4), superior colliculus (AP: -6, ML: ±1, DV: -3.5), reference electrode (AP: +8, ML: -2) and ground electrode (AP: -2, ML: +4). The electrodes for recording in the superior colliculus were stranded electrodes E363/3/Spc (PlasticsOne, VA, US). The other four electrodes were E363/20/2.4/S screw electrodes (PlasticsOne, VA, US). The electrodes were collected in a plastic pedestal MS363 (PlasticsOne, VA, US) and fixed to the skull with RelyX^{TM} Unicem dental cement (3M, Copenhagen, Denmark) and Fuji plus (GC, US) as a chronic implant. The animals were allowed to recover for 14 days before the first exposure to stimuli.

EEG recording

The recordings were made in awake and behaving animals in a home cage with wood bedding. The LEDs were positioned in a frame 40 cm above the bedding. Recordings were made every 30 minutes for the first two hours, then four hours, five hours, seven hours, 24 hours and 28 hours, in

total ten recordings per animal. We used three wavelength conditions to probe the contribution of different cell types (photoreceptors vs RGCs) to the evoked signal, as RGCs have been shown to be sensitive to light in the blue part of the spectrum (Baden et al., 2016; Lagman et al., 2016; Panda et al., 2005).

The animals were exposed to whole-field light flashes of 20 lx white LED (SMD5050), 20 lx blue (455-460 nm), and 5 lx short wave blue (SWB) (405 nm). Each flash had a duration of 10 ms and 400 flashes were applied at a frequency of 1 Hz to record flash-VEPs. Thereafter, the frequency was increased to 14 Hz and the SSVEPs were recorded over a period of 100 s. Light stimulation was controlled with Spike2 software (version 7.20, Cambridge Electronic Design, Cambridge, UK). Spike2 was also used for recording the EEG signal, which was amplified and filtered using a Brownlee amplifier (Model 410, Brownlee precision, CA, US). The amplifier did the primary filtering, bandwidth, and all. The EEG recordings were carried out on four animals, while the exposure data included all eight rats.

Drug administration, pharmacokinetic characterization and histology

The rats received sildenafil citrate extracted from Viagra® (Pfizer, NY, US) 50 mg/kg in 0.1 M HCl, pH adjusted to 4 with NaOH (Abbott et al., 2004). The solution was administered perorally. The rats were chosen based on signal-to-noise ratio of their waveform as recorded in the superior colliculus.

The rats were sacrificed at 15 min (n=4) or 300 min (n=4) after drug administration as the half-life of sildenafil in female rats was reported as 1 hour by (Walker et al., 1999). Trunk blood and the cerebellum was weighed and sampled for exposure profiling of sildenafil. The cerebrum was removed and used for validating the location of the electrodes. The brain was frozen on dry ice and sliced in a freeze microtome in 20µm thick coronal slices and placed directly on glass slides, for microscopy. Though the electrodes have been removed they leave traces in the tissue.

Exposure

The cerebellum was thawed and homogenized using the Covaris 220X. The concentration of sildenafil was quantified in a LC-MS/MS platform (Xevo TQS triple quadrupole (TQ) mass spectrometer operated in electrospray MS/MS mode (multiple reaction mode, MRM) and coupled to a Waters Acquity UPLC controlled by Mass Lynx software version 4.1). Mass spectrometry methods gave the total concentration of sildenafil in the tissue sample. In order to calculate the free concentration of sildenafil in the samples, the unbound fractions of sildenafil were determined to be 7.2% and 3.9% in the blood and brain, respectively.

Data analysis and statistics

The animals are compared to their own baseline recording, to see how the VEP changes after sildenafil administration. The flash VEPs were generated using Spike2 and analyzed in R via R studio. Naming of the peaks in the visual cortex was guided by (Creel et al., 1974; Meeren et al., 1998). The first positive deflection was named P1, the first negative deflection is named N1, the second positive deflection is named P2 and so on. This denomination is used similarly at all time points. For flash VEPs, the amplitude and latency of the peaks were analyzed separately.

The overall effect of sildenafil was assessed by two-way ANOVA, testing the effect of time and wavelength condition using R via Rstudio. As an aim of the study was to characterize the profile of change over time for each of the three wavelength conditions were analyzed separately. The analysis was carried out on four timepoints, to avoid excessive p-value correction. These were based on pharmacokinetic values of sildenafil in female rats suggested to be $t_{½}$=1h, and Tmax=15 min (Walker et al., 1999). Separate ANOVAs were computed for the latency and amplitude of each peak, yielding 72 one-way ANOVAs testing the variance over time (DF=3). These were followed by Tukey post-hoc tests, when the $p<0.05$. The p-values were adjusted for multiple comparisons using the false discovery rate (FDR) method (Benjamini and Yekutieli, 2001).

The SSVEP should provide a more robust response than the transient VEP, but does not provide temporal information as it is summation of previous responses, therefore it should be analyzed in the frequency domain (Norcia et al., 2015). Amplitude would be affected by changes in the noise level between recording sessions the signal-to-noise ratio (SNR) was chosen over amplitude to reduce variation. The first harmonic is at the same frequency as the stimulus (14Hz), where the second harmonic is at 28Hz (Norcia et al., 2015; Regan, 1989).

The SSVEP were analyzed using a script programmed in Matlab 2016a (Mathworks, MA, USA) which fitted sinusoids to determine amplitude and phase and carry out a Fourier transform. To test for an effect of sildenafil, the SNRs of the amplitudes were quantified at 30 minutes and 28h and compared to the baseline condition using a one-way ANOVA as well. The p-values were adjusted using FDR.

Results

Pharmacokinetic profile of sildenafil in rats

Prior to initiation of the electrophysiological experiments, we assessed the pharmacokinetic profile of sildenafil in naïve rats to estimate the temporal dynamics of PDE6 inhibition (Figure 1A). The total concentrations of sildenafil in blood and cerebellum were measured at 15 minutes (Tmax) and at 5hrs after per-oral administration of 50 mg/kg sildenafil, (Figure 1B). The free unbound brain concentration of sildenafil at 15 minutes and 5 hours were 817±298 nM and 380± 159nM (mean ± STD; n=4), respectively. Reported half-maximal inhibitory concentrations (IC_{50}) of PDE6 in cones are 34nM and in rods 38nM, respectively (Wallis, 1999). Based on this, we infer that PDE6 activity was more than 90% inhibited up to 5hrs after sildenafil administration.

Sildenafil-induced changes in VEP amplitude and latency in the visual cortex

The effect of sildenafil is visualized as the grand average of VEPs for visual cortex and superior colliculus, respectively, during the white light condition (Figure 1C and D). Corroborated by the exposure results, the phototransduction is reduced. Generally, sildenafil administration increased the peak latency and reduced the amplitudes of most VEP peaks recorded from the superior colliculus and visual cortex. The overall effects of sildenafil are summarized in the Figure S1 and S2. These show temporal effects in response to administration of sildenafil as well as general effects of the wavelength condition. Further, interactions between the wavelength condition and time points were observed. In the sections below, the data is analysed separately for the three wavelength conditions using the one-way ANOVA (all ANOVAs are summarized in Table S3 and S4), the difference of mean is reported if both the ANOVA and the Tukey post-hoc showed $p<0.05$. Figure 2 depicts the amplitudes of the individual VEP peaks from recordings performed in the visual cortex. Horizontal and vertical panels show wavelength conditions and temporal conditions, respectively. In short, the wavelength conditions are described as the colors white, blue, and short-wave blue (SWB), whereas the temporal conditions include four time points, starting at baseline (10 minutes before administration), 30 minutes after administration, 300 minutes after and 28 hours after administration. As the starting point is time -10 min, the asterisks mark statistically significant differences from the waveform at -10. At 30 minutes after administration of sildenafil for white light there are statistically significant differences in amplitude at P2, N2 and N3. The changes in mean amplitude being (-0.0569, -0.0794 and 0.0716 mV) at time 300 minutes the differences from control are on P2, N2 and N3 (-0.0671, -0.0565 and 0.0659 mV). In the blue condition, the P4 is increased with 0.0203mV in amplitude after 30 minutes. After 300 minutes the P3 is decreased by 0.0320mV, and the N3 have a negative increase of 0.0392mV in amplitude.

The P4 is increased by 0.186mV. At 28 hours, there is a decrease of 0.0321mV in N2. In the SWB, condition there is a statistically significant decrease in amplitude of 0.0742mV of the peak N3 towards the baseline which persists at time 300 minutes. The P4 is decreased 0.0113mV after 30 minutes and 0.0125mV at 5 hours, further there is a 0.0397mV increase of N1, and a 0.0541mV decrease in amplitude of N2. At 28h the P4 have increased by 0.0167 mV.

The latencies of the waveforms for the three wavelengths are depicted in (Figure 3). In the white condition, sildenafil increased the latency of P1, N1, P2, N2, P3, N3 and P4 with statistical significance (0.0125, 0.0231, 0.0245, 0.0391, 0.0825, 0.0957 and 0.11 s) 30 min after administration. 300 minutes after drug administration, the latency of the P1, N1, P3, N3 and P4 components were increased (0.0138, 0.0231, 0.0428, 0.0563 and 0.0576 s). In the blue condition the latency of P1, N1, P2, N3 was increased after 30 min (0.0055, 0.00819, 0.00595, 0.0126 s). The sildenafil-induced effects on P1, N1 and P2 were also detectable after 300 min (0.00419, 0.00646, 0.0053 s), along with a 0.0115 s increase for N2, but not after 28h. For the SWB condition, the latency of the VEP components was increased for all peaks 30 min after sildenafil administration (0.0158, 0.038, 0.0723, 0.0928, 0.128, 0.124 and 0.103 s). After 300 min, the differences of mean latencies of the peaks were (0.0166, 0.0278, 0.0263, 0.0481, 0.0966, 0.0814 and 0.0793s). No changes were detectable after 28h.

Sildenafil-induced changes in VEP amplitude and latency in the superior colliculus

Grand average VEP waveforms recorded from the superior colliculus are displayed in (Figure 4). Going across are the three wavelength conditions, going down are the time points of recording, starting with control at -10 minutes, 30 minutes after administration, 300 minutes after administration and 28h after administration. In the white condition, there is a statistically significant reduction in the amplitude of P1 (-0.0667 mV) and an increase in the amplitude of P2 (0.0395 mV) after 30 minutes. After 300 minutes the amplitude of P1 was reduced (-0.0778 mV) while the amplitude of N1 was increased (0.0579 mV). After 28h, there was no differences in VEP peaks obtained from baseline and sildenafil-treated rats. Sildenafil does not have an effect on the amplitude of the VEP in the blue condition. For the SWB condition, there are statistically significant reductions in the VEP amplitude of P1 and N1 (-0.0607 and 0.0572 mV) after 30 and 300 min (-0.0751 and 0.078 mV, respectively), bringing the peaks even closer to the baseline, further the P3 is reduced with 0.0375mV. After 28h, there was no detectable differences in the VEPs.

(Figure 5) shows graphs of the latencies from the VEPs recorded in the superior colliculus; the asterisks refer to the difference between the baseline and 30 minutes after administration. The plus

signs refer to differences between baseline and 300 minutes after administration. In the white color condition, the latency of all peaks was increased 30 min after sildenafil administration (0.0184s, 0.0378s, 0.0956s, 0.146s and 0.173s). These differences were also present after 300 min (0.0142s, 0.0327s, 0.0437, 0.0497 and 0.0576s). After 28h, there was no effect of sildenafil on the VEPs. In the blue condition, sildenafil increased the latency of the early positive deflections; P1 and P2. The difference of mean is 0.00491s and 0.0122s, respectively. After 300 min, the latencies of both are still increased with a change of 0.0057s and 0.00838, and the latency of N1 was increased with 0.00638 s. 28h after sildenafil administration, there was no detectable differences. In the SWB condition, the latency of all VEP components were significantly increased 30 min after sildenafil administration (0.0214s, 0.0339s, 0.0647s, 0.1s and 0.132s). After 300 minutes, all peaks showed a statistically significant increase in latency (0.0197s, 0.0284s, 0.0429, 0.066s and 0.0888s). After 28h, there are no differences compared to baseline.

Sildenafil induced changes of the SSVEP depend on the nucleus.

Figure 6 shows the impact of sildenafil on the SSVEP recorded in the visual cortex. The amplitudes are depicted as signal-to-noise ratio (SNR), and changes in SNR over all ten timepoints. Similar to the above-mentioned results for the SC a one-way ANOVA was carried out for the same four time points. Across are the three wavelengths, the panels show the first harmonic and second harmonic. The asterisks refer to statistically significant differences in SNR compared to the control using a tukey post-hoc. In the white condition, there are no changes compared to the control condition in either harmonic. In the blue condition ($F(3,25)=4.57, p=0.011$), the post-hoc showed that sildenafil induces a reduction in SNR of the 1st harmonic after 30 minutes.of reduction of 55.78 % and 46.8 % after 300 minutes, which returns to normal at 28h. There are no changes in the 2nd harmonic. In the SWB condition ($F(3,25)=6.85$, $p=0.0032$), there is a similar trend with a statistically significant depression 30 minutes after administration 57.31 % and 49.16 % after 300 minutes, which disappears after 28h. And no effect on the 2nd harmonic.

The SSVEP recorded from the superior colliculus are shown in Figure 7. Both harmonics are affected in the white condition. The 1st harmonic shows a statistically significant effect of sildenafil ($F(3,25)=3.06, p=0.047$) depression after 30 minutes 36,39 %, which is not detectable at time 300 minutes. In the 2nd harmonic, there is also an effect ($F(3,25)=5.76, p=0.0078$). The SNR is a decreased by 30.94% after 30 minutes and 31.53% after 5 hours, the response is normalized at 28h. In the blue condition, there are no changes in the first harmonic, which seemed to contain more variation. In the 2nd harmonic there is a statistically significant ($F(3,25)=6.04, p=0.0062$) depression of the SNR at 30 minutes 35 % and 22.08 % after 5 hours, this is reversed after 28h. In

the SWB condition, there is no significant difference in the SNR, of the 1st harmonic. For the 2nd harmonic, there are ($F(3,25)=4.5, p=0.012$) increases of the SNR at both 30 min 40.08 % and 41.61 % after 5 hours, this is normalized after 28 hours.

Discussion

The purpose of the study was to use sildenafil to investigate the progressive effect of PDE6 inhibition on the visual system by applying two different electrophysiological assays. The visual cortex and superior colliculus were both severely affected by the administration of sildenafil generally causing reductions in amplitude and increases in latency of the majority of the VEP peaks. That sildenafil affects both the superior colliculus and the visual cortex suggests that the compound is primarily impacting early parts of the visual pathway such as rod and cone function, as the SC and the VC are not part of the same downstream functional pathway (Sefton et al., 2014). The observed change in the flash VEP corresponds well to the observed reductions in amplitude of a and b waves more commonly reported from ERG measurements (Nivison-Smith et al., 2014; Vobig et al., 1999). The superior colliculus receives direct input from the retina and may thus represent a `pure´ visual response as opposed to EEG recordings obtained from the visual cortex. This structure does not receive any direct projections from the retina, but integrates information relayed via other nuclei primarily the dorsolateral geniculate nucleus (Sefton et al., 2014). Furthermore, EEG was obtained from the VC using a cortical screw electrode. Consequently, the cortical flash VEPs from this structure may be influenced by volume conduction from other anatomical areas. The latencies are affected more than the amplitudes, probably due to a larger variance in the amplitude data. There is a general trend that the profiles of change observed in the white and the SWB conditions are similar, whereas the blue wavelength condition has fewer affected peaks. Interestingly, there is no detectable change in the amplitude of the VEP from the SC in the blue wavelength condition, but the latency is affected for the early peaks, suggesting a partial compensation of the sildenafil induced changes.

The exposure results after dosing of 50 mg/kg sildenafil suggest full inhibition of PDE6 in both rods and cones at 15 min and 5 hours. Our estimate was based on the free unbound brain concentration, since the blood-brain barrier and the blood-retinal barrier are comparable (Toda et al., 2011).The data are suggestive of a half-life closer to 3h, rather than 1h in female rats as suggested by Walker et al (Walker et al., 1999). The dose described in Walker is 1 mg/kg, which is only 2% of the dose used in this study, and the discrepancy could either come from reaching the threshold of CYP enzymes responsible for metabolizing sildenafil or slower absorption. Even though PDE6 is fully inhibited the visual processing is not fully abolished. PDE6 has different forms in rods and cones as it is a holoenzyme with four subunits α, β and two γ in rods, and a homodimer of PDE6C in cones (Lagman et al., 2016). As there are different IC50 values reported for rods and cones. Thus, these isoforms are probably not equally inhibited by sildenafil. In retinitis pigmentosa the rod cells degenerate first leading to night blindness at the early stages of the disease

(Hartong et al., 2006). The signal recorded in the visual cortex after the administration of sildenafil, differs from what would be recorded in dim light conditions (unpublished data), suggesting that the inhibition of PDE6 is not directly comparable to low-light conditions. Though, sildenafil inhibits PDE6 in both photoreceptor types then (Nivison-Smith et al., 2014) report that a heterozygous mouse model of retinitis pigmentosa show a limited response to the administration of sildenafil compared to wildtype mice. Suggesting that sildenafil and retinitis pigmentosa work by similar mechanisms, if the effect of sildenafil is smaller when PDE6 is compromised.

Studies have shown that the inhibition of PDE5 may contribute to the effect detected. In humans, PDE5 inhibition causes increased flow in the ophthalmic artery (Foresta et al., 2008) and a similar change in rodents ultimately affecting visual processing is not unlikely. Consequently, part of the sildenafil-induced changes in the visual processing may be due to increases in intraocular pressure, over extended periods this can lead to RGC degeneration, and impairing acuity as seen in glaucoma (Jha et al., 2017). A precaution should be made when interpreting the flash VEP results as source-localization is a well-described problem in ERPs (Luck, 2005). Following the change in flash VEP from the visual cortex, suggests that the peaks are 'the same' both at baseline and right after administration of sildenafil.

SSVEPs are becoming popular in the field of brain-computer interfaces where information can be encoded in phase and frequency (Vialatte et al., 2010). In humans it has been suggested that low-frequency SSVEPs originate prior to the cortical areas (Krolak-salmon et al., 2003), supporting the notion that the SSVEP could be generated by cells in the retina (Afsari et al., 2014). Afsari at al. suggest that the first harmonic of a SSVEP is generated at the level of the photoreceptors, and the second harmonic is generated at the level of the RGCs. That ipRGCs project to the VC could explain why the second harmonic of the VC in the SSVEP is not affected in any of the wavelength conditions, as signal from these neurons could compensate for the loss of signal from the photoreceptors. Because of these projections, we would expect the two harmonics from the superior colliculus to be directly coupled. In the white condition, we see the same pattern for the first and second harmonic. In the SWB condition the trend of the first harmonic looks similar to the increase of the first harmonic. An intriguing feature of the ipRGCs is their peak sensitivity being around in blue portion of the visual spectrum more specifically at 480 nm (Panda et al., 2005), correlating well with the results that we saw a smaller change in the blue wavelength (455-460 nm) condition, relative to the others. However, it has been reported in *ex vivo* samples that the response from ON and OFF RGCs can be abolished by sildenafil (Martins et al., 2015).

Conclusion

Here we demonstrate an assay for studying pharmacological changes of visual processing using two EEG techniques. In the present study, both VEPs and the SSVEPs show decreased amplitudes following administration of sildenafil. The profile of change depended on the wavelength condition, given that the response to blue light was modulated to a smaller extend than the response to white or SWB light. Further research should be needed to elucidate the role of retinal ganglion cells in normal and compromised phototransduction.

Funding

This project has received funding from the European Union's Horizon 2020 research and innovation programme under the Marie Sklodowska-Curie grant agreement No 641805 (NextGenVis). HRS holds a 5-year professorship in precision medicine at the Faculty of Health Sciences and Medicine, University of Copenhagen which is sponsored by the Lundbeck Foundation (Grant Nr. R186-2015-2138).

References

Abbott, D., Comby, P., Charuel, C., Graepel, P., Hanton, G., Leblanc, B., Lodola, a, Longeart, L., Paulus, G., Peters, C., Stadler, J., 2004. Preclinical safety profile of sildenafil. Int. J. Impot. Res. 16, 498–504. https://doi.org/10.1038/sj.ijir.3901232

Afsari, F., Christensen, K. V., Smith, G.P., Hentzer, M., Nippe, O.M., Elliott, C.J.H., Wade, A.R., 2014. Abnormal visual gain control in a Parkinson's disease model. Hum. Mol. Genet. 23, 4465–4478. https://doi.org/10.1093/hmg/ddu159

Baden, T., Berens, P., Franke, K., Román Rosón, M., Bethge, M., Euler, T., 2016. The functional diversity of retinal ganglion cells in the mouse. Nature 529, 345–350. https://doi.org/10.1038/nature16468

Benjamini, Y., Yekutieli, D., 2001. The Control of the False Discovery Rate in Multiple Testing under Depency. Ann. Stat. 29, 1165–1188. https://doi.org/10.1214/aos/1013699998

Cote, R.H., 2004. Characteristics of Photoreceptor PDE (PDE6): Similarities and differences to PDE5. Int. J. Impot. Res. 16, S28–S33. https://doi.org/10.1038/sj.ijir.3901212

Creel, D., Dustman, R.E., Beck, E.C., 1974. Intensity of flash illumination and the visually evoked potential of rats, guinea pigs and cats. Vision Res. 14, 725–729. https://doi.org/10.1016/0042-6989(74)90070-4

Foresta, C., Caretta, N., Zuccarello, D., Poletti, A., 2008. Expression of the PDE5 enzyme on human retinal tissue : new aspects of PDE5 inhibitors ocular side effects 144–149. https://doi.org/10.1038/sj.eye.6702908

Hartong, D.T., Berson, E.L., Dryja, T.P., 2006. Retinitis pigmentosa Prevalence and inheritance patterns. Lancet 368, 1795–1809. https://doi.org/10.1016/S0140-6736(06)69740-7

He, Y., Zhang, Y., Su, G., 2014. Recent Advances in Treatment of Retinitis Pigmentosa. Curr. Stem Cell Res. Ther. 10, 258–265. https://doi.org/10.2174/1574888x09666141027103552

Heckenlively, J.R., Arden, G.B. (Eds.), 2006. Principles and Practice of Clinical Electrophysiology of Vision, 2nd ed. The MIT press.

Iwamura, Y., Fujii, Y., Kamei, C., 2003. The effects of certain H1-antagonists on visual evoked potential in rats. Brain Res. Bull. 61, 393–398. https://doi.org/10.1016/S0361-9230(03)00142-4

Jha, M.K., Thakur, D., Limbu, N., Badhu, B.P., Paudel, B.H., 2017. Visual Evoked Potentials in Primary Open Angle Glaucoma. J. Neurodegener. Dis. https://doi.org/10.1155/2017/9540609

Jiang, Z., Yue, W.W.S., Chen, L., Sheng, Y., Yau, K.-W., 2018. Cyclic-Nucleotide- and HCN-Channel-Mediated Phototransduction in Intrinsically Photosensitive Retinal Ganglion Cells. Cell 175, 652–664. https://doi.org/10.1016/j.cell.2018.08.055

Krolak-salmon, P., He, M., Tallon-baudry, C., Yvert, B., Gue, M., 2003. Human Lateral Geniculate Nucleus andVisual Cortex Respond to Screen Flicker. Ann. Neurol. 53, 73–80.

Lagman, D., Franzén, I.E., Eggert, J., Larhammar, D., Abalo, X.M., 2016. Evolution and expression of the phosphodiesterase 6 genes unveils vertebrate novelty to control photosensitivity. BMC Evol. Biol. 1–20. https://doi.org/10.1186/s12862-016-0695-z

Laties, A.M., Zrenner, E., 2002. Viagra® (sildenafil citrate) and ophthalmology. Prog. Retin. Eye Res. 21, 485–506. https://doi.org/10.1016/S1350-9462(02)00013-7

Loughney, K., Ferguson, K., 1996. Identification and Quantification of PDE Isoenzymes and Subtypes, Phosphodiesterase Inhibitors. Academic Press Ltd. https://doi.org/10.1016/B978-0-12-210720-7.50003-4

Luck, S.J., 2005. An Introduction to the Event-Related Potential Technique, 1st ed. MIT press.

Martins, J., Kolomiets, B., Caplette, R., Sahel, J.A., Castelo-Branc, M., Ambrósio, A.F., Picaud, S., 2015. Sildenafil acutely decreases visual responses in ON and off retinal ganglion cells. Investig. Ophthalmol. Vis. Sci. 56, 2639–2648. https://doi.org/10.1167/iovs.14-15964

Meeren, H.K.M., Van Luijtelaar, E.L.J.M., Coenen, A.M.L., 1998. Cortical and thalamic visual

evoked potentials during sleep-wake states and spike-wave discharges in the rat. Electroencephalogr. Clin. Neurophysiol. - Evoked Potentials 108, 306–319. https://doi.org/10.1016/S0168-5597(97)00101-9
Moschos, M.M., Nitoda, E., 2016. Pathophysiology of visual disorders induced by phosphodiesterase inhibitors in the treatment of erectile dysfunction. Drug Des. Devel. Ther. 10, 3407–3413. https://doi.org/10.2147/DDDT.S118015
Nivison-Smith, L., Zhu, Y., Whatham, A., Bui, B. V., Fletcher, E.L., Acosta, M.L., Kalloniatis, M., 2014. Sildenafil alters retinal function in mouse carriers of Retinitis Pigmentosa. Exp. Eye Res. 128, 43–56. https://doi.org/10.1016/j.exer.2014.08.014
Norcia, A.M., Appelbaum, L.G., Ales, J.M., Cottereau, B.R., Rossion, B., 2015. The steady-state visual evoked potential in vision research: A review. J. Vis. 15, (4); 1-46. https://doi.org/10.1167/15.6.4.doi
Panda, S., Nayak, S.K., Campo, B., Walker, J.R., Hogenesch, J.B., Jegla, T., In, 2005. Illumination of the Melanopsin Signaling Pathway. Science (80-.). 307, 600–605. https://doi.org/10.1126/science.1105121
Paxinos, G., Watson, C., 1998. The Rat Brain: in stereotaxic Coordinates, 4th ed. Academic Press, An imprint of Elsevier, San Diego, London.
Regan, D., 1989. Human Brain Electrophysiology: Evoked Potentials and Evoked Magnetic Fields in Science and Medicine. Elsevier Science Publishing Co., Inc., New York.
Reifler, A.N., Chervenak, A.P., Dolikian, M.E., Benenati, B.A., Meyers, B.S., Demertzis, Z.D., Lynch, A.M., Li, B.Y., Rebecca, D., Abufarha, F.S., Dulka, E.A., Pack, W., Zhao, X., Wong, K.Y., 2015. The rat retina has five types of ganglion-cell photoreceptors. Exp. Eye Res. 130, 17–28. https://doi.org/10.1016/j.exer.2014.11.010.The
Sefton, A.J., Dreher, B., Harvey, A.R., Martin, P.R., 2014. Visual System, The Rat Nervous System: Fourth Edition. https://doi.org/10.1016/B978-0-12-374245-2.00030-9
Shiells, R.A., Falk, G., 2002. Potentiation of “on” bipolar cell flash responses by dim background light and cGMP in dogfish retinal slices. J. Physiol. 542, 211–220. https://doi.org/10.1113/jphysiol.2002.019752
Toda, R., Kawazu, K., Oyabu, M., Miyazaki, T., Kiuchi, Y., 2011. Comparison of drug permeabilities across the blood-retinal barrier, blood-aqueous humor barrier, and blood-brain barrier. J. Pharm. Sci. 100, 3904–3911. https://doi.org/10.1002/jps.22610
Vialatte, F.B., Maurice, M., Dauwels, J., Cichocki, A., 2010. Steady-state visually evoked potentials: Focus on essential paradigms and future perspectives. Prog. Neurobiol. 90, 418–438. https://doi.org/10.1016/j.pneurobio.2009.11.005
Vobig, M.A., Klotz, T., Staak, M., Bartz-Schmidt, K.U., Engelmann, U., Walter, P., 1999. Retinal side effects of sildenafil. Lancet 353, 375.
Walker, D.K., Ackland, M.J., James, G.C., Muirhead, G.J., Rance, D.J., Wastall, P., Wright, P.A., 1999. Pharmacokinetics and metabolism of sildenafil in mouse, rat, rabbit, dog and man. Xenobiotica 29, 297–310. https://doi.org/10.1080/004982599238687
Wallis, R.M., 1999. The pharmacology of sildenafil, a novel and selective inhibitor of phosphodiesterase (PDE) type 5. Nippon Yakurigaku Zasshi 114 Suppl, 22P–26P.
Warren, E.J., Allen, C.N., Brown, R.L., Robinson, D.W., 2006. The light-activated signaling pathway in SCN-projecting rat retinal ganglion cells. Eur. J. Neurosci. 23, 2477–2487. https://doi.org/10.1111/j.1460-9568.2006.04777.x
Wert, K.J., Lin, J.H., Tsang, S.H., Brown, S., Biology, C., Jolla, L., 2014. General Pathophysiology in Retinal Degeneration. Dev. Ophthalmol. 53, 33–43. https://doi.org/10.1159/000357294
You, Y., Klistorner, A., Thie, J., Graham, S.L., 2011. Improving reproducibility of VEP recording in rats: Electrodes, stimulus source and peak analysis. Doc. Ophthalmol. 123, 109–119. https://doi.org/10.1007/s10633-011-9288-8

Zhang, X., Feng, Q., Cote, R.H., 2005. Efficacy and selectivity of phosphodiesterase-targeted drugs to inhibit photoreceptor phosphodiesterase (PDE6) in retinal photoreceptors. Investig. Ophthalmol. Vis. Sci. 46, 3060–3066. https://doi.org/10.1088/1367-2630/15/1/015008

15.1 Figures

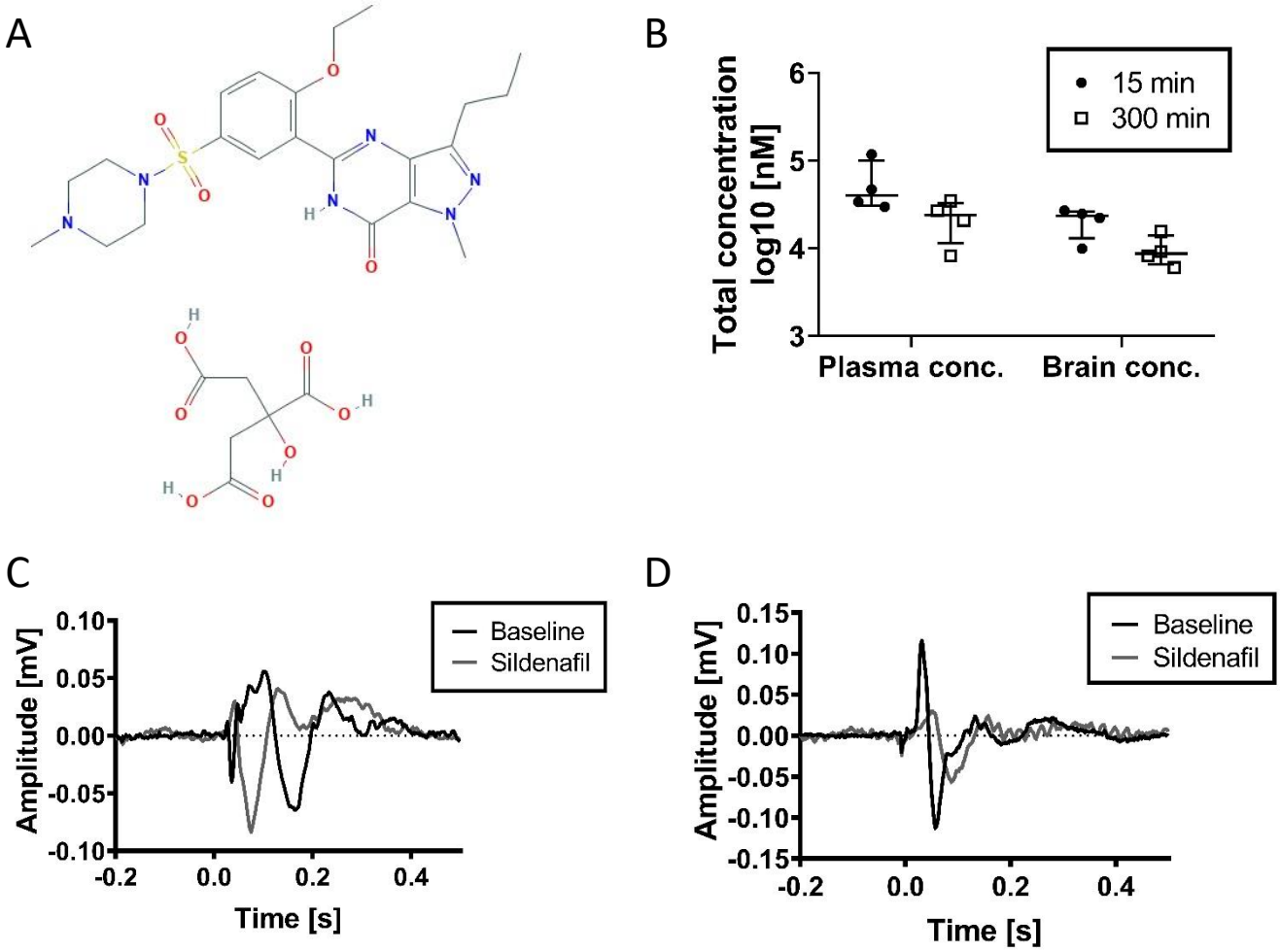

Figure 1 Effect of sildenafil on visual evoked potentials (VEPs) in rats. A) structure of sildenafil citrate B) Total concentration of sildenafil in the plasma and cerebellum. The concentration of unbound sildenafil is depicted with median and interquartile range. C) and D) show grand average VEP waveforms from rat visual cortex and superior colliculus, respectively. Waveforms evoked by a 10-ms white-light flash stimulus are shown at baseline before sildenafil administration (black) and 15 min after (grey) per oral administration of sildenafil.

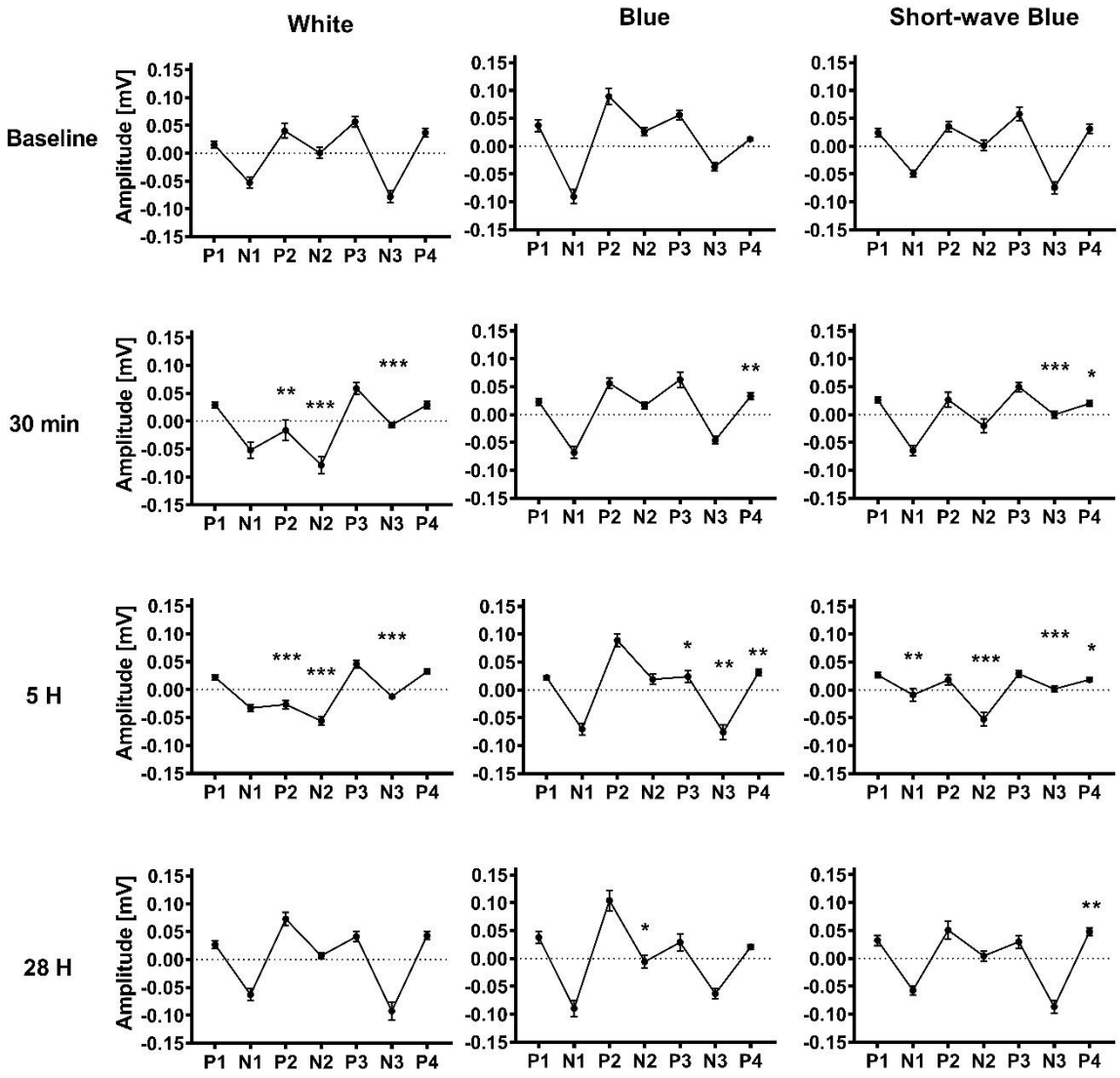

Figure 2 Sildenafil-induced changes in amplitude of visual evoked potentials from rat visual cortex. Amplitudes are plotted as the mean with standard error of mean (SEM). The columns depict data obtained from stimulation with different visual stimuli: white, blue and short-wave blue light. The rows represent time related to dosing: baseline (before dosing), 30 minutes post, 300 minutes post, and 28 hours after administration of sildenafil. The asterisks refer to significant differences after sildenafil administration compared to baseline with significance levels of p<0.05=*, p<0.01=, and p<0.001=***.**

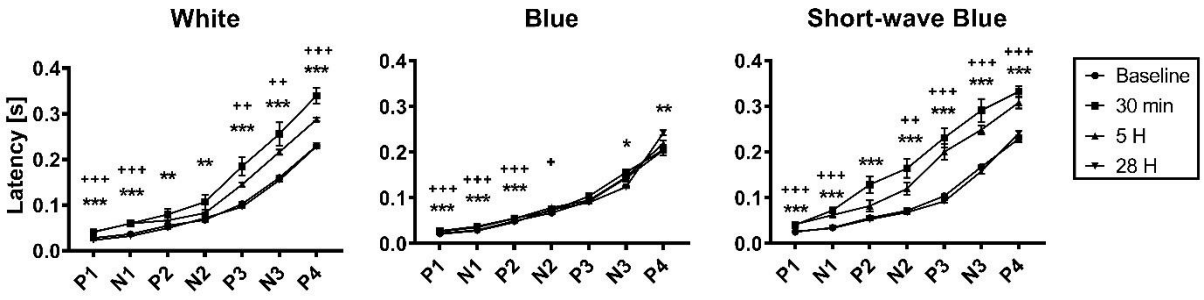

Figure 3 Sildenafil-induced changes in latency of visual evoked potentials from rat visual cortex. Effects are depicted with mean ± SEM. Latency of peaks for each time point, for each color: white, blue and short wave blue light Asterisks refer to significant differences between baseline and 30 min. Plus signs depicts differences between baseline and 300 min.

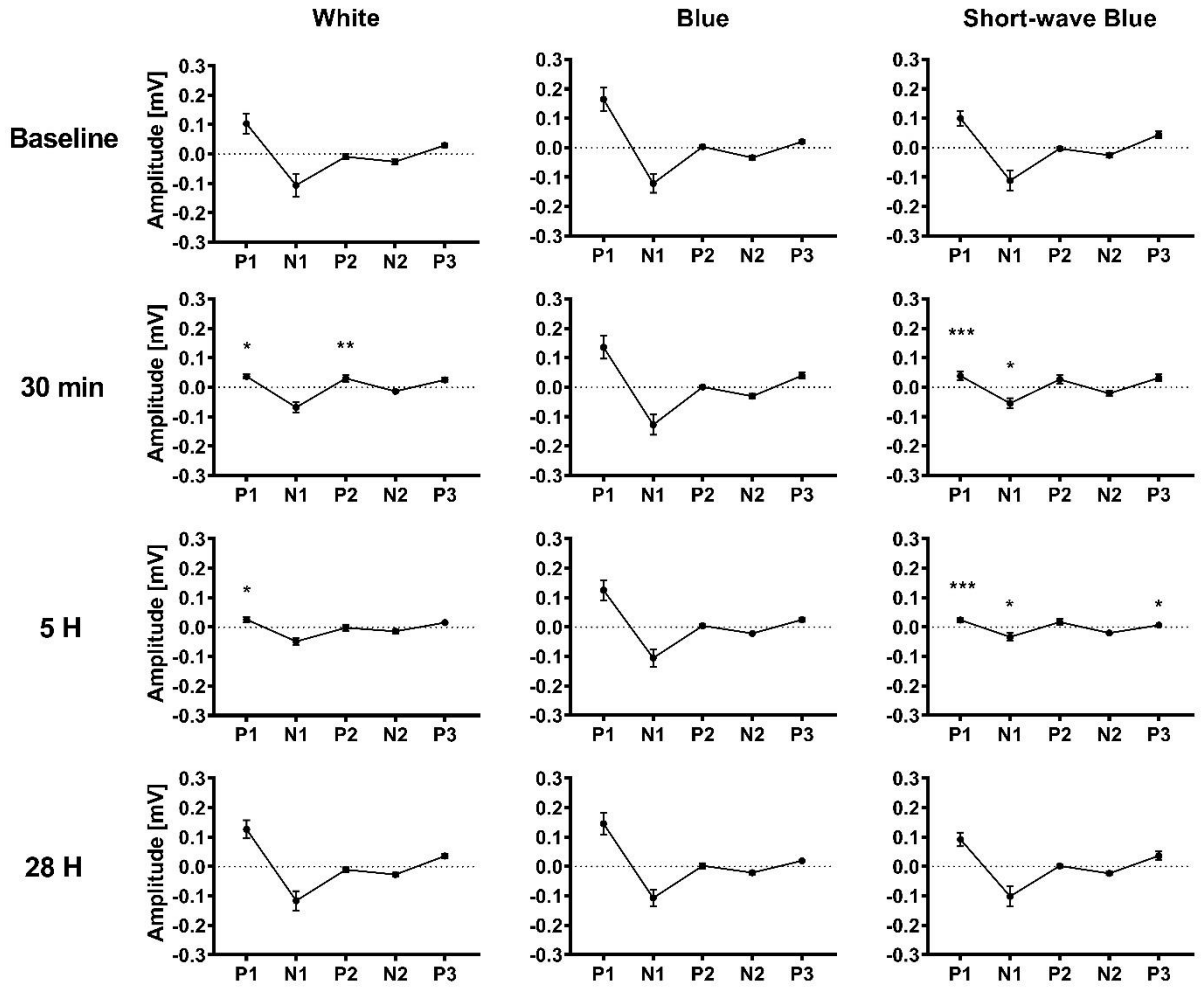

Figure 4 Sildenafil-induced changes in amplitude of visual evoked potentials from rat superior colliculus. The graphs show the mean ± SEM of the amplitude of peaks under three different color conditions at four timepoints. The columns depict data obtained from stimulation with different visual stimuli: white, blue and short-wave blue light. The rows represent the four time points: baseline (before dosing), 30 minutes, 5 hours, and 28 hours after administration of sildenafil.

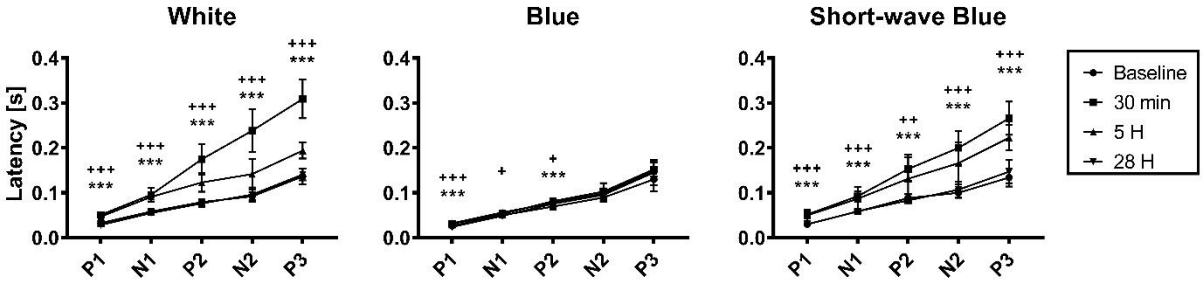

Figure 5 Sildenafil-induced changes in latency of visual evoked potentials from rat superior colliculus across three color conditions and four time points. Effects are depicted with mean ± SEM. Asterisks represent differences between baseline and 30 min. Plus signs delineates differences between control and 300 min.

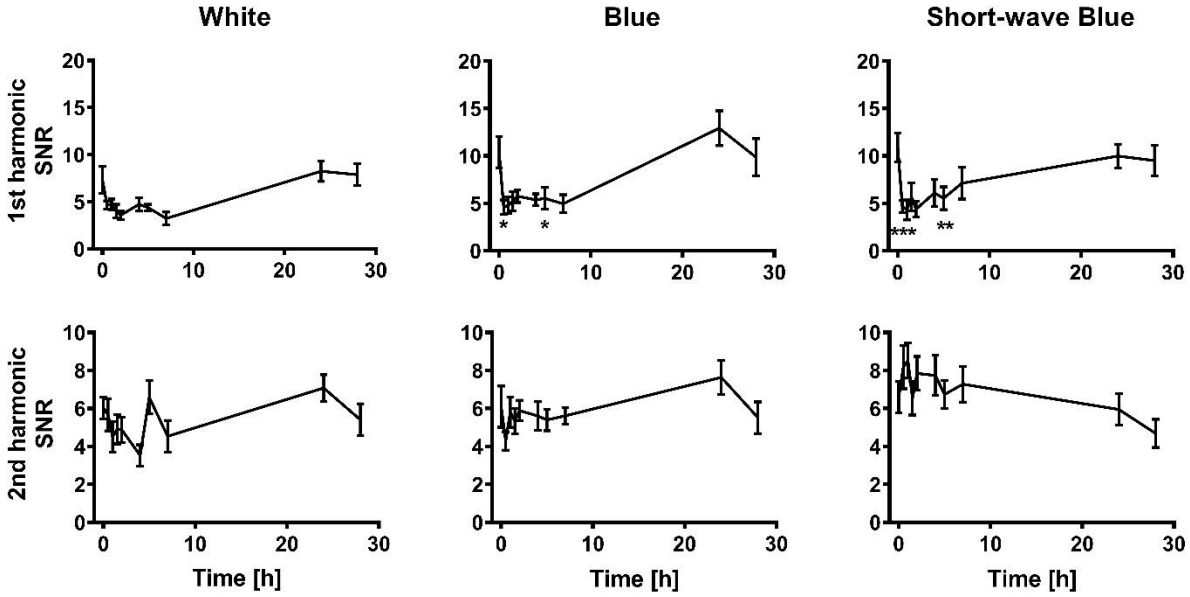

Figure 6 Signal-to-noise ratio of the 1st and 2nd harmonic of steady-state visual evoked potentials from visual cortex is affected by sildenafil. The SNR (mean and SEM) of the SSVEP for 1st and 2nd harmonic of the visual cortex during exposure to white, blue and short-wave blue light. The line plots show time points: 0=baseline; 30min after administration of sildenafil, 1, 1.5, 2, 4, 5, 7, 24 and 28 hours. There are significant changes for the 1st harmonic of the blue and the SWB conditions.

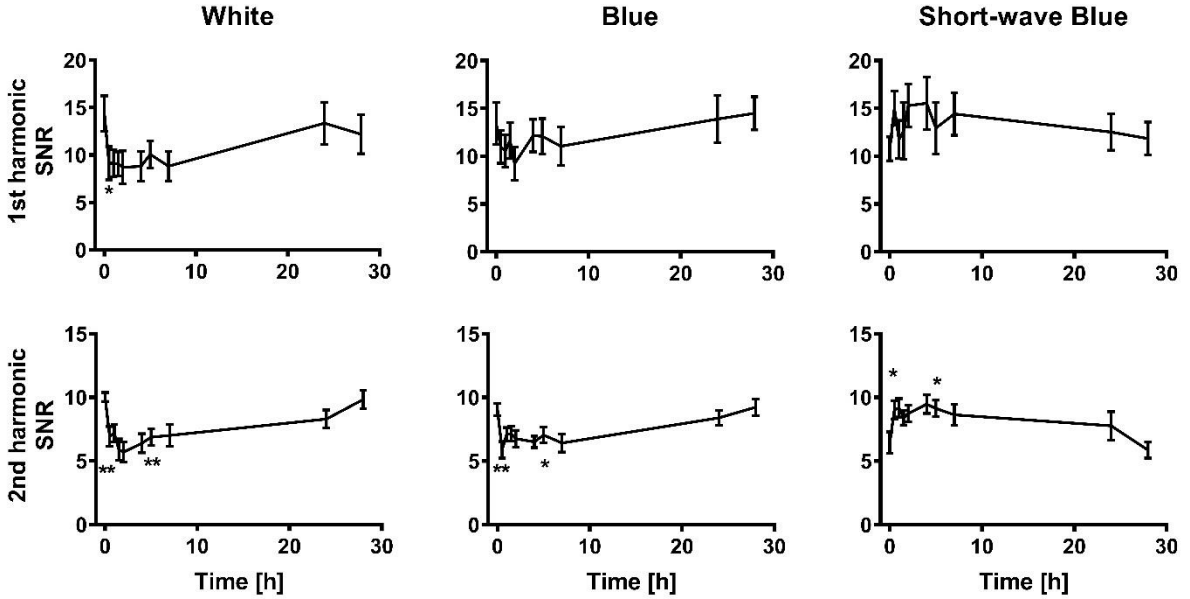

Figure 7 Signal-to-noise ratio of the 1st and 2nd harmonic of steady-state visual evoked potentials from superior colliculus during exposure to white, blue and short-wave blue light. The line plots show the mean and SEM from each time point: baseline at time=0 and the last recording at 28h. There is a significant change in the 1st harmonic in the white light condition, and in the second harmonic for all conditions.

15.2 Supplementary

Visual cortex, amplitude		F-value	P-value	Adjusted p-value
P1	Time F(3,81) Color F(2,81)	1.78 1.91		
N1	Time F(3,81) Color F(2,81)	6.4 14.43	0.0006 <0.0001	0.00071 0.000126
P2	Time F(3,81) Color F(2,81) Interaction F(6,81)	11.55 30 2.77	<0.0001 <0.0001 0.0167	0.000126 0.000126 0.0179
N2	Time F(3,81) Color F(2,81) Interaction F(6,81)	13.35 23.87 7.97	<0.0001 <0.0001 <0.0001	0.000126 0.000126 0.000126
P3	Time F(3,81) Color F(2,81)	6.30 1.05	0.0007	0.000812
N3	Time F(3,81) Color F(2,81) Interaction F(6,81)	36.3 3.4 13.29	<0.0001 0.0383 <0.0001	0.000126 0.0383 0.000126
P4	Time F(3,81) Color F(2,81) Interaction F(6,81)	4.85 8.09 7.9	0.0037 0.0006 <0.0001	0.00421 0.00071 0.000126
Latency				
P1	Time F(3,81) Color F(2,81) Interaction F(6,81)	139.49 101.13 12.19	<0.0001 <0.0001 <0.0001	0.000126 0.000126 0.000126
N1	Time F(3,81) Color F(2,81) Interaction F(6,81)	106.95 76.97 13.04	<0.0001 <0.0001 <0.0001	0.000126 0.000126 0.000126
P2	Time F(3,81) Color F(2,81) Interaction F(6,81)	18.83 16.96 5.55	<0.0001 <0.0001 0.0001	0.000126 0.000126 0.000126
N2	Time F(3,81) Color F(2,81) Interaction F(6,81)	19.33 16.3 7.41	<0.0001 <0.0001 <0.0001	0.000126 0.000126 0.000126
P3	Time F(3,81) Color F(2,81) Interaction F(6,81)	55.9 48.27 13.22	<0.0001 <0.0001 <0.0001	0.000126 0.000126 0.000126
N3	Time F(3,81) Color F(2,81) Interaction F(6,81)	48.61 56.25 7.32	<0.0001 <0.0001 <0.0001	0.000126 0.000126 0.000126
P4	Time F(3,81) Color F(2,81) Interaction F(6,81)	43.41 60.12 17.63	<0.0001 <0.0001 <0.0001	0.000126 0.000126 0.000126

Table S 1 Two-way ANOVA of the amplitude and latency of the waveform from the visual cortex

Superior colliculus, amplitude		F-value	P-value	Adjusted p-value
P1	Time F(3,81)	6.79	0.0004	0.000494
	Color F(2,81)	15.10	<0.0001	0.000126
N1	Time F(3,81)	3.57	0.0177	0.0187
	Color F(2,81)	3.73	0.0282	0.0292
P2	Time F(3,81)	4.82	0.0039	0.00435
	Color F(2,81)	1.31		
N2	Time F(3,81)	1.14		
	Color F(2,81)	1.07		
P3	Time F(3,81)	3.73	0.0144	0.0158
	Color F(2,81)	0.3		
	Interaction (6,81)	2.37	0.0368	0.0374
Latency				
P1	Time F(3,81)	58	<0.0001	0.000126
	Color F(2,81)	44.55	<0.0001	0.000126
	Interaction (6,81)	5.33	0.0001	0.000126
N1	Time F(3,81)	44.99	<0.0001	0.000126
	Color F(2,81)	50.47	<0.0001	0.000126
	Interaction (6,81)	7.32	<0.0001	0.000126
P2	Time F(3,81)	43.52	<0.0001	0.000126
	Color F(2,81)	34.93	<0.0001	0.000126
	Interaction (6,81)	8.90	<0.0001	0.000126
N2	Time F(3,81)	54.97	<0.0001	0.000126
	Color F(2,81)	32.74	<0.0001	0.000126
	Interaction (6,81)	12.6	<0.0001	0.000126
P3	Time F(3,81)	89.83	<0.0001	0.000126
	Color F(2,81)	40.53	<0.0001	0.000126
	Interaction (6,81)	19.03	<0.0001	0.000126

Table S 2 Two-way ANOVA of the amplitude and latency of the waveform from the superior colliculus.

Visual Cortex Amplitude	white			Blue			Short-wave blue		
	F(3,25)	p-value	Adjusted p-value	F(3,25)	p-value	Adjusted p-value	F(3,25)	p-value	Adjusted p-value
P1	2.13	ns		2.18	ns		0.68	ns	
N1	1.66	ns		1.67	ns		7.46	0.001	0.0012
P2	12.69	<0.0001	0.00013	2.87	ns		1.28	ns	
N2	20.96	<0.0001	0.00013	3.55	0.0287	0.031	6.32	0.0024	0.0027
P3	1.03	ns		4.22	0.0151	0.02	2.47	ns	
N3	23.49	<0.0001	0.00013	5.62	0.0044	0.0072	27.63	<0.0001	0.00013
P4	2.98	ns		5.96	0.0033	0.0072	13.96	<0.0001	0.00013
Latency									
P1	47.97	<0.0001	0.00013	29.49	<0.0001	0.00026	81.25	<0.0001	0.00013
N1	64.29	<0.0001	0.00013	35.86	<0.0001	0.00026	38.55	<0.0001	0.00013
P2	6.62	0.0019	0.0023	15.18	<0.0001	0.00026	11.89	<0.0001	0.00013
N2	5.55	0.0046	0.0049	3.28	0.0375	0.038	15.03	<0.0001	0.00013
P3	20.25	<0.0001	0.00013	2.38	ns		43.8	<0.0001	0.00013
N3	16.72	<0.0001	0.00013	11.56	0.0001	0.00026	34.13	<0.0001	0.00013
P4	43.03	<0.0001	0.00013	5.67	0.0042	0.0072	35.91	<0.0001	0.00013

Table S 3 Results of one-way ANOVAs from visual cortex. P-values are adjusted within each wavelength condition

Superior Colliculus Amplitude	white			blue			Short-wave blue		
	F(3,25)	p-value	Adjusted p-value	F(3,25)	p-value	Adjusted p-value	F(3,25)	p-value	Adjusted p-value
P1	5.01	0.0074	0.0074	0.39	ns		10.05	0.0002	0.00025
N1	1.72	ns		0.23	ns		4.47	0.012	0.013
P2	5.56	0.0046	0.0049	0.056	ns		1.94	ns	
N2	1.15	ns		1.09	ns		0.16	ns	
P3	2.73	ns		2.09	ns		3.52	0.0295	0.03
Latency									
P1	25.26	<0.0001	0.00013	27.32	<0.0001	0.00026	20.94	<0.0001	0.00013
N1	45.35	<0.0001	0.00013	3.88	0.0209	0.025	13.2	<0.0001	0.00013
P2	42.56	<0.0001	0.00013	5.34	0.0056	0.0081	13.72	<0.0001	0.00013
N2	45.5	<0.0001	0.00013	1.3	ns		21.33	<0.0001	0.00013
P3	89.3	<0.0001	0.00013	1.69	ns		44.57	<0.0001	0.00013

Table S 4 Results of ANOVAs from superior colliculus

Amplitude of SSVEP	white			blue			Short-wave blue		
Visual cortex	F(3,25)	p-value	Adjusted p-value	F(3,25)	p-value	Adjusted p-value	F(3,25)	p-value	Adjusted p-value
1st	2.87	ns		4.57	0.011	0.011	6.85	0.0016	0.0032
2nd	0.37	ns		0.82	ns		2.39	ns	
Superior colliculus									
1st	3.06	0.0467	0.047	0.93	ns		1.14	ns	
2nd	5.76	0.0039	0.0078	6.04	0.0031	0.0062	4.5	0.0117	0.0117

Table S 5 Results of ANOVAs of the SSVEP data from both the visual cortex and the superior colliculus

16 Manuscript II

Classification of α-synuclein-related pathology in a rat model: identifying PD biomarkers using electrophysiological measurements of visual function

Freja Gam Østergaard[1], Bettina Laursen[1], Marc M. Himmelberg[2], Tim B. Dyrby[3], Hartwig R. Siebner[3], Alex R. Wade[2], and Kenneth Vielsted Christensen[1]

[1]Department of Translational Biology, H. Lundbeck A/S, Ottiliavej 9. DK-2500 Valby, Denmark. [2] Department of Psychology, The University of York, Heslington, York, YO10 5DD, United Kingdom. [3]Danish Research Centre for Magnetic Resonance, Copenhagen University Hospital Hvidovre, Hvidovre, Denmark.

Corresponding author: Freja Gam Østergaard

Target journal: eNeuro

Abstract

Parkinson's disease (PD) is the second most common neurodegenerative disorder. Biomarkers suitable for early diagnosis and monitoring disease progression are the cornerstone of developing disease-modifying treatments for neurodegenerative disease such as PD. Besides motor complications, PD is also characterized by deficits in human visual processing, and recent studies using electrophysiological measurements from the visual system of fly models of PD have identified visual evoked potentials (VEPs) as potential biomarkers for PD associated biologies. Here, we investigate how virally-mediated overexpression of α-synuclein in the substantia nigra pars compacta (SNc) impacts visual processing in a well-established rodent model of PD. Subsequent to a unilateral injection of virus, human α-synuclein was detected in the striatum and superior colliculus (SC). In parallel, there was a significant delay in the latency of the transient VEPs from the affected side of the SC in late stages of the disease. Inhibition of leucine-rich repeat kinase (LRRK2) using PFE360 did not rescue the VEP delay; however, PFE360 increased the latency of the VEP waveform. A support vector machine (SVM) classifier accurately classified rats according to their disease state using steady-state visual evoked potential (SSVEP) profiles. Overall, these findings indicate that the latency of the rodent VEP is sensitive to changes mediated by the overexpression of α-synuclein when the overexpression is fully developed, whereas the SSVEP facilitated detection of α-synuclein across all stages of model progression.

Significance statement

There is a lack of biomarkers for disease progression in the field of Parkinson's disease. This study explores how electrophysiological changes in the rat visual system act as a surrogate biomarker for measuring the progression of disease pathology-relevant expression of human α-synuclein. Identifying subtle differences in neural signalling that persist across time may be beneficial for earlier diagnosis, in prodromal PD if applicable to the human condition, and may support preclinical drug testing in disease models when combined with machine learning classification methods, as these may provide the necessary sensitivity to refine current models.

Introduction

Parkinson's disease (PD) is a progressive neurodegenerative disorder affecting ~0.2 - 3.0% of the population and is characterised by motor symptoms such as bradykinesia, resting tremor, postural instability, and difficulty in initiation of movement (Clarke, 2007; de Rijk et al., 1997). PD is also characterized by secondary non-motor symptoms such as hyposmia, constipation, orthostatic hypotension, depression, sleep disorders, decline in cognitive abilities, and deficits in visual processing. Many of these are present already at early stages of the disease whereas classical motor-related PD symptoms are present in the mid stages of PD (Meissner, 2012; Stern and Siderowf, 2010). Thus, the pathogenesis of PD develops in the prodromal stages of the disease (Noyce et al., 2016). Standard care in PD is symptomatic. Consequently, there is a high unmet need for validation of new biomarkers that can be used to assess new disease-modifying drug treatments in early or prodromal stages of PD (Guo et al., 2018).

According to the Braak staging hypothesis, PD is a progressive synucleinopathic disorder in which six disease stages are associated with a progressive pathology to neurological structures (Braak et al., 2003). Such pathological hallmarks of PD are the degeneration of dopaminergic neurons in the substantia nigra pars compacta (SNc) (Thomas and Beal, 2007) and Lewy bodies (LB) and Lewy neurites; pathological inclusions of aggregated α-synuclein protein in neurons (Giasson et al., 2000; Spillantini et al., 1997). In support, duplications and triplications of the *SNCA* gene encoding the α-synuclein protein are associated with autosomal dominant early onset PD and accompanied by LB (Singleton et al., 2003).

Visual perturbations are common but often overlooked in PD. Some of the most consistent deficits are changes in contrast sensitivity (Ekker et al., 2017; Langheinrich et al., 2000) and delays in visual evoked potentials (VEPs) (Bodis-Wollner and Yahr, 1978; He et al., 2018). The occurrence of these changes in PD have been linked to the spread of α-synuclein aggregates and to reductions of dopamine within the retinal amacrine cells (Miri et al., 2016; Witkovsky, 2004).

In the adeno-associated virus (AAV) α-synuclein rat model of PD, structural pathology originates from the injection site in the SNc, spreading to the striatal and cortical regions (Andersen et al., 2018; Decressac et al., 2012). In rodents, the SNc projects to the superior colliculus (SC) (Comoli et al., 2003), while indirect links exist between the SNc and visual cortex (Hopkins and Niessen, 1976). The SC is believed to be the most prominent retinal target in the rodent, receiving ~90 % of the projections from the retinal ganglion cells (Linden and Perry, 1983; Sefton et al., 2014). Thus, there is potential for α-synuclein expression to affect visual processing in a rodent model of PD.

Recent research reported changes in visual processing using *Drosophila* models of PD, identifying increased contrast sensitivity as a visual biomarker in young *Drosophila* expressing a gain-of-function variant of the human leucine-rich repeat kinase 2 (LRRK2-*G2019S*) causing autosomal dominant PD in humans (Afsari et al., 2014). In the fly, pharmacological inhibition of LRRK2-*G2019S* fully rescued visual perturbations. This research has expanded to include sensitive machine learning classification techniques that allow the investigation of subtle differences in visual function (Himmelberg et al., 2018a; West et al., 2015). Establishing the utility of machine learning techniques to identify new visual biomarkers in animal models of diseases is important, as these techniques can be used as a tool for testing new therapeutic drugs that aim to alter disease progression, and define cross-species biomarkers that could be translated to the human condition (Schapira et al., 2017).

Here, we aim to investigate changes in visual processing caused by α-synuclein related pathology in a rodent model of PD, using electrophysiological measurements of VEP and steady-state visually evoked potentials (SSVEPs), from the visual cortex (VC) and SC. Previous work has established that overexpression of human α-synuclein in the SNc leads to changes in firing pattern in the subthalamic nucleus of the rat (Andersen et al., 2018). Importantly, genetic and pharmacological ablation of LRRK2 using PFE360 rescued the α-synuclein mediated changes in firing (Andersen et al., 2018). From this, we hypothesise that the overexpression of α -synuclein will cause changes in the VEP waveform, and such changes are likely to be rescued by LRRK2 inhibition. Previously, machine learning classifiers have proved successful in classifying *Drosophila* PD models into their correct group based on subtle differences in visual response. Finally, we aim to investigate whether we can similarly classify rodents into their correct group using SSVEP profiles in a sensitive support vector machine (SVM) classifier.

Methods

All animal experimentation was carried out in accordance with the European Communities Council Directive (86/609/EEC), and in accordance with Danish law on care of laboratory animals.

Animals and stereotaxic surgery

26 female Sprague-Dawley (SD) rats, weighing 225g at arrival, were used in the study. Rats were anesthetized using Hypnorm® in saline and midazolam (B.Braun, Melsungen, Germany) in a 2:1:1 relation (equivalent to fentanyl 157 µg/kg) and placed in a stereotaxic frame. Local anaesthetic (Marcain, 2.5mg/ml bupivacaine, AstraZeneca, Albertslund, Denmark) was injected prior to incision. A small drill was used to make seven holes in total: above the SNc (AP: -5.5, ML: +2.0 DV: -7.2) of the left hemisphere. Electrodes were implanted bilaterally in the SC (AP: -6.0, ML: ±1.0, DV:-3.5) and visual cortex (AP: -6.0, ML: ±4.0). Reference electrode was placed at (AT: +8.0, ML: -2.0), and the ground electrode at (AP: -2.0, ML: +4.0).

Electrodes with a 15mm mounting screw (E363/20/2.4/S, PlasticsOne, VA, US) were inserted into the visual cortex, reference, and ground holes. Stranded electrodes with a 25mm mounting screw (E363/3/Spc, PlasticsOne, VA, US) were placed in the SC. Rats were randomly assigned into one of two groups, α-synuclein or null, with 13 rats in each group. The α-synuclein group received an injection of adeno-associated virus (AAV) containing human wildtype *SNCA* (hSNCA) into the left SNc, whereas the null group received an injection of an empty AAV vector. The α-synuclein rats were injected with 3.0 µl of viral particles ($30x10^{10}$ GC) carrying the rAAV2/5 viral vector (Vector biolabs, Malvern, PA, USA) using a 32G Hamilton cannula with an injection rate of 0.2 µl/min. The right hemisphere received no treatment. The electrode leads were gathered in a plastic pedestal (PlasticsOne, VA, US) as a chronic implant attached using dental cement RelyX™ Unicem (3M, Denmark) and Fuji plus (GC, US).

The procedure for all rats was completed over 9 days. Rats were left to recover for 2 weeks. VEP and SSVEP recordings were made at eight time points throughout an 11-week period (see Figure S1), counted from the first day of surgery at 3, 5, 6, 7, 8, 9, 10, and 11 weeks.

VEP and SSVEP stimuli

In the VEP experiment, rats were presented with a single flash of light at 1Hz under 5 wavelength conditions to investigate interactions between α-synuclein overexpression and wavelength. The wavelength were: red light (20 lx, 620-625 nm), green light (20 lx, 525-530 nm), blue light (20 lx, 455 - 460 nm), short-wave blue light (5 lx, 405 nm), and white light (20 lx, 400 - 700 nm). This also benefited our SVM classification analysis by increasing the number of features that could be

included in the classifier. Each rat was presented with 400 repetitions of each wavelength condition of the VEP stimulus at each testing session. Similarly, in the SSVEP experiments, rats were presented with flickering luminance stimuli that flickered with a square wave at a frequency of 14 Hz, with each presentation run lasting 100 seconds. Again, the SSVEP stimulus had five wavelength conditions, identical to the VEP stimuli. Each flash was 10ms in length and there was no light in the cage between flashes. Lux was measured using an LED luxmeter (Extech, MA, US) located in the bottom of the cage. Stimuli were controlled by Spike2 ver. 7.13 (RRID:SCR_000903) (Cambridge Electronic Design Ltd, UK) and were presented using 5050 SMD LEDs.

Data collection

Rats were placed in a standard makrolon cage of polycarbonate and a Plexiglas box (measuring 43.8×35×27.9 cm) placed on top of the makrolon cage, and then placed inside a larger Faraday cage. The LEDs were placed at 40cm above the base of the cage and illuminated the entire Faraday cage. VEPs and SSVEPs were recorded using Spike2 ver. 7.13 while the animals were awake and behaving.

Cylinder test

Eleven weeks after the injection of AAV, the rats were tested for motor asymmetry induced by the injection of α-synuclein in the left SNc. This overexpression affects the striatum ipsilateral of the injection and reduces the use of the contralateral paws. Rats were placed in a transparent plastic cylinder, with one paw dyed red and the other dyed green. The animals were recorded for five minutes using a video camera. The number of touches on the plastic was counted and the ratio of contralateral to total number of touches was computed. The results from the two groups of rats were compared using an unpaired t-test.

Administration and exposure of PFE360

PFE360 is a LRRK2 kinase inhibitor first described in Baptista et al. (2015). The drug was synthesized at Lundbeck A/S (Valby, Denmark) and dissolved in 10% captisol titrated to pH >2 using 1M methanesulphonic acid to a concentration of 3mg/ml. The rats were administered perorally with a dosage corresponding to 7.5 mg/kg of PFE360. The dosing was carried out as a randomized cross-over study 14-15 weeks after the injection of the AAV particles. EEG recordings were initiated 1 hour after administration at the maximum brain concentration (Cmax) (Andersen et al., 2018). The animals were decapitated after the final recording session, approximately 3 hours

after the last PFE360 dosing. The blood and brain tissue from the cerebellum were sampled after the final EEG recordings to determine the peripheral and central exposure of PFE360. The procedure for sampling and determination of the PFE360 concentration is described in detail in Andersen et al. (2018).

Post-mortem assessment of lesion

Brains were divided into three parts for western blotting, assessment of compound concentration in the brain, and histological validation of electrode location. The rostral part containing the striatum was frozen and used for western blotting. The medial part from 13 of the 26 rats (seven control animals and six from the α-synuclein group) was immersion fixed and the medial part from the remaining 13 rats were used for western blotting. The immersion fixed brain parts were used for immunohistochemistry, as the medial region contains the SC. The cerebellum was used to determine the brain concentration of PFE360.

Western blotting for α-synuclein, tyrosine hydroxylase (TH), LRRK2 and LRRK2-pS935

The procedure for tissue preparation and western blotting is described in detail in Andersen et al. (2018). Briefly, tissue punches were taken from the striatum and the SC and were homogenized using a Precellys® lysing kit (Bertin Instruments, France) with CelLytic M buffer (Merck, Germany) and proteases. Protein was isolated and the concentration was determined with BCA Protein Assay (Thermo Scientific, MA, US). For SDS-PAGE and western blotting procedures, 2.5 µg of protein was added in each well. The antibodies were detected using a Licor Odessey system (LI-COR Biosciences, NE, US) with fluorescent secondary antibodies and a Chameleon™ duo pre-stained protein ladder (LI-COR Biosciences, NE, US). Intensity values for the fluorescence of the TH band were measured using the Licor Image Studio Ver. 3.1.4 (LI-COR Biosciences, NE, US).

Histology

The immersion fixed brain parts were cut in slices of 40 µm on a freeze microtome and placed in potassium phosphate buffered saline (KPBS). The tissue was quenched with hydrogen peroxide and washed in KPBS before being incubated with primary antibody. It was then washed before being incubated with the second antibody and exposed using a 3,3-diaminobenzidine (DAB)-reaction. The primary antibodies used were: hWT-α-synuclein (4B12) (Thermo scientific, US).

Four perfusion fixed brains from an earlier study of the AAV-model were kindly donated by Michael Aagaard Andersen. The brains had been extracted at week 10-11 and were stained for hWT α-synuclein (4B12) to investigate the presence of α-synuclein in the SC.

VEP analysis

The peak amplitude and the latencies of the flash VEPs were extracted from the Spike2 waveform display. Here, we defined the peak amplitude as the difference from a baseline to a named peak, measured in millivolts (mV). The latency for any peak was measured relative to the stimulus onset. The SSVEP data was exported from Spike2 and further analysed in MATLAB 2018a (Mathworks, MA, USA).

The latency and amplitude of the peak of the VEP waveform was extracted manually in Spike2. For each rat and waveform condition, average values were computed for each electrode and timepoint over all 400 repetitions. Statistical analysis for the amplitude and latency of the VEP, and the data obtained from the cylinder test, was carried out using the Rstudio interface for R ver. 3.4.2 (RRID:SCR_000432) (RStudio, MA, US).

Individual ANOVAs were conducted for both visual cortex (VC) and SC. This resulted in 24 separate comparisons which were corrected for multiple comparisons using false discovery rate (FDR). As the AAV injection was unilateral, the contralateral side was considered an internal control. This means that an effect of AAV-mediated α-synuclein overexpression would show as an interaction between the treatment group and the side in which the recording was made. The three-way ANOVA included the variables side, group, and colour. The principles of the backward variable elimination strategy was applied to assess whether any of the variables could be discarded (Hocking, 1976). Post-hoc comparisons were carried out using the Tukey multiple comparison test. The three-way ANOVA yielded $p > 0.05$ for third order interactions, indicating they could be removed, and the model was repeated for all possible second order interactions.

For the PFE360 experiments, a four-way ANOVA was applied with drug as an additional factor. The analysis was carried out using the backward variable elimination strategy, followed by Tukey post-hoc comparisons.

SSVEP analysis

SSVEPs are phase locked electrophysiological signals traditionally analysed in the frequency domain, rather than the time domain (Norcia et al., 2015). SSVEP data were analysed separately at each week using MATLAB 2018a (RRID:SCR_001622) (Mathworks, MA, USA). The data comprised 100 1s bins. Figure S2A shows an example of an averaged EEG time course across 1s.

The first 5s and the last 5s of each SSVEP time course were excluded to account for onset transients and offset artefacts, thus retaining 90 1s bins of EEG data per rat for each electrode and wavelength, at each week. These data were transformed into the power spectrum by running a fast Fourier transform (FFT) on each 1s bin. As presented in Figure S2B, amplitude peaks occurred at multiples of our input frequency, namely 1*f* (14Hz) and 2*f* (28Hz). We retained the Fourier amplitudes from these two frequencies as our frequencies of interest.

To filter the data, the mean noise was computed by averaging the amplitudes in the four frequency bins above and below the two frequencies of interest (14Hz and 28Hz). To create a signal to noise (SNR) estimate, we compared the Fourier amplitude at 1*f* and 2*f* to the root mean square (RMS) of the noise calculated from these local side bins. Any amplitude bins that had a SNR lower than 1 were excluded. Thus, all amplitudes retained for further analysis had a Fourier amplitude that was larger than the average noise across the neighbouring bins of 1*f* and 2*f* on the power spectrum. The SNR measurements were used to minimize the variation contributed by noise in the SSVEP.

We used a three-way ANOVA to test the α-synuclein induced differences in SSVEPs within week 11. The variables were side, group, and colour.

Phase was analysed using the CircStat toolbox for Matlab (Berens, 2009). A hktest (two-factor ANOVA, directional statistics) (Harrison and Kanji, 1988) was computed for the pooled wavelength conditions. The independent variables were group and side.

Machine learning classification and bootstrapping

The goal of using the SVM classifier was to accurately classify rats based on multiple features of the SSVEP amplitude drawn from different electrode configurations. Each rat had a total of 40 potential SSVEP amplitude features that could be used in the classification (i.e. amplitudes from 5 illumination wavelengths, 2 harmonics, and 4 electrodes) with 90 1s bins of data for each of these features. It is possible to apply a machine learning classifier to the two groups of rats and compute an overall classification accuracy. However, this can lead to issues of overfitting. To circumvent this, the classification procedure was bootstrapped to perform multiple classification iterations on groups of `synthetic' rats by sampling data from the group-level population.

The classification estimates were bootstrapped by repeatedly sampling (without replacement) from the 1s bin pool of Fourier amplitudes. For each of the four electrodes, this sampling pool contained a maximum of 1170 Fourier amplitude bins (13 rats x 90 1s bins). Wavelength was included as a feature, rather than classifying *into* wavelength, as an increase in features often benefits classification accuracy. We randomly permutated through these amplitude bins, assigning 90 random 1s bins from each feature to each synthetic rat. These 90 1s bins were then averaged

together for each feature. The phase data was not included in the SVM, as the summation of phase response across individual 1s SSVEP bins may yield inaccurate phase information.

This created 13 unique synthetic α-synuclein rats and 13 synthetic control rats. Amplitude responses were normalized by Z-scoring the data across each synthetic rat. The z-score of each feature was entered into the SVM classifier and labelled with the class that the data corresponded to; α-synuclein or control rat. Unique variations of these synthetic rats were run through 1000 bootstrapped iterations of the classifier to derive a mean classification accuracy and corresponding significance value. The mean classification accuracy was deemed significant if less than 5% of the 1000 iterations fell below a 50% chance baseline, equivalent to a *p*-value of .05. In an additional analysis, we shuffled our rat labels on each run. If the SVM is working correctly, we would expect the mean classification accuracy of shuffled data to fall around chance (50%).

Support Vector Machine

The SVM is a robust supervised learning model based on statistical learning theory developed and implemented by Vladimir Vapnik (Vapnik, 1995). The SVM uses a non-linear hyperplane as classification boundary to assign new examples of data to either class, with the output being the accuracy of the SVM in classifying new examples of data (Boser et al., 1992; Cortes and Vapnik, 1995; Wang, 2018). We bootstrapped a SVM classification analysis in MATLAB 2018a using LIBSVM, ver. 3.23 (Chang and Lin, 2011). The SVM had a radial basis kernel function and a 5-sample k-fold cross validation, with 4 groups of data used as the training data and a single group used as the validation data for each run to avoid overfitting.

Results

AAV-mediated overexpression of α-synuclein

To investigate the extent of spreading of the α-synuclein protein to visual regions in the α-synuclein rats, the brains from rats injected with the AAV-h*SNCA* vector were collected at week 10-11 and stained for human wild-type α-synuclein (Figure 1). All brains (n=4) showed an abundance of α-synuclein expression in the ipsilateral SNc and surrounding areas, all ipsilateral to the injection. Immunoreactivity towards human α-synuclein was also observed in the ipsilateral SC. No α-synuclein immunoreactivity was detectable in the contralateral hemisphere, although minor unspecific binding around the edges of the tissue was observed.

α-synuclein is associated with a behavioural motor deficit in the AAV α-synuclein rat

The rats completed the cylinder test in week 11 to assess motor asymmetries associated with the behavioural consequences of α-synuclein overexpression. The cylinder test (Figure S 3A) showed a significant motor asymmetry for the α-synuclein group, but not in the control group. There was a statistical significant difference in the mean ratio of contralateral touches to total number of touches ($t(21)=-3.99$, $p<0.001$). The mean ratio for the α-synuclein rats was 0.34 suggesting that 34 % of touches were with the contralateral paw (i.e. right paw). The control group used the two paws equally, with a mean ratio of 0.49.

Further, as the immunohistochemistry was carried out on brains from a different study (see methods) western blotting was applied to validate the presence of α-synuclein in the striatum and SC of the animals used in the current study. For a representative blot, see (Figure S 3B). The western blots indicated that α-synuclein was present in the SC and striatum ipsilateral to injection in the α-synuclein rats. Although high interindividual variability was observed, visual inspection of the western blot only indicated subtle, if any, changes in the TH levels in the striata ipsilateral to the injection in the α-synuclein group (Figure S 3B).

Measurements of VEP

Visual cortex is not impacted by AAV-mediated α-synuclein overexpression

Next, we investigated whether the overexpression of α-synuclein caused any changes in the VEP measured from the VC. (Figure 2A) shows the grand average waveforms of right and left VC in the AAV α-synuclein group at week 11. There was no significant difference in the amplitude or the latency of the VEP, when comparing between VC of the two hemispheres of α-synuclein and control rats. This finding is corroborated by the histological findings where no evidence of α-synuclein inclusions were present in either hemisphere of the VC (data not shown).

α-synuclein alters VEP responses in the left SC

To investigate whether the overexpression of α-synuclein induced changes in visual processing we tested for differences between ipsi- and contralateral sides using the latency and amplitude data of the rodent VEP by running a three-way ANOVA using the data from week 11 (the final week of testing). The grand average of the waveform is shown in (Figure 2B). The wavelength variable was eliminated as it did not interact with the expression of α-synuclein. There was a significant effect of the interaction between side and group on the latency of P1 measured in the SC ($F(1,24)=12.32$, $p = 0.002$). The post-hoc comparisons revealed a 0.004 s mean latency increase for the left (α-synuclein expressing) SC (0.004s, SE=0.0013, $p = 0.012$) when compared to the right SC in the α-synuclein group. Similarly, post-hoc comparisons found a significant increase in latency (0.003s, SE: 0.0013, $p = .019$) when comparing between left SC in the α-synuclein rats and the control rats. There was no significant difference in latency when comparing between the right SC of α-synuclein group and control group (-0.0019s, SE=0.0013, $p = 0.44$). These findings suggest that the VEP obtained from the side of the injection in the α-synuclein animals is functionally affected, congruent with our histological inspections and results from the cylinder test.

Next, we wanted to know if this difference in response latency was evident at the earliest stage in the model. (Figure 2C) shows that the differences in latency between the right and left hemisphere increases over time in the α-synuclein rats. This is not observed in the control rats. A three-way ANOVA on the effect of side group and colour did not show a significant interaction of side and group on the latency of P1 in week three (w3) ($F(1,24)=2.78$, $p = 0.11$). This suggests that the increase in latency developed over time in parallel with the increase in expression of human α-synuclein. These results indicate that the VEP waveform is sensitive to the overexpression of α-synuclein at the later stages in the model, as evidenced by increases in the latency of P1 in the left SC of the α-synuclein injected rats.

Modulation of the VEP by the LRRK2 inhibitor PFE360

In preclinical PD models, LRRK2 inhibition has been shown to normalize visual processing deficits in LRRK2-*G2019S* transgenic fruit flies (Afsari et al., 2014) and normalize increases in burst firing of the subthalamic nucleus in AAV α-synuclein rats (Andersen et al., 2018). Here, we investigate whether LRRK2 inhibition can rescue the phenotype caused by overexpression of α-synuclein at week 14-15 after injection. (Figure 3A & B) shows the VEP waveforms (superimposed) of the grand averages from the four experimental groups: α-synuclein rats treated with either PFE360 or vehicle, and control rats treated with either PFE360 or vehicle. An increase

in the latency of the waveforms was evident in both the SC and the VC in rats dosed with PFE360. (Figure 3C) shows the unbound concentration of PFE360 measured in the cerebellum after electrophysiological recordings. The mean unbound concentration of PFE360 was 103±46 nM (mean±SD, n=11). A single rat sacrificed 3hr after single administration of PFE360 still had a free unbound brain concentration of 40 nM; significantly higher than the *in vivo*, IC50 of 2.3 nM (Andersen et al., 2018). Thus, suggesting that the LRRK2 kinase was inhibited throughout the recording sessions. Further, western blotting suggested that, the inhibition caused a reduction of phosphorylated LRRK2 as shown in (Figure S 4).

Running a 4-way ANOVA with the backward elimination of variables method (Hocking, 1976) replicated the interaction between group and side, showing a 3 ms increase in the latency of the P1 in the SC (Table S1). Further, there were significant increases in mean latency of the N1 and N2 peaks of the VEP where the differences of mean were 6 ms, and 10 ms, respectively. There was no significant difference in the P2 and P3 peaks between the SC ipsi- and contralateral to the injection (data not shown). There was a significant three-way interaction of PFE360, wavelength, and group on the latency of P4 of the VC, and this peak was excluded from the visualization in (Figure 4). There is a significant additive effect of the PFE360 on the latency for all other peaks in both the VC and the SC, but no detectable interaction between PFE360 and the α-synuclein overexpression (Table S 1). (Figure 4) shows that the latency of the peaks increases from the vehicle to the PFE360 condition. All peaks are shown in the same graph to illustrate the consistency of the observed effect. This suggests that a single acute dose of PFE360 has an impact on the rat visual response that is independent of any changes introduced by the overexpression of α-synuclein.

SSVEP shows an effect in the SNR of the first harmonic

Following the VEP findings, we tested for effects of the α-synuclein overexpression in the SSVEP data at week 11. The signal-to-noise ratio (SNR) of the amplitude data from the first harmonic of the VC showed a significant interaction of side and group (three-way ANOVA, $F(1,244) = 6.84$, $p = 0.009$), however post hoc comparisons found no significant differences. In the SC, there was a significant effect of side in the first harmonic (three-way ANOVA, $F(1,244) = 4.60$, $p = 0.033$), but no significant interaction of side and group. There were no significant changes for the second harmonic. The phase data from the SC showed no significant interaction of side and group in either harmonic and there was no significant difference in phase response from the VC when comparing between α-synuclein rats and control rats.

SVM can accurately classify α-synuclein rats vs. control rats

Currently, SVM is considered to be one of the most efficient methods of classification in real world applications. The goal of the SVM is to find the hyperplane that best separates α-synuclein and control data. To test the ability of the SVM to accurately classify differences in visual processing, visual responses from the α-synuclein rat and control rat groups were compared, with amplitude data from all four electrodes were included as features. The ability to distinguish between these two groups suggests significant variation in the SSVEP of these groups across the visual system. The average classification accuracy of 1000 bootstrapped runs from each week and corresponding significance values are presented in (Table 1) and histograms of these bootstrapped accuracies are visualized in (Figure 5). The SVM was highly accurate in classifying rats into their respective groups at each week, with classifications consistently reaching > 83% accuracy. The SVM was tested with shuffled labels and found that average classification accuracies fell around 50% across all weeks (illustrated by the dotted line in Figure 5). This was similar for both analyses, indicating that the SVM was working as expected. Shuffled label classification accuracies and *p*-values are available in (Table S 2).

SVM can accurately classify SSVEP responses from left and right SC

Second, the responses from the (AAV-α-synuclein treated) left SC and the untreated right SC in α-synuclein group was compared. Here, the ability to distinguish between these two groups suggests significant variations in the SSVEP solely due to the expression of human wildtype α-synuclein. Here, we assessed the ability of the SVM classifier in distinguishing between response amplitudes within the α-synuclein rats when only responses from the left and right SC were included in the analysis. The average classification accuracy of 1000 bootstrapped runs at each week and corresponding significance values are presented in (Table 2) and histograms of these bootstrapped accuracies (and shuffled accuracies) are visualized in (Figure 6). Using the α-synuclein group alone, the SVM was able to accurately classify rats at all weeks, except at week 10 (although this was closely approaching statistical significance). Notably, the SVM performed *better* when all electrodes were included in the analysis, rather than just the electrodes from the SC of the α-synuclein group.

To sum up, these findings suggest that the SVM can accurately classify SSVEP responses in both α-synuclein rats and control rats across different electrode configurations. These results differ from our VEP results due to the highly sensitive nature of the SVM that can pick up nuanced differences in visual response profiles. Overall, it appears that the SSVEP is sensitive to the presence of the

PD-associated gene product from early α-synuclein expression at week 3, through to the fully developed overexpression at week 11.

Discussion

The purpose of this study was to investigate the potential of using VEP and SSVEP responses to detect the overexpression of α-synuclein in a rodent model of PD. First, in the α-synuclein rats, α-synuclein aggregates were localized around the site of injection (the left SNc) and this was accompanied by an increase in the latency of the VEP measured from the ipsilateral SC, after α-synuclein expression was fully developed. Following this, inhibition of LRRK2 using PFE360 could not rescue this increase in latency, but instead caused general increases in the latency of the VEP waveform. Second, the SVM was able to accurately classify rats into their correct group across time using two different electrode configurations.

The overexpression of α-synuclein causes increases in the response latency of the VEP in the left SC, and this is congruent with the accumulation of α-synuclein

We asked whether induced overexpression of α-synuclein caused a detectable electrophysiological change in the rodent visual system, as measured via the VEP and SSVEP. We have demonstrated that an increase in the latency of the VEP measured from the left SC of α-synuclein rats occurs at 11 weeks after injection. Biochemically, our data indicate a subtle decrease in the expression of TH in the left striatum by 15 weeks. The result of our cylinder test suggests that the expression of α-synuclein is fully developed by 11 weeks (Albert et al., 2019; Andersen et al., 2018). Thus, changes in the VEP waveform may only appear after α-synuclein is fully expressed. This difference was also present at 15 weeks, where it seems to have developed further, suggesting that the functional consequences of overexpressing α-synuclein develop slower than the histological phenotype, which should be fully developed at ten weeks. The AAV α-synuclein was massively present in the entire *substantia nigra* both *pars compacta* and *pars reticulata.* In the rodent, the substantia nigra par reticulata (SNr) has direct projections to the SC (Hopkins and Niessen, 1976). This connection may explain how α-synuclein aggregates are detectable in the SC, as the protein is transported and expressed within the cells. It is possible that inclusions in the SC are transported via the GABAergic processes connecting the SC and the SNc (Zhou and Lee, 2011). The exact mechanism by which the aggregated α-synuclein increases the latency of the rodent VEP remains to be elucidated. In humans, α-synuclein clusters have not been found in GABAergic cells (Surmeier et al., 2017). However, they have been identified in the SC (Erskine et al., 2017).

Treating α-synuclein rats with PFE360 caused a general delay in the VEP

Previous studies have found an interaction between LRRK2 and α-synuclein (Andersen et al., 2018; Lin et al., 2009). Thus, the rodent AAV α-synuclein model may be used to monitor disease progression and modulation by pharmacotherapy. Similar to (Andersen et al., 2018), we tested an acute dose of the LRRK2 kinase inhibitor PFE360 to see how this modulated the VEP waveform. PFE360 caused an increase in the VEP latency, for both the control and AAV-α-synuclein group, however it did not show any interaction with α-synuclein. This does not exclude that α-synuclein and LRRK2 interact under other conditions. PFE360 increases the general latencies of the VEP, which could suggest a function for LRRK2 in facilitating post-synaptic potentials. Studies of the rodent brain have localised LRRK2 in the cortex and the striatum (Davies et al., 2013), but not in the SC, yet our data indicates similar effects in both the SC and the VC.

The SSVEP showed changes in amplitude

There were general trends for changes in SSVEPs in α-synuclein rats, however post-hoc tests revealed that these trends were not significant. One limitation of the SSVEP technique is the SSVEP waveform originates from the summation of many repeated waveforms and may yield inaccurate timing information. This may explain why there is no change in SSVEP phase in the SC in either harmonic.

SVM can accurately classify rats into their correct group using SSVEP profiles

Previously, it has been demonstrated that machine learning classifiers are a useful tool for establishing new visual biomarkers in *Drosophila* PD models (Himmelberg et al., 2018a; West et al., 2015). The SVM could accurately classify α-synuclein and control rats into their correct group across differing stages of disease progression. To assess SVM accuracy in classifying rats into either α-synuclein or control rats, SSVEP amplitudes from all four electrodes were included in the SVM. Rats could be classified into their correct group at all weeks with very high accuracy (83.71% - 92.96%). Second, SSVEP amplitudes from the left and right SC of α-synuclein rats were run through the SVM. The differences between these two groups are purely due to the injection of the AAV. We were able to classify rats into their correct group at most weeks – with significant accuracies between 67.23% - 84.48%.

One might expect the highest accuracy in the second analysis, comparing SSVEPs measured from the left SC (where α-synuclein inclusions were localized) with responses from the right SC that did not receive an effect of the AAV-virus and appeared structurally healthy. However, the SVM generally performed better when data from *all* electrodes were included in the classifier. One

reason for this may be that SVM accuracy increases with increased number of features (in the first analysis there were 40 features, in the second there were only 10). Accuracy increasing with more features suggests that these additional features are relevant to the classifier itself, even though this data comes from electrodes where the effect of α-synuclein overexpression was not observable by VEP or immunohistochemistry. This indicates nuanced, but significant differences in the SSVEP amplitudes that occur as a result of the overexpression of α-synuclein. Notably, the classifier identified differences in SSVEP response as early as three weeks after the administration of the AAV vector, and these differences persisted across progression. Previous research has identified cell-to-cell transmission and the formation of exogenous α-synuclein fibrils in animal models expressing mutated *SNCA* (Niu et al., 2018). Although we did not find any physiological α-synuclein in the hemisphere contralateral to the injection, our data suggest that the functional effect of α-synuclein overexpression may cause changes in long-range neural signalling that results in perturbations of the SSVEP measured from the opposing hemisphere.

There are clear benefits in combining electrophysiological measurements of visual processes and novel classification techniques. First, it may enhance early-stage drug discovery using animal disease models. Second, the accuracy (or inaccuracy) of a classifier in differentiating between visual processes recorded from a PD model that has been treated with a therapeutic drug against a healthy control animal allows for the objective assessment of whether a treatment has rescued visual functioning (i.e. are the responses between these two classes now indistinguishable). Further, with evidence for visual biomarkers in a range of simple fly models of PD, and now a more complex rodent model, it may soon be possible to translate such methods and classify human PD patients into their correct genotype based on similar electrophysiological response profiles (Himmelberg et al., 2018b).

Conclusion

First, we have established that the latency of the VEP is sensitive to overexpression of α-synuclein, and this effect is localized to the site of α-synuclein overexpression. Next, administration of the LRRK2 inhibitor PFE360 caused general delays in the VEP which may suggest a function for LRRK2 in facilitating post-synaptic potentials. Finally, we have found that the SSVEP is sensitive to the presence of α-synuclein across multiple stages of α-synuclein overexpression and that such overexpression may cause changes in long-range neural signalling. These findings highlight the utility of the visual system to investigate changes in neural signalling that occur in PD models. Overall, these findings may prove beneficial for producing methods that assist in the early

diagnosis of PD in humans and testing new therapeutic treatments in disease models that aim to rescue neural response.

Acknowledgements

F.G.Ø and M.M.H were supported by the European Union's Horizon 2020 research and innovation programme under the Marie Skłodowska-Curie grant agreement No 641805. HRS holds a 5-year professorship in precision medicine at the Faculty of Health Sciences and Medicine, University of Copenhagen which is sponsored by the Lundbeck Foundation (Grant Nr. R186-2015-2138).

Authors' Contributions

KVC and FGØ conceived and designed the experiments, FGØ performed the experiments, FGØ and MMH analysed the data, FGØ, MMH, KVC, ARW and BL wrote the manuscript.

References

Afsari, F., Christensen, K. V., Smith, G.P., Hentzer, M., Nippe, O.M., Elliott, C.J.H., Wade, A.R., 2014. Abnormal visual gain control in a Parkinson's disease model. Hum. Mol. Genet. 23, 4465–4478. https://doi.org/10.1093/hmg/ddu159

Albert, K., Voutilainen, M.H., Domanskyi, A., Piepponen, T.P., Ahola, S., Tuominen, R.K., Richie, C., Harvey, B.K., Airavaara, M., 2019. Downregulation of tyrosine hydroxylase phenotype after AAV injection above substantia nigra: Caution in experimental models of Parkinson's disease. J. Neurosci. Res. 97, 346–361. https://doi.org/10.1002/jnr.24363

Andersen, M.A., Christensen, K.V., Badolo, L., Smith, G.P., Jeggo, R., Jensen, P.H., Andersen, K.J., Sotty, F., 2018. Parkinson's disease-like burst firing activity in subthalamic nucleus induced by AAV-α-synuclein is normalized by LRRK2 modulation. Neurobiol. Dis. 116, 13–27. https://doi.org/10.1016/j.nbd.2018.04.011

Baptista, M.A.S., Merchant, K., Bryce, D., Ellis, M., Estrada, A.A., Galatsis, P., Fell, M., Fuji, R.N., Kennedy, M.E., Hill, S., Hirst, W.D., Houle, C., Liu, X., Maddess, M., Markgraf, C., Mei, H., Steyn, S., Yin, Z., Yu, H., Fiske, B.K., Sherer, T.B., 2015. LRRK2 Kinase Inhibitors of Different Structural Classes Induce Abnormal Accumulation of Lamellar Bodies in Type II Pneumocytes in Non-Human Primates but are Reversible and Without Pulmonary Functional Consequences Workflow and Study Design 94080.

Berens, P., 2009. CircStat: A MATLAB Toolbox for Circular Statistics. J. Stat. Softw. 31. https://doi.org/10.18637/jss.v031.i10

Bodis-Wollner, I., Yahr, M.D., 1978. Measurements of visual evoked potentials in Parkinson's disease. Brain 101, 661–71. https://doi.org/10.1093/brain/101.4.661

Boser, B., Guyon, I., Vapnik, V., 1992. A Training Algorithm for Optimal Margin Classifiers, in: Proceedings of the 5th Annual ACM Workshop on Computational Learning Theory. ACM Press, pp. 144–152. https://doi.org/10.1145/130385.130401

Braak, H., Del Tredici, K., Rüb, U., De Vos, R.A.I., Jansen Steur, E.N.H., Braak, E., 2003. Staging of brain pathology related to sporadic Parkinson's disease. Neurobiol. Aging 24, 197–211. https://doi.org/10.1016/S0197-4580(02)00065-9

Chang, C., Lin, C., 2011. LIBSVM -- A Library for Support Vector Machines. ACM Trans. Intell. Syst. Technol. 2, 1–27. https://doi.org/10.1145/1961189.1961199

Clarke, C.E., 2007. Parkinson's disease. BMJ 335, 441–5. https://doi.org/10.1136/bmj.39289.437454.AD

Comoli, E., Coizet, V., Boyes, J., Bolam, J.P., Canteras, N.S., Quirk, R.H., Overton, P.G., Redgrave, P., 2003. A direct projection from superior colliculus to substantia nigra for detecting salient visual events. Nat. Neurosci. 6, 974–980. https://doi.org/10.1038/nn1113

Cortes, C., Vapnik, V., 1995. Support-Vector Networks. Mach. Learn. 20, 273–297. https://doi.org/10.1023/A:1022627411411

Davies, P., Hinkle, K.M., Sukar, N.N., Sepulveda, B., Mesias, R., Serrano, G., Alessi, D.R., Beach, T.G., Benson, D.L., White, C.L., Cowell, R.M., Das, S.S., West, A.B., Melrose, H.L., 2013. Comprehensive characterization and optimization of anti-LRRK2 (leucine-rich repeat kinase 2) monoclonal antibodies. Biochem. J. 453, 101–113. https://doi.org/10.1042/bj20121742

de Rijk, M.C., Tzourio, C., Breteler, M.M., Dartigues, J.F., Amaducci, L., Lopez-Pousa, S., Manubens-Bertran, J.M., Alpérovitch, A., Rocca, W.A., 1997. Prevalence of parkinsonism and Parkinson's disease in Europe: the EUROPARKINSON Collaborative Study. European Community Concerted Action on the Epidemiology of Parkinson's disease. J. Neurol. Neurosurg. Psychiatry 62, 10–5. https://doi.org/10.1136/jnnp.62.1.10

Decressac, M., Mattsson, B., Lundblad, M., Weikop, P., Björklund, A., 2012. Progressive neurodegenerative and behavioural changes induced by AAV-mediated overexpression of α-synuclein in midbrain dopamine neurons. Neurobiol. Dis. 45, 939–953.

https://doi.org/10.1016/j.nbd.2011.12.013
Ekker, M.S., Janssen, S., Seppi, K., Poewe, W., de Vries, N.M., Theelen, T., Nonnekes, J., Bloem, B.R., 2017. Ocular and visual disorders in Parkinson's disease: Common but frequently overlooked. Park. Relat. Disord. 40, 1–10. https://doi.org/10.1016/j.parkreldis.2017.02.014
Erskine, D., Thomas, A.J., Taylor, J.-P., Savage, M.A., Attems, J., McKeith, I.G., Morris, C.M., Khundakar, A.A., 2017. Neuronal Loss and A-Synuclein Pathology in the Superior Colliculus and Its Relationship to Visual Hallucinations in Dementia with Lewy Bodies. Am. J. Geriatr. Psychiatry 1–10. https://doi.org/10.1016/j.jagp.2017.01.005
Giasson, B.I., Duda, J.E., Murray, I.V.J., Chen, Q., Souza, J.M., Hurtig, H.I., Ischiropoulos, H., Trojanowski, J.Q., Lee, V.M.-Y., 2000. Oxidative Damage Linked to Neurodegeneration by Selective alpha -Synuclein Nitration in Synucleinopathy Lesions. Science 290, 985–989.
Guo, L., Normando, E.M., Shah, P.A., De Groef, L., Cordeiro, M.F., 2018. Oculo-Visual Abnormalities in Parkinson ' s Disease : Possible Value as Biomarkers The Retina and the Brain. Mov. Disord. 33, 1390–1406. https://doi.org/10.1002/mds.27454
Harrison, D., Kanji, G.K., 1988. The development of analysis of variance for circular data. J. Appl. Stat. 15, 197–223. https://doi.org/10.1080/02664768800000026
He, S., Liu, C., Chen, L., Ye, Z., Zhang, Y., Tang, W., Wang, B., Gao, X., 2018. Meta-Analysis of Visual Evoked Potential and Parkinson's Disease. Parkinsons. Dis. 2018, 1–8. https://doi.org/10.1155/2018/3201308
Himmelberg, M.M., West, R.J.H., Elliott, C.J.H., Wade, A.R., 2018a. Abnormal visual gain control and excitotoxicity in early-onset Parkinson's disease Drosophila models. J. Neurophysiol. 119, 957–970. https://doi.org/10.1152/jn.00681.2017
Himmelberg, M.M., West, R.J.H.H., Wade, A.R., Elliott, C.J.H.H., West, R.J.H.H., Elliott, C.J.H.H., Wade, A.R., 2018b. A perceptive plus in Parkinson's disease. Mov. Disord. 33, 27240. https://doi.org/10.1002/mds.27240
Hocking, R.R., 1976. The Analysis and Selection of Variables in Linear Regression. Biometrics 32, 1–49.
Hopkins, D.A., Niessen, L.W., 1976. Substantia nigra projections to the reticular formation, superior colliculus and central gray in the rat, cat and monkey. Neurosci. Lett. 2, 253–259. https://doi.org/10.1016/0304-3940(76)90156-7
Langheinrich, T., Tebartz, van, Lagrèze, W.A., Bach, M., Lücking, C.H., Greenlee, M.W., 2000. Visual contrast response functions in Parkinson's disease: evidence from electroretinograms, visually evoked potentials and psychophysics. Clin. Neurophysiol. 111, 66–74.
Lin, X., Parisiadou, L., Gu, X.L., Wang, L., Shim, H., Sun, L., Xie, C., Long, C.X., Yang, W.J., Ding, J., Chen, Z.Z., Gallant, P.E., Tao-Cheng, J.H., Rudow, G., Troncoso, J.C., Liu, Z., Li, Z., Cai, H., 2009. Leucine-Rich Repeat Kinase 2 Regulates the Progression of Neuropathology Induced by Parkinson's-Disease-Related Mutant α-synuclein. Neuron 64, 807–827. https://doi.org/10.1016/j.neuron.2009.11.006
Linden, R., Perry, V.H., 1983. Massive retinotectal projection in rats. Brain Res. 272, 145–149. https://doi.org/10.1016/0006-8993(83)90371-2
Meissner, W.G., 2012. When does Parkinson's disease begin? From prodromal disease to motor signs. Rev Neurol. 168, 809–814. https://doi.org/10.1016/j.neurol.2012.07.004
Miri, S., Glazman, S., Mylin, L., Bodis-Wollner, I., 2016. A combination of retinal morphology and visual electrophysiology testing increases diagnostic yield in Parkinson's disease. Park. Relat. Disord. 22, S134–S137. https://doi.org/10.1016/j.parkreldis.2015.09.015
Niu, H., Shen, L., Li, T., Ren, C., Ding, S., Wang, L., Zhang, Z., Liu, X., Zhang, Q., Geng, D., Wu, X., Li, H., 2018. Alpha-synuclein overexpression in the olfactory bulb initiates prodromal symptoms and pathology of Parkinson's disease. Transl. Neurodegener. 7, 1–17.

https://doi.org/10.1186/s40035-018-0128-6
Norcia, A.M., Appelbaum, L.G., Ales, J.M., Cottereau, B.R., Rossion, B., 2015. The steady-state visual evoked potential in vision research: A review. J. Vis. 15, (4); 1-46. https://doi.org/10.1167/15.6.4.doi
Noyce, A.J., Lees, A.J., Schrag, A.-E., 2016. The prediagnostic phase of Parkinson's disease. J. Neurol. Neurosurg. Psychiatry 87, 871–878. https://doi.org/10.1136/jnnp-2015-311890
Schapira, A.H.V., Chaudhuri, K.R., Jenner, P., 2017. Non-motor features of Parkinson disease. Nat. Rev. Neurosci. 18, 435–450. https://doi.org/10.1038/nrn.2017.62
Sefton, A.J., Dreher, B., Harvey, A.R., Martin, P.R., 2014. Visual System, The Rat Nervous System: Fourth Edition. https://doi.org/10.1016/B978-0-12-374245-2.00030-9
Singleton, A.B., Farrer, M., Johnson, J., Singleton, A., Hague, S., Kachergus, J., Hulihan, M., Peuralinna, T., Dutra, A., Nussbaum, R., Lincoln, S., Crawley, A., Hanson, M., Maraganore, D., Adler, C., Cookson, M.R., Muenter, M., Baptista, M., Miller, D., Blancato, J., Hardy, J., Gwinn-Hardy, K., 2003. α-Synuclein Locus Triplication Causes Parkinson's Disease. Science (80-.). 302, 841 LP-841. https://doi.org/10.1126/science.1090278
Spillantini, M.G., Schmidt, M.L., Lee, V.M.-Y.L., Trojanowski, J.Q., Jakes, R., Goedert, M., 1997. Alpha-Synuclein in Lewy bodies Lewy. Nature 388, 839–840. https://doi.org/10.1038/42166
Stern, M.B., Siderowf, A., 2010. Parkinson's at risk syndrome: Can Parkinson's disease be predicted? Mov. Disord. 25, S89–S93. https://doi.org/10.1002/mds.22719
Surmeier, D.J., Obeso, J.A., Halliday, G.M., 2017. Parkinson's Disease Is Not Simply a Prion Disorder. J. Neurosci. 37, 9799–9807. https://doi.org/10.1523/JNEUROSCI.1787-16.2017
Thomas, B., Beal, M.F., 2007. Parkinson's disease. Hum. Mol. Genet. 16, R183–R194. https://doi.org/10.1007/978-1-4939-7880-9_5
Vapnik, V., 1995. The Nature of Statistical Learning Theory. Springer-Verlagy, New York.
Wang, L., 2018. Support Vector Machines: Theory and Applications (Studies in Fuzziness and Soft Computing). Springer-Verlag, Berlin.
West, R.J.H., Elliott, C.J.H., Wade, A.R., 2015. Classification of Parkinson's Disease Genotypes in Drosophila Using Spatiotemporal Profiling of Vision. Sci. Rep. 5, 16933. https://doi.org/10.1038/srep16933
Witkovsky, P., 2004. Dopamine and retinal function. Doc. Ophthalmol. 108, 17–40. https://doi.org/10.1023/B:DOOP.0000019487.88486.0a
Zhou, F.-M., Lee, C.R., 2011. Intrinsic and Integrative Properties of Substantia Nigra pars Reticulata Neurons. Neuroscience 198, 69–94. https://doi.org/10.1016/j.neuroscience.2011.07.061

16.1 Figures

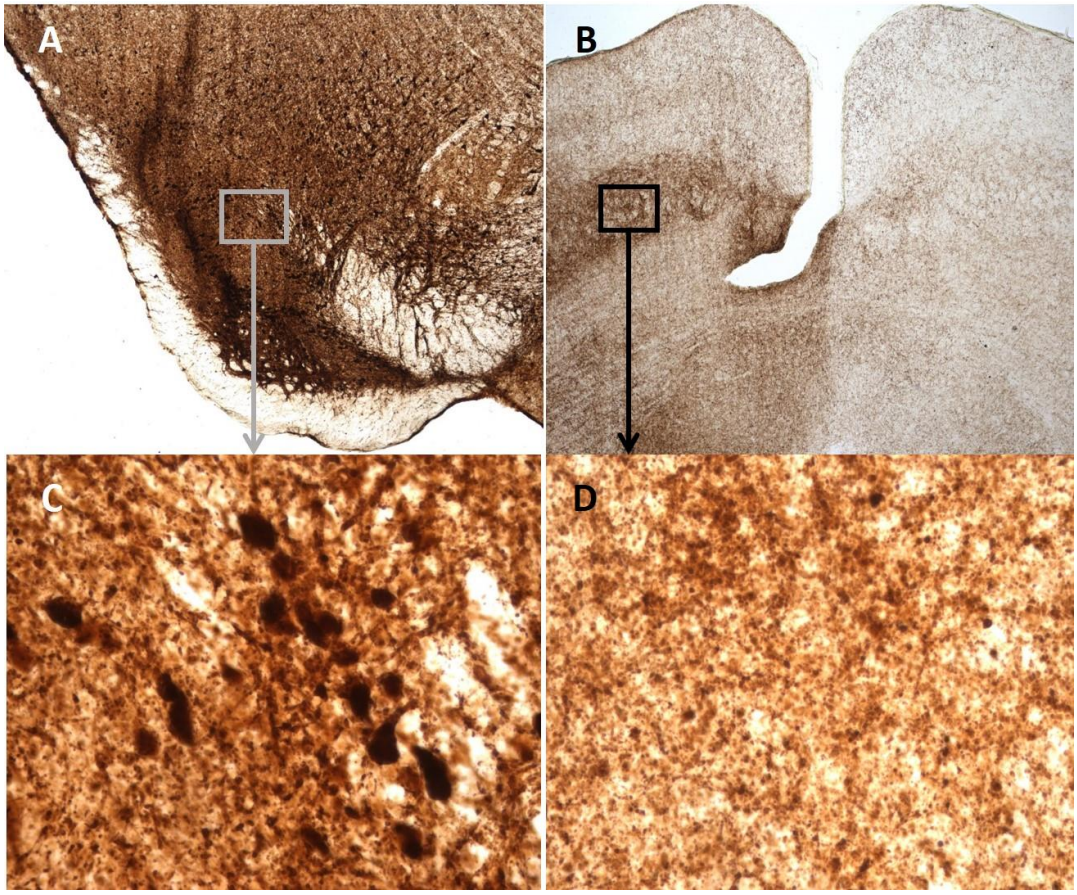

Figure 1 Detection of human α-synuclein immunoreactivity (IR) in the superior colliculus of rats injected with AAV- α-synuclein. A-D, Images of immersion fixed brain slice stained with the 4B12 antibody for human wild-type α-synuclein and magnified 10× and 40×. A, shows human wt α-synuclein IR in the SNc. C, a subsection of the human α-synuclein IR in the SNc at 40×magnification. The magnification highlights cell bodies containing human wt α-synuclein. B and D shows human wt α-synuclein IR appearing as inclusions in the intermediate gray layer of the superior colliculus.

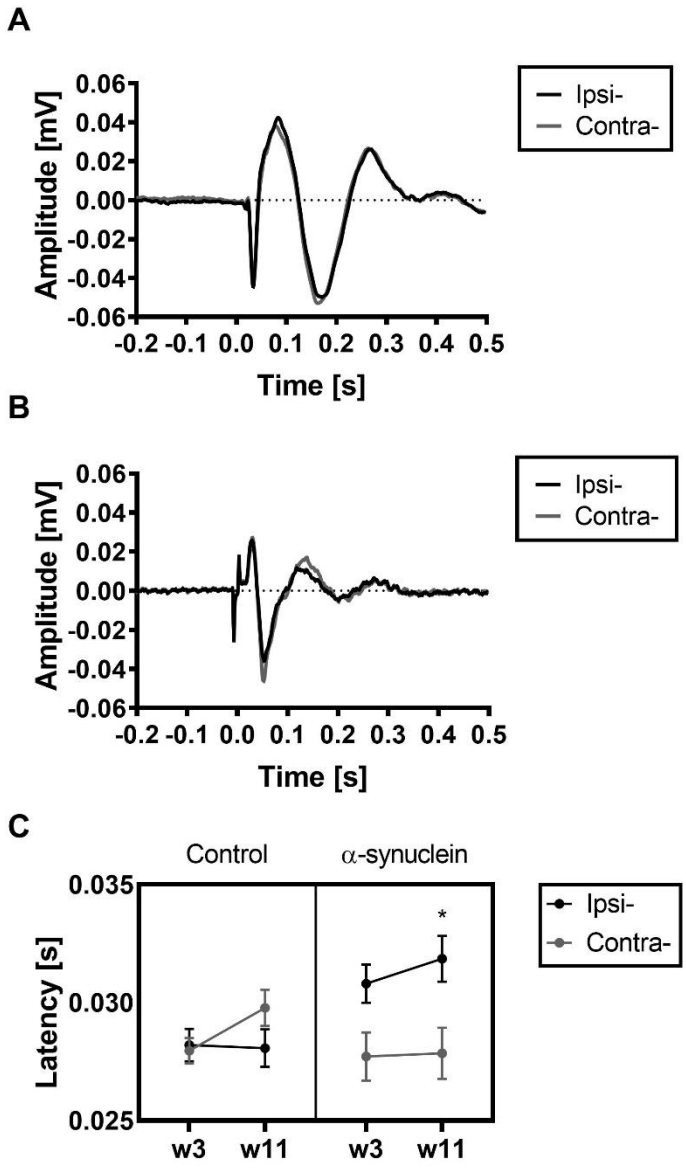

Figure 2 Unilateral α-synuclein overexpression in the SC causes a delay of the first positive peak (P1) of the VEP. A) The grand average VEP waveforms from the visual cortex ipsilateral (black) and contralateral (grey) to the injection of AAV-α-synuclein at week 11 for all colours. Analysis of the peaks amplitude and latency does not show a significant difference between the two waveforms. B) The grand average VEP waveform from the superior colliculus mean for all colors. This only shows data from the animals that had α-synuclein expressed in the left substantia nigra ipsilateral (black) and contralateral (grey) to the injection of AAV-α-synuclein at week 11 for all colours. The peak around time 0 is an artefact from the light stimulus turning on and off. C) Latency of the P1 from the waveform from the superior colliculus shown as mean±SEM at week three (w3) and week 11 (w11) for both α-synuclein and control animals. The P1 recorded ipsilateral to the AAV-α-synuclein injection is significantly delayed at w11 compared to P1 recorded contralateral to the injection. * $p<0.05$

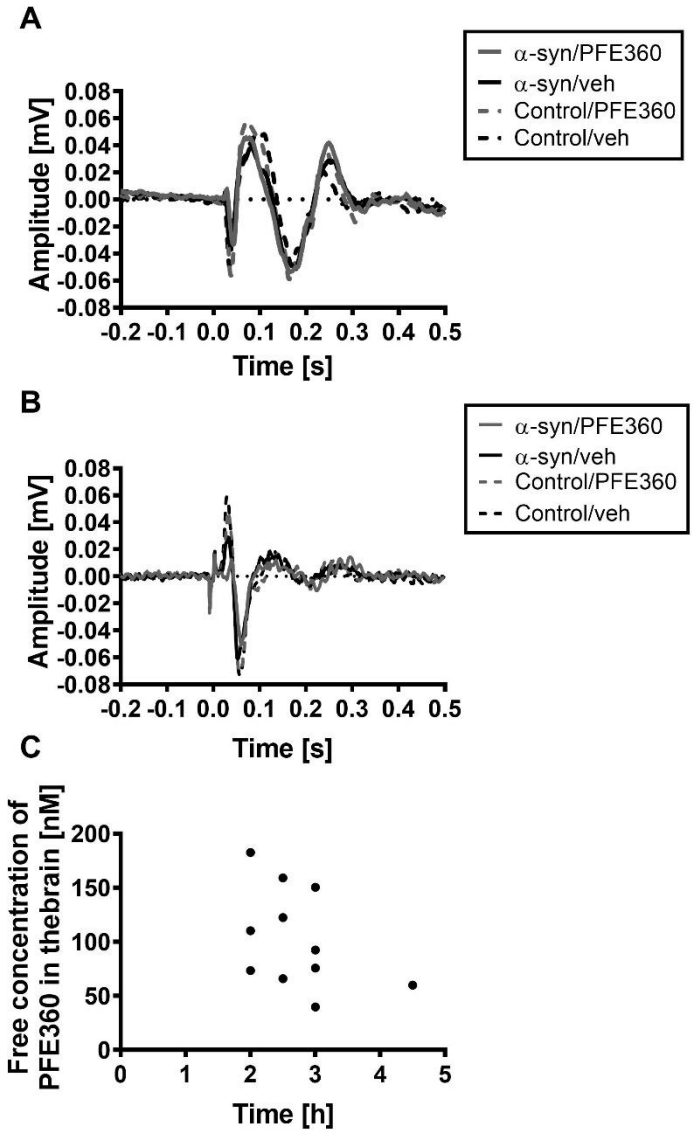

Figure 3 PFE360-mediated LRRK2 inhibition throughout the recording session. A) shows four superimposed VEP waveforms recorded from the visual cortex of rats that had either AAV-α-synuclein injected (solid lines) or the empty AAV vector (dashed lines). Subsequently they were treated with either vehicle (black) or the LRRK2 inhibitor PFE360 (grey). B) four superimposed VEP waveforms recorded from the superior colliculus. C) Free concentration of PFE360 measured in the cerebellum of the rats n=11. X-axis is time since administration in hours. The mean concentration was 102.89 nM with an SD of 45.97nM.

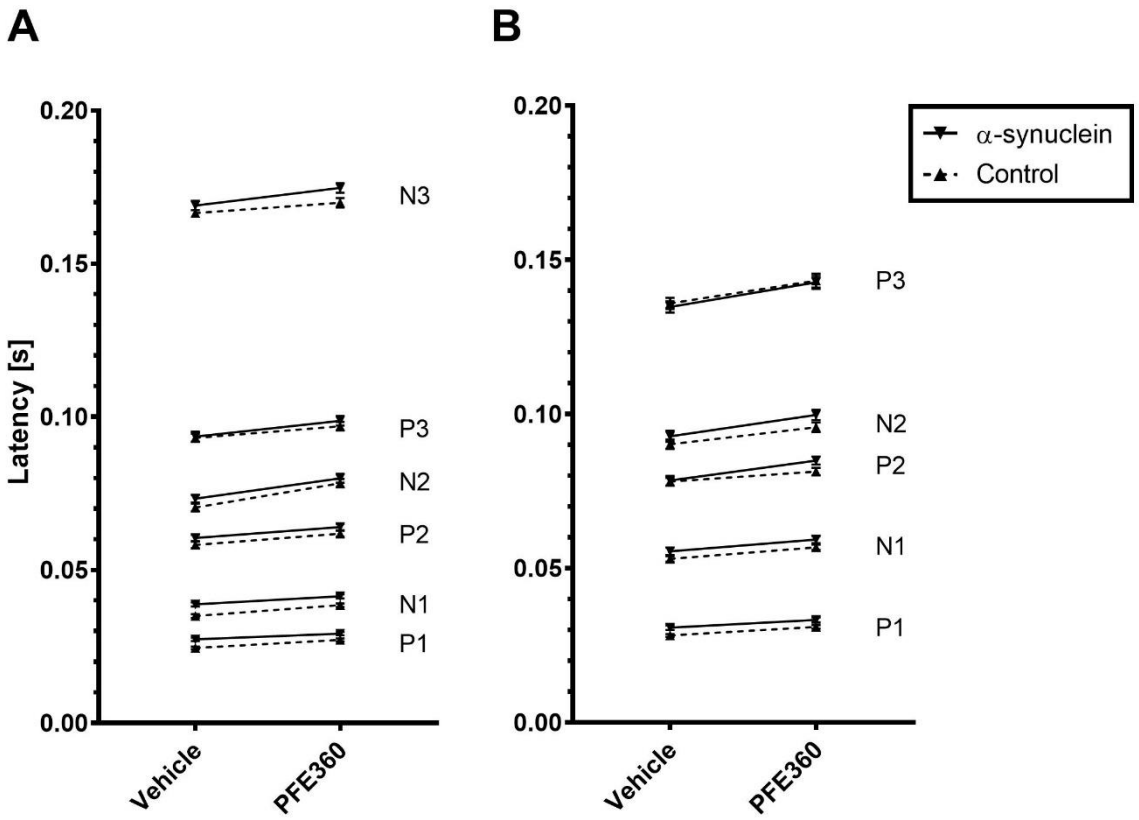

Figure 4 PFE360 causes an increase in latency of the VEP waveforms. All peaks have been stacked in order to show the trend of PFE360 increasing the latencies. A) Latency of each peak from the VEP recorded in the visual cortex after administration of either vehicle or PFE360. There is a statistically significant increase in latency for all peaks. The P4 peak from the visual cortex was excluded as there was a significant interaction of PFE360, wavelength and group. B) Latency of each peak from the VEP recorded in the superior colliculus after administration of either vehicle or PFE360. There is a statistically significant increase in latency for all peaks. Mean±SEM, all differences between vehicle and PFE360 condition were significant with p-values<0.001 (see Table S1).

Week	Accuracy	*p*-value
3	83.71%**	$p < .001$
5	87.98%**	$p < .001$
6	92.28%**	$p < .001$
7	88.99%**	$p < .001$
8	86.79%**	$p < .001$
9	90.16%**	$p < .001$
10	92.96%**	$p < .001$
11	84.12%*	$p = .020$

Table 1 Mean SVM classification accuracy at each age after 1000 bootstrapped runs, classifying α-synuclein rats and control rats into their correct class, when all electrodes are included in the analysis. ** p<0.001, * p<0.05

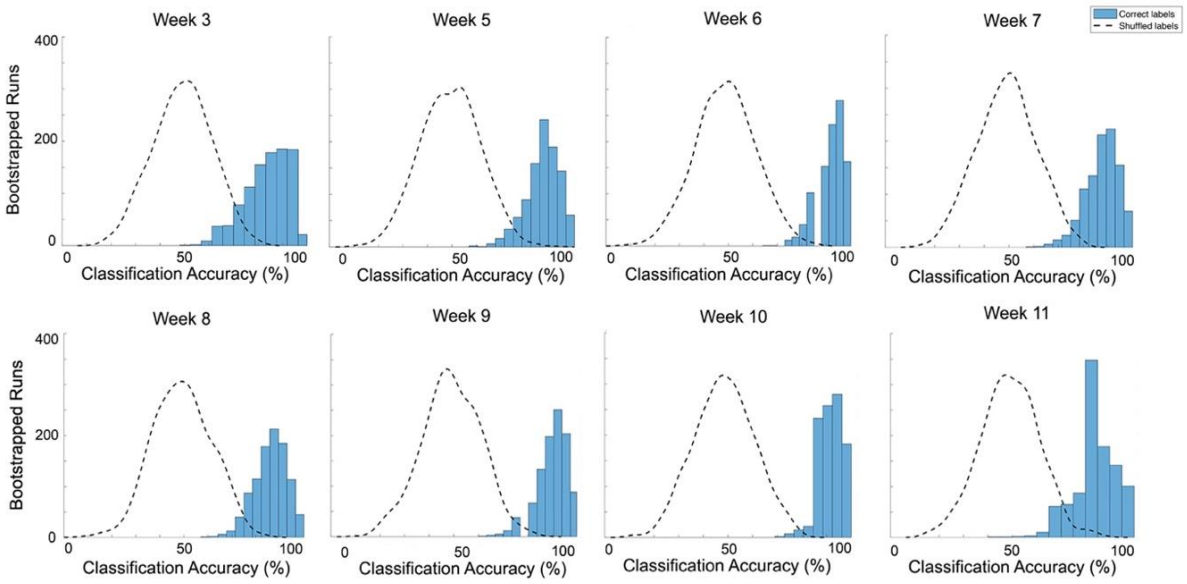

Figure 5 Histogram plots of classification accuracy across 1000 bootstrapped SVM classifications. The SVM is highly accurate in classifying between α-synuclein and control rats at each week when all electrodes are included in the analysis, with virtually no classification runs occurring below the 50% baseline. We include a plot of classification accuracy after shuffling labels, where accuracies fall around the 50% baseline.

Week	Accuracy	*p*-value
3	67.87%*	$p = .042$
5	81.46%**	$p < .000$
6	67.23%*	$p = .047$
7	77.17%*	$p = .002$
8	84.48%*	$p = .000$
9	69.52%*	$p = .036$
10	66.35%	$p = .062$
11	73.01%*	$p = .032$

Table 2 Mean SVM classification accuracy at each age after 1000 bootstrapped runs, comparing between the (treated) left superior colliculus electrode and the (untreated) right superior colliculus electrode within α-synuclein rats. ** p < .001, * p < .05

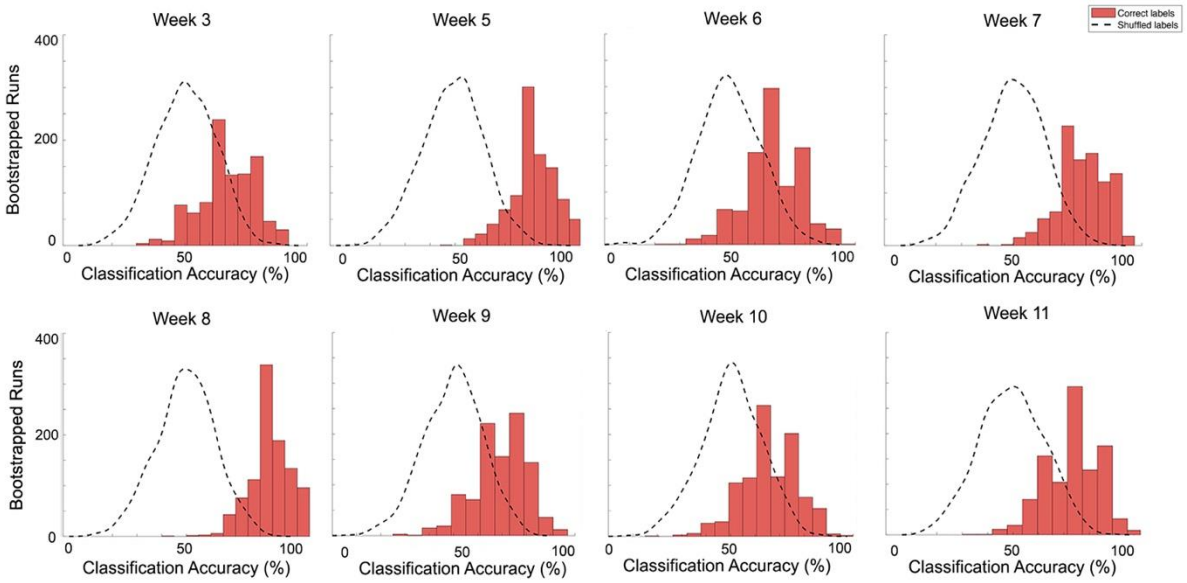

Figure 6 Histogram plots of classification accuracy across 1000 bootstrapped SVM classifications. The SVM is able to classify between the (treated) left superior colliculus and the (untreated) right superior colliculus within α-synuclein rats, expect at week 10. We include a plot of classification accuracy after shuffling labels, where accuracies fall around the 50% baseline.

16.2 Supplementary

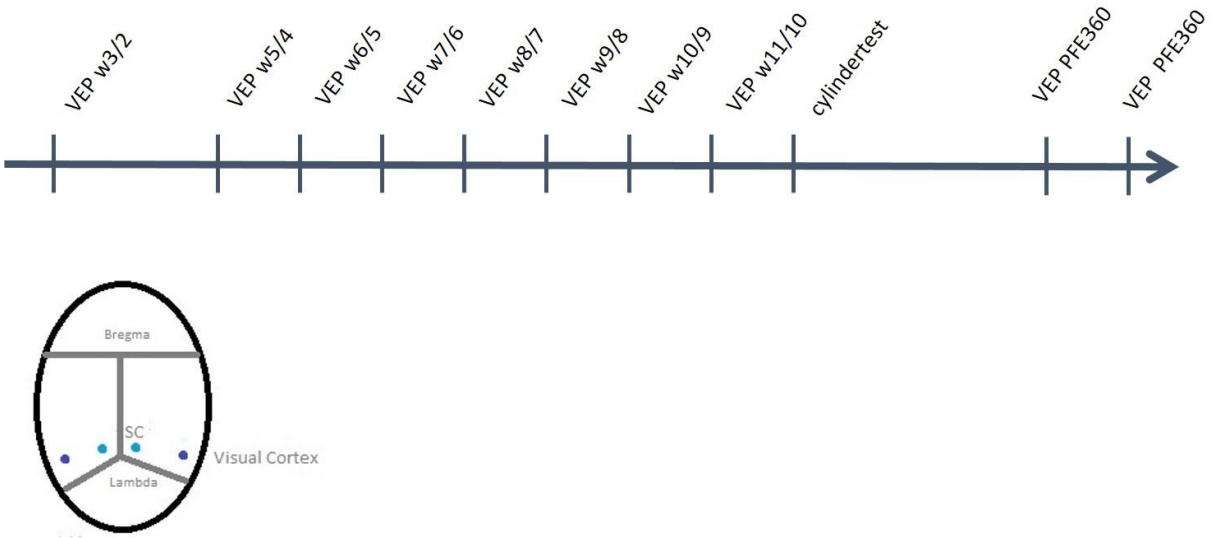

S 1 The animals were allowed to recover for two weeks before being exposed to the stimuli, A) subsequently they were through ten recording sessions, while the lesion developed and then tested in the cylinder test.

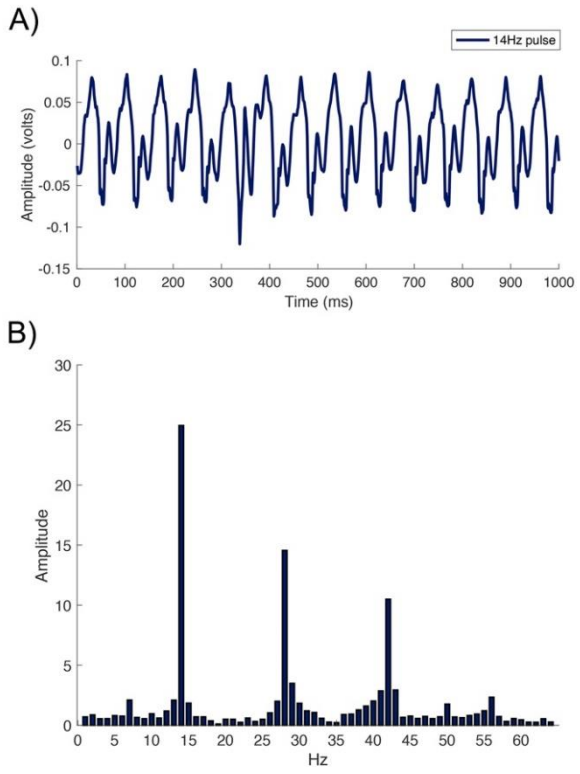

S 2 EEG data is collected in the time domain then transformed into the frequency domain using the FT. In panel A, we present an example of the average EEG time course across a 1000ms bin taken from the right superior colliculus of a 3-week-old control rat. There are 14 peaks across the 1000ms bin, reflecting the 14Hz temporal frequency of our stimulus. In panel B, we present this data in the power spectrum after applying the FT. Peaks occur at multiples of our input harmonic – at 14Hz, 28Hz, and 42Hz (1f, 2f, and 3f, respectively).

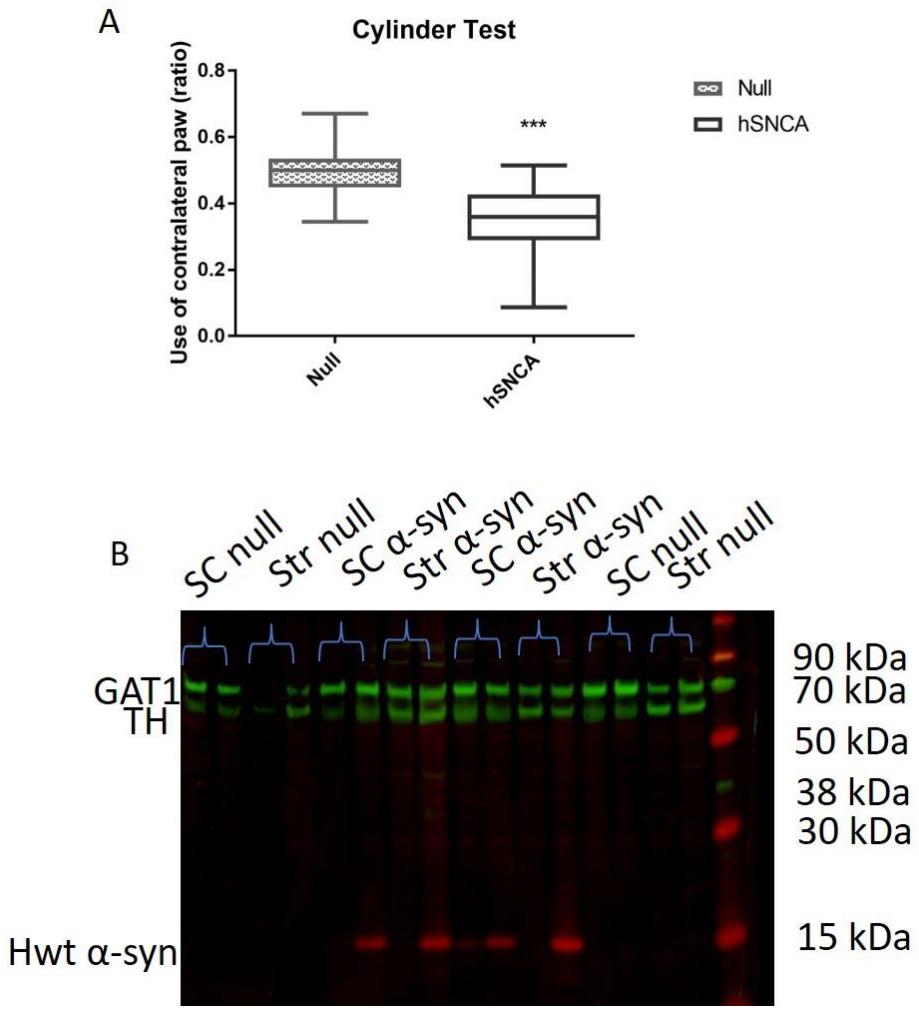

S 3 Alpha-synuclein animals use the contralateral paw less than the ipsilateral. A, shows ratio of contralateral touches over the total number of touches for the animals that had alpha-synuclein expressing AAV injected in the left SNc (in black) and the animals that only had the empty vector injected (grey). The null animals had ratios around 0.5 indicating that they use both paw equally, whereas the alpha-syn animals have ratios around 0.34 biased towards using the paw contralateral of the injection less, due to effects in the striatum. B, Image of a representative western blot showing IR of human α-synuclein, tyrosine hydroxylase (TH) and the GABA transporter (GAT1) in protein lysates from the superior colliculus and the striatum. Human α-synuclein IR is only observed in samples from the ipsilateralhemisphere whereas TH and GAT1 IR is detected in both hemispheres.

Table of F-values (adjusted p-values) from 4-way ANOVA				group	side	drug	color	2nd order interactions group side	group drug	group color	drug side	drug color	3rd order interaction group:drug:color
			numDF	1	1	1	4	1	1	4	1	4	4
Superior Colliculus	amplitude	P1	denDF 456		7.78 (0.0363)		5.21 (0.0033)	27.35 (0.00132)			trend		
		N1	471		13.18 (0.00293)								
		P2	456				8.84 (0.00132)	18.73 (0.00132)					
		N2	456				8.45 (0.00132)	13.23 (0.00293)					
		P3	456		14.27 (0.00189)		5.82 (0.00189)	31.43 (0.00132)	7.58 (0.0363)				
	latency	P1	455		27.91 (0.000471)	60.39 (0.000471)	145.32 (0.000471)	36.28 (0.000471)		4.68 (0.00495)			
		N1	455		8.95 (0.0106)	32.87 (0.000471)	57.32 (0.000471)	44.67 (0.000471)					
		P2	455			21.84 (0.000471)	31.96 (0.000471)	10.96 (0.00484)					
		N2	455			21.22 (0.000471)	19.35 (0.000471)	15.16 (0.000471)				trend	
		P3	455			19.55 (0.000471)	8.36 (0.000471)	10.40 (0.00582)					
Visual Cortex	amplitude	P1	464				4.34 (0.0145)	24.54 (0.000825)					
		N1	479				30.16 (0.000825)						
		P2	479			19.40 (0.000825)	27.55 (0.000825)						
		N2	479				22.30 (0.000825)						
		P3	464				5.41 (0.002933)	8.91 (0.0204)					
		N3	479				7.78 (0.000825)						
		P4	464		trend	trend	9.55 (0.000825)	18.16 (0.000825)				trend	
	latency	P1	479			57.67 (0.000471)	128.43 (0.000471)						
		N1	464	trend		81.14 (0.000471)	196.55 (0.000471)	trend					
		P2	479			28.18 (0.000471)	85.60 (0.000471)						
		N2	479		trend	51.58 (0.000471)	44.69 (0.000471)						
		P3	479			19.80 (0.000471)	34.02 (0.000471)						
		N3	464			16.32 (0.000471)	19.11 (0.000471)	11.89 (0.00308)					
		P4	451	trend			26.49 (0.000471)			4.11 (0.0113)		8.63 (0.000471)	4.46 (0.0066)

Table S 1 Results of 4-way ANOVA shown with F-values and FDR adjusted p-value in parenthesis. 4th order interactions were not significant. Only the interactions that were significant (before p-adjustment) were included in the table. numDF: numerator degrees of freedom, denDF; denumerator degrees of freedom.

Week	Accuracy	*p*-value
3	49.11%	$p = .455$
5	49.39%	$p = .462$
6	48.82%	$p = .476$
7	49.14%	$p = .457$
8	49.35%	$p = .462$
9	49.05%	$p = .479$
10	48.54%	$p = .498$
11	49.04%	$p = .471$

Table S 2 Mean SVM classification accuracy at each week after 1000 bootstrapped runs, classifying α-synuclein rats and control rats into their correct class after labels have been shuffled, when all electrodes are included in the analysis. ** p < .001, * p < .05

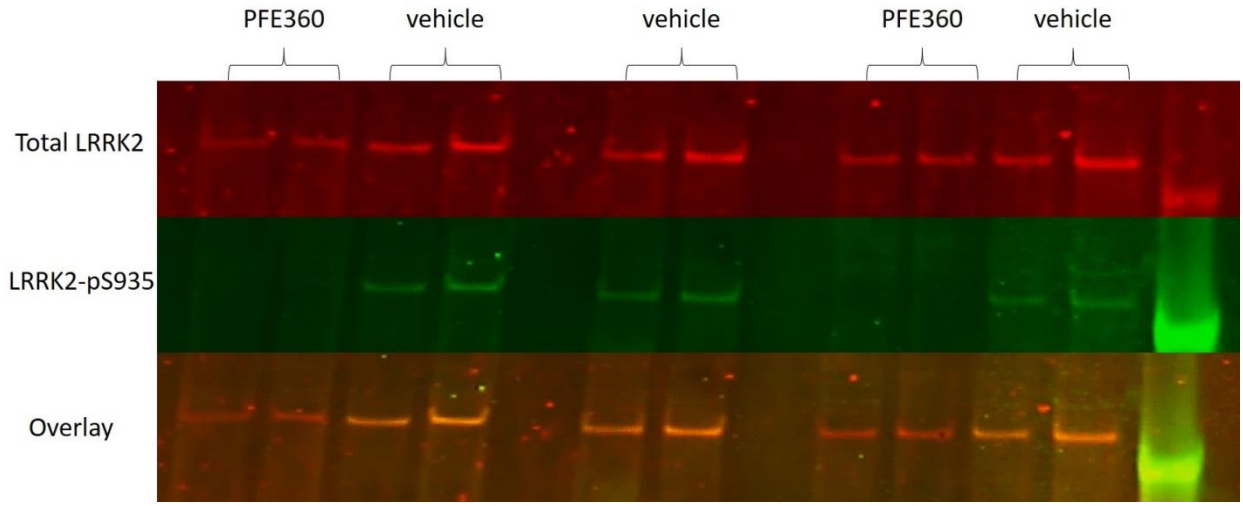

S 4 Expression and phosphorylation of LRRK2 in the rat striatum after PFE360 administration. The top panel shows western blot detection of the total LRRK2 IR in protein lysates from the right and left side of the striatum, respectively. The middle panel shows the signal for phosphorylated LRRK2(pSer935) in the same tissue samples. The bottom panel shows the IR-signals when superimposed. The results confirm that LRRK2 is fully inhibited in animals dosed with PFE360.

17 Manuscript III

Mapping visual processing with functional MRI in a rodent model of α-synuclein overexpression

Freja Gam Østergaard[1], Christian Skoven[3], Alex R. Wade[2], Hartwig R. Siebner[3], Bettina Laursen[1], Kenneth Vielsted Christensen[4] & Tim B. Dyrby[3]

[1] Department of Translational Biology, H. Lundbeck A/S, Ottiliavej 9. DK-2500 Valby, Denmark. [2] Department of Psychology, The University of York, Heslington, York, YO10 5DD, United Kingdom. [3] Danish Research Centre for Magnetic Resonance, Copenhagen University Hospital Hvidovre, DK-2650 Hvidovre, Denmark. [4] Institut de Recherches Servier – IDRS, 125 Chemin de Ronde, 78290 Croissy sur Seine, France

Abstract

Parkinson's disease (PD) is a progressive neurodegenerative disorder that is typically diagnosed late in the course of the disease. Biomarkers suitable for monitoring the disease progression at the early stages are important for the development of therapies to halt or slow the disease. One potential biomarker, α-synuclein, has been found in both the familial version of PD as well as the sporadic version and aggregates of this protein, have been hypothesized to develop decades before PD is diagnosed. Here, we used a virally-induced overexpression of α-synuclein in rats as a mechanistic model of this particular feature of PD. We aimed to investigate if functional magnetic resonance imaging (fMRI) can detect functional changes related to adeno-associated virus (AAV) mediated overexpression of α-synuclein. 16 rats were injected with either AAV-α-synuclein (n=7) or AAV-null (n=9) in the substantia nigra pars compacta of the left hemisphere. Five months after the introduction of the AAV vector, fMRI showed robust blood oxygen level dependent (BOLD) responses to photic stimulation in the visual systems of both control and AAV-α-synuclein animals. However, the presence of AAV-α-synuclein did not appear to significantly alter the BOLD response.

Introduction

Parkinson's disease (PD) is the second most common neurodegenerative disorder (Wirdefeldt et al., 2011) affecting millions of people worldwide (Thomas and Beal, 2007). Though the disease is primarily considered to be sporadic, there are familial versions caused by a mutation in a single gene (Klein and Westenberger, 2012). These hereditable forms of PD have led to the discovery of several susceptibility genes, such as the *SNCA* gene (park1/4) coding for α-synuclein. Abnormal aggregation of α-synuclein is hypothesized to develop long before the diagnostic symptoms of tremor and postural instability (Noyce et al., 2016). The process of α-synuclein aggregation has been suggested to spread progressively from the brainstem into the midbrain and cortex in a process of Braak staging (Braak et al., 2003; George et al., 2013). This hypothesis has been extended to the very early aggregation of α-synuclein in the gut, giving rise to early symptoms such as constipation (Kaye et al., 2006).

Several studies have shown that the visual system is affected in PD (Davidsdottir et al., 2005; Ekker et al., 2017; Satue et al., 2017), but these perturbations have so far failed to give an unambiguous estimate of disease severity (Ridder et al., 2017). This is likely due to PD being diagnosed at a very late stage of disease progression, where patients are prone to suffer from a wide range of visual changes related to normal aging (Ekker et al., 2017). However, there is evidence that PD patients experience changes in contrast sensitivity (Langheinrich et al., 2000) and motion perception (Garcia-Diaz et al., 2018) more often compared to age-matched controls. Further evidence of PD-related changes in vision was provided by *post mortem* studies showing α-synuclein aggregation in the retinae of PD patients (Bodis-Wollner et al., 2014). This finding lead to the hypothesis that α-synuclein aggregation may be the cause of changes in visual processing associated with PD. Although the time course of retinal α-synuclein aggregation is unclear, it has been hypothesized to have potential as a biomarker for the progression and severity of PD (Rahimi et al., 2015).

A rodent model of α-synuclein overexpression in the substantia nigra pars compacta (SNc), mediated by the adeno-associated virus (AAV) has shown to decrease the number of spines of the dopaminergic cells, which in turn have been reported to influence the neuronal firing pattern in the striatum (Andersen et al., 2018). In addition to the striatum the substantia nigra also project to the superior colliculus (SC) which is the primary visual nucleus of rodents. The neuronal firing pattern is measured invasively using electrophysiology making it difficult to apply to humans, therefore a non-invasive technique is desirable. Magnetic resonance imaging (MRI) is a non-invasive bioimaging modality, which have been used to investigate regional changes in brain structure of PD patients (Lehéricy et al., 2014). Functional MRI (fMRI) measures the local changes in blood

volume, flow and oxygenation related to neuronal activity and it has been applied in patients with PD to study changes in function (Pyatigorskaya et al., 2014). Recently, Kuebler et al (2017) demonstrated that fMRI can detect neuronal changes in the dopamine release after a pharmacological challenge in the rodent PD model (Kuebler et al., 2017) also used by (Andersen et al., 2018).

The aim of this study is to use BOLD fMRI, with a purely visual stimulus (flickering full-field illumination) to examine potential functional consequences of overexpressing α-synuclein *in vivo*. The α-synuclein is introduced unilaterally, thereby it is expected to cause an asymmetry of the BOLD response in the visual system. We use two different frequencies as responses to these two frequencies may be governed by different mechanisms (Van Camp et al., 2006), one frequency could be more sensitive to changes introduced by overexpressing α-synuclein.

Methods

Subjects

All experiments were carried out according to EU Communities Council Directives (86/609/EEC) and Danish legislation on care of experimental animals. 20 female Sprague-Dawley™ (SD) rats (Taconic, Denmark), weighing 225g (approx. ten weeks of age) upon arrival, were used.

The rats underwent surgery and cylinder test at the site of H. Lundbeck A/S and were subsequently transported to the Danish Research Centre for Magnetic Resonance (DRCMR) using a transportation company approved for animals. The animals acclimatized to their new housing facility for at least two weeks before imaging. The home cage environment (cages and enrichment) was similar at the two sites.

Surgery

Prior to surgery, each rat was anesthetized using subcutaneous (SC) injections of Hypnorm® (Lundbeck, Valby, Denmark), midazolam 5 mg/mL (B. Braun, Germany) and saline in a 2:1:1 ratio, yielding an injection volume of 1.7 mL/kg. The rat was placed in a stereotaxic frame and Marcain (2.5mg/mL bupivacaine, AstraZeneca, Denmark) was administered locally prior to incision. A small craniotomy (Ø=1mm) was made over SNc of the left hemisphere (AP: -5.5 ML: +2.0 DV: -7.2; (Paxinos and Watson, 1998) to allow for injection of adeno-associated virus (AAV) 2/5, expressing human wildtype α-synuclein (*hSNCA*). This model mimics overexpression of α-synuclein and is considered a mechanistic model of PD (Decressac et al., 2012). Half of the animals acted as controls by having the empty viral vector injected. The animals were post-operatively treated with buprenorphine 0.05 mg/kg, every 8^{th} hour, for four days. The rats were single-housed after the surgery with enrichment in the form of nesting material and a red plastic shelter.

Cylinder test

After ten weeks, the rats were tested for motor asymmetry, induced by the overexpression of α-synuclein. The animals were recorded with a video camera for five minutes, freely moving in a Plexiglass cylinder. Paw touches on the side of the cylinder were counted and the ratio of the touches of paw contralateral to the injection, to total touches was computed. Animals with an overexpression of α-synuclein were hypothesized to use the contralateral paw less than animals receiving the null-vector.

Anesthesia for MRI

Five months after the viral injection, the rats were anesthetized and scanned in a 7T Bruker Biospec (Bruker BioSpec 70/20 USR) MRI scanner with an 80 mm RF transmit quadrature coil and a 20 mm surface receive coil. The receive coil was fixed on the top of the head using masking tape. The signal covered the whole brain but the largest signal was above the region of interest: the superior colliculus, and visual cortex. Sticky tack (Bantex, South Africa) was placed in the ears of the rats to reduce MR scanner noise during scanning. The animals were scanned at the same time of day, on separate days to minimize variation caused by the circadian rhythm.

Anesthesia was induced with isoflurane 5 % and adjusted to 2.5 % while placing a tail-vein catheter. Subsequently, dexmedetomidine (Dexdormitor®, Orion Pharma, Finland) was infused at 0.05 mg/kg/hr. When the heart rate decreased to about 200 bpm, the isoflurane was adjusted to 0.5 % (in 1 L of oxygen:medical air, 8:2). Blood oxygen saturation and heart rate was monitored using pulse oximetry (Nonin, MN, USA). For details of how the anesthetic regime was tested see supplementary methods. The animals breathed spontaneously, and the breathing rate of the animals was continuously monitored by a breathing pad (SA Instruments; NY, USA). The core temperature of the animals was monitored with a rectal probe, and used as feedback to maintain a constant temperature of 37.2 °C using heated air (SA Instruments; NY, USA). After one hour of infusion, the infusion rate of dexmedetomidine was doubled to 0.1 mg/kg/hr. This concentration is lower than what most literature recommend because the vasoconstrictive effects of dexmedetomidine made measuring blood oxygen saturation challenging.

MRI protocols

Structural MRI: Bruker-standard T1_Flash_3D_iso protocol (Paravision 6.0.1). This produces a whole brain structural T1 weighted MRI using a 3D Fast Low Angle Shot (flash) protocol.

The echo-planar image (EPI) MRI had an in-plane voxel size of 0.313 x 0.313 mm with slice thickness of 0.500 mm^3, TR = 1500 ms, and TE = 8.35 ms, slice gab= 0. The Ernst flip angle was determined to 64° was based on T1 measurement of cortical gray matter obtained from a separate session (data not shown). 42 coronal slices covered from the caudal part of the olfactory bulb to the caudal part of the cerebellum.

Visual stimulation was provided by five optical fibers (diameter of 1.5 mm) of "warm white" light provide by a LED source placed outside the scanner. The optical fibers were placed in front of the eyes of the animal. The light intensity was kept at 20 lx measured at the level of the eyes using a LED luxmeter (Extech, MA, US).

The Stimulation Paradigm

The stimulation paradigm used a block design that was generated by a micro1401 data acquisition unit (Cambridge Electronic Design Ltd., UK) controlled from Spike2 ver. 7.20 synchronized to TTL triggers from the scanner. The block design included six task blocks per trial, repeated five times where each task block contained 14 TRs (21s) of either 1 Hz or 14 Hz photic flicker. These two frequencies were chosen as one should be just above 10 Hz while the other should be well below, as 10 Hz has been suggested to be the threshold for saturation of the visual cortex (Van Camp et al., 2006). There were 14 TRs (21s) between repeated task. The fMRI scan was initiated 180 minutes after the infusion of dexmedetomidine was started. The total scan time was approximately four hours.

We addressed whether the fMRI responses were sensitive to unilateral stimuli in two animals (Figure S4). The chiasm of especially albino rats have around 99% of retinal fibers crossing over (Sefton et al., 2014) making an eye patch feasible. The results indicated subtle differences, this subtleness could be due to the quality of the eye patch.

The scanning session was organized to acquire the structural MRI before acquiring the fMRI. We applied at regular time intervals online fMRI correlation analysis using the visual stimuli paradigm. Online fMRI correlation analysis used the analysis of functional neuroimages (AFNI) program integrated into the fMRI sequence (Cox, 1996). The online fMRI analysis ensured to determine when the impact of isoflurane on the neuronal response and BOLD signal was diminished i.e. washed out. Typically, robust regional BOLD responses were obtained after 180 min which was verified with a separate control EEG study with electrodes placed in visual cortex and superior colliculus (supplementary methods).

fMRI Preprocessing

MRI data were analyzed using the FMRIB software library (FSL) (Woolrich et al., 2009). The fMRI data of was aligned within subject using FMRIB's linear image registration tool (FLIRT), then averaged together to construct a standard brain template. This template was used for registration of the data for later analysis.

Visual inspection revealed exclusion of four rats, as these could not be aligned to the standard template leaving 16 to be analyzed; nine controls and seven AAV-α-synuclein animals.

Immunohistochemistry

At the end of the scan session, the animal was given an SC bolus of Hypnorm®/midazolam. The animal was euthanized by intercardial perfusion with KPBS for three minutes, followed by 4 % paraformaldehyde (PFA) premade with methanol. After 10-15 minutes, the rat was decapitated, and the brain extracted. The brain was immersed in 4 % PFA for 24 hours, then placed in phosphate buffer with <1% PFA, and then placed in KPBS.

Brains were fixed in 30% sucrose for 72 hours before sectioning. Once fixed, they were dried and frozen with dry ice, and placed in the freeze microtome for 30 min. 40 µm thick coronal slices were cut and stored in KPBS. All slices were stained within five days.

The brain sections were stained to validate the expression pattern of the hWT-SNCA. Before staining, the tissue was quenched with hydrogen peroxide 3 % to remove any traces of blood. The slices were washed and incubated over night with 4B12 (Thermo Scientific, US) for human α-synuclein as the primary antibody, (concentration 1:1000). Subsequently, the slices were washed and incubated with biotin conjugated anti-mouse secondary antibody (Jackson Immunoresearch Laboratories, MA, US), and exposed using a 3,3-diaminobenzidine (Vector, CA, US). The stained slices were placed on gelatin covered glass slides, and visually examined using a light microscope (Axio scope.A1) (Carl Zeiss Microimaging, Germany).

Statistical analysis

Functional MRI data were analyzed using a three-level statistical analysis pipeline implemented in the FSL expert analysis tool (FEAT). In the first level, the time course of each voxel was fitted with a general linear model (GLM) to produce a statistical map of the z-scores of the correlation for each voxel within each of the scans. Each voxel was corrected for family-wise error with a p-threshold of $p<0.05$. Spatial smoothing was then applied using a Gaussian kernel with full width half maximum of 0.5 mm. In the second level, the z-score maps were averaged for each stimulation frequency within each subject, yielding two averaged statistical maps per animal. Each voxel within the averaged statistical map was corrected for family-wise error with a p-threshold of $p<0.05$. At the third and last level, the averaged statistical maps were averaged within the two groups for each of the two stimulation frequencies. The group statistical maps were compared using an unpaired comparison of the z-score maps between the two groups within each frequency. For the visualization, the statistical maps were superimposed on the high resolution T1.

Structural regions of interest (ROIs) of the superior colliculus and visual cortex (see Figure S5) were defined manually using the standard rat brain atlases (Kjonigsen et al., 2015; Papp et al., 2014; Sergejevaa et al., 2015). The olfactory bulb (ol) was used as a control ROI (not shown). For

each group there would be ROIs for ol, right SC, left SC, right VC and left VC. The mean of contrast of parameter estimates (COPEs) within the ROIs were extracted from the z-statistical map of each rat using FEAT query and further statistical processing was performed in 'R' (R ver. 3.4.2) (R Team, 2008).

The COPEs were analyzed using a three-way ANOVA on a linear mixed effects model with the variables group, ROI and stimulation frequency. Further, a random effect of individual was included in the model to account for the nesting of data as the nuclei of the same rat were influenced by the same physiological changes, e.g. blood oxygen saturation. Using the backward elimination strategy (Hocking, 1976), we tested the 2^{nd} order interaction and additive effects by Tukey post-hoc tests.

Results

Validation of α-synuclein overexpression

To validate the overexpression and impact of α-synuclein in the basal ganglia, α-synclein and control animals were tested for motor asymmetry in the cylinder test (Andersen, Christensen, et al., 2018). Figure 1A shows the change in the use of the forepaw contralateral of the injection site. Control animals used both paws equally (ratio of .5) while α-synuclein animals had significantly different mean ratio pf affected/total touches ratio of 0.35 ($t(14)=2.8$, $p=0.01$). The cylinder test confirmed that the function of the striatum was unilaterally affected in the animals that received the AAV-α-synclein injection.

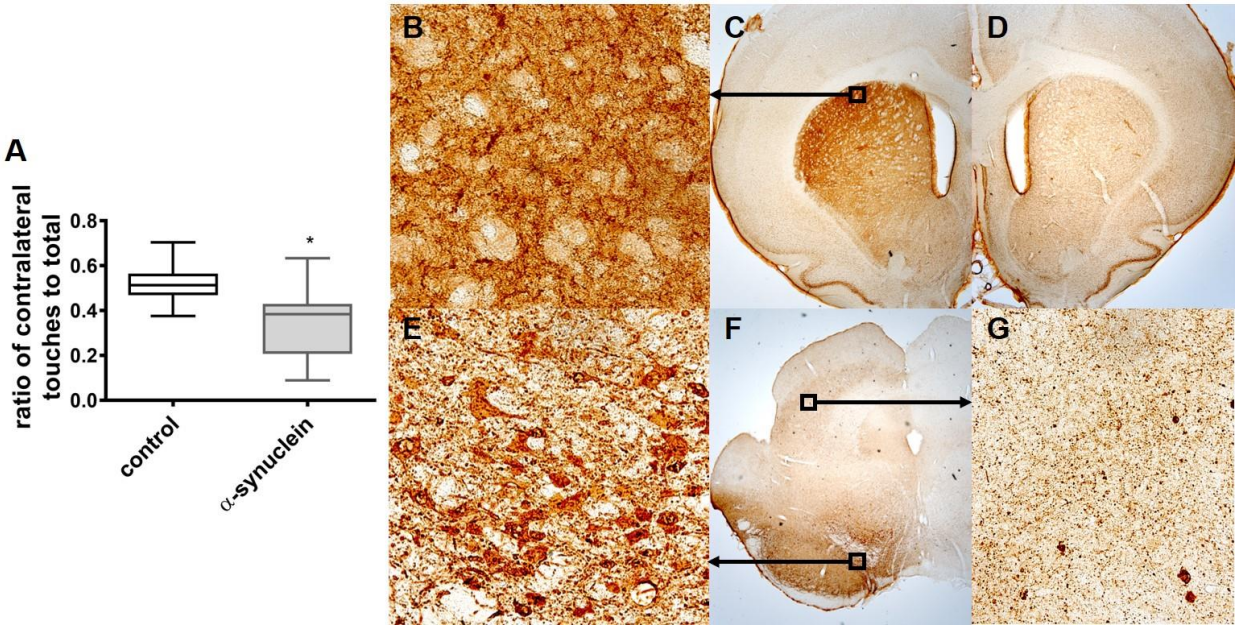

Figure 1 Validation of the AAV-α-synuclein model A) Cylinder test of the animals showing the ratio of touches by the contralateral paw to the total number of touches. The empty vector (null) animals (in black) have a ratio of 0.51 indicating equal use of both paws. The α-synuclein animals (in grey), have a ratio of 0.35 indicating that they use the paw contralateral of the injection less than the ipsilateral paw. B)-G) Representative coronal sections stained for α-synuclein. B) 40x magnification of striatal neurons showing α-synuclein-positive inclusions. C) 2,5x magnification of striatum showing α-synuclein immunoreactivity. D) 2,5x magnification of striatum contralateral to the injection of AAV-α-synuclein. E) 40x magnification showing α-synuclein is present in cell somas in the substantia nigra. F) 2,5x magnification of section showing the substantia nigra and the superior colliculus. G) 40x magnification showing α-synuclein immunoreactivity in the SC. The slices were stained with 4B12 (human WT alpha-synuclein).

Immunohistochemical evaluation showed immunoreactivity (IR) towards human α-synuclein in the SNc (Figure 1 E-F), in areas surrounding the SNc, and in the striatum ipsilateral (Figure B-C) to the injection site. Of particular interest, small inclusions of IR were observed in the intermediate grey layer of the ipsilateral superior colliculus (Figure 1G). Some IR was observed along the edges

of the tissue which were not specific to the injected hemisphere thus considered as unspecific IR. Confirmation of α-synuclein in areas ipsilateral to the injected hemisphere supports the observations from the cylinder test.

fMRI of the visual system

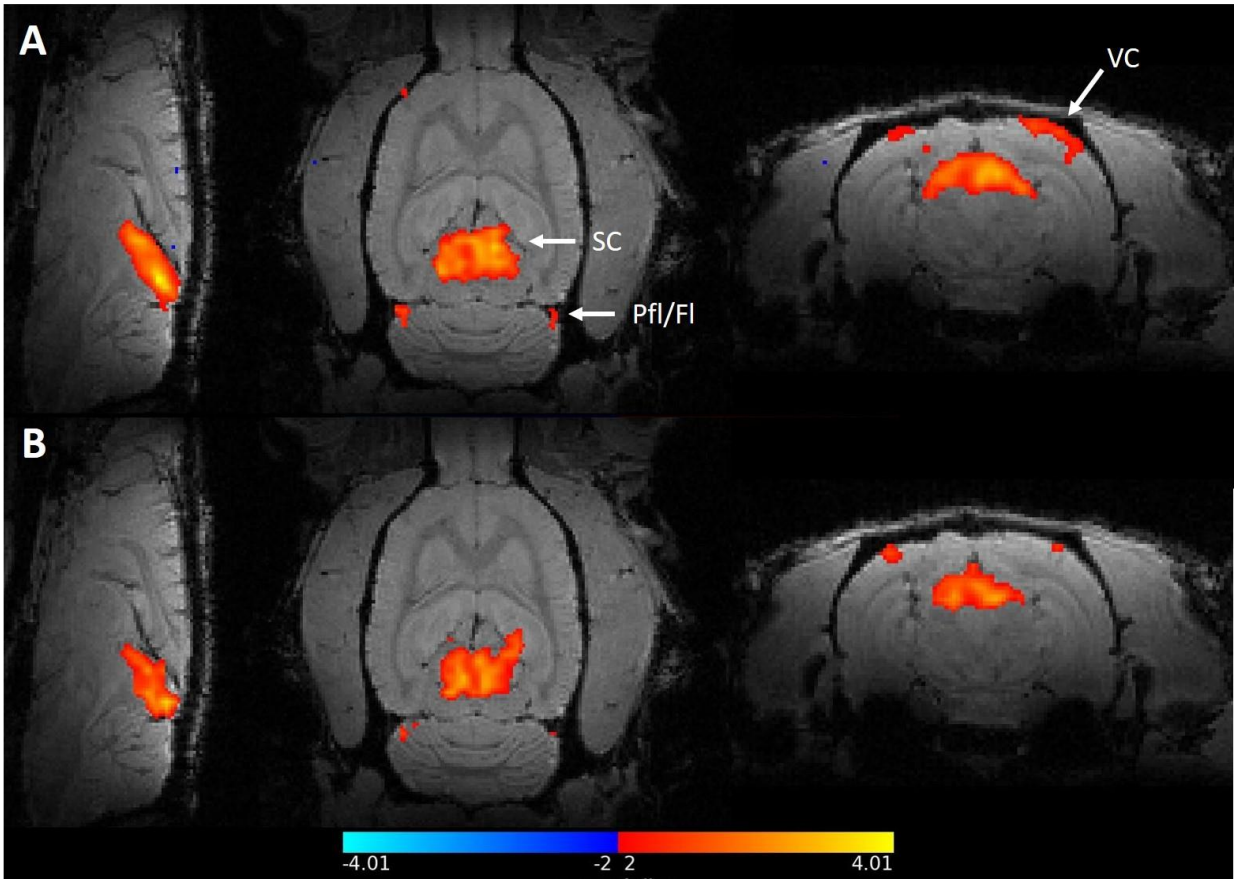

Figure 2 Statistical group maps of BOLD fMRI responses to photic flicker. The color bar shows the thresholds for the z-scores. The figure shows the group averages of activation as computed in the level 3 FEAT analysis. A) control group B) α-synuclein group. Flicker drives robust activation in the superior colliculus (SC), and in the visual cortex (VC). Additionally, the paraflocculus/flocculus complex (Pfl/Fl) was activated.

α-synuclein in the SC could cause decreases in the metabolic demands of the neurons, thereby causing a reduced BOLD signal in the SC ipsilateral of the injection. The z-score maps of the two groups are shown in (Figure 2) registered to a high-resolution anatomical scan. Overall, we found activation of the SC and the VC in both groups. There appears to be a modest activation of cerebellar flocculus complex also shown by (Van Camp et al., 2006) and some response in the lateral geniculate nucleus (LGN) similar to what is reported by (Bailey et al., 2013).

The COPE values from the ROIs of each animal, are visualized as boxplots (Figure 3). Overall, there is no statistically significant effect of overexpressing α-synuclein ($F(1,14)=0.002$, $p=0.962$).

There was a significant effect of ROI ($F(4,130)=59.19$, $p<2\times10^{-16}$). The post-hoc test showed that the SC, but not VC, showed a significant response to the visual stimuli when compared to the olfactory bulb in all conditions.

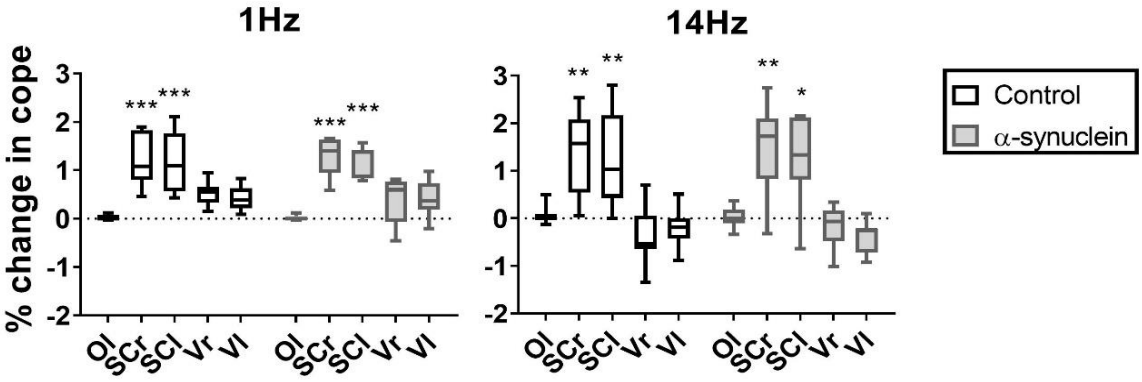

Figure 3 Percent change in contrast of parameter estimates (COPE) in all anatomical regions of interest during 1Hz (left) and 14 Hz (right) light stimulation, respectively. The superior colliculus shows a significant activation. The panels show the median of the COPE values extracted for each region (Ol; olfactory bulb, SC[r,l]; superior colliculus right and left, V[r,l]; visual cortex right and left). Percent change in the group that received the empty viral vector (control) are displayed in black, the results from the animals with α-synuclein expressing animals are shown in grey. The data were analysed with a three-way ANOVA. The asterisks refer to the result of a post-hoc Tukey test. Only the SC differs significantly from the olfactory bulb.

The post-hoc test further confirmed no significant difference between the activation of the ROIs in the right and left hemisphere, suggesting that the overexpression of the α-synuclein was not detectable within animals.

There was a statistically significant interaction between stimulus frequency and ROI ($F(1,130)=6.41$, $p=0.0001$). The post-hoc revealed a significant difference when comparing VC intensity from 1 Hz with the VC at 14 Hz. No significant differences were detected when comparing activation of the olfactory bulb during stimulation with 1 Hz vs. 14 Hz.

Discussion

The purpose of this fMRI study was to examine whether an overexpression of α-synuclein in the SNc is associated with abnormal visually evoked brain activation. We found robust BOLD responses to the visual stimulus in the SC in both groups. There was however no significant difference linked to the group α-synuclein overexpression. This indicates that either the level of neuronal activity measured during visual processing is not altered by overexpression of α-synuclein or that BOLD-fMRI at 7T lacks sensitivity to detect subtle differences between groups. However, there were BOLD responses in rat visual system. This study reproduces the frequency-dependence of the rodent visual cortex (Van Camp et al., 2006). For VC, the visually evoked BOLD responses tends to turn negative at stimulation frequencies above 10Hz (Bailey et al., 2013). The BOLD signal in the SC does not show this frequency-response behavior.

Immunohistochemistry showed that the expression of α-synuclein was fully-developed at the time of scanning. The presence of α-synuclein was detected in the SC ipsilateral to the injection however this did not cause a detectable asymmetry in the BOLD-response of the SC. In a previous experiment the effect of α-synuclein was measured with *in vivo* electrophysiology, here we saw a subtle change in the latency of the VEP in the superior colliculus (unpublished data). The temporal resolution of fMRI makes it insensitive to subtle increases of latency. This could explain the lack of difference between the sides in the α-synuclein animals. There is no direct correlation between ERP and BOLD-fMRI, but the γ-band power (Huettel et al., 2004) and event-related spectral perturbations (Engell et al., 2012) have been reported correlate with BOLD response.

The focus of this paper was to elucidate the functional consequences of overexpressing α-synuclein, both to try and support the electrophysiological study, but also because the AAV-model of PD is not known to cause large anatomical changes. The AAV-model does however, show a loss of dopaminergic cells (Decressac et al., 2012). Kuebler et al. have shown that the change in dopamine can be measured by fMRI/PET using an amphetamine challenge (Kuebler et al., 2017). Generally, the functional consequences of overexpressing human α-synuclein *in vivo* have been shown with other MR-based methods than BOLD-fMRI. A study using diffusion kurtosis imaging, have been shown to image α-synuclein in transgenic mice (Khairnar et al., 2017). This technique looks at the structural changes instead of the changes in oxygen metabolism. A study using MR-spectroscopy found that the bilaterally overexpressing α-synuclein in the striatum caused a changes in energy metabolism (Cuellar-Baena et al., 2016). This technique is sensitive to changes in amounts of metabolites, where BOLD detects changes in the oxygen metabolism of larger populations of neurons. Rodent models of Alzheimer's disease have shown differences in the functional connectivity patterns at an early stage of the protein aggregation using resting state

fMRI (Grandjean et al., 2014). The AAV-model may show similar changes in functional connectivity.

In human patients Zhao et al. have described changes in the BOLD signal of visual areas concerned with the perception of movement (Zhao et al., 2014). Further studies would be needed to study if motion perception is also affected in the AAV-model.

Limitations of the present study are connected to the use of anesthetic in the setup. Consequently, an anesthetic paradigm was established to be used in fMRI studies. Unlike e.g. urethane, and alpha-chloralose, this anesthetic paradigm (supplementary material) has the potential to be used in longitudinal studies. Three hours after the induction of anesthesia, there was a detectable activation of the SC. As the functional changes in the SC are subtle, it cannot be ruled out that variation in the effect of the anesthesia may mask the induced differences.

In summary, this study shows that the fully developed overexpression of α-synuclein did not induce any detectable changes in the BOLD response during visual stimulation.

Conflict of Interest:

Hartwig R. Siebner has received honoraria as speaker from Sanofi Genzyme, Denmark and Novartis, Denmark, as consultant from Sanofi Genzyme, Denmark and as senior editor (NeuroImage) from Elsevier Publishers, Amsterdam, The Netherlands. He has received royalties as book editor from Springer Publishers, Stuttgart, Germany.

Acknowledgements

The authors would like to thank Sascha Gude, Yi He and Milena Kaestner for their technical assistance.

Funding

This project has received funding from the European Union's Horizon 2020 research and innovation programme under the Marie Sklodowska-Curie grant agreement No 641805. HRS holds a 5-year professorship in precision medicine at the Faculty of Health Sciences and Medicine, University of Copenhagen which is sponsored by the Lundbeck Foundation (Grant Nr. R186-2015-2138).

References

Andersen, M.A., Christensen, K.V., Badolo, L., Smith, G.P., Jeggo, R., Jensen, P.H., Andersen, K.J., Sotty, F., 2018. Parkinson's disease-like burst firing activity in subthalamic nucleus induced by AAV-α-synuclein is normalized by LRRK2 modulation. Neurobiol. Dis. 116, 13–27. https://doi.org/10.1016/j.nbd.2018.04.011

Bailey, C.J., Sanganahalli, B.G., Herman, P., Blumenfeld, H., Gjedde, A., Hyder, F., 2013. Analysis of time and space invariance of BOLD responses in the rat visual system. Cereb. Cortex 23, 210–222. https://doi.org/10.1093/cercor/bhs008

Benjamini, Y., Yekutieli, D., 2001. The Control of the False Discovery Rate in Multiple Testing under Depency. Ann. Stat. 29, 1165–1188. https://doi.org/10.1214/aos/1013699998

Bodis-Wollner, I., Kozlowski, P.B., Glazman, S., Miri, S., 2014. a-Synuclein in the Inner Retina in Parkinson Disease. Ann. Neurol. 75, 964–966. https://doi.org/10.1002/ana.24182

Braak, H., Del Tredici, K., Rüb, U., De Vos, R.A.I., Jansen Steur, E.N.H., Braak, E., 2003. Staging of brain pathology related to sporadic Parkinson's disease. Neurobiol. Aging 24, 197–211. https://doi.org/10.1016/S0197-4580(02)00065-9

Cox, R.W., 1996. AFNI : Software for Analysis and Visualization of Functional Magnetic Resonance Neuroimages. Comput. Biomed. Res. 29, 162–173. https://doi.org/10.1006/cbmr.1996.0014

Cuellar-Baena, S., Landeck, N., Sonnay, S., Buck, K., Mlynarik, V., In 'T Zandt, R., Kirik, D., 2016. Assessment of brain metabolite correlates of adeno-associated virus-mediated over-expression of human alpha-synuclein in cortical neurons by in vivo 1H-MR spectroscopy at 9.4 T. J. Neurochem. 137, 806–819. https://doi.org/10.1111/jnc.13547

Davidsdottir, S., Cronin-Golomb, A., Lee, A., 2005. Visual and spatial symptoms in Parkinson's disease. Vision Res. 45, 1285–1296. https://doi.org/10.1016/j.visres.2004.11.006

Decressac, M., Mattsson, B., Lundblad, M., Weikop, P., Björklund, A., 2012. Progressive neurodegenerative and behavioural changes induced by AAV-mediated overexpression of α-synuclein in midbrain dopamine neurons. Neurobiol. Dis. 45, 939–953. https://doi.org/10.1016/j.nbd.2011.12.013

Desai, M., Kahn, I., Knoblich, U., Bernstein, J., Atallah, H., Yang, A., Kopell, N., Buckner, R.L., Graybiel, A.M., Moore, C.I., Boyden, E.S., 2011. Mapping brain networks in awake mice using combined optical neural control and fMRI. J. Neurophysiol. 105, 1393–1405. https://doi.org/10.1152/jn.00828.2010

Ekker, M.S., Janssen, S., Seppi, K., Poewe, W., de Vries, N.M., Theelen, T., Nonnekes, J., Bloem, B.R., 2017. Ocular and visual disorders in Parkinson's disease: Common but frequently overlooked. Park. Relat. Disord. 40, 1–10. https://doi.org/10.1016/j.parkreldis.2017.02.014

Engell, A.D., Huettel, S., McCarthy, G., 2012. The fMRI BOLD signal tracks electrophysiological spectral perturbations, not event-related potentials. Neuroimage 59, 2600–2606. https://doi.org/10.1016/j.neuroimage.2011.08.079

Garcia-Diaz, A.I., Segura, B., Baggio, H.C., Marti, M.J., Valldeoriola, F., Compta, Y., Bargallo, N., Uribe, C., Campabadal, A., Abos, A., Junque, C., 2018. Structural Brain Correlations of Visuospatial and Visuoperceptual Tests in Parkinson's Disease. J. Int. Neuropsychol. Soc. 24, 33–44. https://doi.org/10.1017/S1355617717000583

George, S., Rey, N.L., Reichenbach, N., Steiner, J.A., Brundin, P., 2013. α-Synuclein: The long distance runner. Brain Pathol. 23, 350–357. https://doi.org/10.1111/bpa.12046

Grandjean, J., Schroeter, A., He, P., Tanadini, M., Krstic, D., Keist, R., Konietzko, U., Klohs, J., Nitsch, R.M., Rudin, M., 2014. Early Alterations in Functional Connectivity and White Matter Structure in a Transgenic Mouse Model of Cerebral Amyloidosis. J. Neurosci. 34, 13780–13789. https://doi.org/10.1523/jneurosci.4762-13.2014

Hocking, R.R., 1976. The Analysis and Selection of Variables in Linear Regression. Biometrics

32, 1–49.
Huettel, S.A., McKeown, M.J., Song, A.W., Hart, S., Spencer, D.D., Allison, T., McCarthy, G., 2004. Linking Hemodynamic and Electrophysiological Measures of Brain Activity: Evidence from Functional MRI and Intracranial Field Potentials. Cereb. Cortex 14, 165–173. https://doi.org/10.1093/cercor/bhg115
Kaye, J., Gage, H., Kimber, A., Storey, L., Trend, P., 2006. Excess burden of constipation in Parkinson's disease: A pilot study. Mov. Disord. 21, 1270–1273. https://doi.org/10.1002/mds.20942
Khairnar, A., Ruda-Kucerova, J., Szabó, N., Drazanova, E., Arab, A., Hutter-Paier, B., Neddens, J., Latta, P., Starcuk, Z., Rektorova, I., 2017. Early and progressive microstructural brain changes in mice overexpressing human α-Synuclein detected by diffusion kurtosis imaging. Brain. Behav. Immun. 61, 197–208. https://doi.org/10.1016/j.bbi.2016.11.027
Kjonigsen, L.J., Lillehaug, S., Bjaalie, J.G., Witter, M.P., Leergaard, T.B., 2015. Waxholm Space atlas of the rat brain hippocampal region: Three-dimensional delineations based on magnetic resonance and diffusion tensor imaging. Neuroimage 108, 441–449. https://doi.org/10.1016/j.neuroimage.2014.12.080
Klein, C., Westenberger, A., 2012. Genetics of Parkinson's Disease. Cold Spring Habor Perspect. Med. 2, 1–15. https://doi.org/10.1016/j.jconrel.2014.05.021
Kuebler, L., Herfert, K., Landeck, N., Maurer, A., Amend, M., Thielcke, A., Buss, S., Marciano, S., Stumm, R., Wehrl, H.F., Kirik, D., Pichler, B.J., 2017. Quantification of molecular and functional changes in a rat model of Parkinson's disease using a simultaneaous PET/fMRI protocol.
Langheinrich, T., Tebartz, van, Lagrèze, W.A., Bach, M., Lücking, C.H., Greenlee, M.W., 2000. Visual contrast response functions in Parkinson's disease: evidence from electroretinograms, visually evoked potentials and psychophysics. Clin. Neurophysiol. 111, 66–74.
Lehéricy, S., Bardinet, E., Poupon, C., Vidailhet, M., François, C., 2014. 7 tesla magnetic resonance imaging: A closer look at substantia nigra anatomy in Parkinson's disease. Mov. Disord. 29, 1574–1581. https://doi.org/10.1002/mds.26043
Noyce, A.J., Lees, A.J., Schrag, A.-E., 2016. The prediagnostic phase of Parkinson's disease. J. Neurol. Neurosurg. Psychiatry 87, 871–878. https://doi.org/10.1136/jnnp-2015-311890
Papp, E.A., Leergaard, T.B., Calabrese, E., Johnson, G.A., Bjaalie, J.G., 2014. Waxholm Space atlas of the Sprague Dawley rat brain. Neuroimage 97, 374–386. https://doi.org/10.1016/j.neuroimage.2014.04.001
Pawela, C.P., Biswal, B.B., Hudetz, A.G., Schulte, M.L., Li, R., Jones, S.R., Cho, Y.R., Matloub, H.S., Hyde, J.S., 2009. A protocol for use of medetomidine anesthesia in rats for extended studies using task-induced BOLD contrast and resting- state functional connectivity. Neuroimage 46, 1137–1147. https://doi.org/10.1088/1367-2630/15/1/015008.Fluid
Paxinos, G., Watson, C., 1998. The Rat Brain: in stereotaxic Coordinates, 4th ed. Academic Press, An imprint of Elsevier, San Diego, London.
Pyatigorskaya, N., Gallea, C., Garcia-Lorenzo, D., Vidailhet, M., Lehericy, S., 2014. A review of the use of magnetic resonance imaging in Parkinson's disease. Ther. Adv. Neurol. Disord. 7, 206–220. https://doi.org/10.1177/1756285613511507
Rahimi, J., Milenkovic, I., Kovacs, G.G., 2015. Patterns of tau and α-synuclein pathology in the visual system. J. Parkinsons. Dis. 5, 333–340. https://doi.org/10.3233/JPD-140485
Ridder, A., Müller, M.L.T.M., Kotagal, V., Frey, K.A., Albin, R.L., Bohnen, N.I., 2017. Impaired contrast sensitivity is associated with more severe cognitive impairment in Parkinson disease. Park. Relat. Disord. 34, 15–19. https://doi.org/10.1016/j.parkreldis.2016.10.006

Satue, M., Rodrigo, M.J., Obis, J., Vilades, E., Gracia, H., Otin, S., Fuertes, M.I., Alarcia, R., Crespo, J.A., Polo, V., Larrosa, J.M., Pablo, L.E., Garcia-Martin, E., 2017. Evaluation of progressive visual dysfunction and retinal degeneration in patients with parkinson's disease. Investig. Ophthalmol. Vis. Sci. 58, 1151–1157. https://doi.org/10.1167/iovs.16-20460

Sefton, A.J., Dreher, B., Harvey, A.R., Martin, P.R., 2014. Visual System, The Rat Nervous System: Fourth Edition. https://doi.org/10.1016/B978-0-12-374245-2.00030-9

Sergejevaa, M., Papp, E.A., Bakker, R., Gaudneka, M.A., Okamura-Ohoe, Y., Bolinef, J., Bjaalieb, J.G., Andreas, H., 2015. Anatomical landmarks for registration of experimental image data to volumetric rodent brain atlasing templates. J. Neurosci. Methods 240, 161–169. https://doi.org/10.1016/j.jneumeth.2014.11.005

Team, R.D.C., 2008. R: A language and environment for statistical computing.

Thomas, B., Beal, M.F., 2007. Parkinson's disease. Hum. Mol. Genet. 16, R183–R194. https://doi.org/10.1007/978-1-4939-7880-9_5

Van Camp, N., Verhoye, M., De Zeeuw, C.I., Van der Linden, A., 2006. Light Stimulus Frequency Dependence of Activity in the Rat Visual System as Studied With High-Resolution BOLD fMRI. J. Neurophysiol. 95, 3164–3170. https://doi.org/10.1152/jn.00400.2005

Wirdefeldt, K., Adami, H., Cole, P., Trichopoulos, D., Mandel, J., 2011. Epidemiology and etiology of Parkinson ' s disease : a review of the evidence. Eur. J. Epidemiol. 26, S1–S58. https://doi.org/10.1007/s10654-011-9581-6

Woolrich, M.W., Jbabdi, S., Patenaude, B., Chappell, M., Makni, S., Behrens, T., Beckmann, C., Jenkinson, M., Smith, S.M., 2009. Bayesian analysis of neuroimaging data in FSL. Neuroimage 45, S173–S186. https://doi.org/10.1016/j.neuroimage.2008.10.055

Zhao, Y., Zheng, X., Wang, Q., Xu, J., Xu, X., Zhang, M., 2014. Altered activation in visual cortex: unusual functional magnetic resonance imaging finding in early Parkinson's disease. J. Int. Med. Res. 42, 503–15. https://doi.org/10.1177/0300060513507647

17.1 Supplementary

Anesthesia pilot: The BOLD signal and neuronal activation

A known challenge of preclinical BOLD-fMRI is that measurements are often performed in anesthetized animals, in spite of the risk of impacting both the neuronal signaling and neurovascular dilation thereby attenuating the BOLD-response (Desai et al., 2011). Therefore, we performed an electrophysiological pilot study prior to the fMRI experiment to assess the effect of an anesthetic protocol (isoflurane vs. dexmedetomidine) on visual evoked potentials.

This anaesthesia regime was chosen, as it can be for longitudinal studies compared to urethane, and as scanning awake animals would require training, which might impact the development of the lesion. We chose a combination of dexmedetomidine and a low dose of isoflurane.

Methods

Surgery

16 female SD rats underwent stereotactic surgery where 6 electrodes were implanted. These electrodes where placed bilaterally for visual cortex (AP: -6, ML: ±4), and superior colliculus (AP: -6, ML: ±1, DV: -3.5), additionally a reference electrode (AP: +8, ML: -2) and a ground electrode (AP: -2, ML: +4), coordinates are guided by (Paxinos and Watson, 1998).

Recordings

The stimulation paradigm was 1 Hz of 20 lux warm white LED, continuously presented. Measurements were made freely-moving before induction of anaesthesia (time -10), 30 minutes after induction, 120 minutes, and 180 minutes after induction. The isoflurane was turned off after the recording at 30 minutes, as the VEP varies with the percentage of isoflurane used (data not shown), in the dexmedetomidine/isoflurane condition the isoflurane is reduced to 0.5 % at time 0, and the infusion of dexmedetomidine is started. The EEG signal was averaged directly in Spike2 v7.20 (Cambridge Electronic Design, UK) yielding the VEP. The latency and amplitude information was extracted manually and exported to R for statistical analysis.

Statistical Analysis of the VEP

The electrophysiology was analysed with 48 one-way ANOVAs, testing the influence of time on the latency and amplitude of the individual peaks. The p-values were adjusted for multiple comparisons using false discovery rate (Benjamini and Yekutieli, 2001). The adjusted p-values are shown in Table 2S.

Results

One purpose of the study was to validate an aesthetic regime suitable for fMRI, and with the potential to be used in longitudinal studies. Isoflurane alone causes significant change in the VEP [Figures S1 and S2]. To overcome both the reduction and instability of the signal introduced by

isoflurane a combination of low-concentration of isoflurane and infusion anaesthetic dexmedetomidine (Pawela et al., 2009) was employed, as it does not impair the neuronal activity too much compared to awake. After 180 min of the combination anesthetic the VEP of the visual cortex have almost normalized. The VEP from the SC have gained in amplitude. A small pilot was carried out in the scanner using one animal. Figure S 3 shows a larger BOLD-response at time 180 compared to time 120.

Initiation		Maintenance		Paper	Stimuli	Activation
Isoflurane	4%	Urethane	1.3g/kg bolus (IP), 0.13g/kg supplements (IV)	(Bailey et al., 2013)	RGB LEDs, optical cables	SC+VC+ dLGN
Isoflurane	2.5%	Medetomidine, Pancuronium bromide	0.1mg/kg/h 2mg/kg/h	(Pawela et al., 2008)	5ms, 465nm (blue) LED	SC+VC+ dLGN
Ketamine, **Xylazine**	75 mg/kg 5 mg/kg	Medetomidine	Bolus 0.08mg/kg -> 0.15mg/kg/h (IM)	(Van Camp, Verhoye, De Zeeuw, & Van der Linden, 2006)	Strobe unit (bi-, monocular)	SC+VC
Isoflurane	4%	Isoflurane	1%	(Lau, Zhang, et al., 2011; Lau, Zhou, Cheung, Chan, & Wu, 2011)	Green LED 10Hz, Fiber optics	SC+dLGN+(VC)
Isoflurane	2%	Medetomidine	Bolus 0.04mg/kg -> 0.08mg/kg (SC)	(Niranjan et al. 2016)	cold white LED	SC+VC+ dLGN
Isoflurane	5→2.5%	Isoflurane Dexmedetomidine	0.5% 0.05→0.1 mg/kg/h (IV)	This study	White LED, fiber optics	SC+VC+(dLGN)

Table 1 S Comparison of anaesthetic regimes used in the literature with visual stimulation. (IV) intravenous; (IM) intramuscular; (SC) subcutaneous.

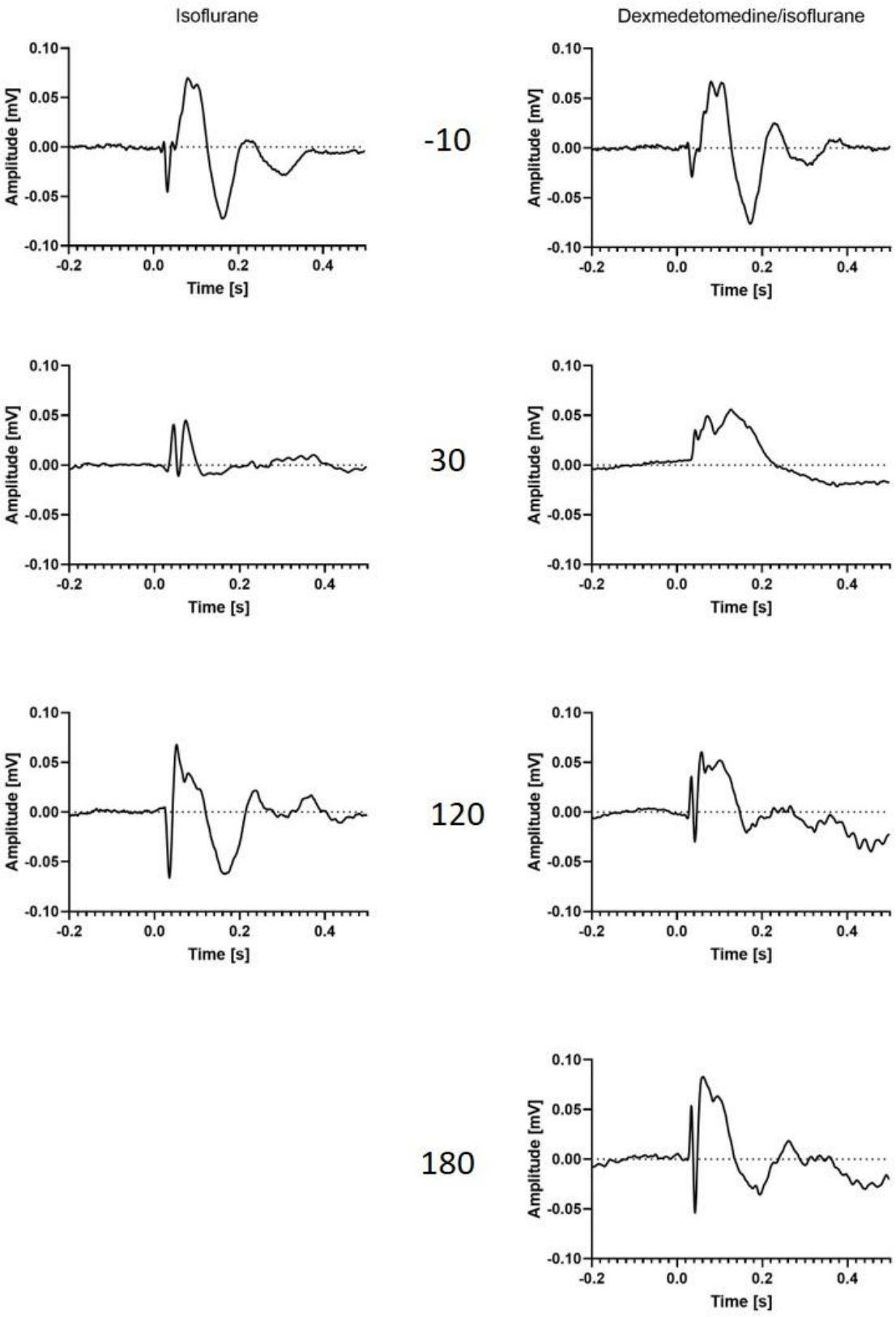

S 1 Anaesthesia affects the VEP in the visual cortex. The numbers between the columns refer to time since initiation of anaesthesia. For the isoflurane condition the animals are only anesthetized at time 30 (the EEG response varies with the level of isoflurane), right after the recording the anaesthesia was removed. At 120 the animals had been awake for 60-70 minutes. In the dex/iso condition the animals are anesthetized throughout the recording session, and anaesthesia is removed after the recording at 180 minutes.

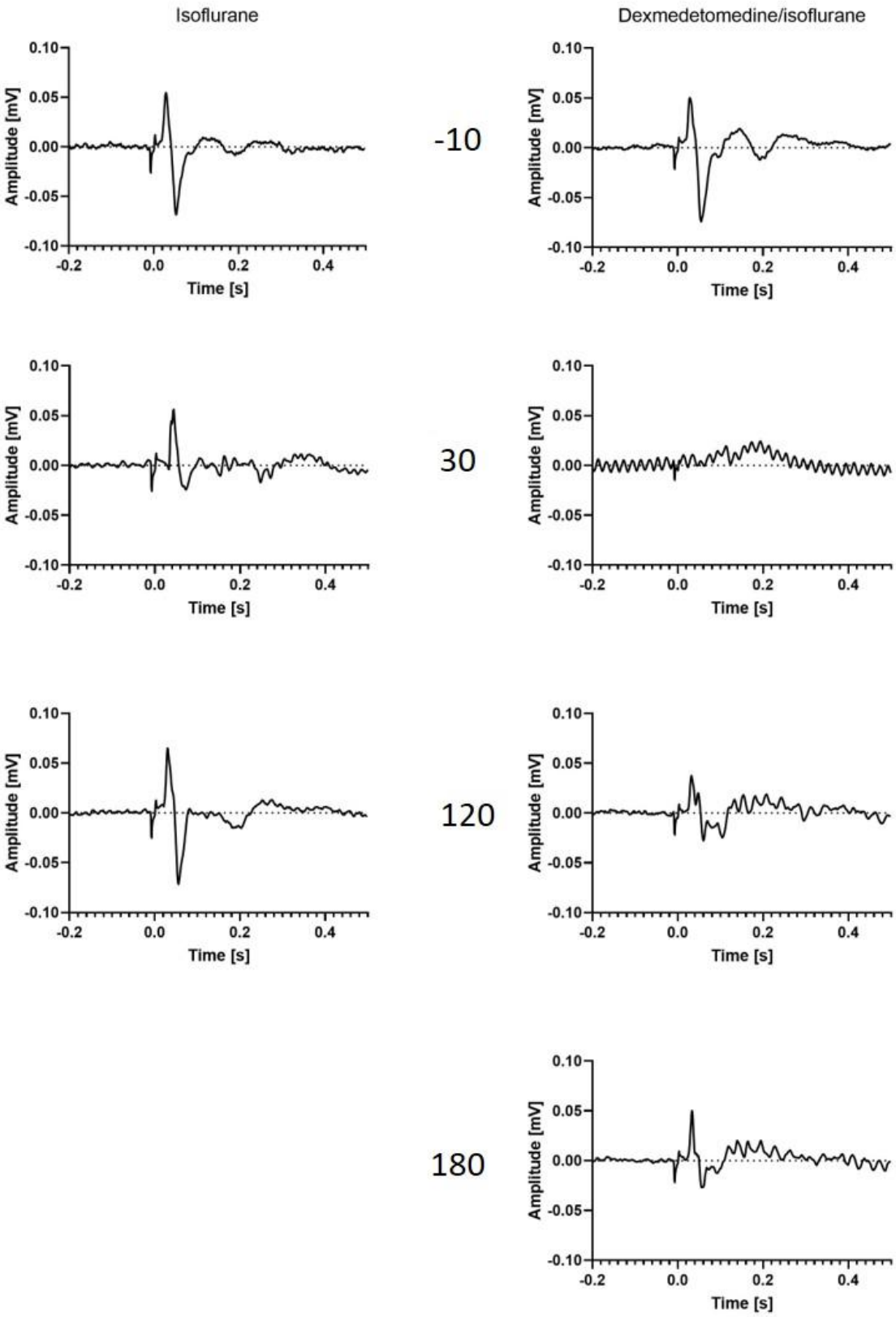

S 2 Anaesthesia affects the VEP in the superior colliculus. The numbers between the columns refer to time since initiation of anaesthesia.

Adjusted p-values from oneway ANOVAs			Isoflurane → awake			Isoflurane/dexmedetomidine		
			30	120	180	30	120	180
Superior colliculus	Amplitude	P1						
		N1	0.01996					
		P2	0.00965					
		N2	0.0289					0.00476
		P3						
	Latency	P1	0.0101			9.31E-06	0.00251	0.00227
		N1				3.61E-03		0.04056
		P2				0.00776		
		N2				0.042		
		P3				0.001585	0.000775	
Visual cortex	Amplitude	P1					0.015165	0.000499
		N1				2.15E-05		
		P2	trend				0.008477	3.56E-07
		N2	0.03983					0.00713
		P3	0.000585		7.66E-05			
		N3	0.000748			2.90E-12	0.00262	
		P4				2.41E-04		
	Latency	P1				1.81E-05	6.16E-09	1.03E-06
		N1				0.04116	0.00632	
		P2				1.75E-03	0.00234	
		N2				0.00127	3.15E-05	0.01058
		P3				0.0013	7.31E-05	
		N3	0.00239			1.93E-04	0.001188	
		P4					1.86E-05	8.86E-05

Table 2 S Table of p-values from the 48 one-way ANOVAs from the quantifications of VEPs. All results refer to the difference to the control.

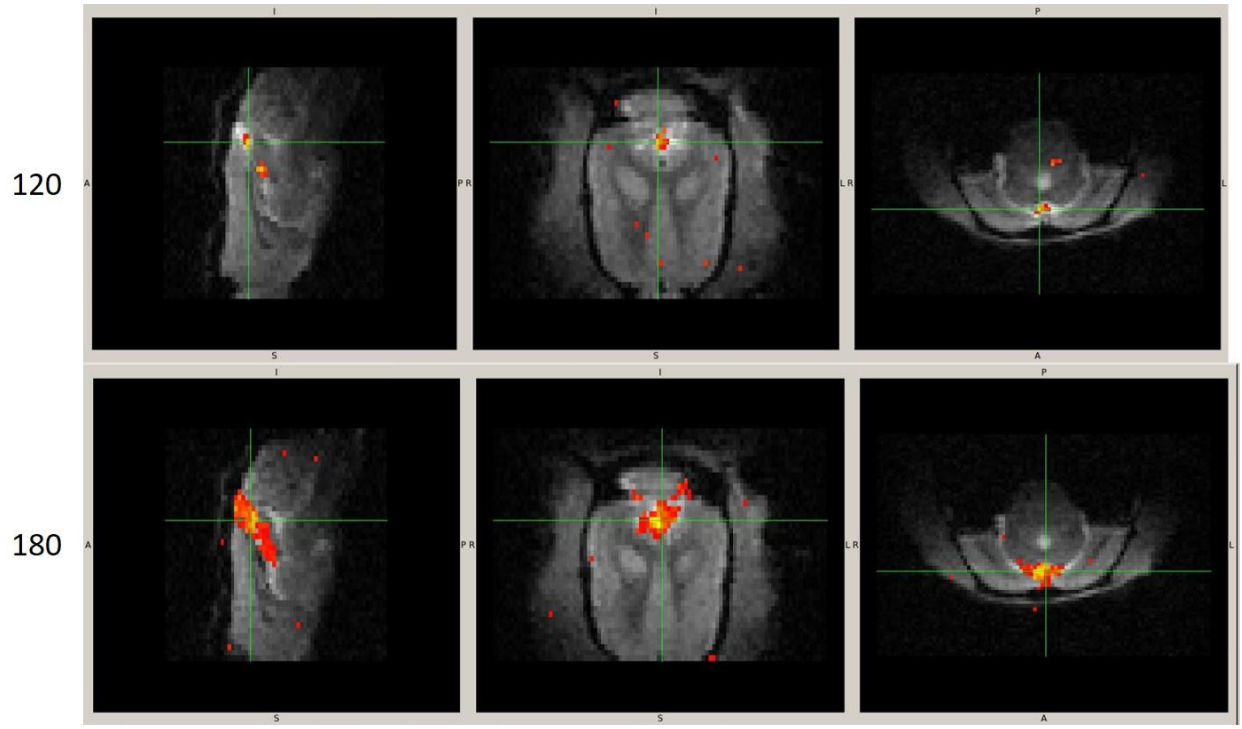

S 3 Effect of anaesthetic on BOLD (n=1). The first row shows the BOLD 120 minutes after the dexmedetomidine infusion has been started. The second row shows the same animal after 180. There is no spatial smoothing and the threshold is the same (min=3.5 SD from zero).

17.2 Supplementary Figures

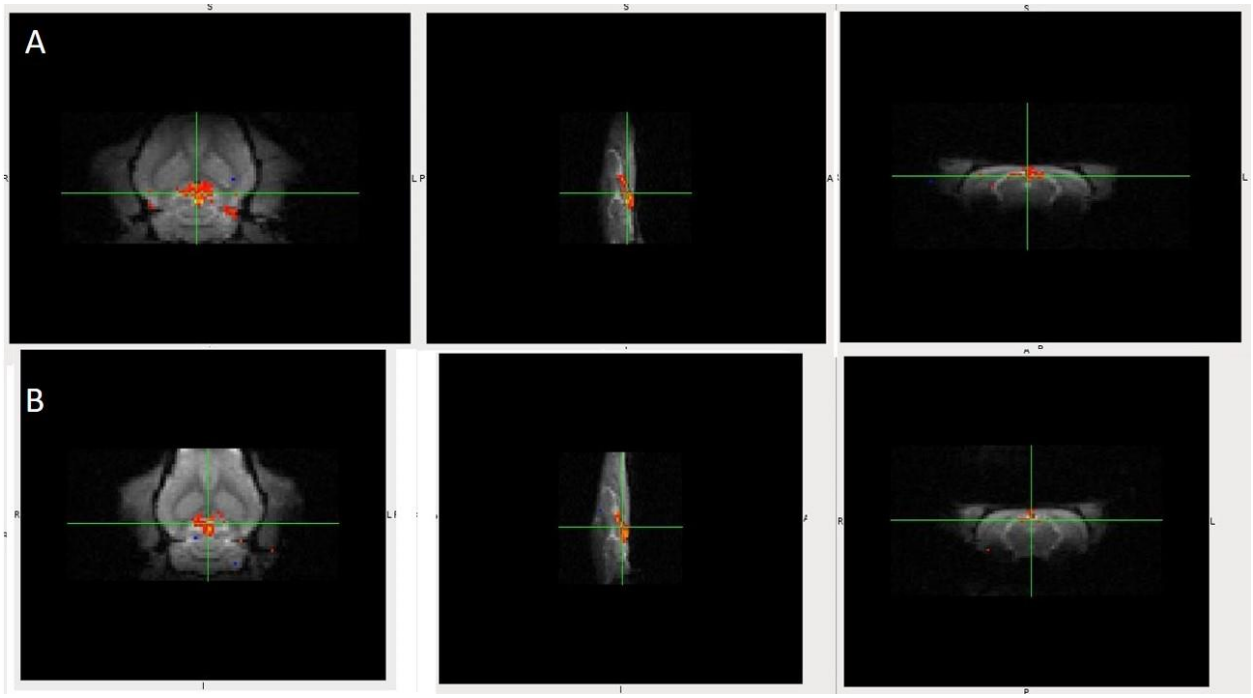

S 4 Unilateral differences introduced with an eye patch A) right eye patched causing a reduction of signal in the left side. B) left eye patched causing a reduction of signal in the right side. There peculiar squeezing is caused by erroneous setting of the resolution during scanning.

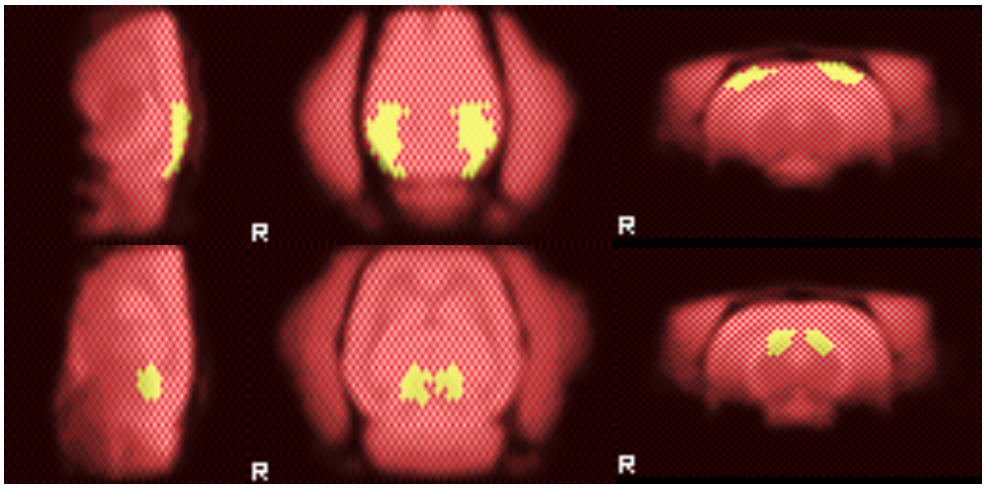

S 5 Masks used for extracting estimates. Top panel, shows the masks for right and left visual cortex. Lower panels show the masks used for right and left superior colliculus.

Study Report

18 Study Report

Electrophysiological Investigation of the Role of LRRK2 in Visual Processing of Rats

Introduction

Leucine-rich repeat kinase 2 (LRRK2) was formerly known as *PARK8.* It is associated with both familial and sporadic Parkinson's disease (PD) (Zimprich et al., 2004). Mutations in this gene are primarily found in familial PD, but also in 1% of sporadic cases. The most common PD-associated mutation, the G2019S, is a gain-of-function mutation increasing the kinase activity 2-3 times.

LRRK2 is a large protein expressed in the entire body especially lungs, kidneys and the immune cells (Herzig et al., 2011). Chronic inhibition of LRRK2 have shown to cause accumulation of lipids in the kidneys (Andersen, Wegener, et al., 2018; Baptista et al., 2013). The substrates are believed to be RabGTPases, but the cellular role of LRRK2 is poorly understood (Steger et al., 2016). In neurons, LRRK2 has been associated to endocytosis (Rivero-Ríos et al., 2015), autophagy (Roosen & Cookson, 2016) and suggested to affect the localisation of the dopamine transporter (Longo et al., 2017), further it has been shown to interact with other PD-related proteins such as α-synuclein (Daher et al., 2015; Tong & Shen, 2009) and PINK1 (Bonello et al., 2019). LRRK2-KO animals have been studied to examine the risks of LRRK2 inhibition as a potential therapeutic for PD (Baptista et al., 2013).

PD patients with LRRK2 mutations have been reported to perform worse in colour discrimination tasks compared to PD patients not carrying LRRK2 mutations (Marras et al., 2011). A study in *drosophilae* showed that the G2019S mutation in LRRK2 causes a significant change in contrast gain-control (Afsari et al., 2014). The visual evoked potential (VEP) measures the electrophysiological integrity of the visual system. Here the VEP is used to study the role of LRRK2 in visual processing.

The aim is twofold, to investigate how the systemic loss of LRRK2 affects the VEP of a LRRK2-knockout rat compared to a wildtype, and if administering a LRRK2 kinase inhibitor to the two genotypes, would cause any electrophysiological differences to minimize.

Methods

Animals

The work in this study is in compliance with EU and Danish legislation on animal experimentation. The LRRK2-knockout (KO) rat is a homozygous genotype with a 10 bp deletion in exon 30, developed by SAGE laboratories in collaboration with the Michael J. Fox foundation.

15 LRRK2-KO female rats, and 15 wildtype (WT) female rats from SAGE laboratories, US. arrived weighing approx. 225g (ten weeks of age). They were housed in pairs until their surgery. After surgery, they were single-housed to prevent damages to the implants. They were housed in reverse daylight with a 12/12 light/dark cycle, lights off at 06:00. Their home cages contained wooden bedding and enrichment, food and water was available *ad libitum.*

Surgery

The animals were anesthetized using subcutaneous (SC) injections of Hypnorm® (Lundbeck, Valby, Denmark), midazolam 5mg/ml (B.Braun, Melsungen, Germany) and saline in a 2:1:1 relation (2.0 ml/kg), yielding 157µg/kg fentanyl. Norodyl (carprofen 5mg/kg) (ScanVet, Fredensborg, Denmark) and Noromox prolongatum (amoxicillintrihydrat 150mg/kg) (ScanVet, Fredensborg, Denmark) were administered during surgery and for five days post-surgery. The animals were mounted in a stereotactic frame and Marcain (2.5mg/ml bupivacaine, AstraZeneca, Albertslund, Denmark), was administered locally (SC) prior to incision. Coordinates were guided by (Paxinos & Watson, 1998). Holes were made bilaterally for visual cortex (AP: -6, ML: ±4), superior colliculus (AP: -6, ML: ±1, DV: -3.5), reference electrode (AP: +8, ML: -2) and ground electrode (AP: -2, ML: +4). The electrodes for recording in the superior colliculus were stranded electrodes E363/3/Spc (PlasticsOne, VA, US). The other four electrodes were E363/20/2.4/S screw electrodes (PlasticsOne, VA, US). The electrode leads were collected in a plastic pedestal MS363 (PlasticsOne, VA, US) and fixed to the skull with RelyX^{TM} Unicem dental cement (3M, Copenhagen, Denmark) as a chronic implant. The sutures were removed under sevoflurane anaesthesia after 5-7 days, dependent on the healing of the animals. The animals were allowed two weeks for recovery before being exposed to any experimentation.

Recording

The recordings were made in awake and behaving animals in a home cage with wood bedding. The homecage was placed in a cabinet shielded from light and electrical noise. The rats were exposed to 400s of 1Hz, 10ms light flashes from LEDs placed 40 cm above the floor of the cage. The first recording the rats were exposed to five different wavelengths (supplementary): short-

wave blue (405 nm), blue (455-460 nm), green (525-530 nm), red (620-625 nm) and white 5050 SMD LEDs. The blue LEDs was chosen for further investigation, as this condition showed the largest cumulative difference between genotypes.

PFE360

PFE360 is a LRRK2-kinase inhibitor (Baptista et al., 2015). It was dissolved in 10 % captisol and pH adjusted with methanesulphonic acid, and administered per oral in a randomized cross-over study, reaching the concentration of 7.5 mg/kg, where we expected full kinase inhibition (Andersen, Christensen, et al., 2018). All recording was carried out 1 hour after administration as this is considered the Tmax (Andersen, Christensen, et al., 2018). To rule out time variance the randomization of day one was repeated with one week in between. The final sequence became Day1-Day1-Day2 with the dashes representing a week. This enabled us to compare the e.g. WT animals given the vehicle to themselves a week later. When comparing the amplitude and latency data of the first recording with the second there is no significant difference between the vehicle condition of the KO or the WT (data not shown).

Post-mortem assessments

The animals were sacrificed at 1 H (n=8), 3 H (n=8) and 6 H (n=6) after administration of PFE360. The blood and cerebellum was sampled for exposure to confirm previously reported values for T½ of PFE360 (Andersen, Christensen, et al., 2018). The cerebrum was used to assess the location of the electrodes histologically.

Data analysis

The flash VEPs were generated and recoded using Spike2 7.20. Naming of the peaks in the visual cortex was guided by (D. Creel, Dustman, & Beck, 1974; Meeren, Van Luijtelaar, & Coenen, 1998). The first positive deflection was named P1, the first negative deflection is named N1, the second positive deflection is named P2 and so on. For flash VEPs, the amplitude and latency of the peaks were extracted manually and analyzed separately.

The SSVEP should provide a more robust response than the transient VEP, but does not provide temporal information as it is summation of previous responses, therefore it should be analyzed in the frequency domain (Norcia, Appelbaum, Ales, Cottereau, & Rossion, 2015). Amplitude would be affected by changes in the noise level between recording sessions the signal-to-noise ratio (SNR) was chosen over amplitude to reduce variation. The first harmonic is at the same frequency as the stimulus (14Hz), where the second harmonic is at 28Hz (Norcia et al., 2015; Regan, 1989).

The SSVEPs were analyzed using a script programmed in Matlab 2016a (Mathworks, MA, USA) which fitted sinusoids to determine amplitude and phase and carry out a Fourier transform. To test for an effect of sildenafil, the SNRs of the amplitudes were quantified at 30 minutes and 28h and compared to the baseline condition using a one-way ANOVA as well. The p-values were adjusted using FDR.

Statistics

The data was analyzed in R (R 3.4.2) via R studio. The model for analysis of PFE360 data was a two-way repeated measures ANOVA, which included the variables genotype, and drug. The analysis is carried out separately for each peak for each nucleus giving 24 ANOVAs, the results from these tests were adjusted with false discovery rate (FDR) for multiple comparisons. This was followed by Tukey test with FDR adjustment, if the $p<0.05$.

Results

Interaction of colour and genotype

To investigate whether the knockout of LRRK2 would interact with the wavelength of the stimulus. VEPs were recorded from the visual cortex and superior colliculus, using five wavelength conditions. This pilot study is presented in the supplementary material. Figure S1 shows the waveforms from the visual cortex of the two genotypes. Cumulating the differences of means of both latency and amplitude showed a larger discrepancy between the LRRK2-KO rats and the wildtypes, when using the blue condition. This wavelength was chosen as stimulation condition for subsequent investigation using PFE360.

PFE360 affects both KO and WT rats

To study the effect of modulating LRRK2 activity, the LRRK2 kinase inhibitor PFE360 was administered to both the LRRK2-KO and the WT, in a randomized cross-over study. Figure 1 A-B shows the waveforms recorded from the visual cortex and the superior colliculus, after the administration of either vehicle or PFE360, and stimulating with blue wavelength [455-460 nm]. Figure 1C shows the concentration of PFE360 at three time points after administration. 1 hour after administration the unbound concentration is 137.4 nM, which is more than 10 times the IC50 of 2.3 nM reported by (Andersen, Christensen, et al., 2018).

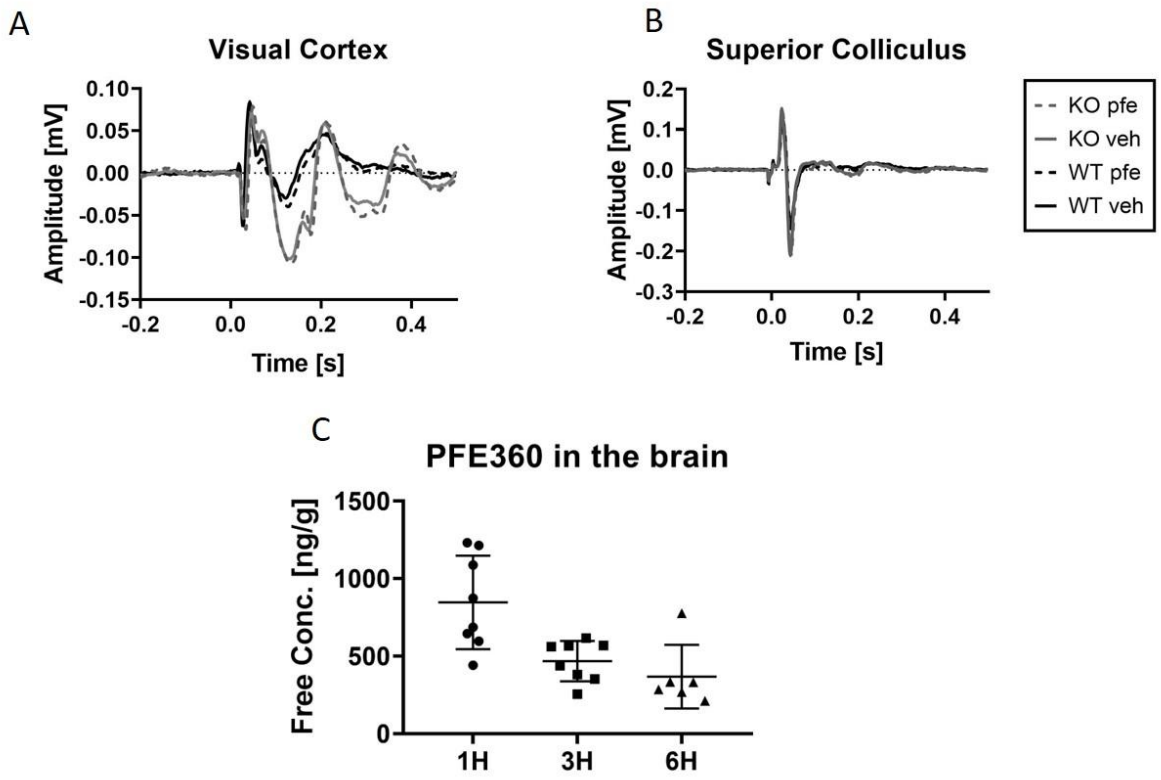

Figure 1 The effect of PFE360, and pharmacological profile. A) and B) shows the four waveforms of the WT with vehicle (black line) and one hour after administration of PFE360 (dashed, black line), and the KO with vehicle (grey line) and PFE360 (dashed, gray line). C) shows the total concentration of PFE360 in the cerebellum at three time points after the administration of PFE360.

Visual cortex

The amplitudes of the waveform from the visual cortex are quantified in Figure 2. The results of the overall two-way ANOVAs are shown in Table 1. They reveal statistically significant effects of LRRK2-KO on the peaks P1, N3 and P4. Further there is an effect of the drug on the N1 and P2 of the WT, and no detectable effect of the drug in the KO. In the detail the P1 peak, show an overall effect of the genotype, where the amplitude of the KO animals is reduced by 0.0099±0.0018 mV compared to the WT. For both the N2, and the P3 there is an effect of the drug on the WT, causing reductions in the amplitude (-0.017±0.0045 mV and -0.019±0.0056 mV respectively). Furthermore, the N3 peak form the KO rats is -0.086±0.0055 mV larger compared to the wildtype. The amplitude of the P4 peak is increased by 0.015±0.0032 mV in the KO compared to wildtype.

Amplitude of peaks in visual cortex		*Two-way ANOVA*		
			F-value	Adjusted p-value (if p<0.05)
P1	Gene	F(1,27)	13	0.0014
	Drug	F(1,304)	0.69	
N1	Gene	F(1,27)	0.033	
	Drug	F(1,304)	0.88	
P2	Gene	F(1,27)	0.65	
	Drug	F(1,304)	0.036	
N2	Gene	F(1,27)	4.3	0.049
	Drug	F(1,304)	23	0.00021
P3	Gene	F(1,27)	1.1	
	Drug	F(1,304)	33	0.00021
N3	Gene	F(1,27)	64	0.00021
	Drug	F(1,304)	0.45	
P4	Gene	F(1,27)	9.9	0.006
	Drug	F(1,304)	0.0079	

Latency of peaks in visual cortex		*Two-way ANOVA*		
			F-value	Adjusted p-value (if p<0.05)
P1	Gene	F(1,27)	0.079	
	Drug	F(1,304)	16	0.00021
N1	Gene	F(1,27)	16	0.00064
	Drug	F(1,304)	117	0.00021
	interaction	F(1,304)	15	0.00036
P2	Gene	F(1,27)	53	0.00021
	Drug	F(1,304)	54	0.00021
N2	Gene	F(1,27)	0.80	
	Drug	F(1,304)	96	0.00021
P3	Gene	F(1,27)	0.010	
	Drug	F(1,304)	69	0.00021
N3	Gene	F(1,27)	15	0.0008
	Drug	F(1,304)	20	0.00021
P4	Gene	F(1,27)	0.77	
	Drug	F(1,304)	10	

Table 1 The overall statistical results from the ANOVA of the amplitude and latencies from the visual cortex waveforms. The p-value is displayed after FDR adjustment.

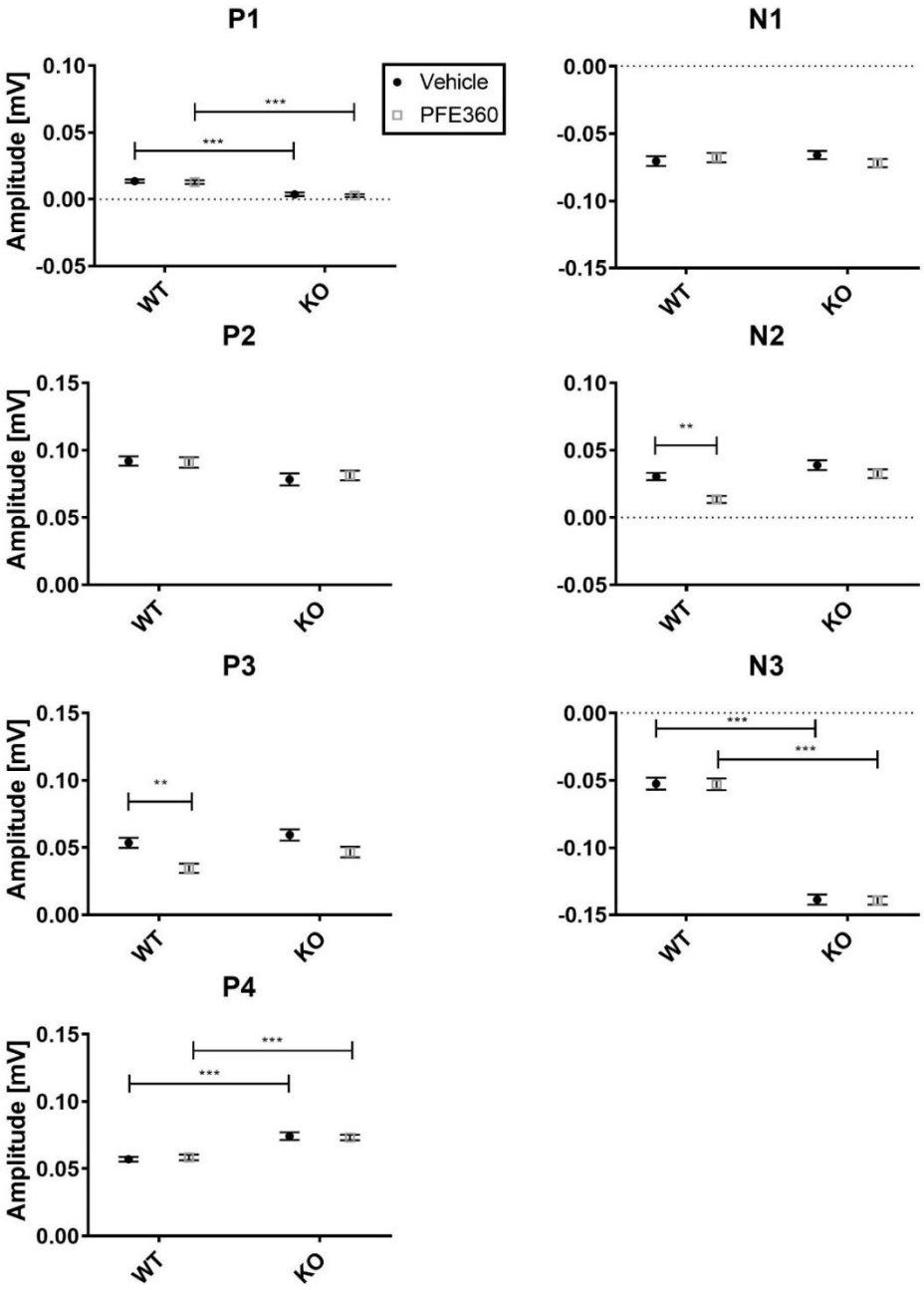

Figure 2 Amplitude of the peaks in the waveform from the visual cortex shown as mean±SEM. The amplitudes of all peaks are shown on the same scale, but different parts of the scale to accommodate the nature of each peak. Asterisks refer to results from the post-hoc tests: * p<0.05, ** p<0.01, *** p<0.001.

Figure 3 shows the grand means of the latency data from the visual cortex waveform. The results of the ANOVAs are shown in Table 1. PFE360 cause increases of latency ranging from 1.2 ms to 5.6 ms in both wildtype and LRRK2-KO. The knockout of LRRK2 show latencies increased with 2.5 ms and 5 ms on the N1 and P2, respectively, but 20 ms in the latency of N3. There are no statistically significant changes in P4 peak.

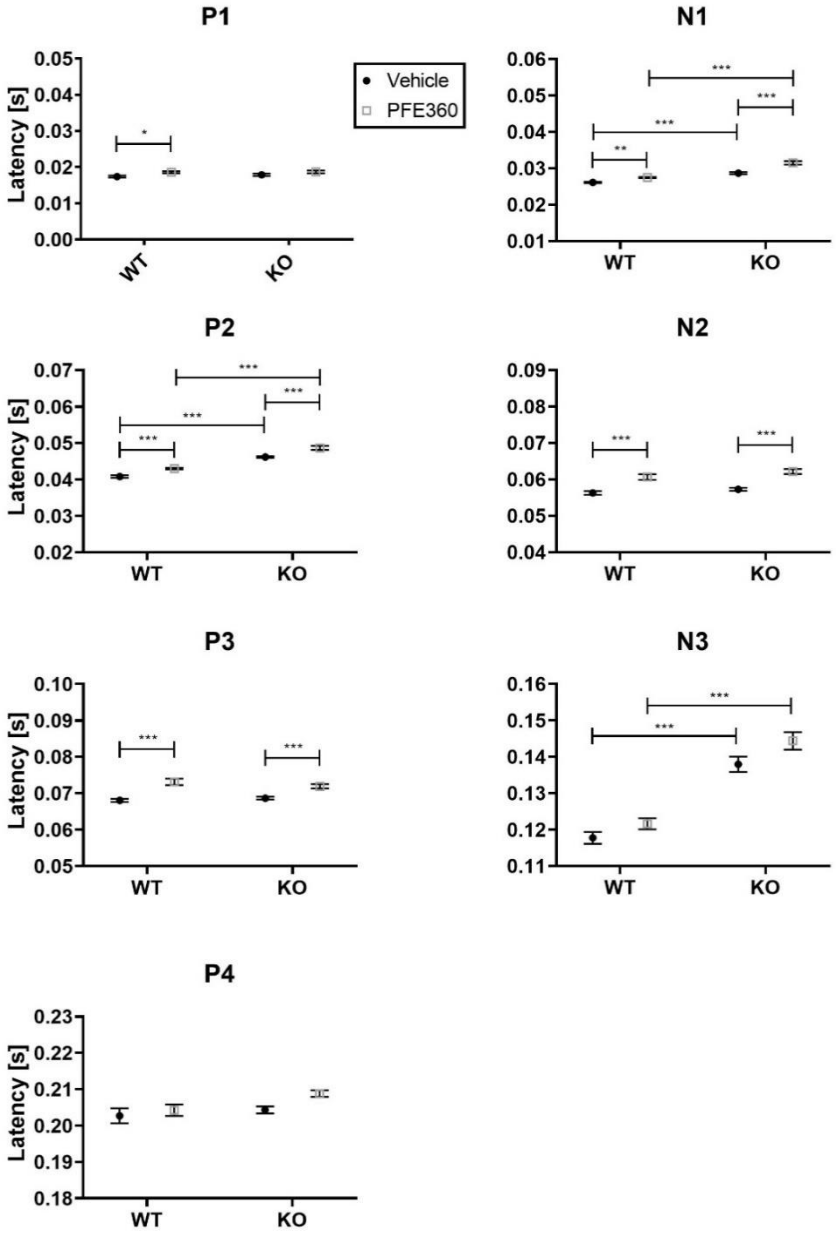

Figure 3 Latency of the peaks in the waveform from the visual cortex, shown as mean±SEM. The scale is 50 ms for all peaks. Asterisks refer to results from the post-hoc tests: * p<0.05, ** p<0.01, *** p<0.001.

PFE360 induces changes in the superior colliculus

The grand amplitudes of the peaks from the superior colliculus are displayed in Figure 4. The results of the overall two-way ANOVAs testing for the effect of gene and drug, are shown in Table 2. Both the P1 and N1 show significant effects of gene, where there are effects of PFE360 in the amplitudes of P2 in the KO and N2 in the WT. Specifically, the P1 in the KO displayed an increase of 0.043±0.0083 mV, the N1 the KO show a negative increase in amplitude of 0.08±0.011 mV. In the P2 the is an increase of amplitude caused by the drug in the KO 0.0083±0.0030 mV, but not in

the WT. The N2 show a significant decrease in the amplitude of the WT 0.0055±0.0032 mV, caused by adding PFE360. There are no changes in the amplitude of P3.

Amplitude of peaks in superior colliculus	*Two-way ANOVA*			
			F-value	Adjusted p-value (if p<0.05)
P1	Gene	F(1,27)	6.5	0.019
	Drug	F(1,273)	0.0070	
N1	Gene	F(1,27)	14	0.0012
	Drug	F(1,273)	0.065	
P2	Gene	F(1,27)	1.7	
	Drug	F(1,273)	0.87	
	interaction	F(1,273)	13	0.00064
N2	Gene	F(1,27)	0.96	
	Drug	F(1,273)	20	0.00021
P3	Gene	F(1,27)	0.66	
	Drug	F(1,273)	5.5	0.021

Latency of peaks in superior colliculus	*Two-way ANOVA*			
			F-value	Adjusted p-value (if p<0.05)
P1	Gene	F(1,27)	8.3	0.009
	Drug	F(1,273)	137	0.00021
N1	Gene	F(1,27)	3.2	
	Drug	F(1,273)	84	0.00021
P2	Gene	F(1,27)	19	0.00036
	Drug	F(1,273)	14	0.00036
	interaction	F(1,273)	3.9	0.049
N2	Gene	F(1,27)	7.3	0.013
	Drug	F(1,273)	12	0.00076
P3	Gene	F(1,27)	3.1	
	Drug	F(1,273)	25	0.00021

Table 2 Statistics for the two-way ANOVA of the amplitudes and latencies from the superior colliculus. The p-values are adjusted using FDR for all 24 ANOVAs.

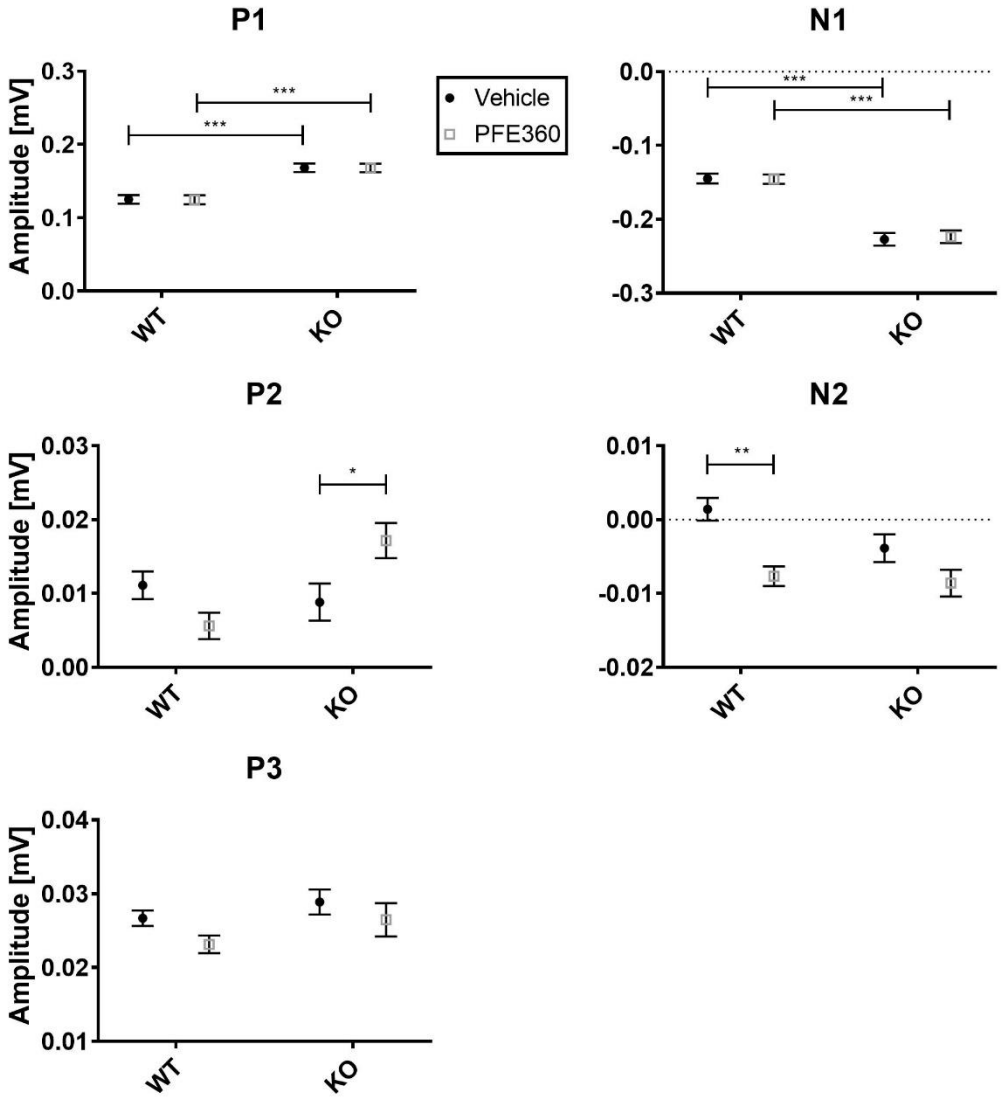

Figure 4 Amplitudes of the superior colliculus, displayed with mean±SEM. There is effects of genotype on P1 and N1. Asterisks refer to results from the post-hoc tests: * p<0.05, ** p<0.01, *** p<0.001.

The grand latencies of the superior colliculus are shown in Figure 5. The results of the overall two-way ANOVAs are shown in Table 2. There are significant effects of genotype, and PFE360 in both the P1, and the N1, collectively these are in the range of 1-3 ms. In the P2 and N2 there are effect of genotype, causing decreases of latency range from 5-9 ms. There are also effects of PFE360 on the KO, causing increases in latency of 4-5 ms. For the P3, there is an effect of the genotype in the vehicle condition causing a decrease of 7.4±2.3 ms, the addition of the drug seems to normalize this effect for the KO, by increasing the latency with 7.4±2.3 ms.

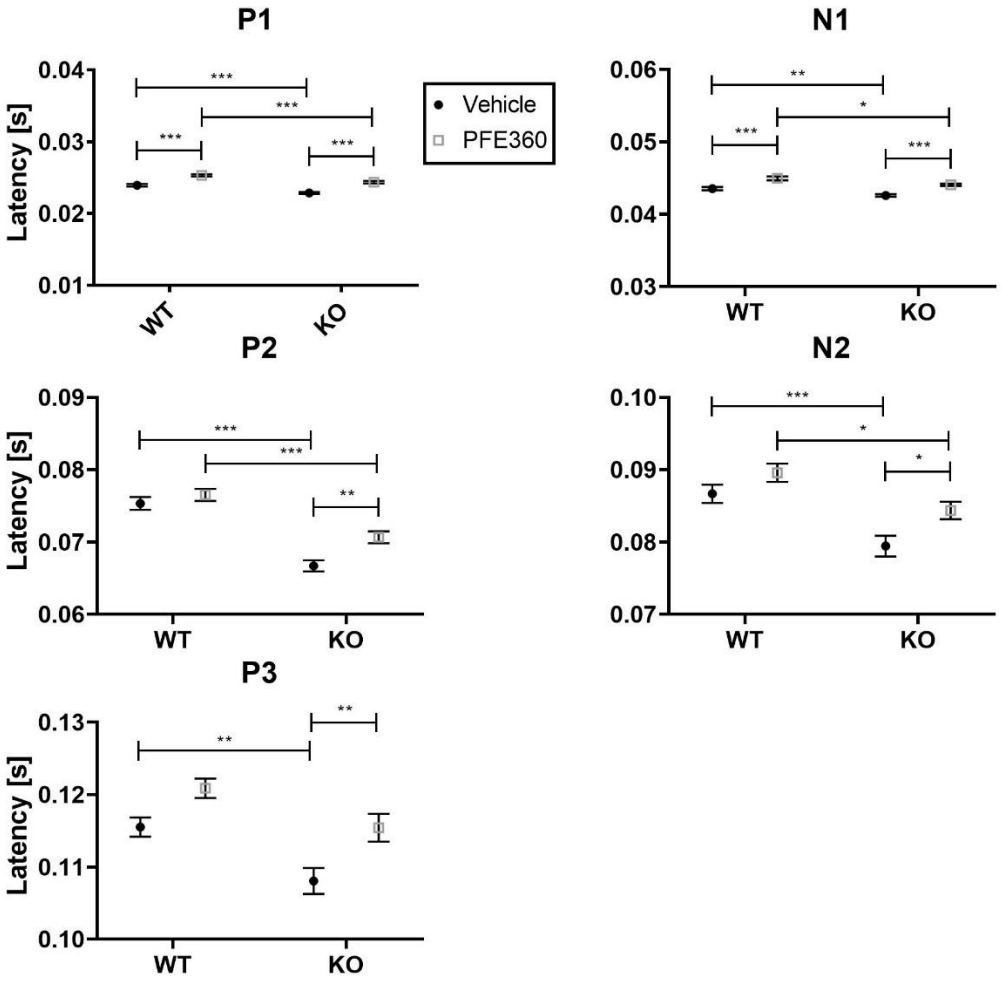

Figure 5 Latencies of the superior colliculus, shown as mean±SEM. Asterisks refer to results from the post-hoc tests: * p<0.05, ** p<0.01, *** p<0.001.

SSVEP changes in response to LRRK2 modulation

In addition to the VEPs the SSVEPs were measured in the visual cortex and superior colliculus. The SNRs of the harmonics are displayed in Figure 6. The two-way ANOVA of the SNR of the 1st harmonic from the visual cortex shows a trend for an interaction between drug and gene ($F(1,54)=3.27$, ns). The test for the 2nd harmonic shows no significant effects.

In the superior colliculus there was no detectable differences when testing the SNR of the 1st harmonic, but the 2nd harmonic shows a significant effect of gene ($F(1,54)=6.44$, $p=0.01$).

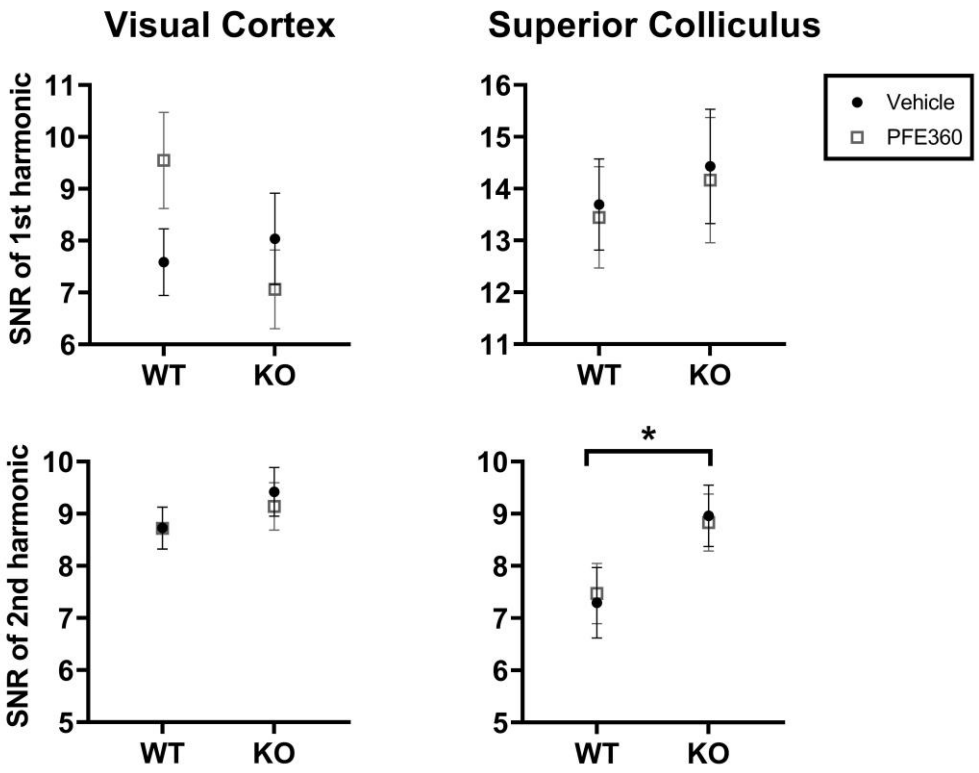

Figure 6 SSVEP from visual cortex and superior colliculus shown with grand mean±SEM. There is a trend of and interaction for the first harmonic of the visual cortex. There is a statistically significant effect of gene on the second harmonic of the superior colliculus.

Discussion

The purpose of the study was to investigate the role of LRRK2 in visual processing. VEPs and SSVEPs were recorded from the superior colliculus and the visual cortex of both LRRK2-KO and wildtype rats. Subsequently, the LRRK2 kinase inhibitor PFE360 was administered in a randomized cross-over design. Previously the knockout model has been studied for toxicological purposes, with respect to using LRRK2 inhibition as a therapy for PD. These studies have primarily shown adverse effects on lung and kidneys (Baptista et al., 2013; Fuji et al., 2015), here we report changes in the electrophysiology of the visual system. There was a significant difference in the overall VEP waveform when just comparing between the knockout and the wildtype. The magnitude of this difference depended on the wavelength of the stimulus presented. Interestingly, human patients with LRRK2-linked PD perform worse in the Farnsworth-Munsell 100-hue test when compared to idiopathic PD, as well as comparing G2019S-carriers with non-mutation carriers from the same families (Marras et al., 2011). Our results show an interaction between genotype and wavelength, suggesting that LRRK2 may be involved in the transduction of wavelength information. In flies the expression of LRRK2-G2019S has been reported to cause a progressive loss of photoreceptors (Hindle et al., 2013). Further investigation would be needed to determine if LRRK2 is present in the retina of rodents.

In the rodent brain, LRRK2 is enriched in the subthalamic nucleus and the, even the visual cortex, but not in the superior colliculus (Davies et al., 2013; Higashi et al., 2007). This could explain why the differences in the overall VEP seem more pronounced in the visual cortex. Further, there were consistently peaks after the P4 of the visual cortex of the KO animals, suggesting that the lack of LRRK2 changes the duration of the post-synaptic response. When comparing the VEPs and SSVEPs from the superior colliculus, there is a significant difference between the LRRK2-KO and the wildtypes, suggesting that LRRK2 has a function in this region. However, this function may be developmental. LRRK2 is expressed in neural progenitor cells suggesting a role in neurodevelopment. An *in vitro* study of LRRK2 deficiency have been reported to induce changes in neurite outgrowth possibly via retinoic acid interaction (Schulz et al., 2011). An *in vivo* study has detected LRRK2 in the ventricular and subventricular zones associated with neurogenesis in embryonic animals (Zechel, Meinhardt, Unsicker, & von Bohlen und Halbach, 2010). Collectively, these results suggest a role for LRRK2 in the development of neurons. These studies were carried out in mice, but LRRK2 is well-conserved between the two species (Zimprich et al., 2004).

The LRRK2 kinase inhibitor PFE360, affected the electrophysiological responses of both the LRRK2-KO rats and the WTs. This inhibitor was described by Baptista to have very little off-target effects (Baptista et al., 2015). The dose have been shown to be specific for the kinase domain of LRRK2 (Andersen, Christensen, et al., 2018). The LRRK2-KO rats show shorter latencies of their peaks in the superior colliculus, but longer latencies in the visual cortex. An acute dose of PFE360 caused longer latencies in both nuclei, similar to the effect in the wildtype rats, supporting off-target effects of the LRRK2 kinase inhibitor (Thirstrup et al., 2017). Testing the vehicle condition twice in the same animals shows that the week between the first test and the cross-over does not introduce change in the waveform of the VEP, suggesting a robustness in the measurement of the VEP, further suggesting that the changes in the VEP of the knockout are induced by PFE360. Some of the suggested off-target kinases are: MST 1/2, RSK2 (Baptista et al., 2015), MAP3K5, MAP3K15 and MAP3K6 (Thirstrup et al., 2017). These enzymes have very diverse functions, but the MAP3K5 have been associated to stress induced death of retinal ganglion cells in glaucoma (Seki & Lipton, 2008). Whether acute inhibition can affect visual processing remains to be elucidated.

Future perspective

In consistency with studies of both flies and humans, modulation of LRRK2 affects colour vision. Further investigation of the underlying mechanism may help elucidate the consequences of LRRK2 modulation.

References

Afsari, F., Christensen, K. V., Smith, G. P., Hentzer, M., Nippe, O. M., Elliott, C. J. H., & Wade, A. R. (2014). Abnormal visual gain control in a Parkinson's disease model. *Human Molecular Genetics*, *23*(17), 4465–4478. https://doi.org/10.1093/hmg/ddu159

Andersen, M. A., Christensen, K. V., Badolo, L., Smith, G. P., Jeggo, R., Jensen, P. H., … Sotty, F. (2018). Parkinson's disease-like burst firing activity in subthalamic nucleus induced by AAV-α-synuclein is normalized by LRRK2 modulation. *Neurobiology of Disease*, *116*(April), 13–27. https://doi.org/10.1016/j.nbd.2018.04.011

Andersen, M. A., Wegener, K. M., Larsen, S., Badolo, L., Smith, G. P., Jeggo, R., … Thougaard, A. (2018). PFE-360-induced LRRK2 inhibition induces reversible, non-adverse renal changes in rats. *Toxicology*, *395*(December 2017), 15–22. https://doi.org/10.1016/j.tox.2018.01.003

Baptista, M. A. S., Dave, K. D., Frasier, M. A., Sherer, T. B., Greeley, M., Beck, M. J., … Fiske, B. K. (2013). Loss of leucine-rich repeat kinase 2 (LRRK2) in rats leads to progressive abnormal phenotypes in peripheral organs. *PLoS ONE*, *8*(11), 1–16. https://doi.org/10.1371/journal.pone.0080705

Baptista, M. A. S., Merchant, K., Bryce, D., Ellis, M., Estrada, A. A., Galatsis, P., … Sherer, T. B. (2015). LRRK2 Kinase Inhibitors of Different Structural Classes Induce Abnormal Accumulation of Lamellar Bodies in Type II Pneumocytes in Non-Human Primates but are Reversible and Without Pulmonary Functional Consequences Workflow and Study Design, 94080.

Bonello, F., Hassoun, S.-M., Mouton-Liger, F., Shin, Y. S., Muscat, A., Tesson, C., … Brice, A. (2019). LRRK2 impairs PINK1/Parkin-dependent mitophagy via its kinase activity: pathologic insights into Parkinson's disease. *Human Molecular Genetics*, *00*(00), 1–16. https://doi.org/10.1093/hmg/ddz004

Creel, D., Dustman, R. E., & Beck, E. C. (1974). Intensity of flash illumination and the visually evoked potential of rats, guinea pigs and cats. *Vision Research*, *14*(8), 725–729. https://doi.org/10.1016/0042-6989(74)90070-4

Creel, D. J. (2012). Visually Evoked Potentials. In *The Organization of the Retina and Visual System* (pp. 1–28). https://doi.org/NBK107218 [bookaccession]

Daher, J. P. L., Abdelmotilib, H. A., Hu, X., Volpicelli-Daley, L. A., Moehle, M. S., Fraser, K. B., … West, A. B. (2015). Leucine-rich repeat kinase 2 (LRRK2) pharmacological inhibition abates α-synuclein gene-induced neurodegeneration. *Journal of Biological Chemistry*, *290*(32), 19433–19444. https://doi.org/10.1074/jbc.M115.660001

Davies, P., Hinkle, K. M., Sukar, N. N., Sepulveda, B., Mesias, R., Serrano, G., … Melrose, H. L. (2013). Comprehensive characterization and optimization of anti-LRRK2 (leucine-rich repeat kinase 2) monoclonal antibodies. *Biochemical Journal*, *453*(1), 101–113. https://doi.org/10.1042/bj20121742

Fuji, R. N., Flagella, M., Baca, M., S. Baptista, M. A., O'Mahony, J., Roose-Girma, M., … Warming, S. (2015). Effect of selective LRRK2 kinase inhibition on nonhuman primate lung. *Science Translational Medicine*, *7*(273), 273ra15-273ra15. https://doi.org/10.1126/scitranslmed.aaa3634

Herzig, M. C., Kolly, C., Persohn, E., Theil, D., Schweizer, T., Hafner, T., … Shimshek, D. R. (2011). LRRK2 protein levels are determined by kinase function and are crucial for kidney and lung homeostasis in mice. *Human Molecular Genetics*, *20*(21), 4209–4223. https://doi.org/10.1093/hmg/ddr348

Higashi, S., Moore, D. J., Colebrooke, R. E., Biskup, S., Dawson, V. L., Arai, H., … Emson, P. C. (2007). Expression and localization of Parkinson's disease-associated leucine-rich repeat kinase 2 in the mouse brain. *Journal of Neurochemistry*, *100*(2), 368–381. https://doi.org/10.1111/j.1471-4159.2006.04246.x

Hindle, S., Afsari, F., Stark, M., Adam Middleton, C., Evans, G. J. O., Sweeney, S. T., & Elliott, C. J. H. (2013). Dopaminergic expression of the Parkinsonian gene LRRK2-G2019S leads to non-autonomous visual neurodegeneration, accelerated by increased neural demands for energy. *Human Molecular Genetics*, *22*(11), 2129–2140. https://doi.org/10.1093/hmg/ddt061

Longo, F., Mercatelli, D., Novello, S., Arcuri, L., Brugnoli, A., Vincenzi, F., … Morari, M. (2017). Age-dependent dopamine transporter dysfunction and Serine129 phospho-α-synuclein overload in G2019S LRRK2 mice. *Acta Neuropathologica Communications*, *5*(1), 22. https://doi.org/10.1186/s40478-017-0426-8

Marras, C., Schuele, B., Munhoz, R. P., Rogaeva, E., Langston, J. W., Kasten, M., … Lang, A. E. (2011). Phenotype in parkinsonian and nonparkinsonian LRRK2 G2019S mutation carriers. *Neurology*, *77*(4), 325–333. https://doi.org/10.1212/WNL.0b013e318227042d

Meeren, H. K. M., Van Luijtelaar, E. L. J. M., & Coenen, A. M. L. (1998). Cortical and thalamic visual evoked potentials during sleep-wake states and spike-wave discharges in the rat. *Electroencephalography and Clinical Neurophysiology - Evoked Potentials*, *108*(3), 306–319. https://doi.org/10.1016/S0168-5597(97)00101-9

Norcia, A. M., Appelbaum, L. G., Ales, J. M., Cottereau, B. R., & Rossion, B. (2015). The steady-state visual evoked potential in vision research: A review. *Journal of Vision*, *15*(6), (4); 1-46. https://doi.org/10.1167/15.6.4.doi

Paxinos, G., & Watson, C. (1998). *The Rat Brain: in stereotaxic Coordinates* (4th ed.). San Diego, London:

Academic Press, An imprint of Elsevier.
Regan, D. (1989). *Human Brain Electrophysiology: Evoked Potentials and Evoked Magnetic Fields in Science and Medicine*. New York: Elsevier Science Publishing Co., Inc.
Rivero-Ríos, P., Gómez-Suaga, P., Fernández, B., Madero-Pérez, J., Schwab, A. J., Ebert, A. D., & Hilfiker, S. (2015). Alterations in late endocytic trafficking related to the pathobiology of LRRK2-linked Parkinson's disease. *Biochemical Society Transactions*, *43*(3), 390–395. https://doi.org/10.1042/BST20140301
Roosen, D. A., & Cookson, M. R. (2016). LRRK2 at the interface of autophagosomes, endosomes and lysosomes. *Molecular Neurodegeneration*, *11*(1), 1–10. https://doi.org/10.1186/s13024-016-0140-1
Schulz, C., Paus, M., Frey, K., Schmid, R., Kohl, Z., Mennerich, D., … Gillardon, F. (2011). Leucine-rich repeat kinase 2 modulates retinoic acid-induced neuronal differentiation of murine embryonic stem cells. *PLoS ONE*, *6*(6). https://doi.org/10.1371/journal.pone.0020820
Seki, M., & Lipton, S. A. (2008). Targeting excitotoxic/free radical signaling pathways for therapeutic intervention in glaucoma. *Progress in Brain Research*, *173*(08), 495–510. https://doi.org/10.1016/S0079-6123(08)01134-5
Steger, M., Tonelli, F., Ito, G., Davies, P., Trost, M., Vetter, M., … Mann, M. (2016). Phosphoproteomics reveals that Parkinson's disease kinase LRRK2 regulates a subset of Rab GTPases. *ELife*, *5*, 1–28. https://doi.org/10.7554/eLife.12813
Thirstrup, K., Dächsel, J. C., Oppermann, F. S., Williamson, D. S., Smith, G. P., Fog, K., & Christensen, K. V. (2017). Selective LRRK2 kinase inhibition reduces phosphorylation of endogenous Rab10 and Rab12 in human peripheral mononuclear blood cells. *Scientific Reports*, *7*(1), 1–18. https://doi.org/10.1038/s41598-017-10501-z
Tong, Y., & Shen, J. (2009). α-Synuclein and LRRK2: Partners in Crime. *Neuron*, *64*(6), 771–773. https://doi.org/10.1016/j.neuron.2009.12.017
Zechel, S., Meinhardt, A., Unsicker, K., & von Bohlen und Halbach, O. (2010). Expression of leucine-rich-repeat-kinase 2 (LRRK2) during embryonic development. *International Journal of Developmental Neuroscience*, *28*(5), 391–399. https://doi.org/10.1016/j.ijdevneu.2010.04.002
Zimprich, A., Biskup, S., Leitner, P., Lichtner, P., Farrer, M., Lincoln, S., … Gasser, T. (2004). Mutations in LRRK2 Cause Autosomal-Dominant Parkinsonism with Pleomorphic Pathology families, we have found six disease-segregating muta- tions (five missense and one putative splice site muta- tion) in a gene encoding a large, multifunctional pro- kinase. *Neuron*, *44*, 601–607. https://doi.org/10.1016/J.NEURON.2004.11.005

18.1 Supplementary

Pilot of interaction between genotype and wavelength condition

The purpose of this pilot was to test for interactions between wavelength of the stimulus presented and the genotype of the animal. This was investigated by recording the VEP of both wildtypes and LRRK2-KO during five different wavelength conditions:

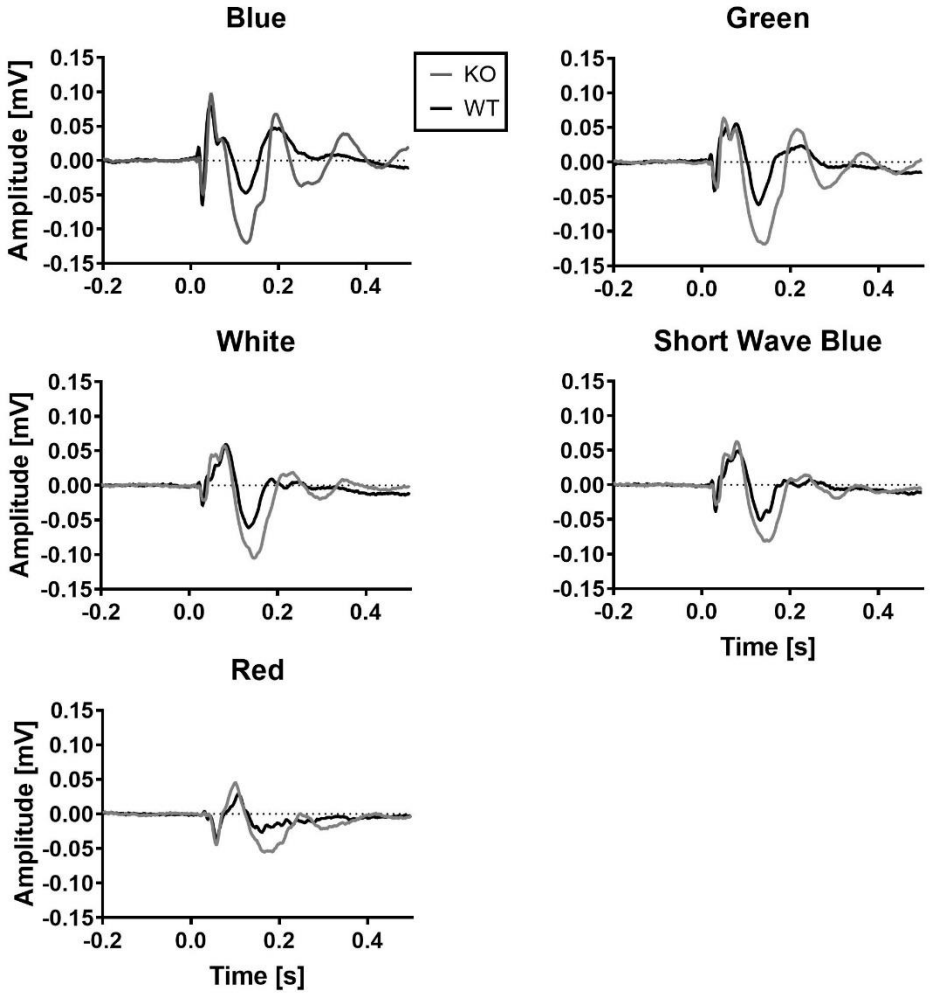

Figure S 1 Waveforms in the visual cortex. The grey is the LRRK2 knock-out and black is the wildtype. The difference between the KO and the WT depend on the wavelength of the light. The difference between the means was largest for blue light.

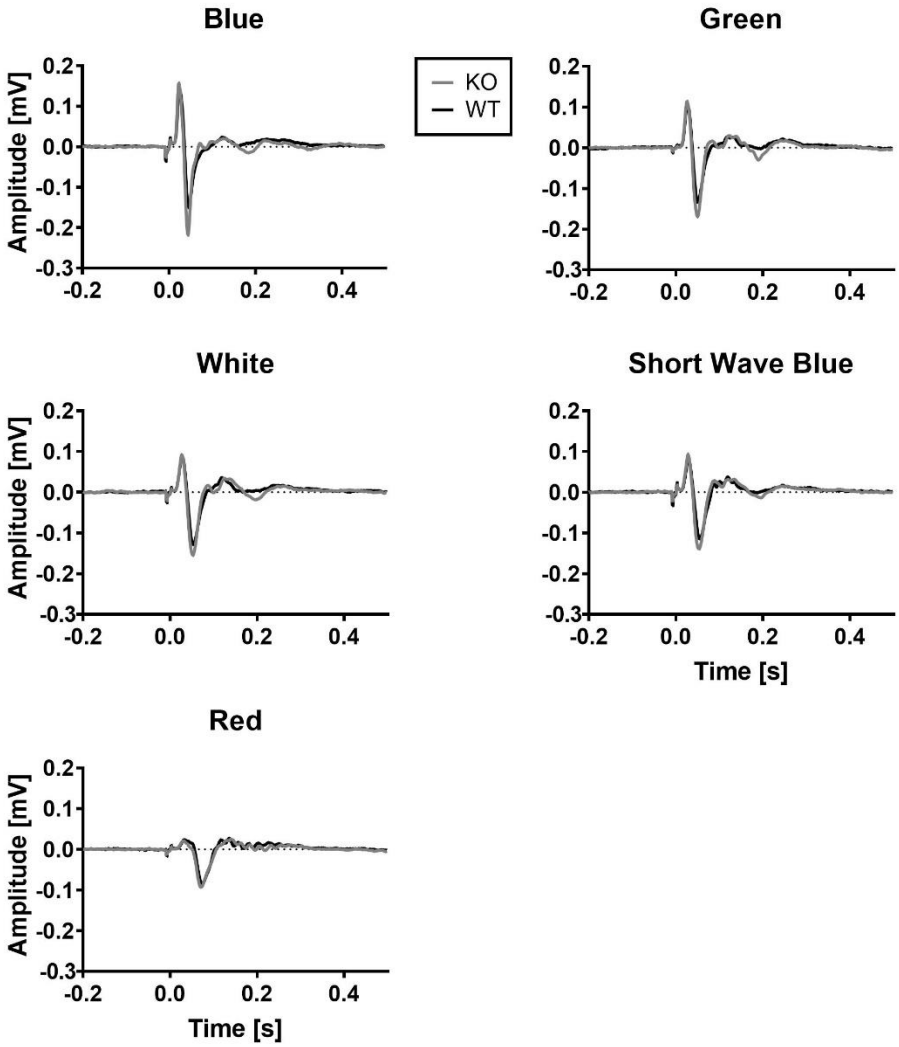

Figure S 2 Grand average waveforms from the superior colliculus recorded during five different wavelength conditions. The grey is the LRRK2 knock-out and black is the wildtype.